Organic-Inorganic Hybrid Polyoxometalate Extended Structures: Self-Assembled and Configured

University of Glasgow

A thesis submitted to the University of Glasgow for the degree of **Doctor of Philosophy**

School of Chemistry

College of Science and Engineering

Presented by

Naomi Anna Bechmann Johnson

(BSc)

August 2019

“C’est le temps que tu as perdu pour ta rose
qui fait ta rose si importante”

Antoine de Saint-Exupéry
Le Petit Prince

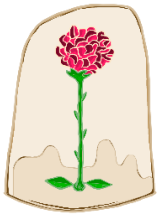

Acknowledgement

The work presented here was carried out between July 2014 and December 2018 in the Cronin Group within the School of Chemistry at the University of Glasgow. The help and support I have received during and leading up to this period was immeasurable and I am truly grateful. To recognise and name everyone would double the size of this document, but I am especially indebted to the following people.

First and foremost, I thank **Prof Lee Cronin** for seeing potential in me at a time when the doors to the world of academic research felt firmly shut. I have since maintained this faith in my own abilities through the example Lee sets: highly valuing the space for alternative free thinking, pushing ideas to their limit and being authentic to yourself.

Dr Andrew Macdonell took me under his wing when I first joined the group and introduced me to research projects with the greatest care. This not only grounded my start but also sparked a lifelong friendship. I have been very lucky. Thank you!

A thanks also goes to **Dr Vladislav Kulikov**, **Dr Andrew Surman** and **Dr Guillaume Marie** for their mentorship and practical training when I was very new to chemistry research. This support was later relayed and maintained by team leaders and senior members: **Dr Ross Winter**, **Dr Weimin Zhang**, **Dr Nancy Watfa**, **Dr Yousef Abul-Haija**, **Dr Shan She**, **Dr Geoffrey Cooper** and **Dr Deliang Long**.

I would like to thank my project students, **Eduard Garrido Ribó** and **Zoë Sinclair** for the fresh perspectives they brought to this work. I am astonished to see their relentless optimism has not tarnished during lab experience and life difficulties. I am very excited to see how this growing resilience against the challenges ahead continues to develop.

A warm thank you goes to my fellow PhD students, the soon-to-be **Drs**: **David Doran**, **Edward Lee**, **Stephanie Marie Colon-Santos** and **Dario Caramelli** with whom the comparison of parallel personal struggles has softened the load at various crisis moments whether in the form of a passing grimace or joke, a comforting hug, or heart-felt conversation.

To alumni of the **Cronin Group** whose friendships over the years have formed the distinct chapters of my time in the group, **Kevin Donkers**, **Dr Lorna Christie**, **Dr Leanne Bloor**, **Dr Laurie Points**, **Dr Christoph Buche**, **Dr James Taylor**, **Dr Vasilis Duros**, **Dr Mercé Martin**, **Dr Qi Zheng** and those of you who are still here and bring little glimmers of magic to my daily life, **Manuel Kupper**, **Andrius Bubliauskas** and **Dr Juan Manuel Parrilla Gutierrez**. I cannot list all the special moments we have shared that keep us connected no matter where life takes us individually. Thank you for the joy, fear, laughter, love, wonder, conversation, company and food we have had together and I am particular grateful to the office, lunch and coffee break pals for toppling me daily into a bottomless pit of conversation and exploration of human existence. A big thanks also to **Dr Laia Vilà-Nadal** and **Silke Asche** with whom I have shared adventure and trusted in crisis and the helpful strangers **Matt**, **Chris** and **Josh** to which the three of us owe a great deal. For proofreading my thesis, I would like to thank **Richard**, **Vasilis**, **Stephanie**, **Manuel, Dr Eric Janusson, James McAllister** and **Robert Pow**.

Immense thanks to **Jim McIver**, **Dr Diana Castro**, **Dr Jennifer Mathieson**, **Amanda McGarvey**, **Stuart Marshall** and **Laia**, the oil in the cogs of the Cronin Group, without which daily work would be impossible. This recognition also extends further to fellow occupants, **Stuart Mackay, Ted Easdon, Karen McLachlan** and **Finlay Smith** to name but a few, of the **Joseph Black Building** itself: a living, thriving, ever-changing community with many layers of history and intertwining personal journeys of researchers, technicians, contractors, students, cleaners and lost visitors. It has been a pleasure to work within these walls for almost a decade, where a passing smile, ray of sunlight or interesting shadows in the corridor never fails to lift my mood.

Sincere thanks to my mentor **Dr Jenny Scott** not only for her alternative perspective and sound advice, but also the stories and laughter we have exchanged these last 6 years.

I would like to express my gratitude to the individuals encountered at the crossroads of my life which would ultimately lead me to the start of this PhD journey, in particular: **Mr Patrick Youmans**, **Mr Keith House** and **Mr Angus Gregson** who kindled my initial fascination for the physical sciences, **Prof Geoffrey Eglinton** who highlighted to me the importance of creative minds within the sciences, **Matthew Ireland**, **Mark Johnson** and

Prof Bob Hill for drawing me to the city of Glasgow and finally **Dr Louis Farrugia** who unknowingly opened a portal through which I discovered the Cronin Group wonderland.

I cannot express how lucky I am to have received the support of innumerable friends many of which have helped me a lot at specific moments throughout these years. In particular, I would like to extend heart-felt thanks to **Francesca Stephens** and soon-to-be **Dr Corentine Laurin** for their companionship during the first year of my postgraduate experience, I am deeply thankful to **Nicholas Joyce** for the solid anchor of support and encouragement he has provided throughout the ups and downs of my PhD. Finally, a very special thanks goes to **Jamie Johnstone** who has, since his reappearance a year ago, always been there when I pick up the phone for daily revitalisation.

Lastly, I am extraordinarily grateful to my family, the ones who have been by my side for the longest, who truly understand how far I have come and profoundly shape who I am. Thank you to **Eve Bechmann-Johnson** the wisest person I know, **Richard Johnson** the most earnest of role models, **Jeremy Johnson** for his laughter and joy in the face of the impossible and **Miriam Johnson** for her strength, grounding and discernment.

Abstract

The high oxidation state metal oxide clusters known as polyoxometalates (POMs) are interesting not only because of their unusual physical and chemical properties but also because they are complex structures that self-assemble from basic building blocks, a process that is not well understood. Synthetic chemists generally begin by developing an in-depth understanding of matter which can then be used to manipulate it; however, POM researchers tend to spend less time exploring the mechanisms of POM self-assembly and instead focus simply on the search for new clusters or the modification of existing ones. This approach can in some ways be compared to the life science fields in which researchers work with systems that may be too complex to fully understand yet are still able to manipulate processes for many applications. As a result, these researchers learn more about the system itself.

Instead of focusing on the synthesis or self-assembly of POMs themselves, this thesis explores the formation of inter-cluster assemblies: starting with a self-assembling POM-based network and then moving on to explore the directed synthesis of inter-POM assemblies. Just like the self-assembly of POMs themselves, the way in which clusters arrange themselves on a supramolecular level takes place spontaneously, forming crystals and sometimes gels. Alternatively, there are methods in which inter-POM assemblies can be designed and engineered entirely by chemists. For this to be possible the incorporation of organic chemistry is necessary as the mechanisms are far better understood and manipulation is carried out with high precision and control. Organic moieties can be grafted onto POM clusters directly through covalent bonds forming organic-inorganic POM hybrids which can then be modified with a level of control comparable to pure organic chemistry. This is achieved through functionalisation of the organic ligands using reaction conditions that do not disturb the inorganic clusters to which they are fused. Herein both the intermolecular self-assembly and covalently connecting directed synthesis of organic-inorganic POM hybrid extended structures and oligomers are explored. In doing so, tentative comparisons with biomolecular configurable polymers, namely polypeptides and nucleic acids are made.

The first section explores the extended structure of a self-assembled POM hybrid formed through the acidification of molybdate and the biological molecule, 5’-guanosine

monophosphate. On crystallisation of the resulting bi-functionalised hybrid clusters, the guanosine Strandberg monomers, stack into double-helix structure with dimensions almost identical to Z-DNA. The formation of such a complex structure through spontaneous self-assembly of simple building blocks is interesting to those familiar with the inorganic origin of life theory proposed by Cairns-Smith. Further investigations using AFM and CD are made to explore the nature of the guanosine Strandberg in solution with results suggesting an ordered structure is present.

The second section contrasts with the self-assembly of POM hybrid extended structures by controlled synthesis of discrete POM hybrid oligomers using asymmetric Mn-Anderson hybrids. This is achieved via the development of azide or alkyne-functionalised Mn-Anderson monomers isolated through chromatography and then used in a “Click” reaction to form dimers and trimers. These chains are then further extended with the addition of a monomer to each end resulting in a tetramer and pentamer. The resulting four oligomers are verified using ESI-MS and NMR and compared via SE-HPLC and IMS-MS where evidence for two conformers of the tetramer chain is observed.

The last section builds directly from the previous section by working on expansion of the “Click” coupled POM hybrid oligomerisation to include other clusters. This concept is inspired by the configurable nature of polypeptide chains that result in structures with properties of an astonishing variety. Building blocks appropriate for such a task must be easily made in large quantities in order to function as a starting material. For example, the vanadium-based Lindqvist hybrid is deemed inappropriate for use as a building block due to low yields. Adaptation of the asymmetric Mn-Anderson method is applied to the Fe-Anderson hybrids where Fe acetate replaces the Fe acac starting material resulting in a purer product and an additional FMOC protection step added to avoid problematic basic properties of the TRIS ligand during material formation. An attempt at Co-Anderson hybrid synthesis unexpectedly results in the formation of a tri-functionalised cobalt-centred hybrid with three hydroxyl groups instead of amine groups, the post-modification of which is unsuccessful. Synthesis of an asymmetric Cr-Anderson hybrid building block is achieved through consecutive stepwise reactions. The resulting Mn-, Fe- and Cr-Anderson building blocks are then used for the formation of a Mn/Fe/Mn-Anderson trimer from which a Cr/Mn/Fe/Mn/Cr-Anderson pentamer is attempted.

Table of Contents

Publications

Configurable Nanosized Metal Oxide Oligomers via Precise "Click" Coupling Control of Hybrid Polyoxometalates. Macdonell, A.; Johnson, N. A. B.; Surman, A. J.; Cronin, L. *J. Am. Chem. Soc.* **2015**, *137*, 5662–5665.

Spontaneous Assembly of an Organic–Inorganic Nucleic Acid Z-DNA Double-Helix Structure. Kulikov, V.; Johnson, N. A. B.; Surman, A. J.; Hutin, M.; Kelly, S. M.; Hezwani, M.; Long, D-L.; Meyer, G.; Cronin, L. *Angew. Chem. Int. Ed.* **2017**, *56*, 1141–1145.

Abbreviations

In addition to standard notation, the following abbreviations were used in this thesis:

acac	Acetylacetone
AFM	Atomic Force Microscopy
CD	Circular Dichroism
CuAAC	Copper(I)-Catalyzed Alkyne-Azide Cycloaddition
DCC	N, N'-Dicyclohexylcarbodiimide
DEPTQ	Distortionless Enhancement by Polarisation Transfer with retention of Quaternaries
DFT	Density Functional Theory
DIEA	N, N-diisopropylethylamine
DLS	Dynamic Light Scattering
DMF	N, N-Dimethylformamide
DMSO	Dimethyl Sulfoxide
DOSY	Diffusion Ordered Spectroscopy
EEDQ	2-Ethoxy-ethoxycarbonyl-1,2-dihydroquinoline
ELSD	Evaporative Light Scattering Detector
equiv.	Equivalent
ESI-MS	Electrospray Ionisation Mass Spectrometry
Et_2O	Diethyl Ether
FMOC	9-Fluorenylmethyloxycarbonyl
GMP	Guanosine Monophosphate
HPLC	High-Performance Liquid Chromatography
IMS-MS	Ion-Mobility Spectrometry–Mass Spectrometry
IR	Infrared
LC	Liquid Chromatography
MeCN	Acetonitrile
NHS	N-Hydroxysuccinimide
NMR	Nuclear Magnetic Resonance Spectroscopy
OAc	Acetate
POM	Polyoxometalate
RP	Reverse Phase
SPPS	Solid-Phase Peptide Synthesis
TBA	Tetra-n-butylammonium
TEA	Triethyl amine
TEM	Transmission Electron Microscopy
TRIS	Tris-(hydroxylmethyl)-aminomethane
Trt	Trityl
UV	Ultra-Violet
XRD	X-Ray Crystallography

1 Introduction

The complexity of the living world inspires many to explore the manipulation of matter. In the case of chemists, this compulsion exhibits itself as a desire to investigate and work with systems at a molecular level with the aim of gaining control over the transformation of substances. The level of control researchers possess depends on the depth to which they understand the systems they work with, many of which are incredibly complex and so it takes generations of hypothesis, trial, error and luck before a satisfactory level of knowledge is achieved.

The field of *polyoxometalate* chemistry is an example of a subject where full understanding is still under development. When working with this system, it is possible to seemingly spontaneously assemble extraordinarily complex structures from very simple starting materials. To some, this "simple-to-complex" characteristic is particularly fascinating because of the parallels that can be drawn between polyoxometalate and biological systems and so arguably the study of one could advance understanding of the other. This is particularly striking since very few of the components of either system overlap with one another.

Studying polyoxometalates with such an aim in mind can be approached in a number of ways such as encouraging the life-like characteristics of a polyoxometalate system to display itself, attempting to develop mechanisms involving polyoxometalates that are inspired by biological systems or simply mixing the two systems together and observing the result. The following sections introduce the polyoxometalate field and some of the biological systems that this work explores.

1.1 Polyoxometalates

Polyoxometalates are a class of inorganic materials composed of high oxidation state transition metals and oxygen atoms, connected together to form discrete clusters.[1] These almost always negatively charged clusters can vary in size from molecular to nano-scale[2] and form a remarkable variety architectures for which they receive much attention. Polyoxometalate (POM) synthesis involves deceptively straightforward one-pot reactions in which simple building blocks *self-assemble* into complex polyanions which are isolated

through crystallisation. Although there is limited understanding of the self-assembly process, experts in the field can control the structure formation by varying the exact experimental conditions such as pH, temperature and concentration. In addition to their complex structures, POMs also attract interest for their unique electronic and redox properties caused by the nature of the transition metals, most commonly molybdenum, tungsten and vanadium, from which they are made. These characteristics are also affected by other elements included in the structure and the cations that balance the system, components that can vary enormously. As a result application of POMs in electronics[3,4], catalysis[5,6], materials[7–11], magnetism[12,13] and medicine[14,15] is frequently demonstrated.

1.1.1 A History of Polyoxometalates

The first alleged observation of what would later come to be known as the *molybdenum blues* was ilsemmanite, a naturally occurring mineral responsible for the intense blue colour of the modern day Idaho Springs, Colorado and The Valley of Ten Thousand Smokes, Alaska. The first documented observations of POM compounds were made initially by Swedish chemists in 1778 where Carl Wilhelm Scheele recorded some unknown blue molybdenum oxides[16] and the second in 1826, where Jöns Jacob Berzelius described how a reaction of ammonium molybdate and phosphoric acid produced a yellow precipitate, which would later be confirmed to form $(NH_4)_3[PMo_{12}O_{40}]\cdot xH_2O$, a classic POM structure known as the Keggin.[17] In 1862, the Swiss chemist Jean-Charles Galissard de Marignac used a titration to determine the elemental composition for silicotungstic acid, also a Keggin, with surprising accuracy considering the limit of the analytical techniques available during that period. Despite not being able to identify the exact structure, Galissard de Marignac did propose the existence of two geometries, now recognised as the α- and β- species.[18,19]

During the following hundred years, a number of different theories were proposed in attempts to predict and understand the nature of these metal oxide clusters. It was not until 1893 that the basic principles of coordination chemistry were laid out and the idea that metal ions within a compound could be linked to several oxygen atoms was proposed by a Swiss chemist, Alfred Werner.[20] Fifteen years later, Werner's concepts were applied to metal oxide clusters by Miolati[21] and further developed in 1917 with the

Miolati-Rosenheim theory, suggesting that heteropolyacids form through replacing the oxo ligands of a parent acid with [MO_4^{2-}] or [$M_2O_7^{2-}$].[22] A decade later, an alternative theory was proposed by Linus Pauling suggesting that octahedral [MO_6] units surrounded a central tetrahedral [XO_4] unit to form the clusters, but was limited by the fact Pauling argued that these units would only allow for corner sharing of oxo ligands and not edge or face-sharing which is now known to be commonly seen within polyoxometalate structures.[23]

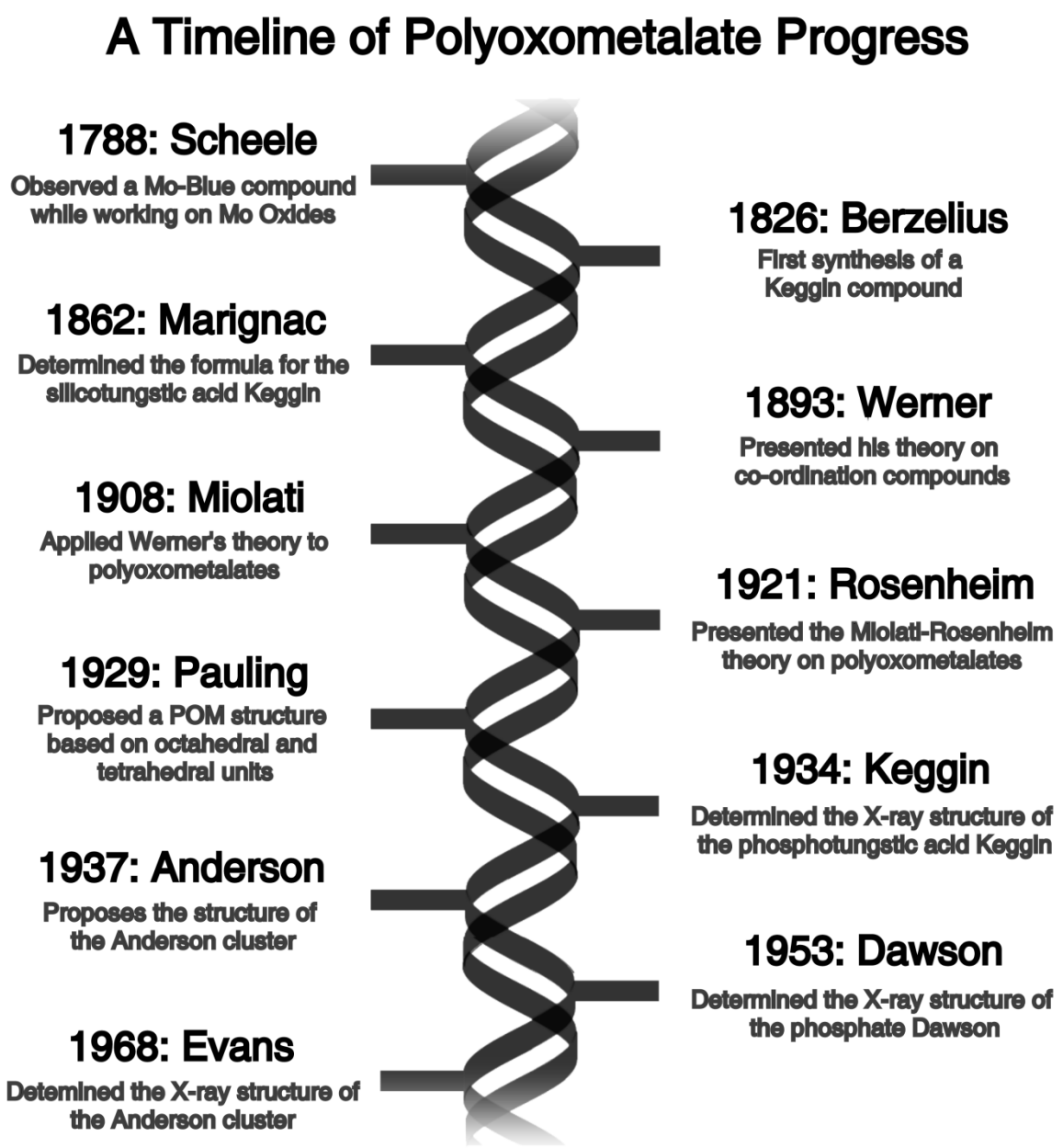

Figure 1 A timeline summarising some of the major developments in the polyoxometalate field.

The development of single crystal X-ray diffraction (XRD) in 1913, finally provided a more definitive understanding of the structure of these clusters.[24,25] The first polyoxometalate structure to be solved was 12-phosphotungstic acid in 1933 by James Fargher Keggin,

showing a structure formed of twelve edge and corner sharing polyhedra.[26,27] Although this breakthrough took about a decade to be fully accepted, the solved structure did then allow for the structures of several other clusters to be predicted in advance of their verification via XRD, namely the Wells-Dawson[28] and the Anderson-Evans.[29,30]

These ideas and techniques continued to be developed by a handful of research groups such as Souchay (Paris), Baker and Pope (Georgetown), who over the years laid the foundations of POM chemistry.[31,32] Breakthroughs such as the discovery of the wheel-shaped molybdenum blues[33] and other large clusters, for example the "blue lemon"[2] established polyoxometalates as a nanomaterial[34] and brought wider interest to the field. In more recent years, the additional use of analytical methods such as nuclear magnetic resonance (NMR), mass spectrometry (MS) and computational modelling has continued to deepen our understanding of the structural characteristics and assembly of polyoxometalates.[35] The major milestones of polyoxometalate chemistry described here are also summarised in timeline form (**Figure 1**).

1.1.2 Structure and Nomenclature

Nomenclature within the field of polyoxometalates is not fully standardised although there are a reasonable number of commonly used terms. The word *polyoxometalate* itself describes a compound containing three or more metal centres connected through bridging oxygen atoms. The term *metal-oxygen cluster* is an alternative, self-explanatory description for polyoxometalate but is rarely used.[36] Instead, it is more common to encounter *polyanion*, or to a lesser extent *polyoxoanion* which reflects the fact that polyoxometalates are, with the exception of a few examples, cations but fails to highlight the metal-containing aspect of a polyoxometalate and therefore cover a much broader range of clusters, not specific to POMs alone.[28,37]

Polyoxometalates are formed of three component parts: oxo bridges, addenda and heteroatoms (**Figure 2**). The *addenda* are the major metal centres involved in holding together the POM structures and according to Baker, have the following characteristics:[32] (1) Upon polymerisation in solution their coordination number can vary from 4 to 7, (2) they are one of the smallest metal ions capable of octahedral packing, (3) they possess a high positive charge and finally, (4) they are capable of forming terminal M=O bonds via

dπ-pπ interactions. For these reasons, addenda are mostly found to be early transition metals in their highest oxidation states with configurations of d^0 and d^1, most commonly Mo^{VI} and W^{VI} and sometimes V^V, Nb^V and Ta^V.[38] Addenda have also been seen formed from other hexavalent (Tc, Re, Ru and Os), pentavalent (Cr, Mo, W, Tc and Re), tetravalent metals (Ti, V, Cr, Mo and W)[31] as well as noble metals (Pd, Pt and Au).[39]

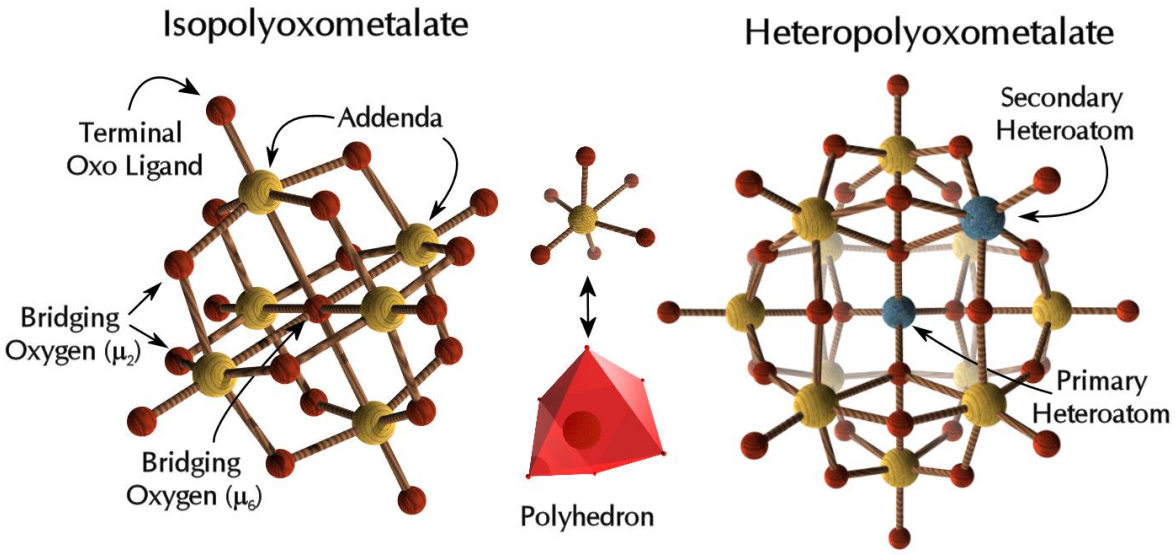

Figure 2 Common polyoxometalate nomenclature labelling models of a typical isopolyoxometalate structure (the Lindqvist) and a heteropolyoxometalate structure (the Keggin).

Heteroatoms are the remaining non-addenda atoms found within the polyoxometalate structure, most commonly elements of the p-block such as Si, P, S, Ge and As although by no means are they restricted to this. Almost any element can act as a heteroatom, metals and non-metals alike, so long as it is capable of bonding to three or more atoms. A *primary* or *central* heteroatom is one which is crucial to the POM structure itself whereas *secondary* or *peripheral* heteroatom can be removed without destroying the cluster. When a POM has a secondary heteroatom missing, a cavity known as a *lacuna* is left and the POM itself can be referred to as *lacunary*.

Polyoxometalates can be split into two categories (**Figure 2**): isopolyoxometalates and heteropolyoxometalates, with the respective general formulae of $[M_nO_y]^p$ and $[X_aM_nO_y]^p$ where a<n, M = addenda, X = heteroatoms and p is the overall charge of the cluster, most likely negative. *Isopolyoxometalates* are POMs made purely of primary heteroatoms and oxygen atoms whereas *heteropolyoxometalates* contain structurally essential primary heteroatoms and secondary heteroatoms on the peripheral. Although, in most cases this classification seems straightforward, there are times where the isopolyoxometalate and

heteropolyoxometalate terminology is unclear.[31] This ambiguity stems from the fact that a second transition metal found within a POM cluster can be classified as either a heteroatom or an addenda atom. An Anderson-Evans-type structure for instance, can have either a transition metal or a non-metal at its centre and so switches between isopolyoxometalate and heteropolyoxometalate depending on what atom occupies this central position despite the cluster shape remaining the same.[40] Another example of confusion occurs when comparing a classic isopolyoxometalate, the $[Mo_6O_{19}]^{2-}$ Lindqvist cluster with another Lindqvist where one molybdenum has been replaced with a vanadium to form $[VMo_5O_{19}]^{3-}$ which can be classed either as a heteropolyoxometalate or a mixed-addenda isopolyoxometalate.[41]

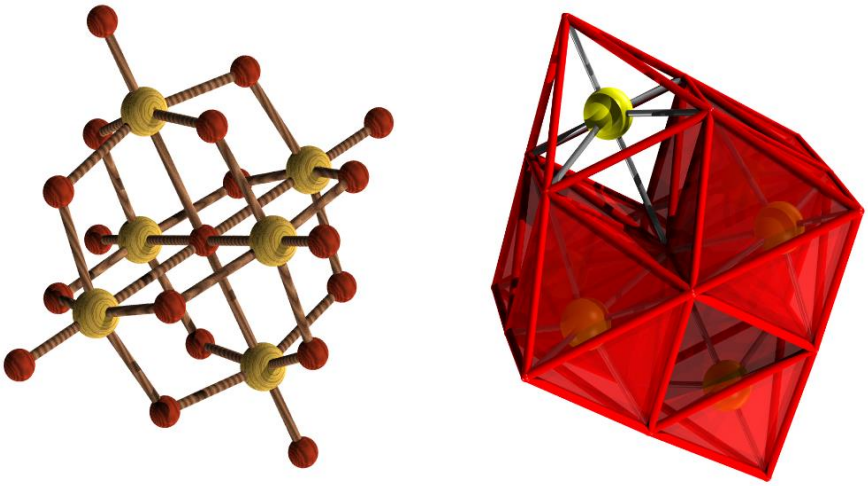

Figure 3 Comparison of the ball-and-stick (left) and polyhedral (right) representations of the Lindqvist POM.

Finally, the oxygen atoms within a polyoxometalate cluster can either be described as bridging or terminal. A *bridging* oxygen atom is bound to two or more addenda whereas a *terminal* oxo ligand forms a double bond with a single metal centre on the edge of the cluster. The geometric shape that oxygen atoms surrounding a single metal centre form is known as a *polyhedron* and is often depicted in figures to make a clearer representation of the POM cluster (**Figure 3**). These $[MO_x]$ polyhedral units, where x=4-7, but most commonly 6, are generally seen to be the simplest structural element (or *synthon*) of a polyoxometalate and recur within even the biggest and most complex POM clusters (**Figure 4**).

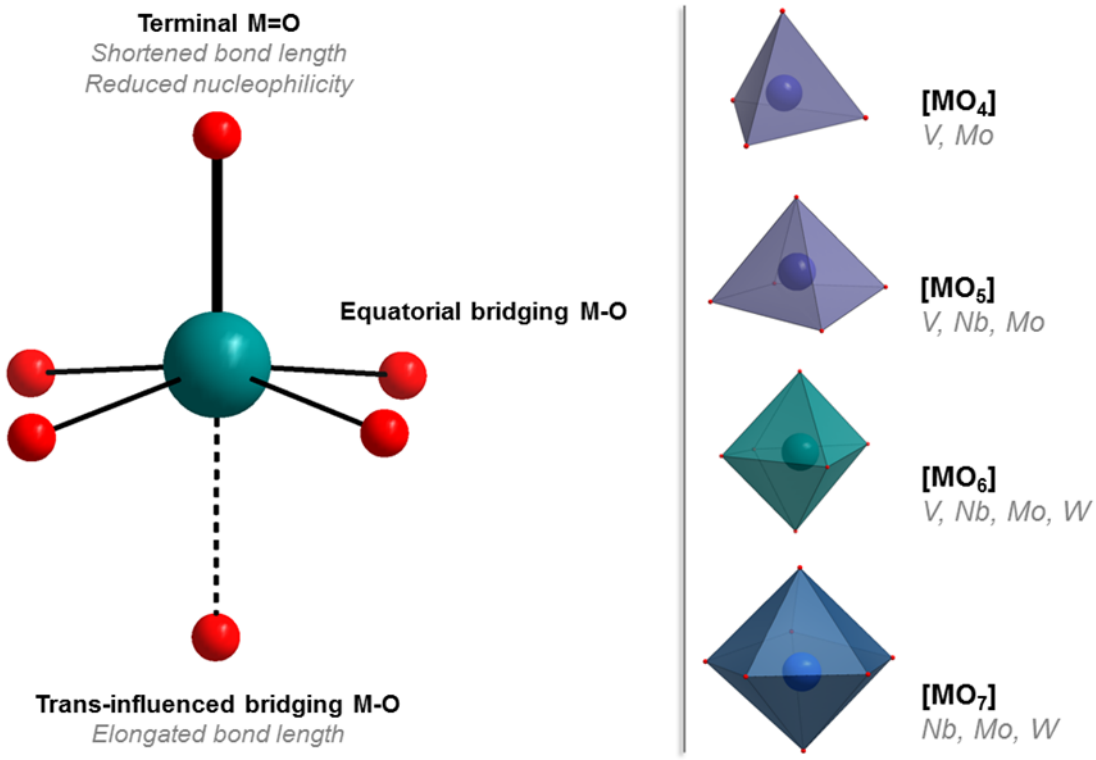

Figure 4 Labelled representation of a typical [MO_6] polyhedral unit found in polyoxometalate structures (left) and highlighting the trans-influence. The polyhedral units of a cluster can vary from 4 ligands all the way up to 7 (right).

In order to understand how it is possible for these metal oxides to form as discrete, well defined clusters and not infinite, extended structures such as with the iron oxides responsible for rust, it is necessary to understand the nature of the metal to oxygen bonding and discuss some coordination theory,[20] in particular the distortion that occurs in the bonding between transition metal and oxygens bonded tetrahedrally.[42] The *trans*-influence is the weakening of a metal-ligand bond in a square planar or octahedral geometry due to the ligand coordinated to the opposite side of the metal.[43] The ligands *trans* to one another are sharing the same orbital of the central metal and so their bonding stability will be altered depending on the electron accepting and donating abilities relative to one another. This influence can either result in a structural change where the bond length increases and the geometry distorts or has a kinetic impact resulting in loss of stability of the bond and therefore becomes more labile and reactive. In the case of the coordination observed in polyoxometalates, the terminal oxygen ligands (M=O bonds) are a much better electron donor to the addenda atom compared to the bridging oxygen ligands (M-O bonds) and so the trans-effect is observed in the shortening of the M=O bonds and distortion of the polyhedrons such that the addenda atoms are located closer to the terminal oxygen atoms, sometimes up to an Ångström difference in length (**Figure 4**).[43] The positioning of the terminal oxo ligands and central

oxo bridging ligands due to the *trans*-influence results in polarisation throughout the cluster with the outer surface having a higher positive charge than would perhaps be expected and the inner core being somewhat electron rich. As a result, the terminal oxo groups are not very susceptible to protonation and therefore stabilise the cluster as a whole. In addition, the electron rich core provides flexibility to the centre of clusters, providing space for a multitude of heteroatoms and geometries to comfortably arrange themselves, which is one reason for the observed diversity of polyoxometalate architectures. This also goes some way into explaining how it is that larger polyoxometalate building blocks are not generally formed from the simple polyhedra synthons, described previously but rather from a combination of ready-made simpler polyoxometalate clusters.

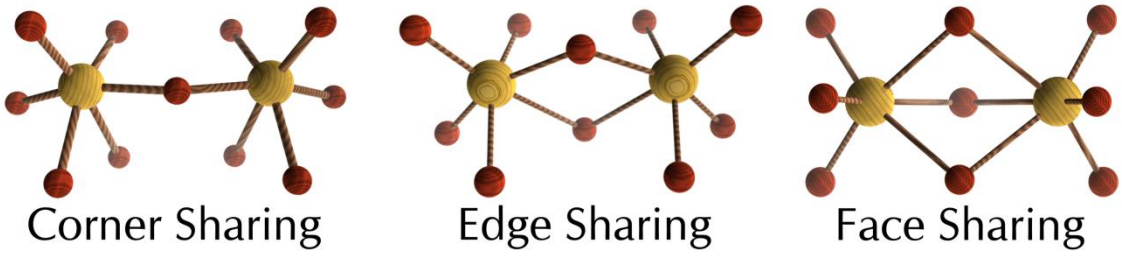

Figure 5 Demonstration of corner, edge and face-sharing between [MO_x] units.

Acid-mediated condensation can result in polymerisation of the [MO_x] (generally MO_6) building blocks via corner, edge or face sharing (**Figure 5**) so long as the *Lipscomb Principle*[44] is followed which rules that no polyhedra can have less than two unshared terminal oxygens, although there are a handful of molybdate-based structures that do break this rule.[45–47] This results in three categories of POM clusters being possible, those possessing octahedra with only one M=O terminal bond being *type I*, those containing two being *type II* and a mixture of both being *type III*.[48] This classification reflects not only structural difference but also a resulting chemical behavioural difference. Type I and type III POMs are reversibly redox active because the LUMO of these octahedra will be non-bonding, the most notable within this category being the molybdenum blues and browns.[3,49–51] Type II clusters on the other hand, are POMs that will generally decompose if reduced due to the strong anti-bonding character of the cis-dioxo [MO_6] units.[31,50]

1.1.3 Lacunary Structures

Classical POM structures such as the Wells-Dawson or the Keggin structure with missing heteroatoms are known as lacunary structures.[1] They can be formed from the classic clusters themselves, usually by raising the pH to sufficiently destabilise the POM or alternatively they can be synthesised directly in a one-pot reaction under conditions disfavourable for the formation of the completed structure. As a general rule, removal of an additional metal centre will be adjacent to an already missing addenda site and never at opposite ends of the cluster (**Figure 6**).

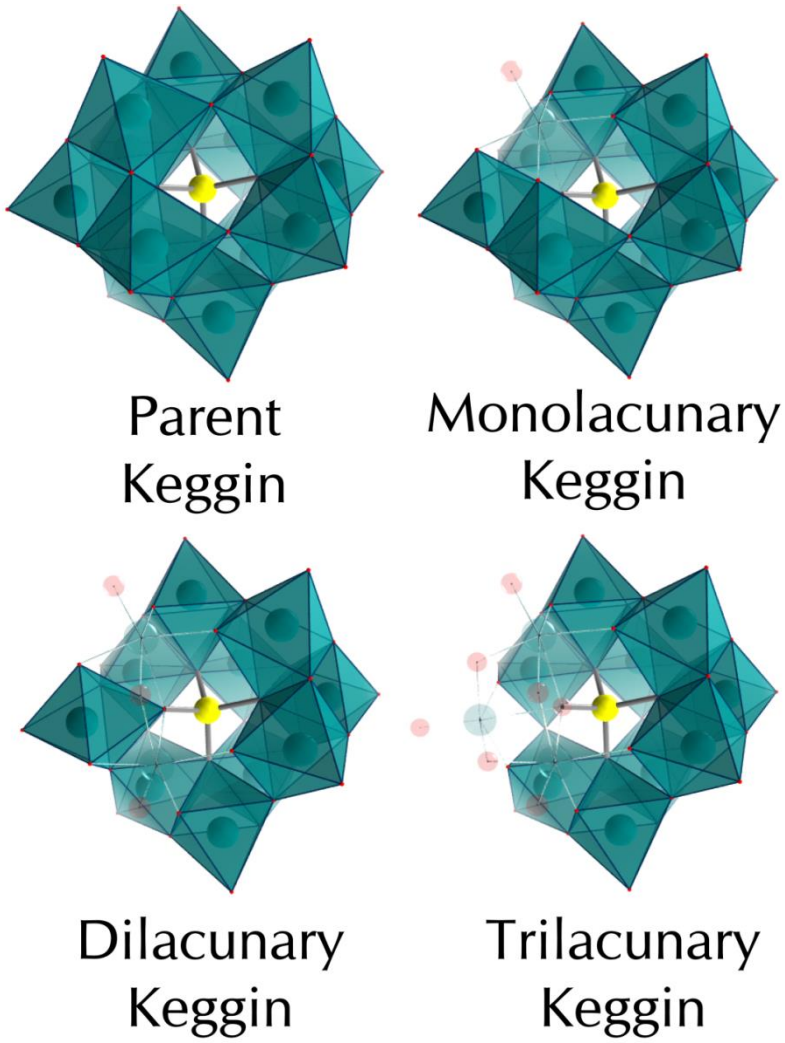

Figure 6 Example of the lacunary structures based off the Keggin structure, demonstrating sequential removal of addenda atoms starting from the parent cluster to give the W_{11}, W_{10} and W_9 species (removed atoms are shown as transparent to indicate their former position).

Lacunary structures can allow for the formation of mixed-metal POMs by filling of lacuna with other addenda metals, lead to larger, more complex POM architectures through condensation of lacunary units or linking through transition metals and even act as a starting material for the formation of POM hybrids, discussed in a later section. This is

due to the uneven charge distribution of a lacunary POM where the increased nucleophilicity of the exposed oxygen atoms of a lacuna make it more reactive with electrophiles.

1.1.4 Synthesis

By acidifying aqueous solutions of transition metal oxyanions, $[MO_x]^{n-}$ the Lewis acidity of the metal centres increases resulting in a series of condensation reactions bringing the metal centres together to form the larger, more complex geometries of polyoxometalates (**Figure 7**). The architecture of these structures varies enormously depending on the reagents used and the reaction and purification conditions.

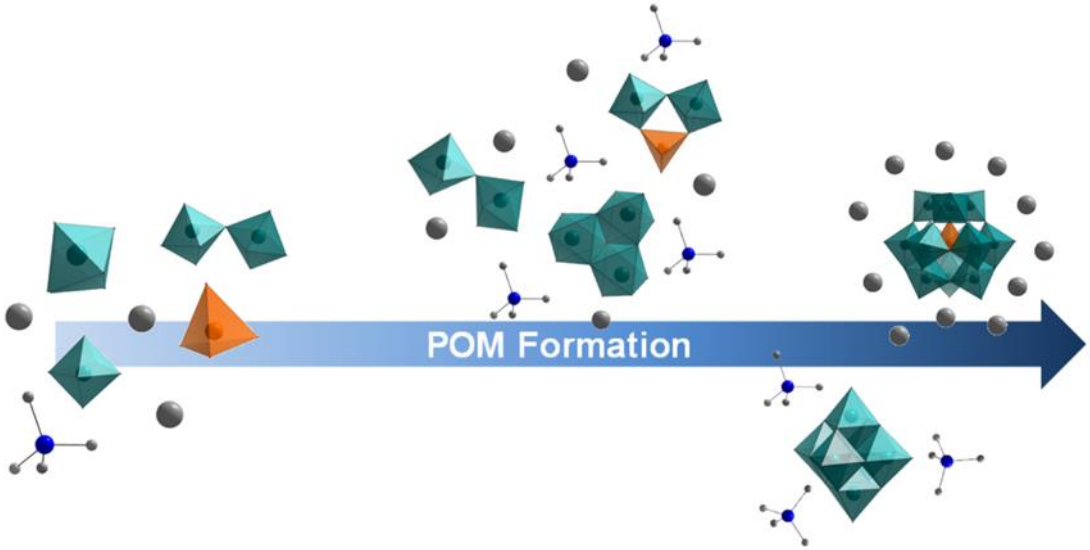

Figure 7 Representation of the way in which polyoxometalates are assembled from smaller building blocks and subunits.

The majority of POM synthesis is carried out in aqueous one-pot reactions. As well as the metal oxide starting material, reagents used frequently include heteroatoms, reducing or oxidising agents, cations and organic ligands. There are also a lot of options possible for conditions such as pH, temperature, time, concentration and ionic strength, all with the potential to dramatically influence the outcome of an experiment.[52]

In addition to the standard aqueous one-pot reaction under mild conditions, alternative approaches can be used very effectively. Although water is the solvent most commonly used for POM synthesis, carrying out experiments in polar organic solvents (especially

acetonitrile, *N,N*-dimethylformamide or dichloromethane) can result in different POM clusters forming than in the equivalent aqueous setup.[53–57]

A lot of POMs are synthesised at relatively low or even room temperatures, but sometimes by carrying out a reaction far from equilibrium conditions, metastable POMs crystallise that would not otherwise be obtained. For this to occur, it is necessary to carry out the reaction at greatly elevated temperatures and pressures and so hydrothermal or solvothermal conditions are used. This approach has been demonstrated using water[58–60] organic solvents[61–63] and ionic liquids.[64–66]

Often instead of, or in addition to, the simple [MO_4] starting material, small pre-formed polyoxometalate clusters themselves are used, which may either be some of the archetypal POM structures (which shall be described later) or lacunary polyoxometalates. Lacunary POMs make particularly good building blocks because of the reactivity of their lacuna: the pockets left behind on the removal of an addenda atom are especially electron rich. If pre-formed POMs are used in a reaction, then the synthesis can no longer by definition really be referred to as *one-pot* and is instead a series of reactions building one from another. There are also other unconventional approaches, including those taken by Cronin and co-workers, such as continuous flow[67,68] or inside purpose-built 3D printed cartridges.[69,70]

Crystallisation is a crucial element of POM synthesis, purification and isolation. It is often the only way for some polyoxometalates to be obtained and in a lot of cases, formation of the desired clusters is directed by the crystallisation process itself. Crystal growth can be a delicate task where variables such as solution concentration, air humidity and temperature and flask shape and size all make significant contributions to the quality, quantity and type of crystals obtained, which will occasionally only grow at certain times of the year or not be reproducible outside the laboratory in which they were first isolated.[48]

This reproducibility issue due to the need for experimental preciseness is not an uncommon problem within the POM field and highlights the importance of detailed experimental procedure documentation. There are some POMs that have a number of valid synthesis pathways and can be made with relative ease, but many only form within

a very small and specific window of reaction conditions, which may be very difficult to pin down and often it is not possible for even an expert within the field to make a compound without direct oversight and training from another researcher experienced with that particular POM.

1.1.5 Self-Assembly

Speculation over the assembly pathway of polyoxometalates has resulted in numerous studies being carried out using X-ray crystallography and NMR, from which a number of different theories have developed. More recently, mass spectrometry (MS) studies have resulted in a more concrete understanding of the self-assembly mechanisms for such clusters.[71–73] By combining electrospray ionisation mass spectrometry (ESI-MS) and density functional theory (DFT) studies for example, a mechanism for the formation of the Lindqvist POM was proposed where the cluster assembles one metal-centre at a time, with each sequential condensation alternating between exothermic and endothermic until a large enough exothermic reaction takes place to allow the cluster to form.[74] In another example, Cronin et al. analysed the formation of a gigantic palladium wheel structure by using a combination of electrophoresis, size-exclusion chromatography and (SEC) and ESI-MS to analyse the reaction mother liquor as a function of real time. This approach allowed them to propose formation of the $\{Pd_{84}\}$ wheel would build up over the course of several days from 14 $\{Pd_6\}$ subunits (**Figure 8**).[75] A similar method was then also applied to the analysis of formation of a series of smaller Pd wheels.[76]

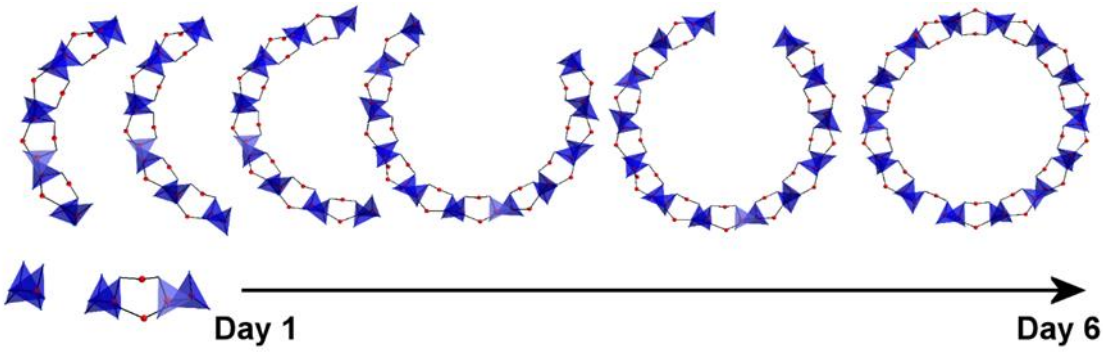

Figure 8 Proposed mechanism for the build-up of $\{Pd_{84}\}$ from $\{Pd_6\}$ subunits over 6 days. Only the $\{Pd_6(\mu_4\text{-}O)_2\}$ core (blue tetrahedra), and bridging μ_2-O ligands (red) are shown for clarity.

The seemingly extensive assembly pathway of the Lindqvist, which is considered one of the most simple POM structures, highlights how complex the self-assembly mechanism of larger clusters is to understand. This lack of mechanistic understanding results in one of

the biggest challenges faced by POM chemists. *Directed* self-assembly is a reaction set up with a specific target in mind, and although this approach does get used within the field, the unpredictability of POM formation means this method is not a guaranteed success. An equally valid approach to searching the polyoxometalate *chemical space* is to set up reactions, varying the synthetic conditions with no specific structure in mind. This *serendipitous* or *undirected* self-assembly approach allows for more pockets of novel POM cluster families to be unearthed which would otherwise not be predictable. This concept is taken a step further in the Cronin group where algorithms are designed to allow robots to carry out reactions as they search though chemical space (**Figure 9**).[77,78]

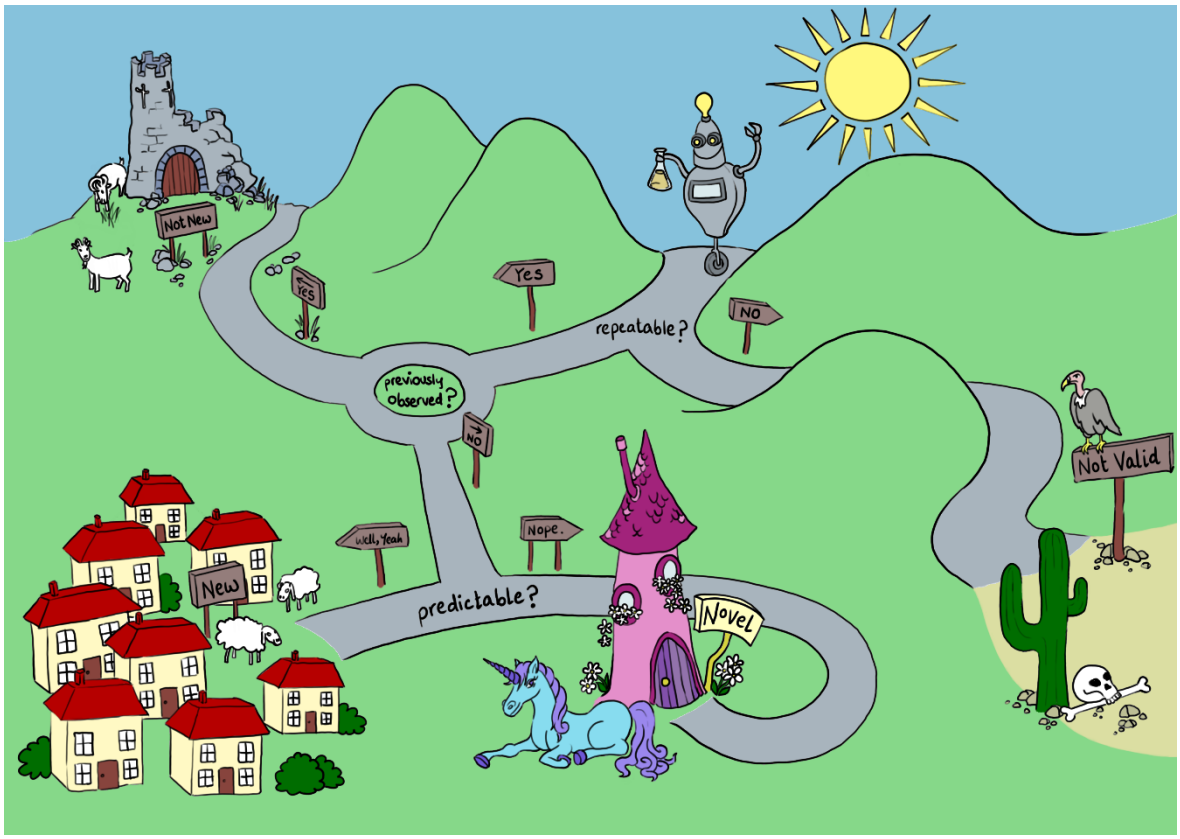

Figure 9 A cartoon representing how chemical-handling robots or platforms can use algorithms to search "chemical space" for novel, unpredictable structures.

1.1.6 Counterions

As polyoxometalates are almost always anionic, structures and solutions contain cations to balance the charge, these counterions can range from *hard* to *soft* species; that is alkali metals (Na^+, K^+) to organic compounds (generally amine derivatives either protonated or simply as their quaternary salts) and can play an important structural role or even influence what species within a POM solution crystallise out.[79–83]

Sometimes the effect counterions have on the formation of structures is used to direct the assembly of new POMs. Depending on whether triethanolammonium ($TEAH^+$) or dimethylammonium ($DMAH^+$) is used for example, a reaction may yield a peanut-shaped Dawson $(TEAH)_6[H_2W_{18}O_{57}(SO_3)]$ or a *Trojan Horse* type cage $(DMAH)_8[W_{18}O_{56}(SO_3)_2(H_2O)_2]$.[84] Other uses of $TEAH^+$, or *inorganic crown ether* as an encapsulating organic cation resulted in the formation of a *celtic ring* shaped cluster or a family of isopolyoxotungstate, Dawson-like cages.[85,86]

In addition to directing cluster formation, cations are also known to influence the supramolecular micro-structures that POM species self-assemble into, such as microtubes,[87–90] membrane-like architectures,[91–94] colloidal structures[95] and even "iCHELLS" (inorganic chemical "cells").[96]

1.2 Polyoxometalate Hybrids

As outlined in the previous section, the cations of a polyoxometalate have a big influence on the assembly and properties of the resulting system. Sometimes these counterions are more complex organic molecules than the commonly used amine derivatives (such as TBA^+, $DMAH^+$ etc.) and in these cases, the system is referred to as an *organic-inorganic POM hybrid*. In fact, any POM system containing any significant associated organic molecules whether or not they behave as counterions falls under the POM hybrid category and more specifically, a *Type 1* POM hybrid.[97,98] Type 1 organic-inorganic POM hybrids make interesting compounds as they bring together the high charge, unique architectures and multiple stable redox states of the inorganic clusters with the already well-developed range of structural and electronic properties of organic molecules. Examples of such compounds include a helical coordination polymer formed from an Al-Anderson POM cluster and a copper (II) complex fragment,[99] the single-molecular magnet (SMM) behaviour displayed by a complex formed of Al- or I-Anderson POMs and $\{CuTbL_{schiff}\}$ ligands[100] and the photocatalytic network formed of Ag-containing ligands, hydrogen bonded to Strandberg-type clusters (**Figure 10**).[101]

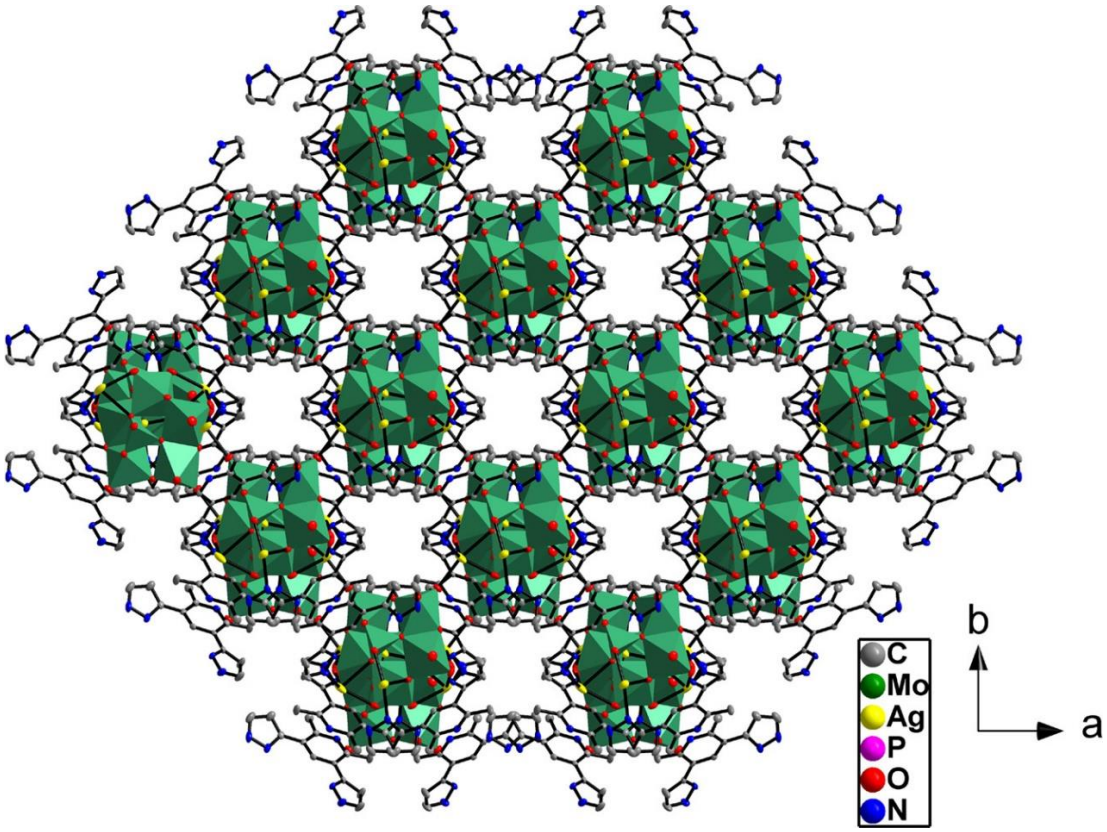

Figure 10 An example of a Type 1 organic-inorganic polyoxometalate hybrid where the organic (silver complex) and inorganic (Strandberg POM) are connected through supramolecular interactions forming a 3D network. Reproduced with permission.[101]

However, these Type 1 compounds have their downside due to the limitation posed by the nature of the bonding between the organic and inorganic parts of the system, where the intermolecular interactions will only remain intact in the solid phase. This is the factor that puts the *Type 2* organic-inorganic POM hybrids at an advantage over Type 1 hybrids. A Type 2 hybrid has an organic component covalently linked to an inorganic polyoxometalate core, via either a terminal oxygen atom (or a substitute for this ligand) or via a secondary heteroatom. With a covalent association instead of a supramolecular one, these hybrids share the same interesting features as the Type 1's but with the added stability and control that discrete molecules bring. Not only does the cluster-ligand arrangement remain intact in solution, but grafting these compounds onto a surface or incorporation of them into another system becomes possible. These options are what make Type 2 hybrids stand out from the "classical" purely inorganic polyoxometalate aspect of the field since POM chemistry contains a high level of unpredictability due to the limited understanding of their self-assembly. On the other hand, when working with Type 2 POM hybrids it is possible to accurately and reliably design synthetic procedures, giving the chemist a level of control over architectural design, which is not possible with the pure inorganic clusters (**Figure 11**).

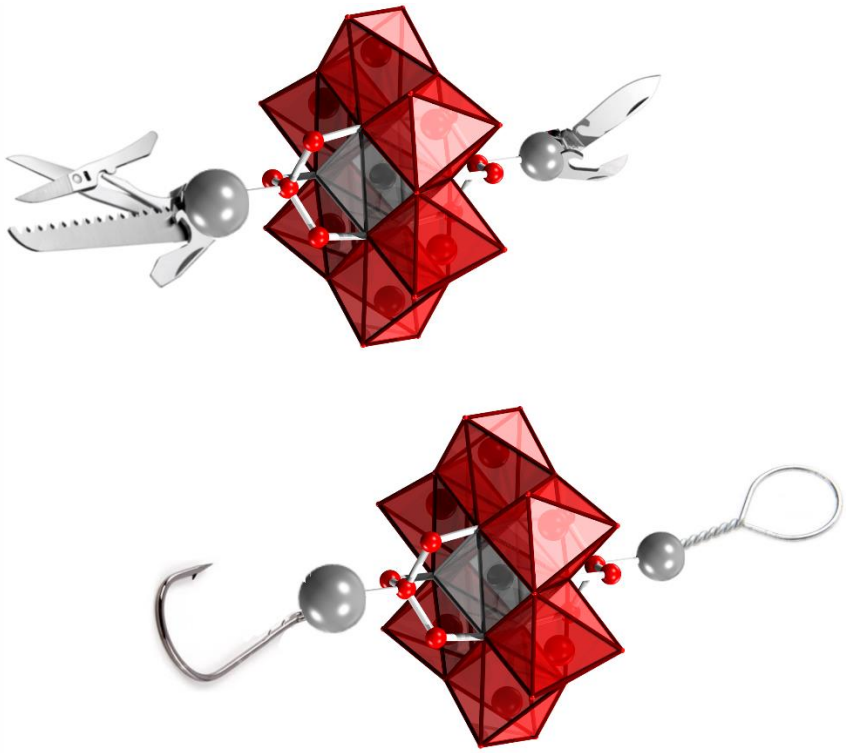

Figure 11 A cartoon representation of a Type 1 organic-inorganic polyoxometalate hybrid; an Anderson cluster core with metal tools symbolising the covalently connected organic ligands. This imagery reflects the versatility and synthetic control available to Type 1 POM hybrids.

As the work outlined in this thesis does not involve any Type 1 organic-inorganic polyoxometalate hybrids, for simplicity the term "POM hybrid" will be used as an abbreviation for "Type 2 organic-inorganic polyoxometalate hybrid".

1.2.1 Structure and Synthesis

As previously described POM hybrids can be covalently linked to organic moieties via either a terminal oxo ligand or a secondary heteroatom. Most POM hybrids have a central inorganic core with the geometry of an archetype polyoxometalate such as an Anderson-Evans or a Wells-Dawson, some of which have more than one linking mechanism available to them. In other cases, the POM core is only stable in conjunction with the organic counterpart (**Figure 12**).[102]

POM hybrids can be made via one-pot or stepwise synthesis, where the hybrid assembles directly from all the starting materials or the ligands are added (together or sequentially) to a pre-formed POM cluster, respectively. Modification of the POM hybrid moieties can be separated into two categories: pre-functionalisation and post-functionalisation. *Pre-functionalisation* refers to any ligand adjustments made to the moieties before they are

grafted to the POM core whereas *post-functionalisation* are the modifications made to the ligands once the POM hybrid is complete.

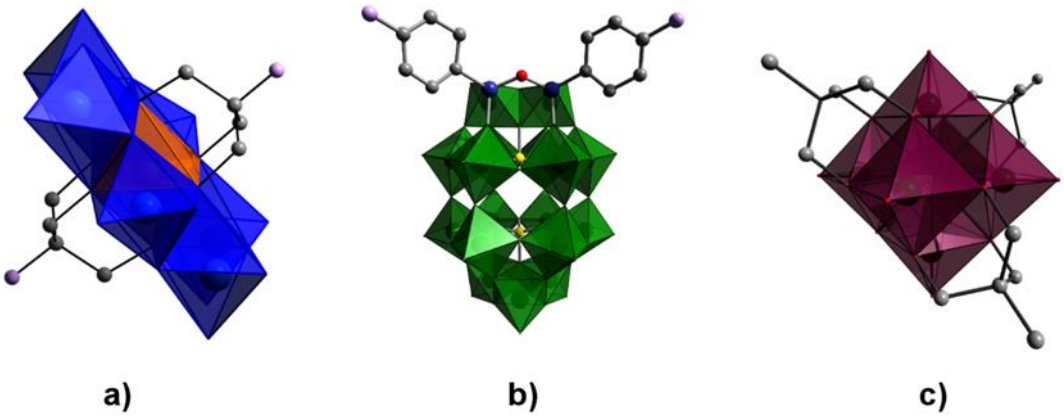

Figure 12 Polyoxometalate hybrids are typically represented using polyhedral for the inorganic core and ball-and-stick for the ligands. Common structures include (a) TRIS Mn-Anderson,[103] (b) organo-silyl hybridised Wells-Dawson[104] and (c) the {V_6} Lindqvist cluster stabilised by the surrounding TRIS ligands.[105]

1.2.2 Organic Ligands

The organic moieties can also vary from simple organic structures to recognisable biomolecules. The triol group, tris(hydroxymethyl) and its derivatives are the most frequently recurring organic POM hybrid moieties (**Figure 13**). With its three hydroxyl groups, it is able to connect to a POM core via three of its adjacent terminal oxo groups leaving one free functional group, which is often a methyl, hydroxyl or amine group. The most versatile tris(hydroxymethyl) group is the tris(hydroxymethyl)aminomethane (TRIS base or simply TRIS) because of the ease with which the nitrogen can be converted into other groups, such as amides, imines and amines. Since its initial use as a POM hybrid ligand in 1983,[106] it and its derivatives have become the most commonly used linker for Lindqvist, Wells-Dawson and Anderson-Evans hybrids.

In some instances it is possible to fully utilise the merging of an inorganic metal cluster with an organic compound by using a moiety that allows for electronic interaction to pass between POM core and ligand. Hasenknopf et al. successfully achieved this by connecting a ligand to a metal cluster via unsaturated bonds such that the inorganic and organic parts are directly conjugated. This alternative to the TRIS linker, 2-acetamido-2-ethyl-1,3-propanediol, uses a carboxyl oxygen as a substitute for one of the three hydroxyl groups and has been successfully grafted to a Dawson cluster.[107,108] The resulting conjugation

effect is not necessarily seen for all carbonyl-containing TRIS derivatives, as seen with the linker used to functionalise an Anderson by the Wei group.[109]

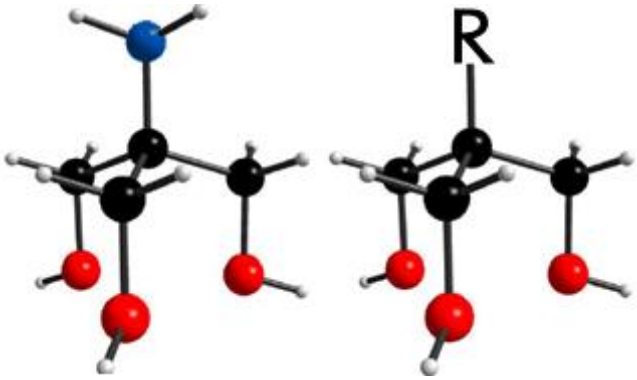

Figure 13 The tris(hydroxymethyl) moiety (right) is frequently used to hybridise POMs, the most common derivative being tris(hydroxymethyl)aminomethane (TRIS) (left).

1.2.3 Click Chemistry for POM Hybrids

Unlike pure POM clusters themselves, organic-inorganic POM hybrids have the potential to be functionalised. This post-functionalisation has the major limitation of organic reaction compatibility with POM cores which are rarely stable at low or very high pH, may decompose in the presence of redox active reagents, can undergo cation exchange with positively charged species and often have limited solubility in organic solvents. This highly restrictive compatibility is an issue which is also encountered in the field of biochemistry where it is often necessary to modify parts of a complex biomolecule without resulting in the decomposition of the entire system. Nwe and Brechbiel address this issue by outlining a series of *Click reactions* suitable for biomolecular chemistry, many of which have characteristics suitable for use in POM hybrid modification.[110] The concept of Click chemistry was developed by Barry Sharpless and describes a set of reactions which resemble processes observed in biology and focuses on carbon-heteroatom bond rather than carbon-carbon bonds. To be included in the Click chemistry category, a reaction must meet a tough set of criteria: it must be modular, wide in scope, high yielding, stereospecific, simple to purify and be achievable in mild reaction conditions, with inoffensive or no by-products and readily available starting materials.[111] Common examples of Click reactions include Diels-Alder, nucleophilic substitutions, non-aldol carbonyl chemistry and the most popular, the azide-alkyne cycloaddition which is often referred to as *the* “Click” reaction.[112]

1.2.4 Post-functionalisation of POM Hybrids

The following examples show what sorts of reactions are suitable for organic post-functionalisation of POM hybrids.

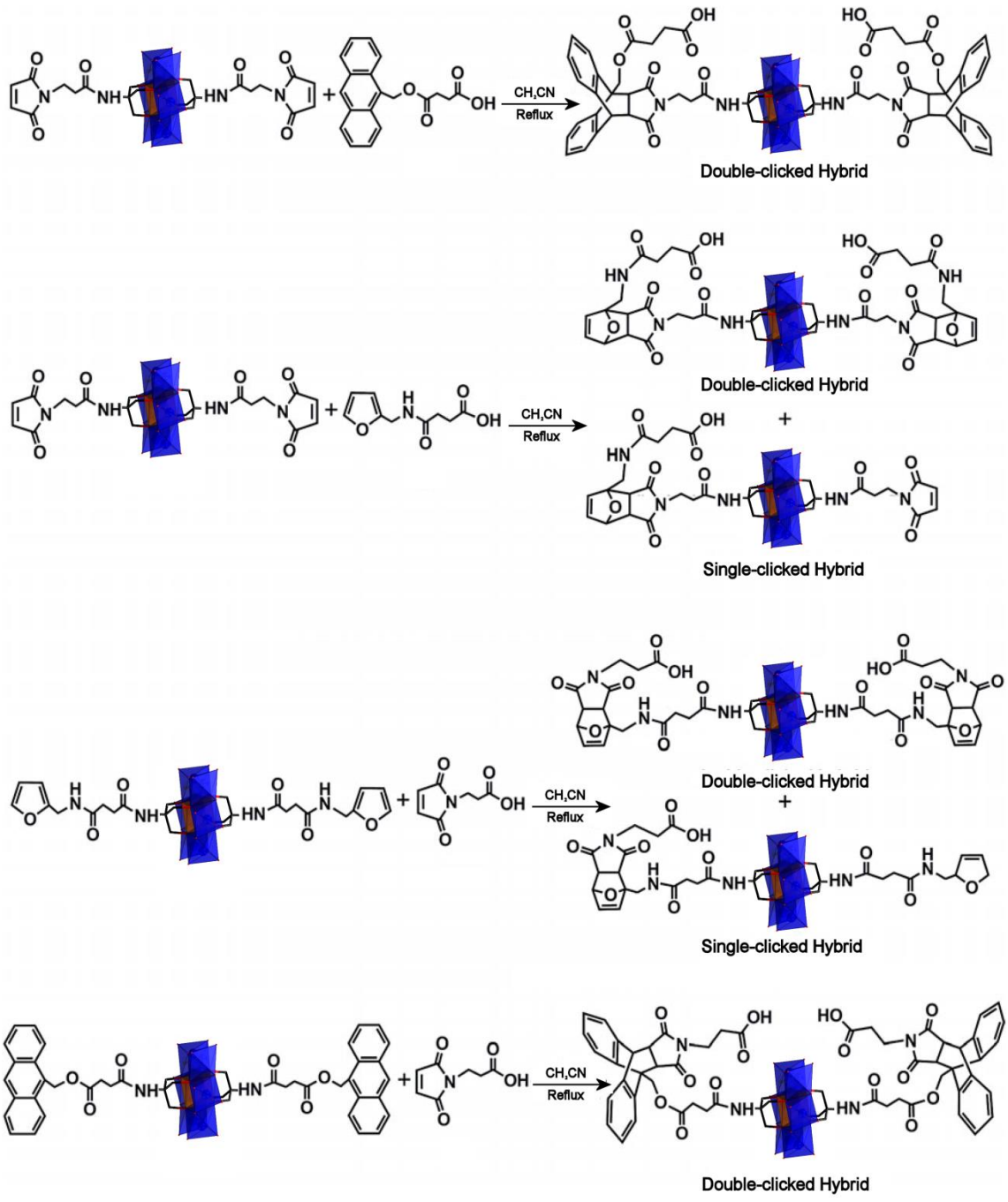

Figure 14 Reaction schemes showing the double and single-clicked hybrids formed from the various Diels-Alder reagent combinations. From top to bottom, the pairs are: maleimide Mn-Anderson and anthracene carboxylic acid, maleimide Mn-Anderson and furan carboxylic acid, furan Mn-Anderson and maleimide carboxylic acid and anthracene Mn-Anderson and maleimide carboxylic acid. Reproduced with permission.[113]

A series of furan and maleimide substitution Diels-Alder reactions were carried out on Mn-Anderson hybrids (for more on this structure, see section 1.3.9) in a two-step post-

functionalisation.[114] To start with, furan, maleimide and anthracene functionalised Mn-Anderson hybrids were synthesised by refluxing their respective carboxylic acid derivates with a TRIS Mn-Anderson cluster and 2-ethoxy-1-ethoxycarbonyl-1,2-dihydroquinoline (EEDQ) in MeCN for 24 hours. The three resulting aromatic Mn-Anderson hybrids were further functionalised with the appropriate diene or dienophile by means of a metal-free Diels–Alder Click reaction, resulting in a series of Mn-Anderson hybrids with complex organic ligands (**Figure 14**).[113]

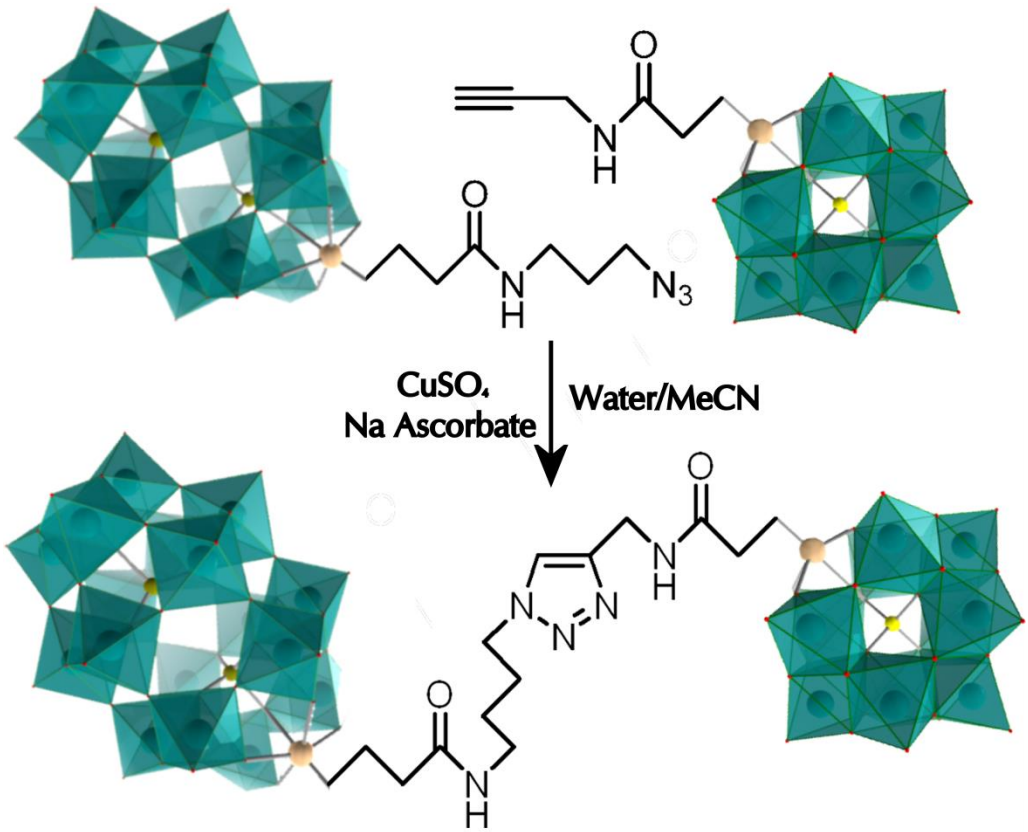

Figure 15 Reaction scheme showing the CuAAC coupling of an alkyne-functionalised Sn-Keggin and an azide-functionalised Sn-Dawson hybrid, forming a 1,2,3-triazole linked dimer. Reproduced with permission.[115]

The first example of a copper-catalysed azide-alkyne cycloaddition was used to connect a Dawson and a Keggin hybrid (for more on these structures, see sections 1.3.5-1.3.7) together, resulting in a POM dimer. This cycloaddition was successfully carried out in a water-acetonitrile mix and with copper sulfate and sodium ascorbate to couple an amine-functionalised Dawson hybrid with an alkyne-functionalised Keggin hybrid (**Figure 15**). The same paper also demonstrated the possibility of using these conditions to further functionalise the POM hybrids organic moieties such as, sugars, short peptides or common organic ligands.[115]

1.3 Classical POMs and POM Hybrids

Within the field of POM research, there are a selection of structures that frequently recur due to their stability and reproducibility. These classic POMs may not only form with a variety of addenda atoms and heteroatoms, but they and their derivatives are the substructures of the majority of the larger polyoxometalates. They are also the structures from which the common polyoxometalate hybrids are derived. The following sections will give a brief overview of some of these archetype POMs with a particular focus on those that are known to form organic-inorganic hybrid structures and are relevant to the work described in later chapters.

1.3.1 Lindqvist

First reported by Swedish chemist Ingvar Fritz Lindqvist in 1950,[116] the smallest and simplest archetypical POM is a "super-octahedral" assembly made of six edge-sharing $[MO_6]$ units with six metal centres, twelve bridging oxo ligands and six terminal oxo ligands (**Figure 3**). The Lindqvist is an isopolyoxometalate with the general formula $[M_6O_{19}]^{n-}$ and can be synthesised with addenda of Nb,[117,118] Ta,[119] Mo[120,121] and W.[122] It is also possible to form the Lindqvist structure out of V, making $[V_6O_{19}]^{8-}$ but will decompose without the stabilisation of organic ligands, resulting in a hybrid.[102,123,124] This is also the case with the Fe-based Lindqvist structure.[125] A number of *mixed-addenda* forms have been isolated, including $[V_xW_{6-x}O_{19}]^{(2+x)-}$ (x = 1, 2)[126,127] and $[Nb_3W_3O_{19}]$,[5-128] and some have shown to display photocatalytic activity.[129]

As with any of the classic POM clusters, the Lindqvist structure can be recognised as a building block within more complex POM architectures. Examples of this include a POM-based single molecular magnet (SMM) made from a lanthanide-linked Lindqvist dimer,[130] a mixed-metal coordination polymer [131] and a cobalt-containing sandwich structure.[132]

Much of the Lindqvist POM-based work focuses on the hybridised versions of these structures.

1.3.2 Lindqvist Hybrid

The weakly basic and strongly electronegative properties of the terminal oxygen atoms make substitution of an oxo ligand and hybridisation with organic moieties possible.[133] This was first achieved in 1992 by Maata et al. who successfully replaced a terminal oxygen atom of a {Mo_6} Lindqvist with an aromatic phosphinimine using an imido substitution by stirring at 85°C for 48 hours in anhydrous pyridine.[134] This lead to a number of similar phosphinime substitutions of up to 6 {Mo_6} terminal oxygen ligands,[135–138] as well as alternatives such as isocyanates and aromatic amines.[139,140]

Almost a decade later, optimisations were made to allow for example, the reaction of $[Mo_6O_{19}][(C_4H_9)_4N]_2$ with aromatic amines to take place faster (16 hours) and under milder conditions by use of dicycohexylcarbodiimide (DCC) as a dehydrating agent (**Figure 16**).[141] This was further improved when a octomolybdate $[Mo_8O_{26}][(C_4H_9)_4N]_4$ and amine hydrochloride was shortened down to 6 hours and the amine no longer specifically required to be part of an electron-donating aromatic ring.[142,143] Adaptation of these methods for the {W_6} Lindqvist cluster proved successful only when carried out as a one-pot reaction.[55]

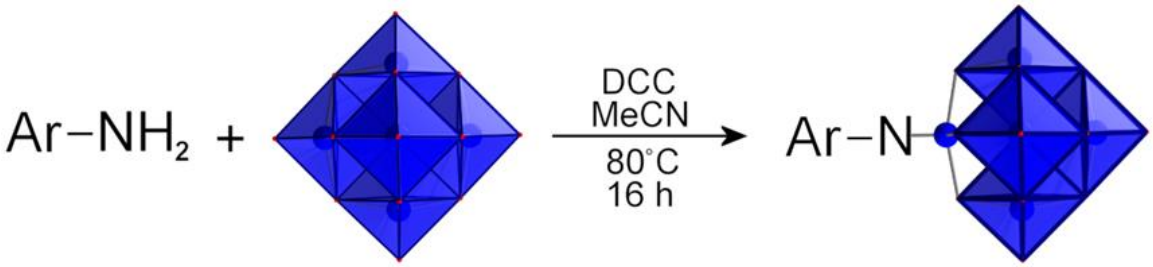

Figure 16 A reaction scheme showing the synthesis of an organoimide Mo_6O_{18} cluster using dicyclohexylcarbodiimide (DCC) as a dehydrating agent. MoO_6 polyhedra are shown in blue.

During this period, the first example of a covalently bound Type 2 POM-based donor-acceptor hybrid system was developed: an {Mo_6} cluster connected to a ferrocenyl isocyanate in pyridine (**Figure 17**).[144] This coordinate bond holds the donor and acceptor components together, allowing the system to remain intact in solution and cyclic voltammetry measurements of the compound show a clear shift from the starting materials. Another example used the DCC method to connect four {Mo_6} to a central porphyrin which not only displayed a shift in reduction and oxidation potentials but also catalytic activity.[145] To add to these hybridisation possibilities, work was done to

demonstrate a post-synthetic modification where the Sonogashira coupling was carried out on a 4-iodophenyl functionalised {Mo_6} in order to further extend the organic component.[146]

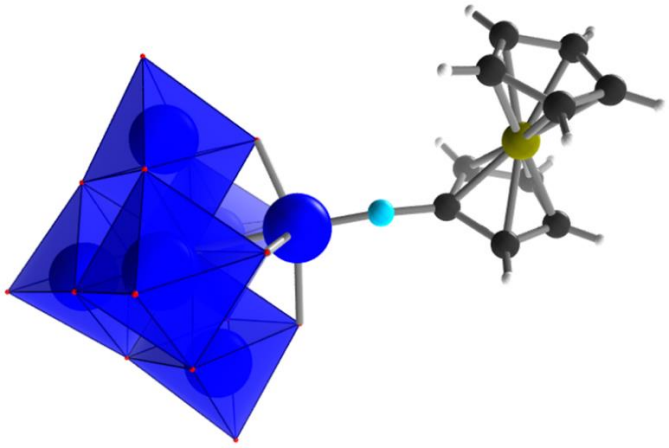

Figure 17 The crystal structure of the ferrocenylimido Lindqvist cluster $[Mo_6O_{18}(FcN]^{2-}$ with a molecular donor-acceptor system.

Although vanadium-based Lindqvist POMs show a lot of interesting redox[124] and photo-reductive properties,[147] they are only stable in their hybrid form, the first of which was a pentamethylcyclopentadienyl ruthenium functionalised {V_6} cluster isolated almost 40 years after the initial "superoctahedron" cluster was reported.[102] Tris(hydroxymethyl) groups were then found to also stabilise the {V_6} cluster, where the three hydroxyl groups of the ligand would replace adjacent terminal oxo groups of the POM and forming not only di-functionalised hybrids,[148] but also tri- and tetra-substituted clusters (**Figure 18**)[149] using hydrothermal conditions. In addition to these TRIS substitutions, the paper reported a {V_6} hybrid with a fluoride in place of the oxygen atom in the centre of the cluster, resulting in distortion to the inorganic core. Chromium and iron-centred analogues to this fluoride-substituted Lindqvist hybrid have now also been reported.[150]

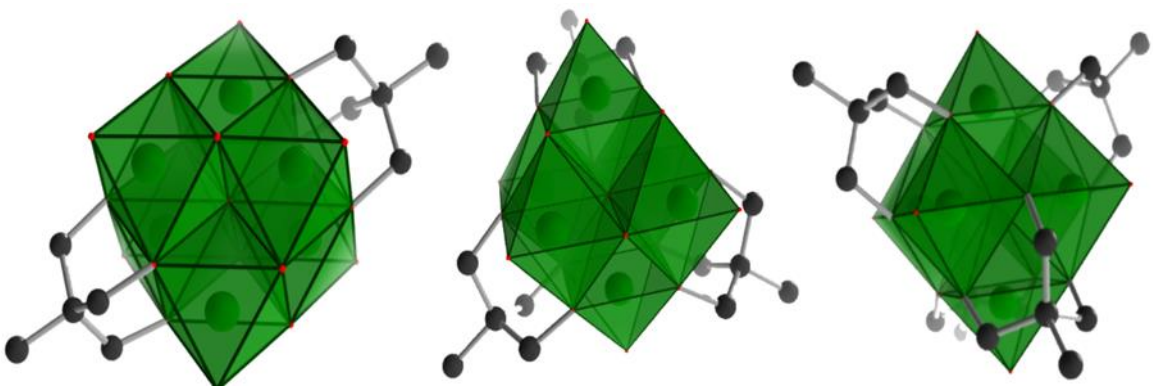

Figure 18 Crystal structures of bi-, tri- and tetra-TRIS functionalised {V_6} hybrid clustetrs.

Examples of work involving the TRIS-substituted {V_6} hybrid are, despite the cluster's apparent interesting properties and functionality, rare due to the challenging nature of the POM's synthesis which is unfortunately unreliable. Electronic communication was observed and measured between ruthenium- and zinc-centred tetraphenylporphyrin and pyridyl-functionalised Lindqvist clusters.[151] The electronic properties of a ferrocene-hybridised Lindqvist were studied and found to have minimal effect on the POM cluster and an explanation was given with the help of DFT calculations.[152] The amphiphilic properties of a hexavalent Lindqvist hybrid were used to act as an "emulsion catalyst" in deep desulfurisation reactions.[153]

1.3.3 Octamolybdate

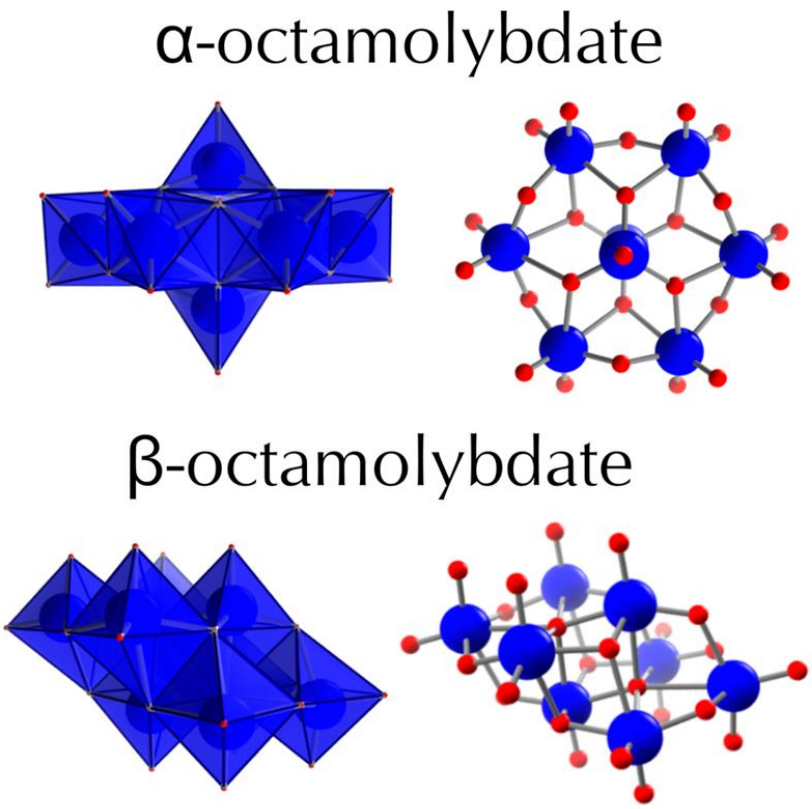

Figure 19 The two most common isomers of {Mo_8}, α- and β-octamolybdate in polyhedral and ball-and-stick representations.

Octamolybdate, $[Mo_8O_{26}]^{4-}$ is an isopolymolybdate known to form a number of structural isomers (α, β, γ, δ, ε, ζ, η and θ),[154–157] the most common of which are the α and β (**Figure 19**). The α-isomer has an approximate D_{3d} symmetry consisting of a ring of edge-sharing [MoO_6] octahedra capped by two [MoO_4] tetrahedra and the β-isomer is a parallelepiped structure consisting of two planes each composed of four [MoO_6] octahedra each sharing a central oxygen that also binds to a metal centre on the other plane. These two isomers

can be selectively precipitated from solutions, using large cations to isolate the α-octamolybdate and small cations for the β-octamolybdate.

Both of these isomers can be used as starting material for the Anderson-Evans-type hybrid (discussed in later sections) despite their structural differences and MS studies have shown their fragmentation during synthesis to be similar.[56] Before this was established, Anderson hybrids were made purely from the α-octamolybdate as the [MoO_6] ring of the α-isomer resembles the Anderson core.[103]

1.3.4 Strandberg

In 1973, Rolf Strandberg isolated and solved the structure of $Na_6Mo_5P_2O_{23}(H_2O)_{13}$.[158] This thereafter named *Strandberg* POM, $Mo_5X_2O_{23}^{6-}$ consists of a ring of five [MoO^{6-}] octahedral subunits, all edge sharing except for one corner, and is capped at both ends with tetrahedral [XO^{4-}] subunits (where X is a heteroatom) via three bridging oxo ligands (**Figure 20**). The resulting structure has a twofold rotational axis of symmetry and the twelve protruding oxygen atoms give the clusters a ball shape. Most of the time, the polyanions are linked together via counterions forming a crystal structure and balancing the charge and compared to other commonly studied POMs, the Strandberg is smaller in size and has a higher charge density.[101]

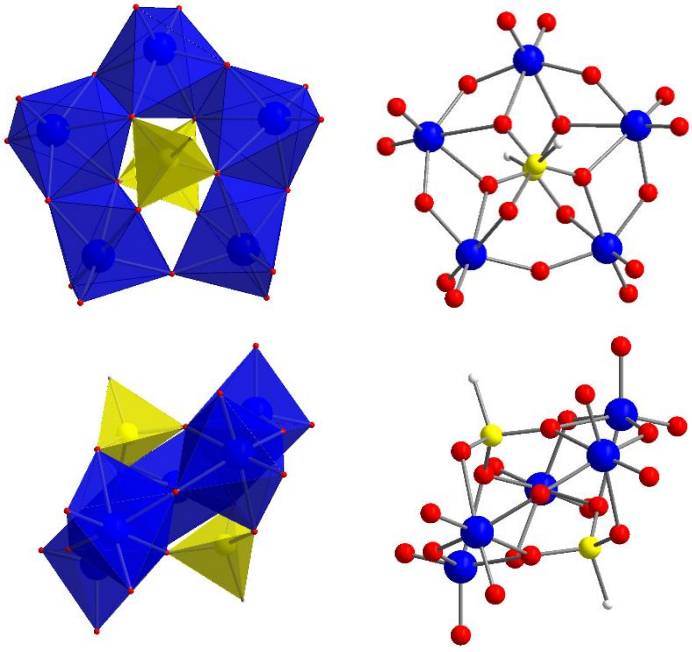

Figure 20 Polyhedral (left) and ball-and-stick (right) representation of the Standberg structure $Mo_5P_2O_{23}^{6-}$ from face (top) and side (bottom) views. Colours: blue – molybdenum, red – oxygen, yellow – phosphorus.

Typically, the two heteroatom units [XO^{4-}] are phosphorus atoms, but other atoms such as sulfur[159] and selenium[160] are also possible. The location of these two heteroatoms provides a straightforward method for hybridisation as organic ligands can covalently connect to them directly. The first examples of such organic-inorganic Strandberg hybrids were reported only a couple of years after the POM cluster itself was originally found, isolating a number of alkane and amine functional groups[161] which were observed using XRD not long after.[162] In addition, the cluster, its hybrid and associated molybdophosphates have been studied using a range of techniques including XRD,[163] NMR,[164] capillary zone electrophoresis[165] and density functional theory (DFT) methods.[166]

Despite the ease of formation of the hybrid, not very many structures have been built using the Strandberg-type POM, although in recent years a number of studies of various macrostructures (including helices,[101] 2D and 3D networks[167] and) of the Strandberg POM or hybrid coordinating to ions such as Co, Ni, Cu, Zn, Ag and Ca[101,168,169] have been made (**Figure 10**). Some reports have also demonstrated antiferromagnetic properties[170] and catalytic[171] or biological activity.[172] One study used chiral organic moieties to form a Strandberg hybrid resulting in a compound that stacked in solution, forming a gel network that displayed optical activity.[173] Another report demonstrated the chiral properties of the $[S_2Mo_5O_{23}]^{4-}$ POM itself by showing how the compound displayed the *Pfeiffer effect* when interacting with L- and D-arabinose.[159] The Pfeiffer effect is observed when a chiral compound interacts with one enantiomer of a racemic mixture resulting in displacement of the equilibrium.

1.3.5 Keggin

The Keggin is a heteropolyoxometalate whose simple structure and derivatives are seen frequently throughout polyoxometalate chemistry.[174] The POM is commonly composed of Mo, W or V with a p-block element heteroatom such as B, Si, Ge, P or S[175,176] although the cluster has also been documented to form entirely of Al[177], Ga[178], Fe[179] and Mn,[180] although these structures are not strictly POMs. With the formula $[XM_{12}O_{40}]^{p-}$, the Keggin's central heteroatom is surrounded by 12 metal centres and 40 oxygen atoms, 4 of which link metal centres to the heteroatom, 24 that bridge between metal centres and the 12 remaining form the terminal oxo ligands. The structure can be broken down into four $[M_3O_9]$ subunits each composed of three edge-sharing metal octahedrons. These

subunits form a cage by corner-sharing to each other and tetrahedrally coordinating to the heteroatom in the centre via an oxygen atom shared between the three metal centres of each subunit. The orientation of the $[M_3O_9]$ subunits relative to one another determines which of the five α, β,[181] γ,[182] δ,[183] or ε [184] isomers the Keggin cluster is, which decrease in stability with increased W-O-W bond strain (**Figure 21**).

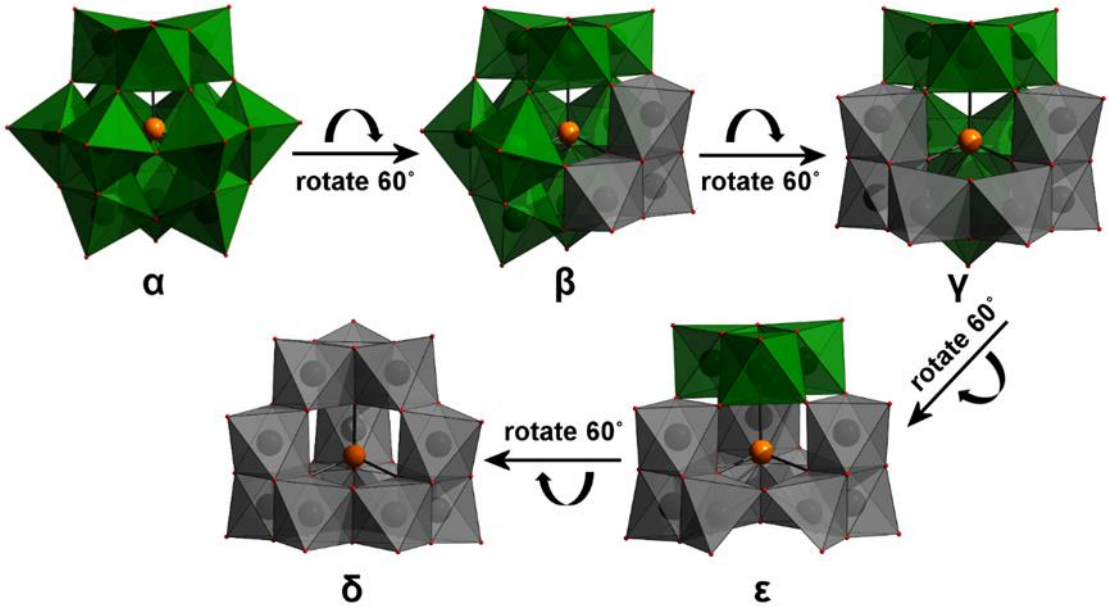

Figure 21 Polyhedral representation of how the α, β, γ, δ and ε -isomers of the Keggin structure differ by a sequential 60° rotation of the $[M_3O_9]$ subunits. Colours: O = red; X = orange; $\{M_3O_{13}\}$ triad = green; rotated $\{M_3O_{13}\}$ triad = grey.

1.3.6 Wells-Dawson

The Wells-Dawson (commonly abbreviated to "Dawson"), $[X_2M_{18}O_{62}]^{p-}$ is a structure that forms under similar conditions to the Keggin and in fact resembles a pair of fused Keggins each with a $[M_3O_9]$ triad missing, forming a *central belt* of 12 corner-sharing octahedral addenda capped by two edge sharing $[M_3O_{13}]$ units. It has two tetrahedral $[XO_4]$ heteroatomic sites where X is often Si,[185,186] P,[28,187] S,[188] or As.[187]

These 8 heteroatom bonded oxygens along with 36 bridging oxo ligands between metal centres and 18 terminal oxo ligands making a total of 62 oxygen atoms altogether.[189] The addenda environments within the Dawson are not all equivalent resulting in different properties such as the central belt's greater favourability towards reduction (**Figure 22**).[190]

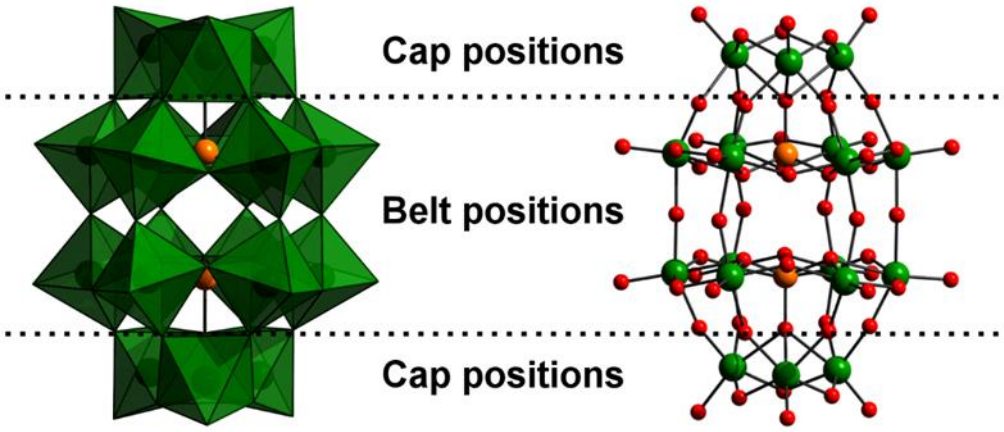

Figure 22 Polyhedral and ball-and-stick representations of the Dawson structure showing the cap and belt positions. Colours: M = green, O = red, X = orange, {MO_6} = green polyhedra.

As with many classic POM structures, the Dawson has a number of isomeric forms available to it, with six possibilities proposed by Baker and Figgis.[191] The α, β and γ isomers result from 60° rotations of the [M_3O_3] caps relative to one another and can then be converted to α*, β* and γ* isomers by 60° rotation of the half-Dawson unit [XM_9O_{36}], so pivoting at the central belt such that the tetrahedral [XO_4] stagger. As it stands, only α,[28] β,[187,192] γ[187] and γ*[193] have been synthetically isolated and this can be explained by the relative stabilities hypothesised through DFT calculations.[194] In addition to these rotational-based isomers, a number of unconventional Dawsons result from non-traditional heteroatoms with pyramidal or octahedral templates, causing deviation from the classic Dawson architecture. When the pyramidal heteroatomic template of say [AsO_3],[195,196] [BiO_3][197] and [SO_3],[198] is used for example, a Dawson-like cluster with a characteristic *peanut-shape* is formed. In contrast, octahedral heteroatomic templates such as [IO_6],[199] [SbO_6],[200] [TeO_6][201] and [WO_6][86] result in a cluster containing a single tetrahedron instead of two tetrahedral heteroatom units, such as [$H_4W_{18}O_{56}(WO_6)$]$^{6-}$. In some instances a single heteroatom may also be observed along with a vacant site for the pyramidal templates.[196]

Interesting redox properties are displayed by [IO_6] and [TeO_6] templates on reduction of Te^{VI} and I^{VII} to Te^{V} and I^{VI}. Unlike the conventional electron delocalisation over the POM surface, a trapped electron on the central heteroatom within the POM shell is observed, leading to more tuneable electronic properties.[202]

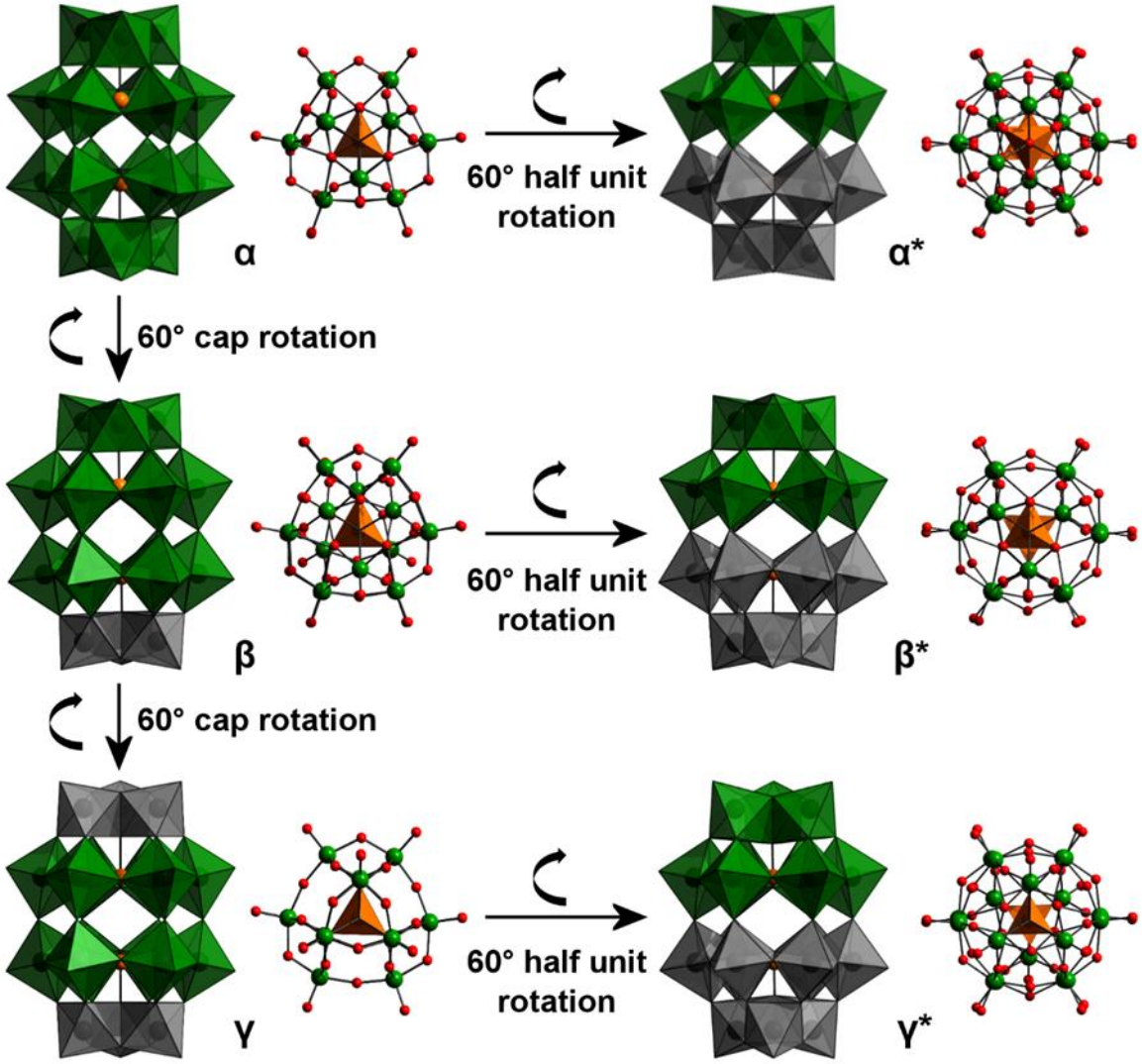

Figure 23 Diagram showing the relationship between Dawson -isomers that differ each by e sequncial 60° cap rotation and how the -isomers differ from a respective 60° half unit rotation. Polyhedral representation seen from the side and ball-and-stick representation giving a top view highlighing the eclipsed or staggered conformation of the central tetrahedral $\{XO_4\}$. Colours: O = red, M = green, X = orange, $\{M_3O_{13}\}$ triad = green polyhedra, rotated $\{M_3O_{13}\}$ triad = grey polyhedra, $\{XO_4\}$ unit = orange polyhedra.

1.3.7 Keggin and Dawson Hybrids

POM hybrids of Keggins and Dawsons are generally formed from their lacunary derivatives as the nucleophilic pockets provide an ideal reaction site for organic ligands. Positioning of the organic moiety on a Dawson may vary as the heteroatom missing may be removed from either the cap or the belt of the cluster. Most of these hybrids will be made with tungsten-based POMs as they have more stable lacunae. In order to make a molybdenum Dawson or Keggin hybrid, it is necessary for the lacunary derivatives to be formed in situ during a one-pot reaction.[203]

The monolacunary derivatives $[XW_{11}O_{39}]^{p-}$ and $[X_2W_{17}O_{61}]^{p-}$ for example, can hybridise to organic moieties containing a p-block element such as germanium, silicon or tin. This was first achieved in 1979, when Knoth reacted a series of organometal and organometalloidal halides ($RSnCl_3$, $RSiCl_3$, $RGeCl_3$, $RAsCl_2$, and $C_5H_5TiCl_3$) with the monolacunary equivalents of the Keggins ($[W_{12}SiO_{40}]^{4-}$, $[W_{12}PO_{40}]^{3-}$ and $[Mo_{12}SiO_{40}]^{4-}$ resulting in POM hybrids with one or two ligands fused to the cavity.[204] Similar work was carried out by Pope,[205] where organotin and organogermanium was monosubstituted into Dawson structures, $[P_2W_{17}O_{61}]^{10-}$ and $[As_2W_{17}O_{61}]^{10-}$ in addition to Keggins. Later, Mayer showed organosilicon could mono- and disubstitute to POMs in the same way, notably also a paper which used mass spectrometry to identify the clusters (**Figure 24**).[206]

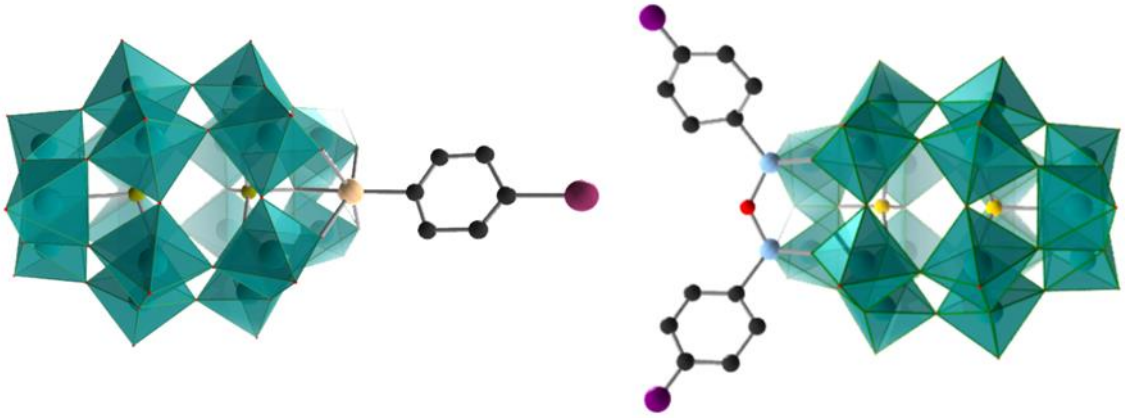

Figure 24 Crystal structure of a single-chain tin-anchored Dawson hybrid ($[P_2W_{17}O_{61}SnC_6H_4I)]$ - left) and a double-chain silicon anchored Dawson hybrid ($[P_2W_{17}O_{61}(O\{SiC_6H_4I\}_2]$ – right).

A significant amount of work was also carried out in the development of post-functionalisation techniques for the organic ligands of these POM hybrids. These methods have been much explored by the Proust group who have demonstrated the potential to further functionalise hybrids using coupling reactions to 4-iodo aryl, terminal alkyne and amino groups.[207] For example, a Sonogashira coupling was used to attach a pyrene moiety to an alkyne group of silicon-based Keggin and Dawson hybrids to give a photoactive antenna.[208] This same technique was then used in the synthesis of a heteroleptic iridium-POM hybrid designed for light harvesting[209] and electro(chemical) or peptidic couplings were used to attach a Keggin-type POM to a gold or glassy carbon surface.[210] Similarly, the Neumann group showed how a Keggin hybrid could be used to stabilise the formation of Pd-nanoparticles which were found to be effective in the catalysis of Suzuki-, Heck-, and Stille-type reactions.[211]

Biomolecular-inorganic hybrids have been produced using Dawson clusters to bind to amino acids via a tin linker. To begin with a POM hybrid was synthesised with a pendant carboxylic acid moiety to which simple amino acids could be attached in a post-functionalised coupling.[212] This hybrid was a diastereomer due to the chiral nature of both the monosubstituted Dawson isomer and the amino acid itself, where differences in their NMR measurements were observed.[213] A further study then demonstrated a method for optimisation, isolation and characterisation of a single tripeptide-Dawson hybrid enantiomer with high purity.[214]

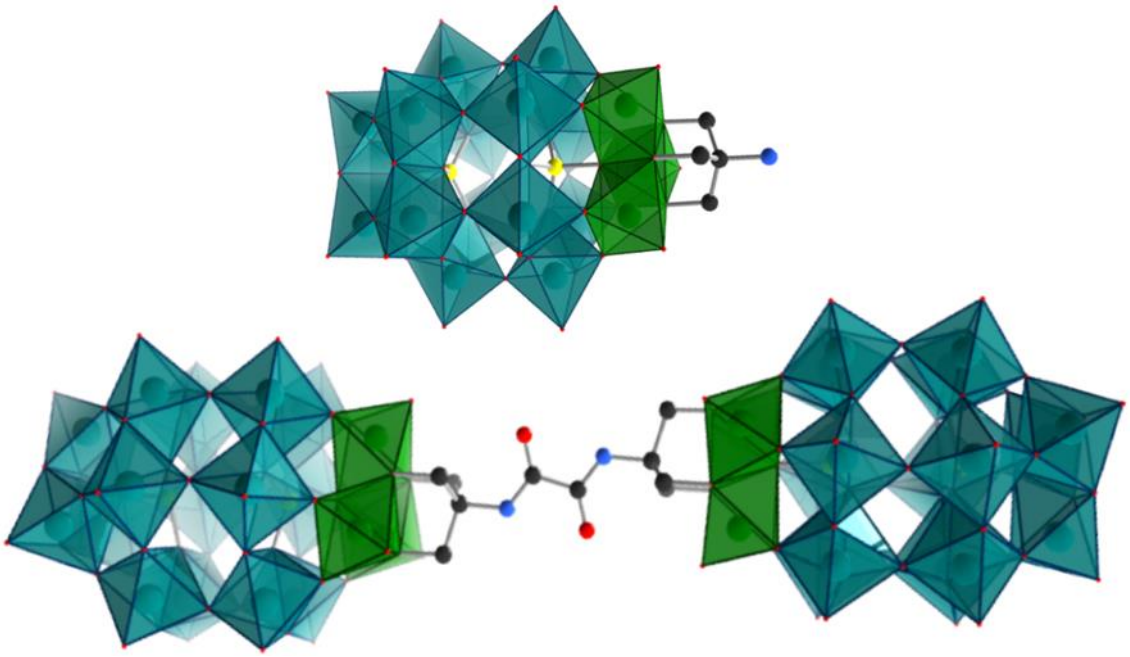

Figure 25 Crystal structure of the TRIS Dawson hybrid [$P_2W_{15}V_3$], which when linked together via a diamide linker can form a dumbbell-shaped dimer [$P_2W_{15}V_3$].

A TRIS Dawson hybrid was first achieved in 1993 and involved substituting one [W_3] cap of a tungsten Dawson with [V_3] so that the labile V-O-V bonds are able to connect to the tris(hydroxymethyl) linker (**Figure 25**).[215] Notably, the vanadium substitution results in a variety of oxidation sates being available to the cluster.[216] X-ray crystallography and cryospray mass spectrometry were used to explore the supramolecular interactions formed by the TRIS Dawson hybrid as a crystal structure and in solution.[217] Variations on the TRIS linker allowed four Dawson clusters to be linked together via a dendrimeric tris(hydroxymethyl) group (**Figure 26**)[218] and a Dawson hybrid trimer based around a TRIS-functionalised central aromatic ring to be designed.[219] The amphiphilic nature of a dumbbell-shaped dimer made of two {$P_2W_{15}V_3$} clusters were linked via a di-TRIS ligand was studied (**Figure 25**).[220] The polar heads allowed for the formation of vesicles in

water/acetone solutions, the properties of which were tuneable through altering the cations or the bridging organic connection.[221]

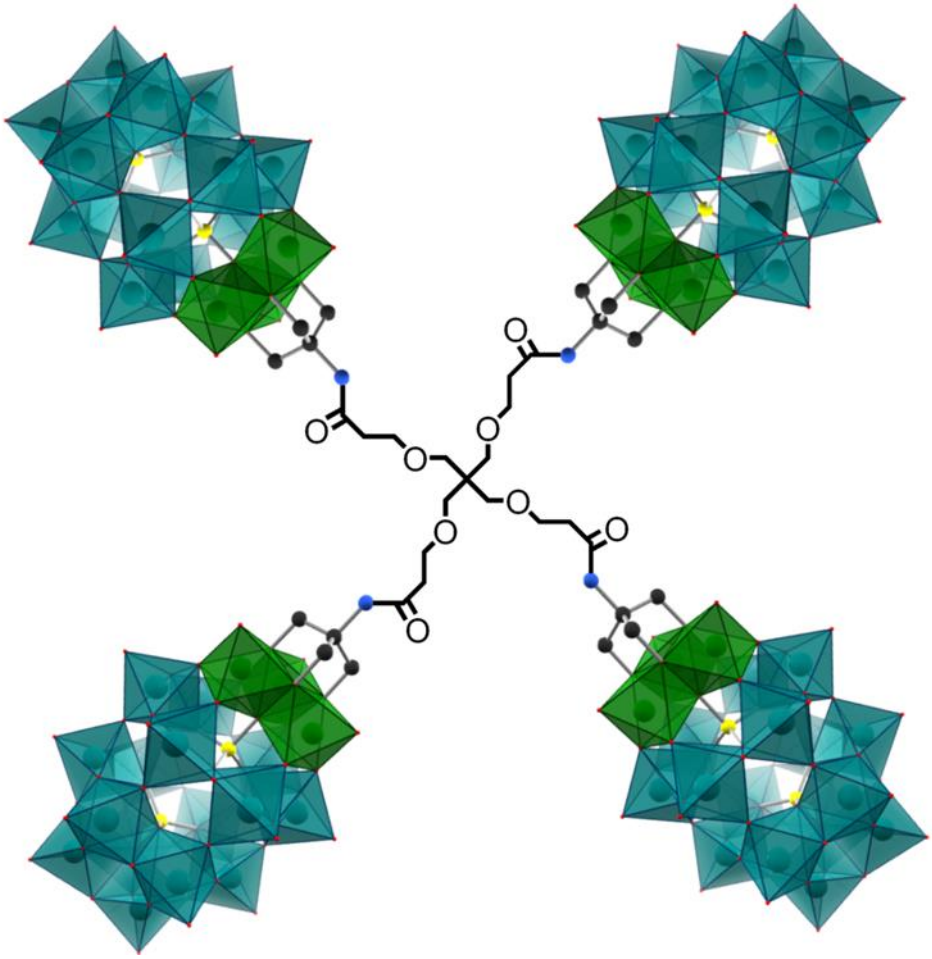

Figure 26 Representation of the dendrimer structure formed of four $P_2W_{15}V_3$ units linked via an amine-based TRIS dendrimer with a pentaerythritol core.

1.3.8 Anderson-Evans

In 1937, John Stuart Anderson predicted the structure for a molybdenum POM composed of six edge-sharing polyhedra arranged in a ring surrounding a central, octahedrally coordinated heteroatom.[29] About a decade later the described structure, specifically $K_6[TeMo_6O_{24}]$ was isolated and confirmed crystallographically by Howard T. Evans Jr. [222,223] and since then, there have been many POMs found with the same structure, summarised as $[H_y(XO_6)M_6O_{18}]^{n-}$, where y = 0–6, n = 2–8, M = Mo^{VI} or W^{VI} addenda atoms and X = central heteroatom.[52] Although the POM is named after both of these individuals, the Anderson-Evans is generally abbreviated to "Anderson" for convenience and will be referred to as such for the remainder of this thesis. Since the Anderson's initial discovery, this cluster-type has been synthesised with molybdenum addenda and to a lesser extent,

tungsten addenda and with many different central heteroatoms (in the $\{XMo_6O_{24}\}$ case, X = Cr,[224] Mn,[225] Fe,[226] Co,[227] Ni,[228] Cu,[229] Zn,[230] Ga,[231] Al,[232] Te,[222] Rh,[233] Ru,[234] Pt[235] and I[236]).

The 24 oxygens of the cluster can be separated into bridging oxo ligands, of which six are triple-bridged, six are double-bridged, and the twelve remaining are terminal oxo ligands around the edge (**Figure 27**). The Anderson can exist in a non-protonated (A-type) or protonated (B-type) form depending on the heteroatom present. High oxidation state heteroatoms, such as Te^{VI} [237] or I^{VII} [236] lead to the A-type with the general formula $[X^{n+}M_6O_{24}]^{(12-n)-}$. Conversely, heteroatoms of low oxidation state will form B-type Andersons where the six triple-bridged oxygens surrounding the heteroatom are protonated, giving a formula of $[X^{n+}(OH)_6M_6O_{18}]^{(6-n)-}$ (X = e.g.,Cr^{III} [224], Fe^{III} [238]). In 1988, a β-isomer of the Anderson structure was discovered which has been isolated with a Sb[239] and a Pt[240] metal centre and is bent, forming the shape of a butterfly.

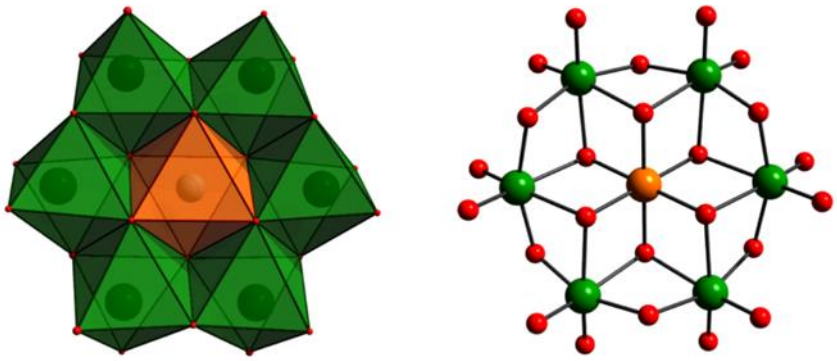

Figure 27 Polyhedral and ball-and-stick representations of the Anderson structure, of general formula $[H_yXM_6O_{24}]^{n-}$. Colours: M = green; X = orange; O = red.

The majority of the chemical and physical properties of the Anderson structure are directed by the choice of heteroatom, counter cation and hybridisation. However, most of the compounds do have a characteristic $p_\pi(O_t) \rightarrow d_{\pi^*}(Mo)$ ligand-to-metal charge-transfer transition and an absorption of ~210nm with a 240nm shoulder.[40,241–245] Additional studies have been undertaken investigating its thermal stability[40,234,244–248] and others its hydrolytic stability,[40,249,250] which are interesting for biological applications. Heteroatom-dependent properties include redox,[227,248,251–254] magnetic behaviour and luminescence.[242,255–259]

1.3.9 Anderson Hybrids

With the exception of the Type 1 hybrid structures build out from a terminal oxo ligand of the cluster,[100,260] it is the tris(hydroxymethyl) linker that is primarily used to functionalise the Anderson with the three hydroxyl groups replacing adjacent oxygen atoms on the POM's face. These TRIS groups can bind either to the three oxygens linking directly to the heteroatom or with one oxygen at the edge of the cluster instead, referred to as the δ and χ isomers, respectively[103], with the functionalisation known to occur on both faces of the Anderson as well as on a single side.

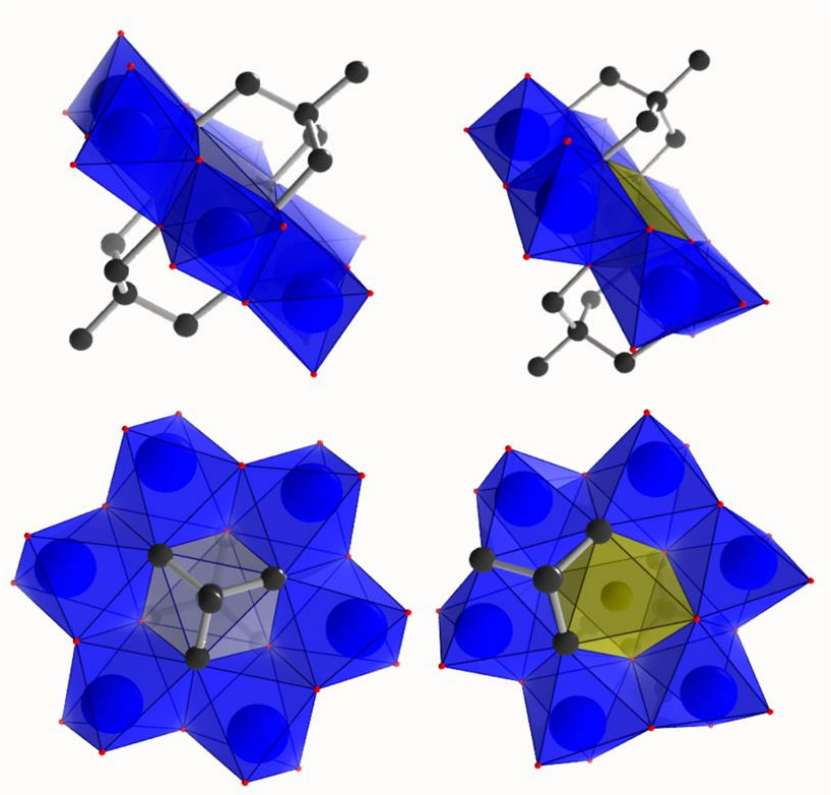

Figure 28 A side and top view of the crystal structure of the tris(hydroxymethyl)methane –capped (C_5H_9) derivatives of $[MnMo_6O_{24}]^{3-}$(left) and $[H_2ZnMo_6O_{24}]^{3-}$ (right) and showing the δ and χ isomers, respectively.

The TRIS Anderson hybrid is almost exclusively observed for the $[XMo_6]$ cluster (X = Cr, Mn, Fe, Ni, Zn, Ga and Al),[261] with one tungsten-containing exception of a single-sided $[NiW_6]$ hybrid[262] and a doubly functionalised β-isomer of the Cr-Anderson.[263] The heteroatom is what influences whether the δ-isomer forms (in the cases of Mn and Fe) or the χ-isomer (seen for Ni and Zn).[103] Some of these hybrids, such as the Mn-Anderson, are synthesised directly from the ligands and a source of molybdate (such as the octomolybdate described in section 1.3.3) in a one-pot reaction. Others, like the Cr-Anderson hybrid, are formed in a series of reactions where the ligands are added

sequentially to the pre-formed Anderson structure.[109] Interestingly, in the case of the Fe-Anderson hybrid, both the one-pot[151,264] and the stepwise methods have been shown to be effective.[40]

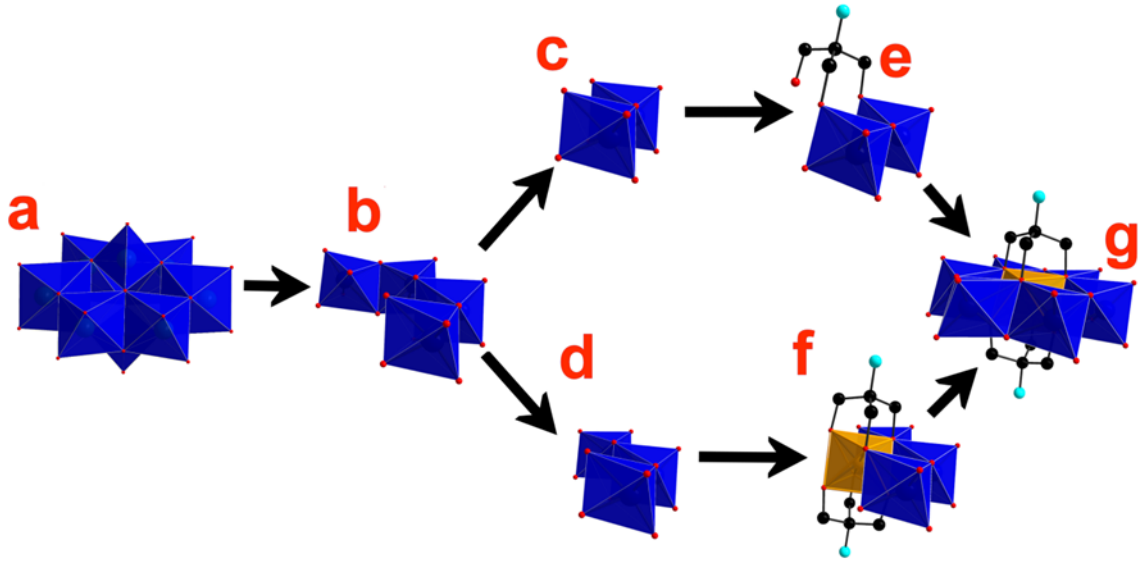

Figure 29 A scheme showing the proposed mechanisms for the build up of TRIS Mn-Anderson from the octomolybdate {Mo_8} starting material.

Cronin et al. studied TRIS functionalised Mn-Anderson hybrids using Ion-Mobility Mass Spectrometry in order to gain more information on the build-up of the compound in solution[265] and detect the two different geometric isomers formed (**Figure 29**).[266]

1.3.9.1 Mn-Anderson Hybrid Post-Functionalisation

The majority of Anderson hybrid studies use the Mn-Anderson cluster due to the reliability of its synthesis and crystallisation. In 2002, Hasenknopf and Gouzerh first synthesised a tris(hydroxymethyl)methane derivative Anderson hybrid and observed the formation of the two isomers.[103] A year later, the post-functionalisation of a TRIS Mn-Anderson was demonstrated[267] and observations were made of the chemical gel formed by the coordination of pyridyl Mn-Anderson hybrid with metal centres.[268] Further study on the coordination of pyridyl-POM hybrids with porphyrins showed reversible redox and fluorescence properties.[151] In fact, it was possible for copolymers to form between porphyrins and polyoxometalate hybrids using anodic electropolymerisation, resulting in sheets and wires. These copolymers were also shown to catalyse the photoreduction of Ag(I) (**Figure 30**).[269]

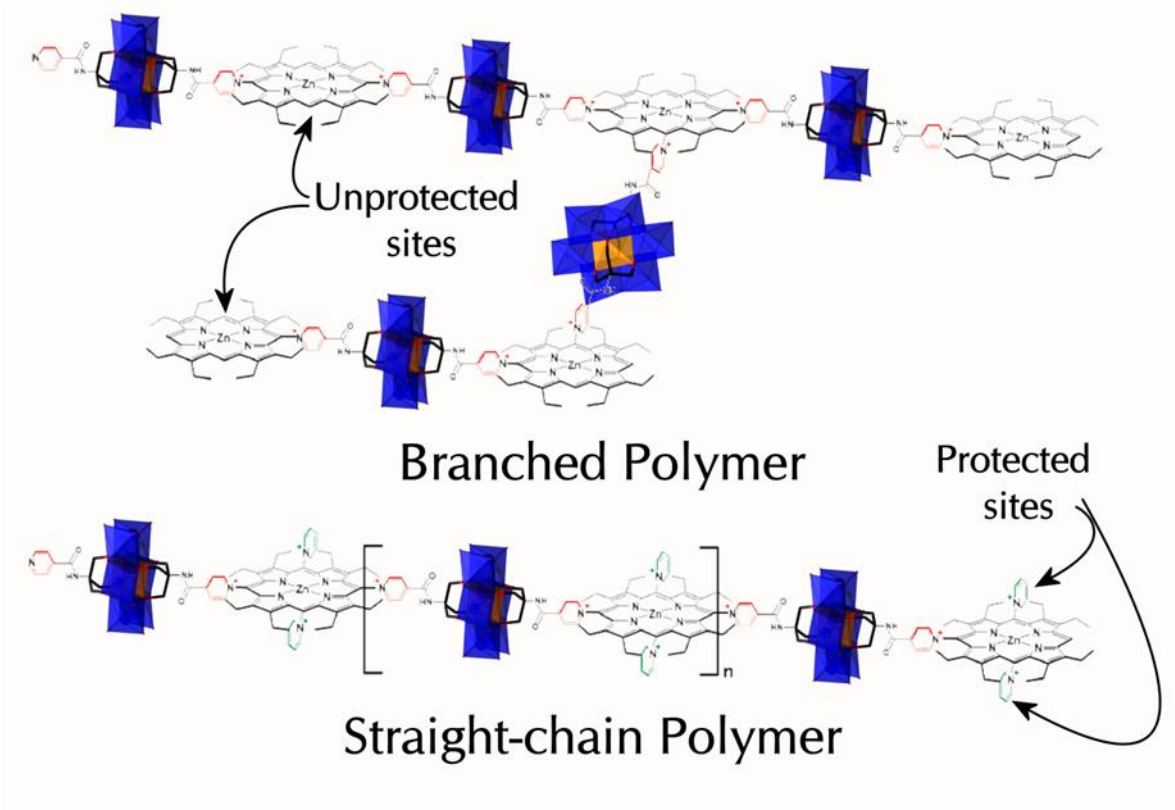

Figure 30 Diagram of the porphyrin Mn-Anderson hybrids that can polymerise to form sheets when the ZnOEP porphyrin ligands has four sites available for nucleophilic attack and wires when the porphyrin is protected at the 5 and 15 positions: 5,15-ZnOEP(py)$_2^{2+}$.

Other interesting assemblies where observed when C-6, C-16 and C-18 alkyl chains were grafted onto Mn-Anderson hybrids and the TBA^+ cations exchanged for dimethyldioctadecyl ammonium ($DMDOA^+$) cation resulting in an amphiphile from the surfactant enclosed hydrophilic POM.[270] Alkyl-functionalised Mn-Anderson hybrids were observed forming vesicles as the molecules behaved like surfactants with their polar POM heads and the hydrophobic carbon chains as tails.[271]

1.3.9.2 Asymmetric Anderson Hybrid

In 2008, the first asymmetrically functionalised Mn-Anderson hybrid was formed from a one-pot reaction giving a statistical mixture of products, 50% of which was the asymmetric where a single cluster was functionalised differently on either side (**Figure 31**).[272] This product was isolated via fractional crystallisation and then post-functionalisation could be carried out on one side of the Mn-Anderson leaving the other ligand unchanged. The following year this technique was used to bond such asymmetric POM hybrids to a patterned gold surface.[273] These asymmetric Mn-Andersons were also used in studies exploring the formation of planar, 2D and 3D nanostructure assemblies.[274,275] Scanning probe microscopy was used to explore how different cations

affect the patterning of the 2D nanostructures during Langmuir-Blodgett deposition of Mn-Anderson hybrids. The resulting nanostructures were shown to be remarkably stable under ambient conditions but self-patterning on heating as well as showing dielectric behaviour and reversible capacitive properties.[276]

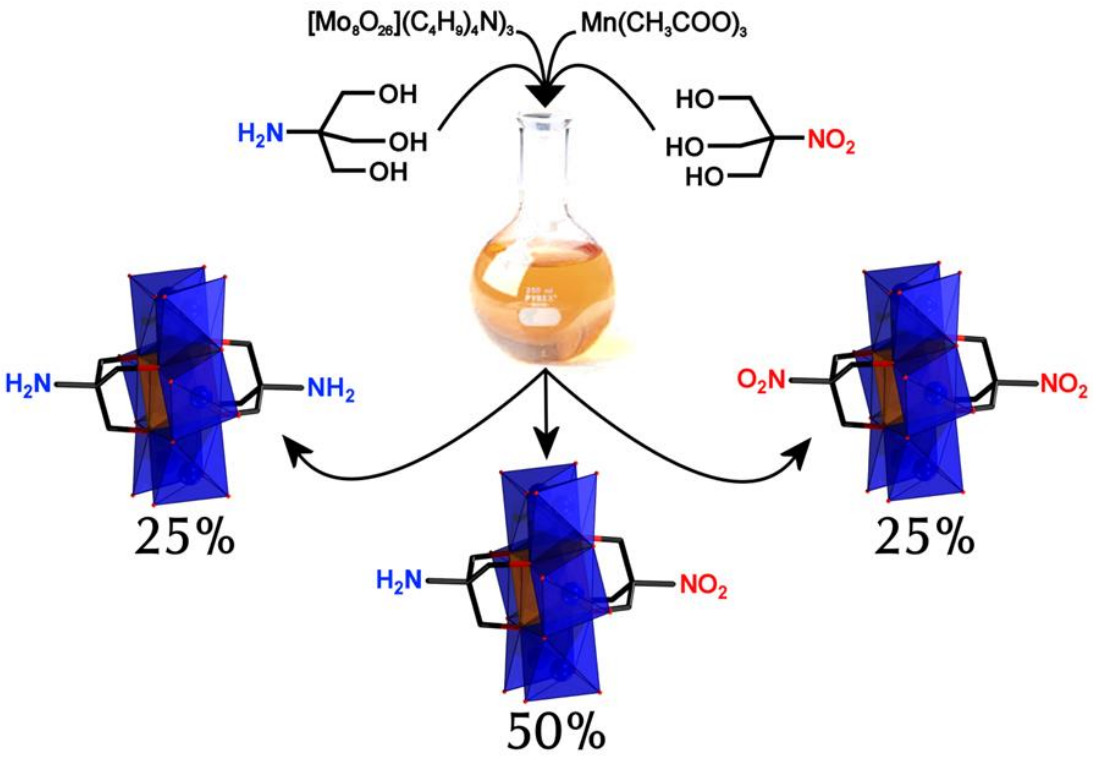

Figure 31 Diagram illustrating the synthetic procedure for the formation of an asymmetric Mn-Anderson from tris(hydroxymethyl)aminomethane and tris(hydroxymethyl)nitromethane starting materials. The symmetric Mn-Anderson products also form at statistical ratios.

The exploration of the asymmetric Mn-Anderson compounds was limited by the challenges of separation. As the synthesis involved the use of two different TRIS ligands, the resulting mixture contained symmetric and asymmetric products. These hybrids were separated using fractional crystallisation, a technique which unfortunately resulted in very low yields and purity. For small-scale studies like the ones just described, this was not an issue but for the many other potential applications an asymmetric hybrid might be used for, a method for pure product isolation on a larger scale was required. Such a technique was developed by Cronin et al. in 2013.[277] On measuring the crude mixture of an asymmetric Mn-Anderson one-pot reaction using reverse phase HPLC, it was possible to clearly separate out the three different products based on their polarity. Adapting this method to reverse phase liquid chromatography (RP-LC) allowed large batches of crude product to be reliably separated provided the two moieties had a significant difference in their polarity (**Figure 32**).

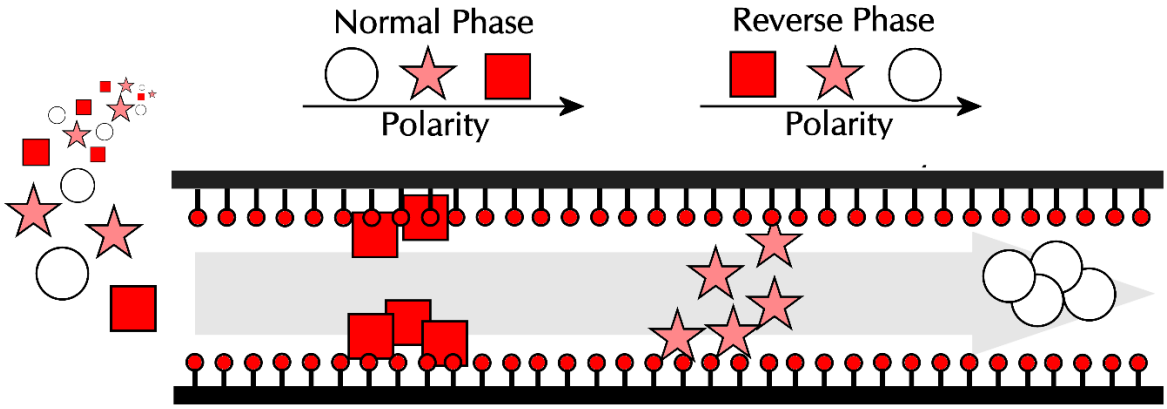

Figure 32 Cartoon illustrating the basic concept of column chromatography. Different components of a mixture pass through the column at varying rates depending on whether they have greater affinity to the stationary (red pins) or mobile (grey arrow) phase. In normal phase liquid chromatography, the stationary phase is a hydrophilic material whereas in reverse phase liquid chromatography it is hydrophobic.

In order to synthesise an asymmetric Mn-Anderson hybrid with moieties of similar polarity, an additional step involving the use of a "universal" asymmetric Mn-Anderson precursor, was added. This precursor, FMOC/TRIS Mn-Anderson hybrid, was synthesised in a one-pot reaction using the classic TRIS and an FMOC-TRIS ligand, resulting in three products: symmetric FMOC Mn-Anderson, symmetric TRIS Mn-Anderson and the desired asymmetric product itself, which was isolated using the RP-LC separation method just described. The TRIS moiety of this compound could be post-functionalised and the FMOC protecting group subsequently removed to reveal a second TRIS group available for further functionalisation, in this way allowing for a Mn-Anderson hybrid to be made containing two different ligands with similar polarity (**Figure 34**). Access to these asymmetric Mn-Anderson hybrids has opened the doors to many synthetic possibilities, including the design of sequence polymers or similar, an example of which is discussed in a later section.

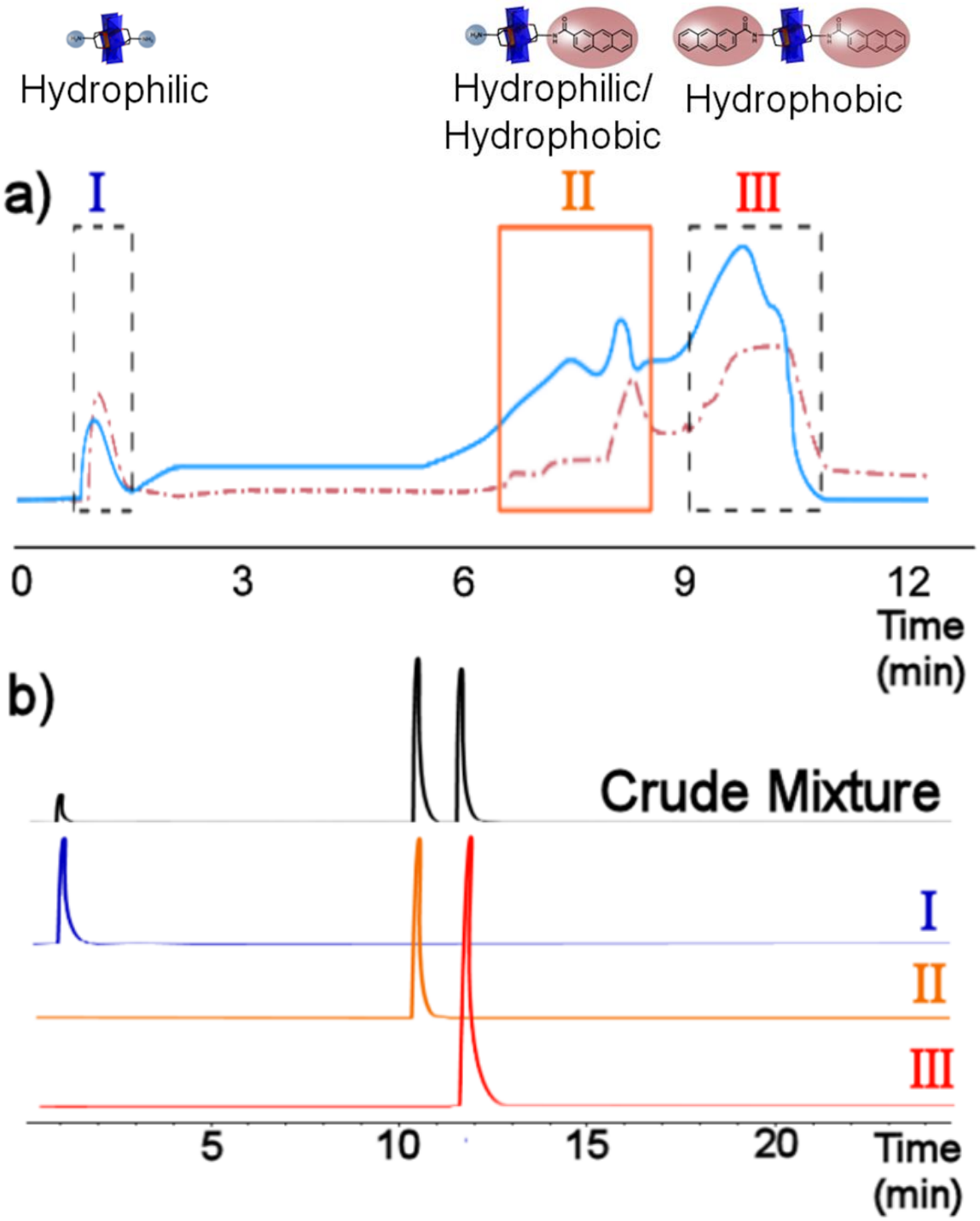

Figure 33 (a) UV and ELSD trace for the reverse phase liquid chromatography separation of TRIS/anthracene Mn-Anderson and its symmetric by-products and (b) the corresponding HPLC UV traces of pure samples and crude mixture. Hybrids with polar moieties pass through the column faster than those with hydrophobic side chains.

An alternative approach to acquiring asymmetric Anderson hybrids involves the stepwise hybridisation and has been developed for Mn-, Al- and Cr-Anderson by Wei et al.[278] To begin with the Anderson POM cluster itself is synthesised by acidification of a small molybdate species.[279] Then the POM is functionalised with an organic ligand on one side only,[280,281] which must take place in aqueous conditions as this prevents the second side from being reacting[109] and carefully pH controlled to ensure formation of the δ-isomer.[282]

Finally the second side of the hybrid can be functionalised with a different TRIS-type ligand and this time organic solvent was used to drive the reaction to completion.[278] Although this method involves three synthetic steps, it does hold an advantage of forming only a single product resulting in a higher yield and easier isolation.[283]

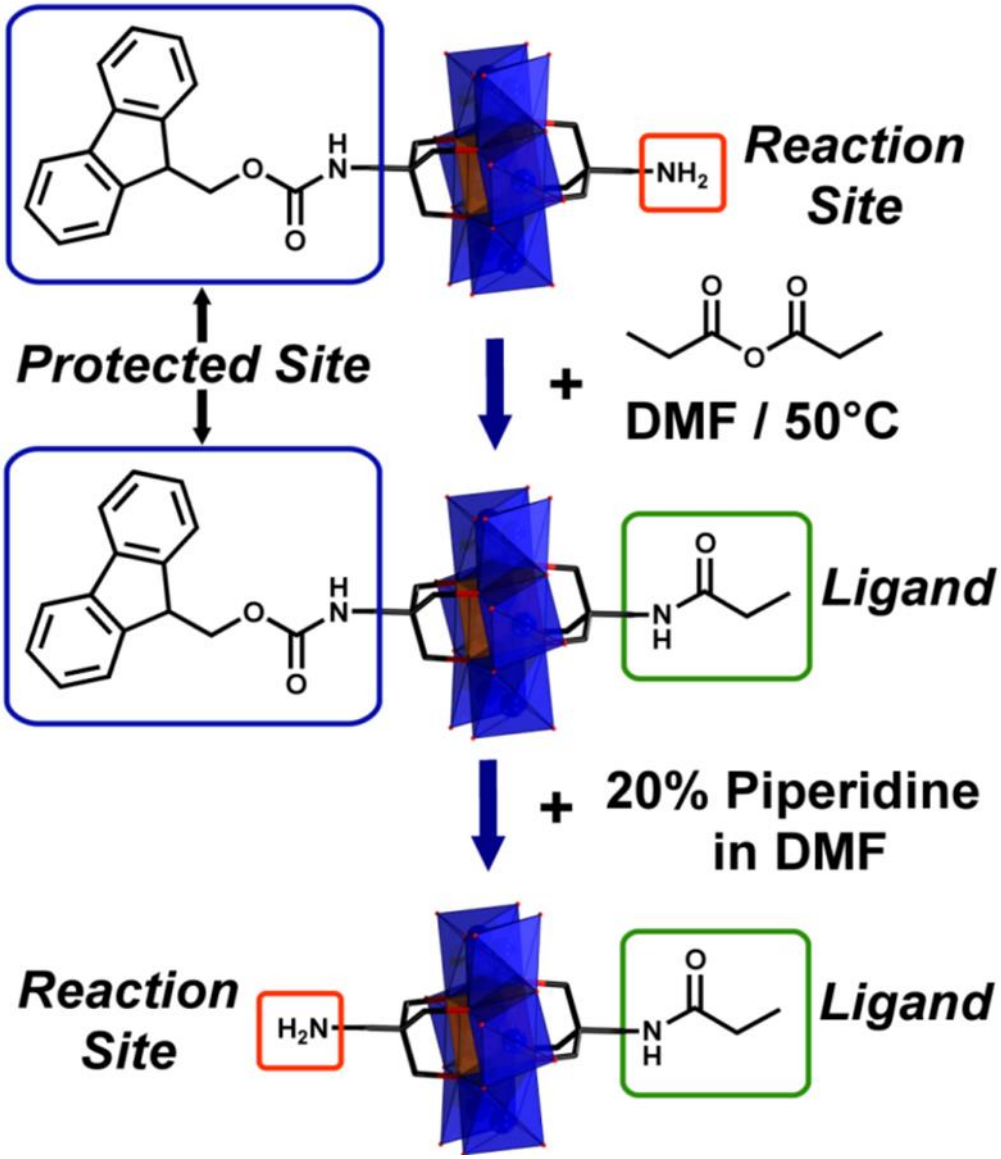

Figure 34 Reaction scheme demonstrating how the "Universal" FMOC/TRIS Mn-Anderson can be used as starting material for the synthesis of an asymmetric Mn-Anderson with moieties of similar polarity, which cannot be purified via RP-LC. Here, the unprotected site reacts with propionic anhydride then the FMOC group is removed using piperidine, leaving a second reactive site.

1.4 POM Hybrid Polymers

This section gives an overview of the ways in which polyoxometalate hybrids have been incorporated into polymer chains as a result of post-functionalisation of the clusters.

Conventional free radical-induced copolymerization was used to link styrylimido-functionalised Lindqvist hybrid monomers and 4-methylstyrene molecules together forming a polystyrene chain with the cluster as a pendent group at a ratio of 1:3.[284] In a different example, Lindqvist clusters were added to a polymer after the chain had formed. The $\{Mo_6\}$ was attached as a pendent side-chain to the free aryl amines of a rod-coil diblock copolymer (DCP) via a post-polymerisation reaction in NMP, a commonly compatible solvent.[285]

There are also examples of POM-polymer hybrids involving Dawson clusters. Norbornene-Dawson hybrid monomers were polymerised in the presence of a Grubbs catalyst and mild conditions resulting in an organic polynorborene backbone structure with pendent Dawson clusters. The polymer formed despite concern over potential steric-hindrance issues with a well-defined structure, high molecular weight and was used to form solution-processed thin films and catalyse the oxidation of a sulfide.[286]

The Dawson was also used as the terminal group of a polystyrene chain, a system which was studied at length by Wang et al.[287] The POM-polymer hybrid was synthesised using atom transfer radical polymerization (ATRP) to build up a polystyrene chain (**Figure 35**). On substitution of the TBA^+ counterions with protons, the Dawson hybrid displayed amphiphilic behaviour. The use of TEM imaging revealed how these POM-polymer hybrids formed large vesicles in DMF, an irreversible process suggesting the organic tails were protecting the POM cores.[288] In addition to this, it was also found that these vesicles would transform into tubular aggregates, which would eventually stack together in a thermodynamic process caused by annealing treatment.[289]

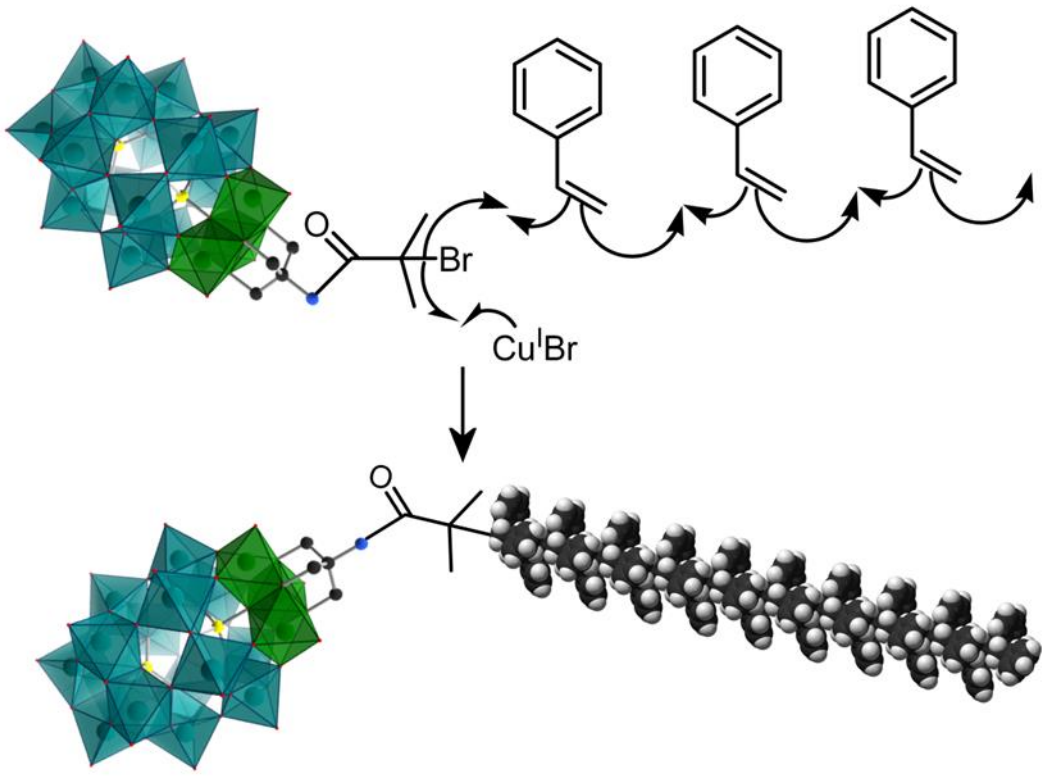

Figure 35 Scheme illustrating the build-up of a chain via atom transfer radical polymerisation (ATRP) using CuBr as a catalyst, starting from a $P_2W_{15}V_3$ bromoisbutyryl hybrid.

In contrast to all these examples, the doubly-functionalised core of the Mn-Anderson hybrid allows for the cluster to be directly incorporated into the chain rather than behave as a pendent group. Polymer chains were, for example, built up on either side of a pentaerythritol functionalised Mn-Anderson hybrid via a ring-opening polymerisation of ε-caprolactone catalysed by $Sn(Oct)_2$. The cluster within the polymer was shown to have an influence on the crystallisation of the polymer.[290] In a final example, coumarin-functionalised Mn-Anderson hybrids were used in a light-driven polymerisation. This reaction was reversible, resulting in extraction of the hybrid monomers under the right conditions.[291]

1.5 Gel Macrostructures

Having discussed what types of extended structure can be formed from POMs and their hybrids, this section next moves away from the polyoxometalate field but remains within the intermolecular, extended assembly theme by looking at macrostructures that result in gelation.

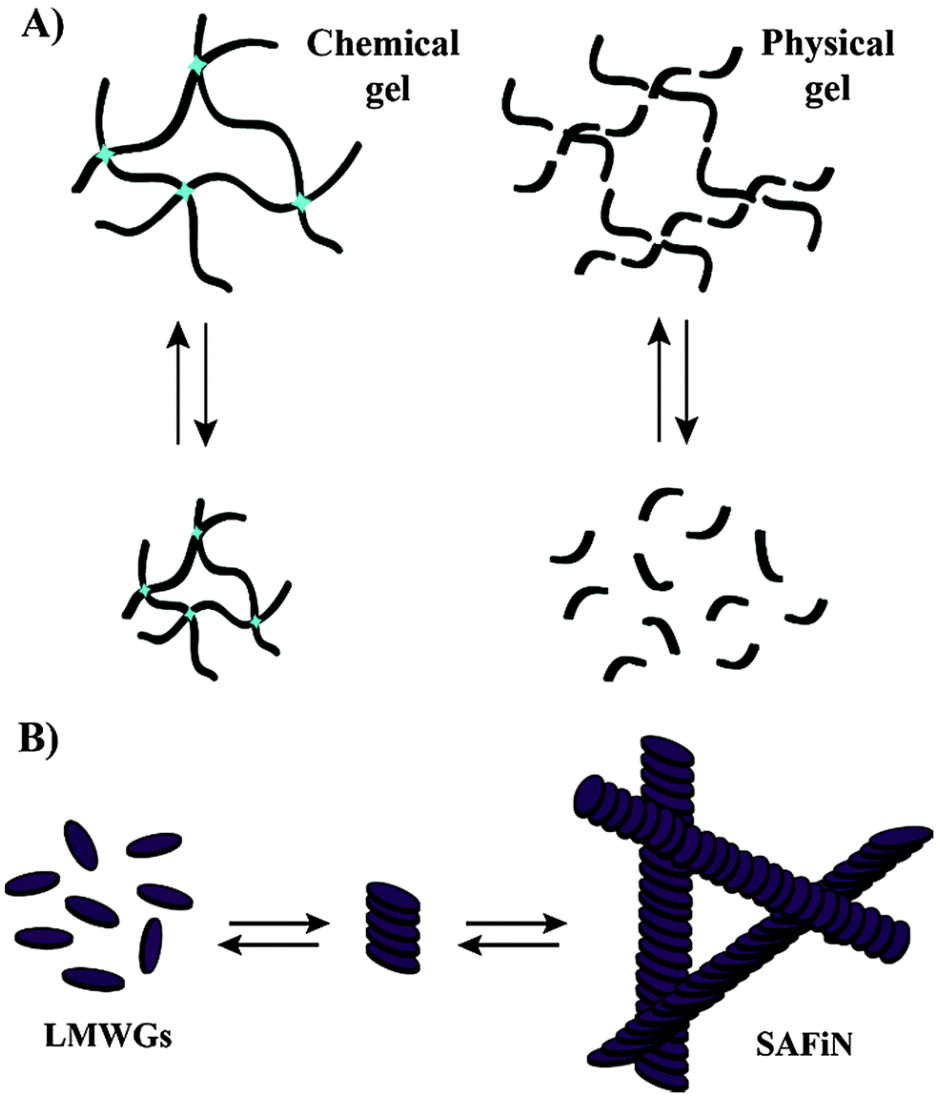

Figure 36 Diagrams explaining how A) the covalent bonds of a chemical gel make it more stable under varying conditions than a physical gel and B) low molecular weight gelators form ordered structures called self-assembled fibrillary networks. Reproduced with permission.[292]

For a material to be classed as a gel, it must meet a couple of criteria, the first of which is that the material must have an extended microstructure that remains permanent on a macroscale, long enough for an analytical measurement to be taken.[292–294] The second requirement is that despite displaying rheology that resembles a solid, a gel's structure in fact consists mostly of liquid, which when organic forms an *organogel* and when aqueous, a *hydrogel*. This liquid is referred to as the *sol* and held together via a solid network,

known as the *gel*. When this gel network is held together through covalent bonds, then a *chemical gel* is formed which has the ability to remain intact if exposed to environmental changes, such as dehydration where the gel reversibly shrinks. *Physical gels* on the other hand, are less permanent because the gel network consists of noncovalent interactions such as Van der Waals forces, hydrogen bonds and Coulombic interactions (**Figure 36a**). If the crosslinking of a physical gel is made up of compounds with a molecular weight of 3000 Da or less, then it is known as a *low molecular weight gelator* (LMWG) and will generally be formed from an ordered packing structure: a *self-assembled fibrillary network* (SAFiN) (**Figure 36b**).[295] The ordered, yet non-permanent nature of the supramolecular interactions found in LMWGs makes them particularly interesting and has a number different of applications. Although LMWGs can be made from a wide variety of compounds, the majority are formed from natural products and in particular, nucleotides, nucleosides and nucleic acids due to their ability to H-bond and π-stack. Gels of nucleobase analogues are interesting because of their relative robustness and versatility when it comes to application in biology which can include drug delivery, tissue engineering and diagnostics.[296–298]

1.5.1 Nucleobases

Nucleosides, nucleotides and nucleic acids are compounds that all have a nitrogen-containing heterocycle known as a *nucleobase* of which there are two types the *purines* and the *pyrimidines*. The purines have a bicyclic structure resulting in potential for hydrogen bonding to occur from several sides whereas the pyrimidines are formed of a single ring with only one edge available for hydrogen bonding.[299]

Nucleosides are molecules made from a nucleobase connected to a D-ribose via a glycosidic bond and become *nucleotides* when this ribose is (mono-, di- or tri-) phosphorylated. Combining sugar and phosphate elements to nucleobases give these compounds additional supramolecular structure and function (**Figure 37**). This can be seen with the 5'-nucleotide building blocks that assemble to form the *nucleic acids*: DNA and RNA structures which will be discussed further in section 1.6.1.[300]

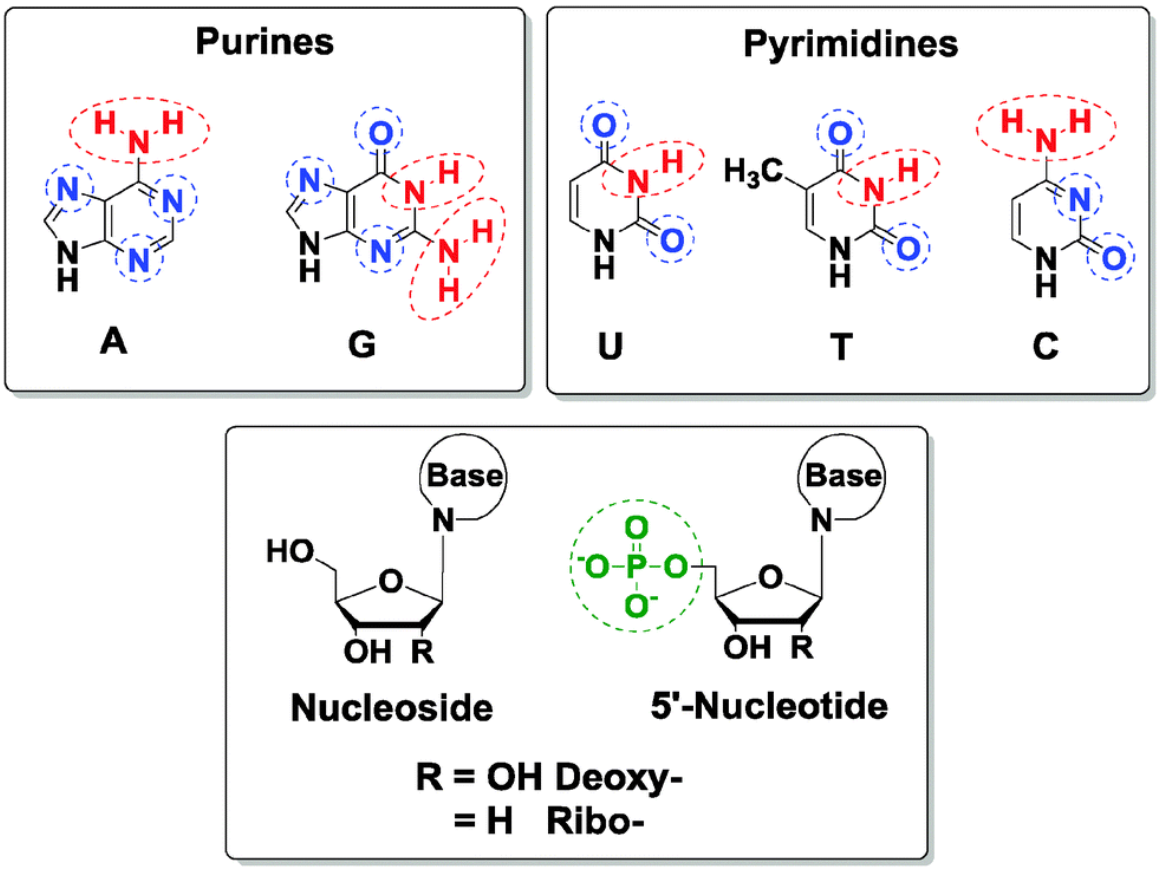

Figure 37 Diagram showing the two categories of nucleobase: purines (adenine A and guanine G) and pyrimidines (uracil U, thymine T, and cytosine C) that connect via a glycosidic bond to D-ribose forming a nucleoside and a nucleotide on phosphorylation. Reproduced with permission.[292]

There are 28 possible ways in which pairs of the common nucleobases can interact and in the case of the purines with their additional hydrogen bonding donors and acceptors, the intermolecular interaction can extend out to more than one other molecule.[301] Some of the possible intermolecular interactions are shown in **Figure 38**, including the Watson-Crick base pairing well known for its role within deoxyribonucleic acid (DNA).

Of course, due to their hydrogen bonding and π-stacking potential, nucleobases are also able to interact with themselves, often self-assembling into extended structures and gels. This is most notably the case for the guanine ring and its derivatives where the structures formed exist within biological systems.[302,303] Gels formed from other nucleobases will not generally occur unless derivatised with hydrophobic functional groups; guanosine along with its derivatives is the only nucleobase that does not require derivatisation in order for gelation to occur.[304] This is due to its tendency to assemble into G-ribbons, G4-quartets and G-quadruplexes.

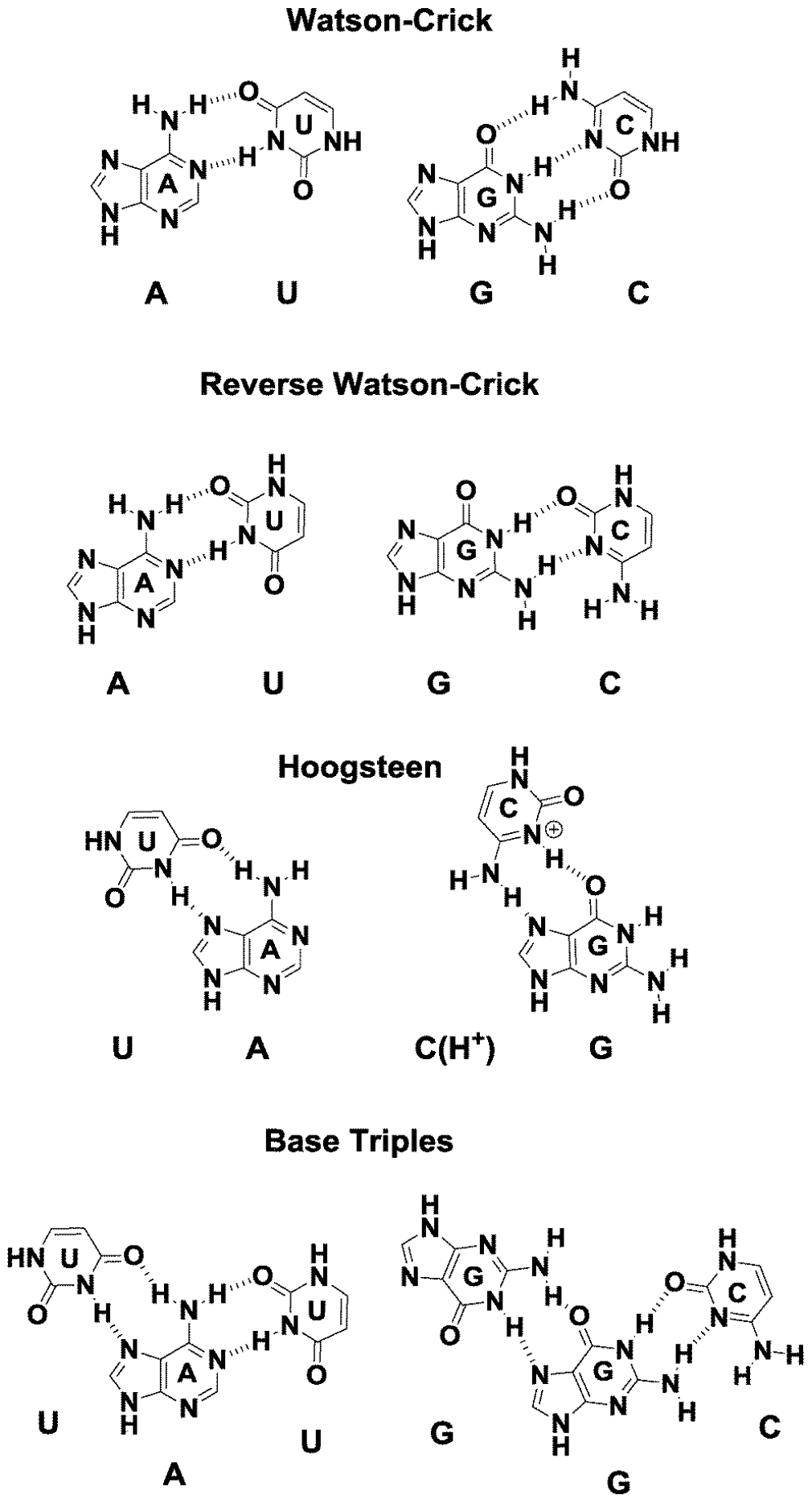

Figure 38 Four examples of binding motifs available to hydrogen bonding interactions between nucleobases: Watson-Crick, Reverse Watson-Crick, Hoogsteen and Base Triples. Reproduced with permission.[292]

1.5.2 Guanosine

In order for guanosine-based gels to form from organic solvents, derivatisation of the guanosine is necessary which can be done with relative ease as the ribose ring is readily functionalisable.[292] The most commonly known structures formed by guanosine derivatives are the G-ribbons, G4-quartets, G-quadruplexes and G-wires, shown in **Figure 39**. The G-ribbons are formed from the hydrogen donors and acceptors interacting to make strands of guanosine. The G4-quartets on the other hand, are hydrogen bonded planar tetramers and generally (though not always[305]) have to be stabilised with a central coordinating metal cation. The G-quadruplexes and G-wires are formed from stacks of these G4-quartets. In addition, it has been observed that G-rich nucleic acid sequences aggregate to form interesting structures.[306]

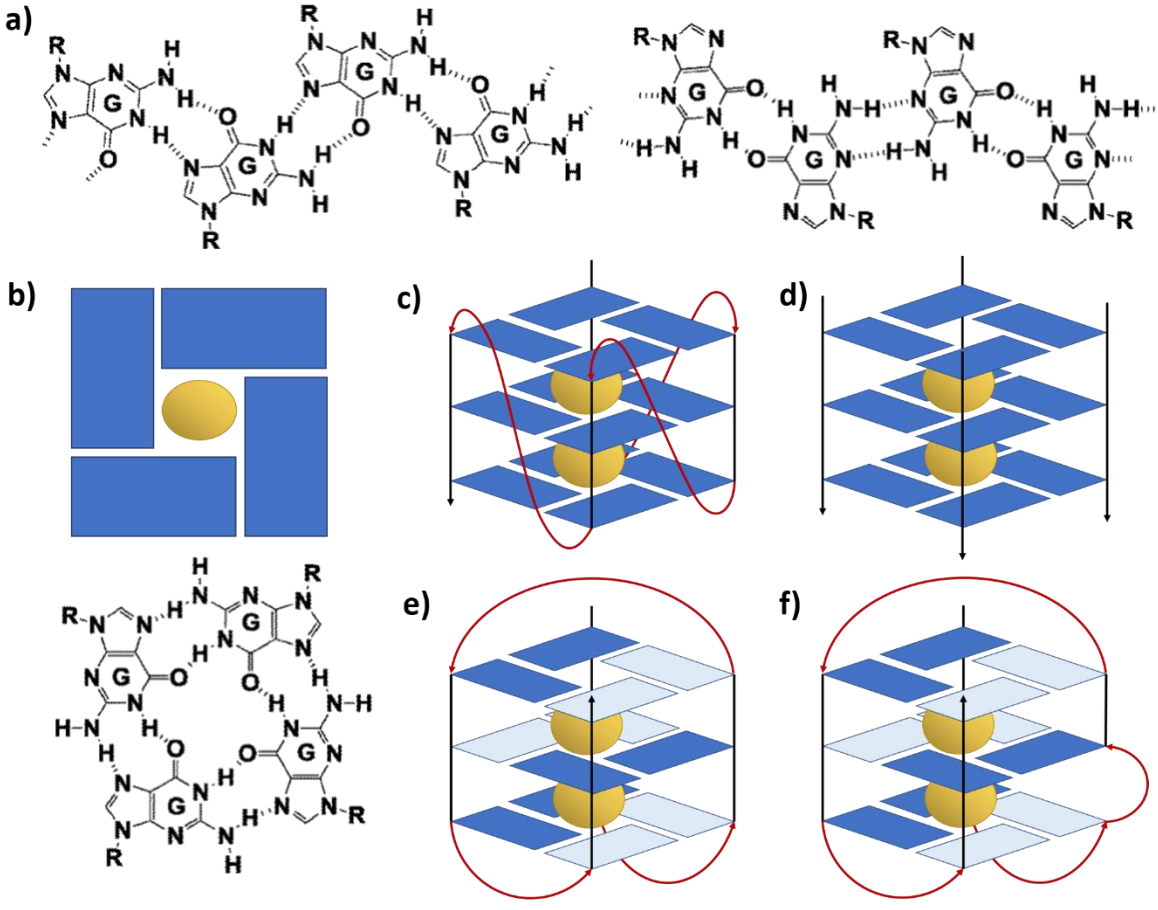

Figure 39 Diagrams of the hydrogen bonding interactions between guanine bases that lead to the formation of a) two types of G-ribbons and b) G4-quartets which stack into G-quadruplexes which are found in c) unimolecular parallel, d) tetramolecular parallel, e) unimolecular antiparallel or f) unimolecular bulged arrangements.

Guanosine-based hydrogels were first reported in 1910 by Ivar Bang[307] and more closely examined by Levene and Jacobs, two years later.[308] However it was not until 1962 that

Gellert, Lipsett, and Davies began to determine the structures of guanosine monophosphate through diffraction experiments of dried gels[309] and since then exploration of guanosine derivative gels has greatly expanded, due to their interesting range of potential applications in bio- and nano-technology. This potential is not exclusively due to their interesting structures such as columns (G-wires) and thin films (nanoribbons),[306,310] but also the compatibility and stability in biological systems,[311] their reversible and controllable tuneablilty,[302,309] the chiral selectivity[312,313] and separation potential.[314,315] Studies on guanosine-based hydrogels use techniques such as visual detection, bulk physical measurements, absorption and circular dichroism spectroscopies, X-ray diffraction, light scattering, neutron scattering, and NMR for a comprehensive analysis.[316–323]

1.6 Configurable Biomolecules

Section 1.4 gave some examples of POM hybrids that had been incorporated into polymer chains in a variety of ways including pre- and post-functionalisation methods. It was seen how in a number of these cases, the POM-polymer hybrids would self-assemble through intermolecular interactions forming nanostructures such as vesicles or nanotubes. Section 1.5 continued with the theme of supramolecular assembly by discussing the gel structures formed by nucleobases with a particular focus on guanine derivatives, molecules that play a key role in biological processes. This section will discuss the way molecules such as guanine, make up complex *information-containing* polymers seen in living systems, namely nucleic acids and proteins both of which are built from a pool of monomers that influence the structure and function of the chain depending on the order and conditions in which they are assembled. The section will then go on to give some examples of biomolecule-inspired structures, including biomolecule-POM hybrids.

1.6.1 Nucleic Acids

Nucleic acids are the polymers made of nucleotide monophosphate monomers (see section 1.5.1) that are linked together through phosphodiester bridges, broken down into the following components: a nucleobase, a sugar and a phosphate group. The resulting polymer has a *sugar-phosphate* backbone with pendent nucleobases (**Figure 40**). An assembly where the sugar is ribose and the nucleobases are adenine, guanine, cytosine

and uracil is known as *ribonucleic acid* (RNA) and when the sugar is deoxyribose and thymine is used instead of uracil, the polymer is called *deoxyribonucleic acid* (DNA).[299]

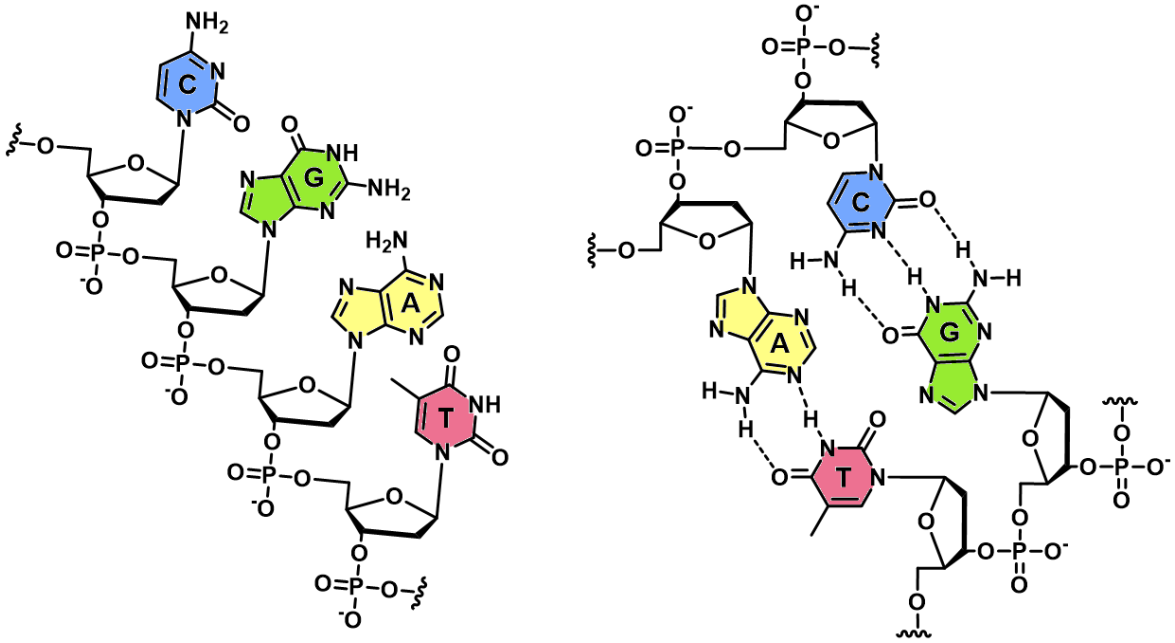

Figure 40 (a) A molecular structure of a single strand of deoxyribonucleic acid (DNA): a sugar-phosphate polymer with pendant nucleobases (C – cytosine, G – guanine, A – adenine, T – thymine). (b) A pair of DNA strands connecting via hydrogen bonds between nucleobases: CG, AT.

DNA has the primary biological function of storing the "instructional" code used by the *ribosome*, an enzymatic machinery that build proteins (see section 1.6.2), and is also the genetic information that is transferred from a living organism onto its offspring, resulting in the defects which allow evolution to occur.[324] DNA is sometimes seen as a single strand (ssDNA) but mostly as a double strand (dsDNA). Double-stranded DNA is recognised for its iconic double helix structure caused by the hydrogen bonding and π-stacking between the pendent nucleobases of opposing DNA strands. The hydrogen bonding is the interaction described in section 1.5.1 known as Watson-Crick base pairing between a purine and a pyrimidine; either adenine and thymine (AT) or guanine and cytosine (GC). The π-stacking is a result of the faces of these base pairs aligning over one another in the core of the structure around which the two sugar-phosphate backbones spiral. In order for every nucleobase to have a matching Watson-Crick pair, it is necessary for the two strands of dsDNA to be *complementary* to one another, and this feature is essential for the replication mechanism used by the genetic code. The DNA double helix is a relatively stable structure (in water) not only due to these intermolecular forces between the rigid nucleobase rings, but also because all the hydrophobic elements are at the core of the

structure, shielded from the aqueous environment by the outer polar sugar-phosphate backbone.

Environmental conditions, deoxyribose conformation and the exact nucleobase makeup can impact the dimensions of the DNA double helix, resulting in the A-DNA, B-DNA and Z-DNA structures (**Figure 41**). All three structures consist of two *antiparallel* chains coiled around the Watson-Crick paired bases, the A- and B-type DNA however, is right-handed whereas Z-DNA coils in a left-handed direction. A-DNA is the widest and shortest type with slightly tilted base pairs and is characteristic of dehydrated DNA and B-DNA has base-pairs perpendicular to the axis and is favoured in hydrated environments. Z-DNA is named after the *zigzagging* of the sugar-phosphate backbone; it is the narrowest form of DNA and is favoured by guanine-cytosine-rich sequences.[325]

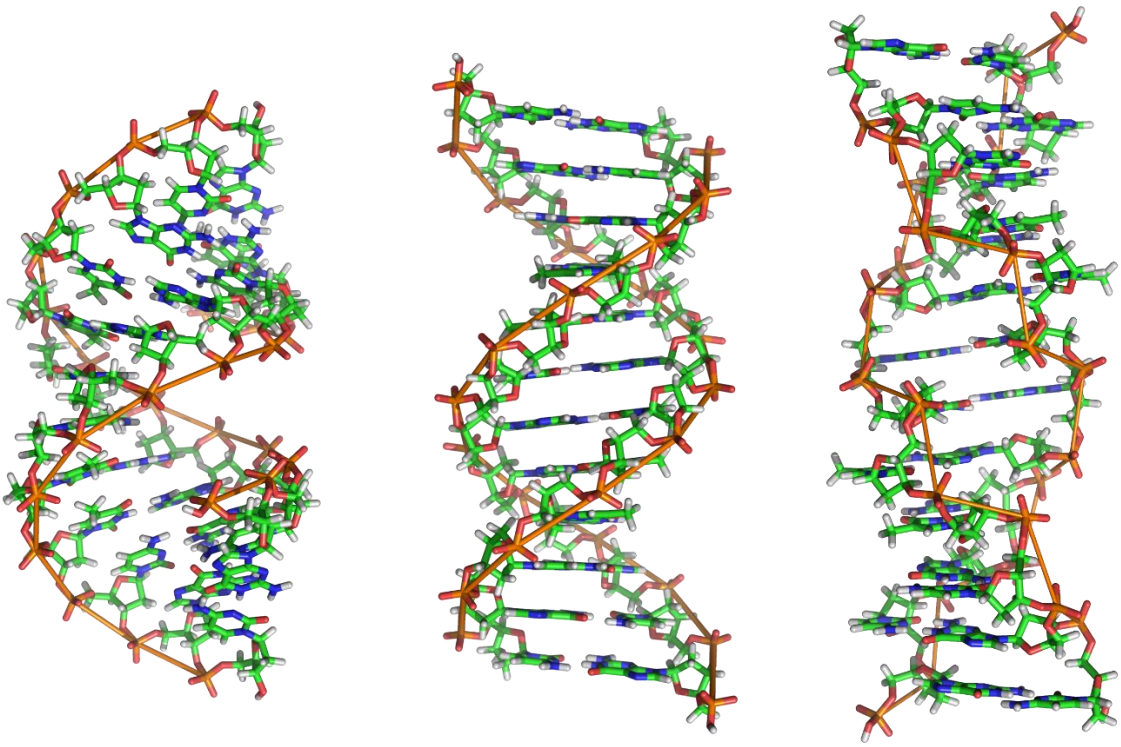

Figure 41 Double helix structures of A-, B- and Z-DNA shown from left to right. Reproduced from Wikimedia Commons.

Although RNA does not make a complementary double helix structure with itself, it is still found in many different forms, including messenger RNA (mRNA), transfer RNA (rRNA) and ribosomal RNA (rRNA) all of which have very different structures and functions. Messenger RNA is used in the process of *translation* where it carries a fragment of genetic code (copied from DNA) to be read by the ribosome. Transfer RNA is a 75 nucleotides-long strand that folds into a *cloverleaf* shape and has the function of carrying amino acids

into the ribosome (**Figure 42**). Ribosomal RNA, of which there are three types: (a) 3700, (b) 1700 and (c) 120 nucleotides-long, is the major component of the ribosome structure and behaves as a catalyst in the formation of proteins (section 1.6.2).[326]

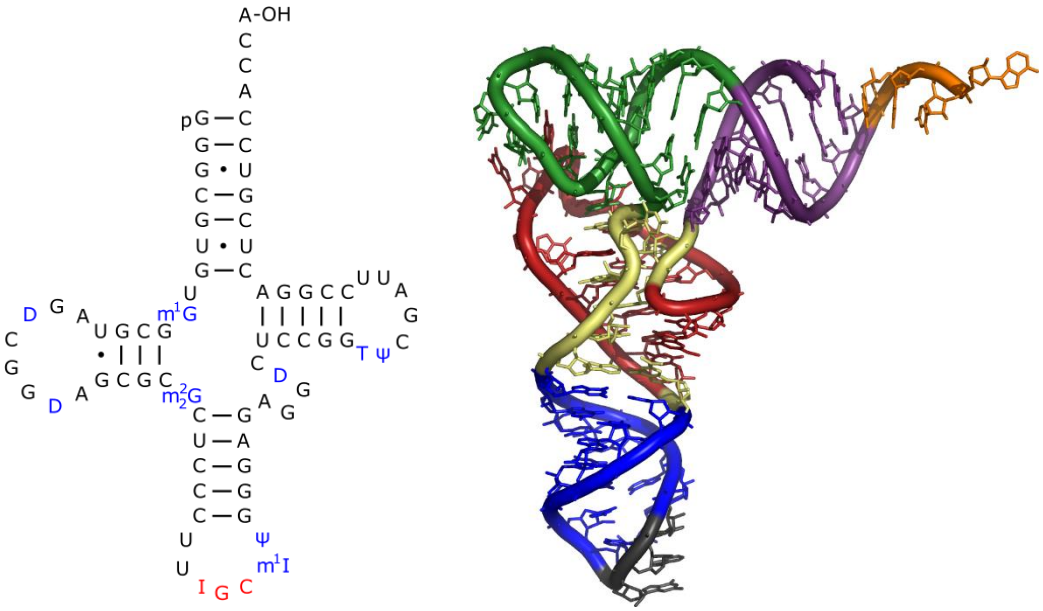

Figure 42 The nucleobase sequence and hydrogen bonding of a transfer-RNA (left) and its 3D structure and folding (right). Reproduced from Wikimedia Commons.

1.6.1.1 Helical Structures

Helical structures are observed relatively frequently and over a wide range of scales in biology. Common examples include collagen, agar, α-amylose and the α-helices formed by proteins.[327] The ubiquitous example is of course the DNA double helix, central to the existence of life and with a particularly aesthetically pleasing and mesmerising shape; it is not surprising that other double helix formations are often compared to this classic structure. One approach to mimicking the DNA double helix shape has involved the modification of the pre-existing nucleic acid assembly[328] or the use of non-biological organic molecules instead.[329] In fact, there are many examples within organic chemistry of helical structures,[330] formed via inter- and intramolecular hydrogen bonds,[331,332] metal coordination[333,334] and molecular templating.[335] The left- or right-handedness of a helix is often influenced by the chirality of the components of a polymer[336] although it is possible for one sense to be favoured even when the moieties are non-chiral.[337] In general however, if monomers of a system display no chirality, helix formation must be induced via external templating and notably, examples of non-templated inorganic helical structures are extremely rare (an observation that makes an interesting contrast with the

arguments made in section 1.6.3).[338] Having said this, helical macrostructures can form during crystal growth simply as a result of the stacking arrangement of non-chiral monomers, where they are tilted one relative to another, a structural effect can be observed in the gel formation (**Figure 43**).[339,340] In fact, there are many examples of defect-containing situations that result in spiral-type shapes from forming.[327]

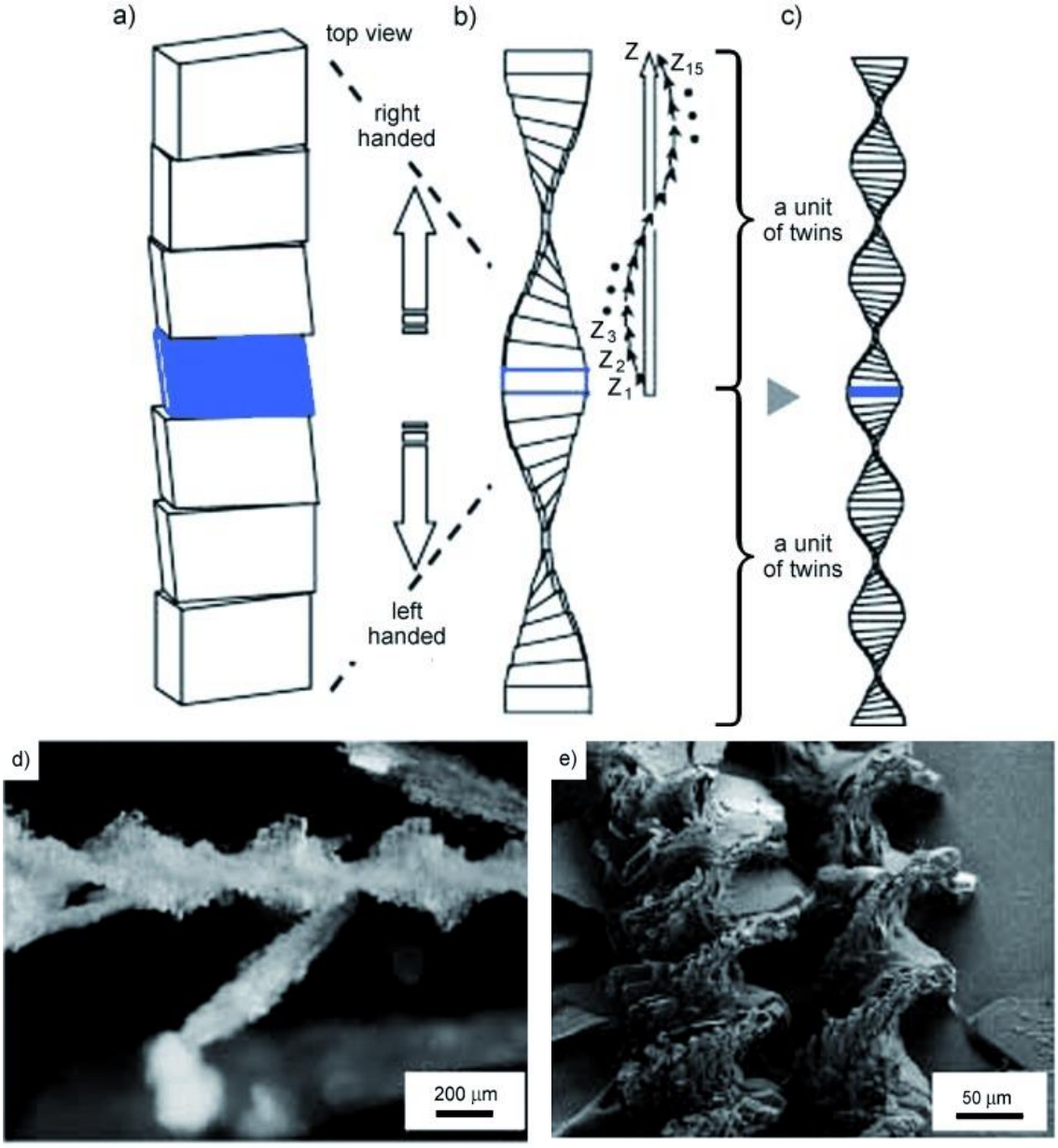

Figure 43 (a-c) Diagram showing how the regular arrangement of non-chiral crystal units can result in a helical structure. (d+e) Optical microscopy and field-emission scanning electron microscope (FESEM) images of the twisted morphology. Reproduced with permission.[327]

While many examples of single-helical based structures have been observed in inorganic chemistry, double-helix formations are rare[327] and most of them use templates to induce the double helix formation, or are still primarily carbon-based structures and do not

display any of the interesting electronic properties expected from inorganic molecules.[341,342]

One example of a purely inorganic double helix formed without templating is the SnIP structure.[343] Made from Sn, SnI_4 and P_4 cooled slowly from 923K in a sealed container, the double helices consist of a [P^-] strand and a [SnI^+] strand intertwined forming right- and left-handed helices in equal amounts (**Figure 44**). This results in bundles of helices that can be separated using scotch tape, similarly to graphene and display electronic and optical properties.

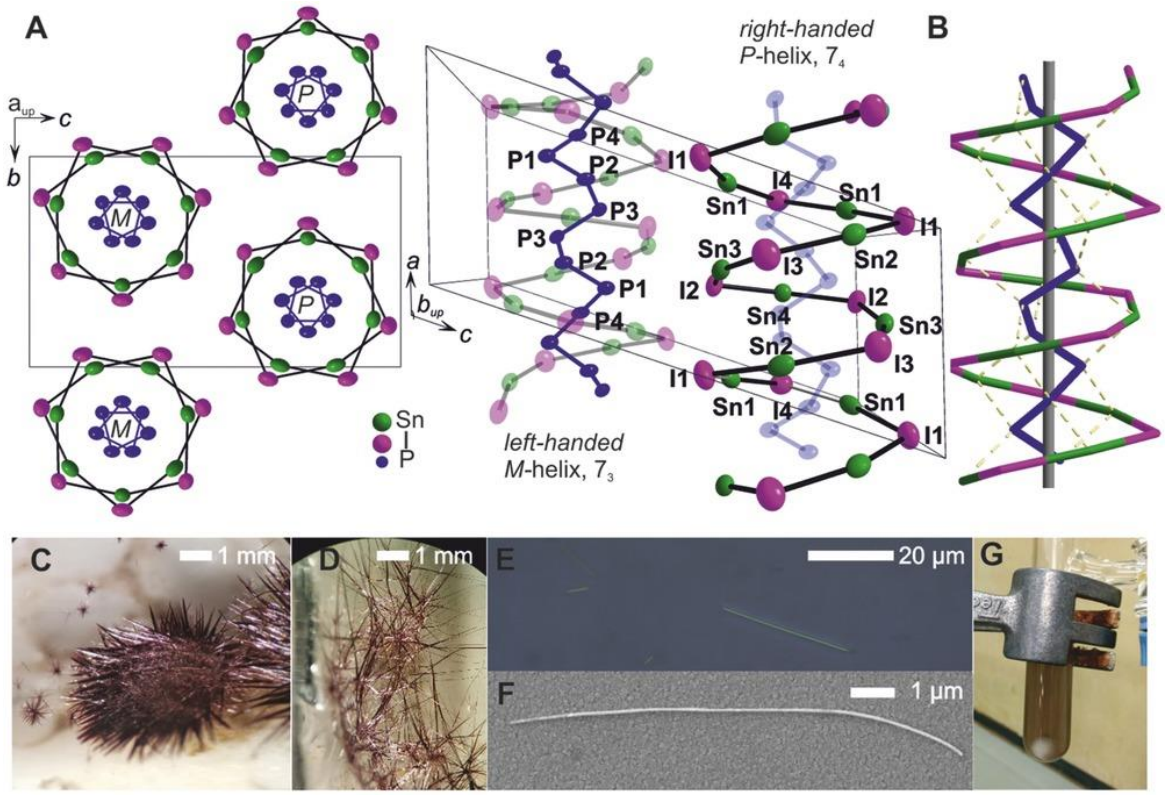

Figure 44 The double-helix structure formed from intertwined [P^-] and [SnI^+] strands, shown from (a) above and (b) below, (c-d) SnIP crystal growth, mechanically exfoliated (e) microscope imaging, (f) scanning electron microscope (SEM) imaging and (g) suspension of SnIP in chloroform. Reproduced with permission.[343]

In conclusion, despite a fascination for the DNA molecular structure, any double helices that have been synthesised so far are not dimensionally comparable to the nucleic acid structure unless the materials used are close derivatives of the original polymer itself.

1.6.2 Peptides

The genetic code carried by the DNA strands described in section 1.6.1, are the instructions used for constructing a different biological polymer, called a *polypeptide* or

protein. Like DNA, proteins play a central role in biology and have a fascinating structure, but for different reasons. Proteins are the molecules responsible for carrying out the majority of functions in living things and this is due to the incredible architectural diversity made possible by the multiple structural layers of these polymers, known as primary, secondary, tertiary and quaternary (**Figure 46**).[344]

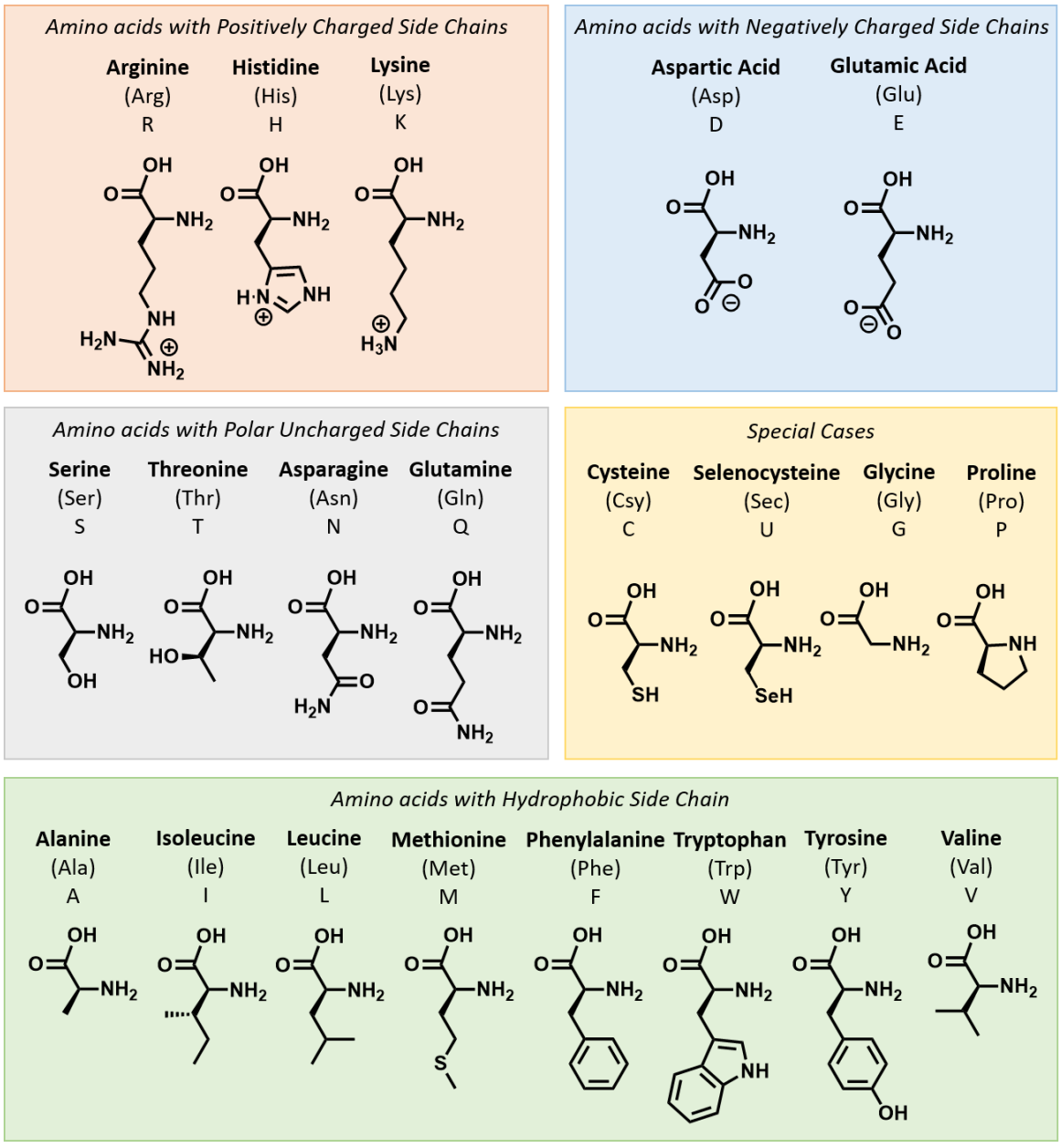

Figure 45 Molecular structures and categories of the 21 amino acids that make up peptide sequences.

The *primary structure* of a protein corresponds to the order in which the monomers are linked together. These monomers (residues) are a set of small organic molecules called *amino acids*, 21 of which are naturally occurring,[345] and will always be the L-isomer in biological systems (**Figure 45**). Amino acids have a carboxylic acid (C-terminus), an amine

(N-terminus) and a functional R-group surrounding a central tetrahedral carbon. The 20 different R-groups of amino acids have a variety of different properties and can be split into four categories: hydrophobic, polar, acidic and basic. The amine and carboxylic acid groups allow for these monomers to link together via a condensation reaction resulting in a peptide bond, a group which is planar, kinetically stable and contains both a H-bond donor and acceptor. As the chain has a direction, the convention is to write out sequences from the amino to carboxyl (or N- to C-) terminus and if the sequence is shorter than about 50 amino acids then the term *(poly)peptide* is used over *protein*.

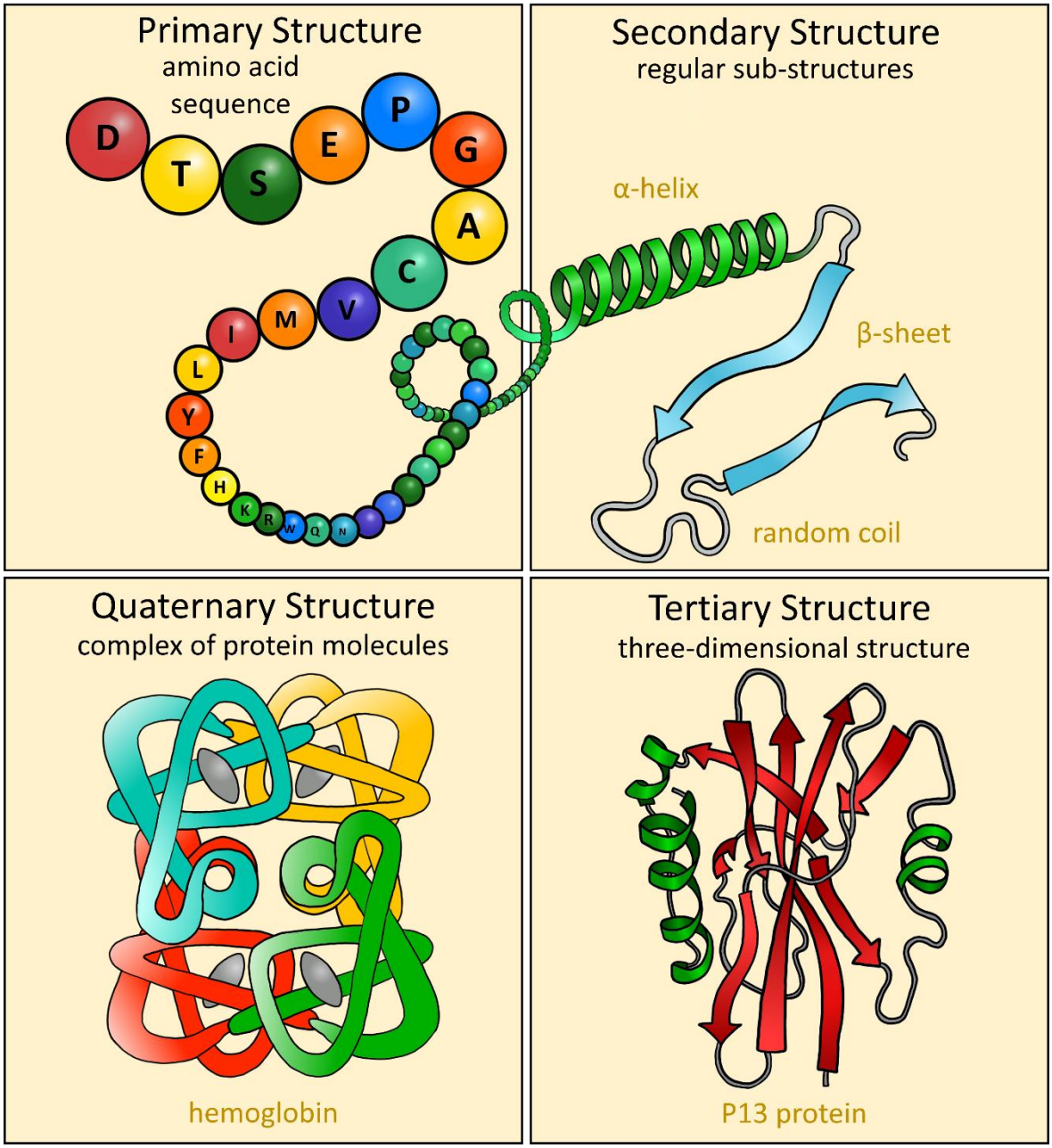

Figure 46 Representation of the four levels of structure that are found in proteins.

The *secondary structure* of a protein is the manner in which the local areas of a peptide chain interact with and fold around themselves, forming arrangements such as *α-helices*, *β-sheets, loops* and *turns*. These supramolecular interactions are very dependent on the properties of the amino acids in the primary structure. In an α-helix, the C=O group of each amino acid forms H-bonds with the N-H of a residue four spaces along the chain and may result a left- or right-handed screw axis. The β-sheets also form through C=O and N-H forms hydrogen bonds between strands that may run parallel, antiparallel or mix to one another.

The overall shape this folded chain makes is referred to as the *tertiary structure,* which will often include carefully shaped reactive pockets with specific catalytic functions. Usually a hydrophilic core and hydrophobic exterior or vice versa is observed, adapted for the protein's environment (aqueous or membrane-bound) and function (e.g. a pore, transporter, enzyme or structural component).

Some larger proteins are made up of multiple peptides fixed together through intermolecular interrelations or covalent connections such as *disulfide bridges* (S-S), formed between the S-atoms of cysteine residues and all of these parts combined is known as the *quaternary structure*. In addition, this overall structure may contain some non-amino acid components such as a porphorin (e.g. a hemegroup) or a coordination metal (e.g. Zn^{2+} or Mg^{2+}).[326]

The shape, size and properties of proteins can vary enormously and are crucial to their function within biological systems (**Figure 47**). The variety of properties seen in proteins make them interesting and valuable molecules. In some cases, artificial synthesis of peptides can be easier than extracting them from living systems and allows for the exploration of sequences that do not occur naturally. Solid phase-peptide synthesis (SPPS) is the technique used for manually making peptides.[346–348] It involves insoluble and filterable cross-linked PS supports from which the chain is extended, one amino acid at a time from C-terminus to N-terminus. Apparatus are commercially available for carrying out automated SPPS because although the procedure is relatively straightforward, the number of steps involved in the process is large, and the tasks very repetitive.[349]

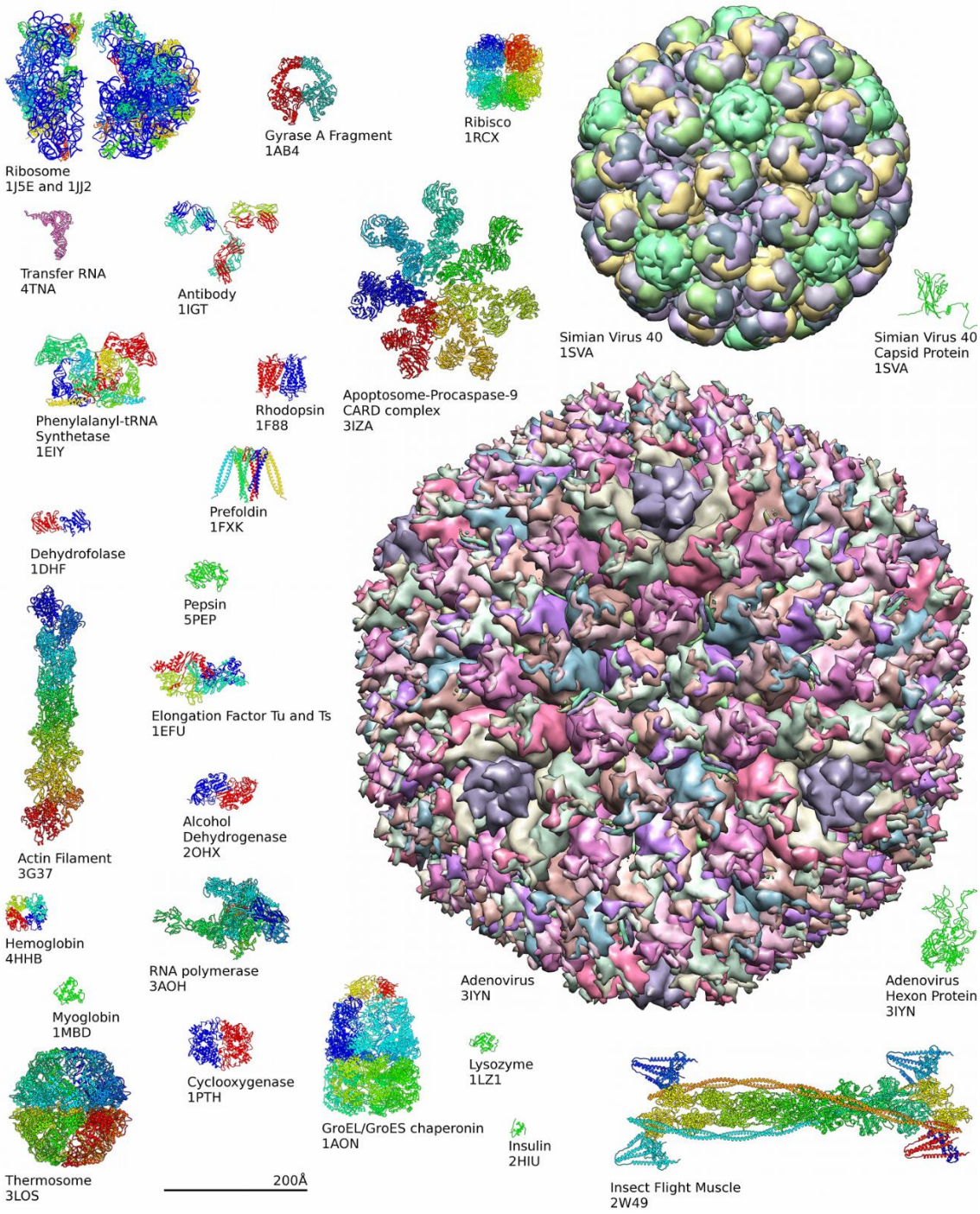

Figure 47 Examples demonstrating the enormous structural diversity available to proteins. Reproduced from Wikimedia Commons.

1.6.2.1 Mn-Anderson Peptide Hybrids

This section follows on from section 1.4 which described a number of POM-polymer hybrids, but this example has been left separate as it takes direct inspiration from the bio-polymer system just described and incorporates an inorganic cluster into a peptide chain.

In a process developed by Cronin et al., individual amino acids, dipeptides, tripeptides were bound to a Mn-Anderson hybrid as well as incorporated into a small peptide

chain.[350] The precursor used was synthesised from a succinic Mn-Anderson hybrid functionalised with NHS ester-activated groups which would bind to single amino acids or small peptides when stirred in the presence of DIEA for 24 hours. This approach allowed for two identical peptides to be attached to a Mn-Anderson at both ends. In order to incorporate a Mn-Anderson hybrid into a peptide as an "inorganic amino acid", an asymmetric version of the NHS ester-activated Mn-Anderson hybrid had to be used (section 1.3.9.2). This is due to the embedded directionality of biologically-inspired peptides, in which amino acids are joined from C to N and so an effective artificial amino acid also needs to have direction. This asymmetric Mn-Anderson hybrid had an NHS ester-activated group on one side and an FMOC protecting group on the other (**Figure 48**).

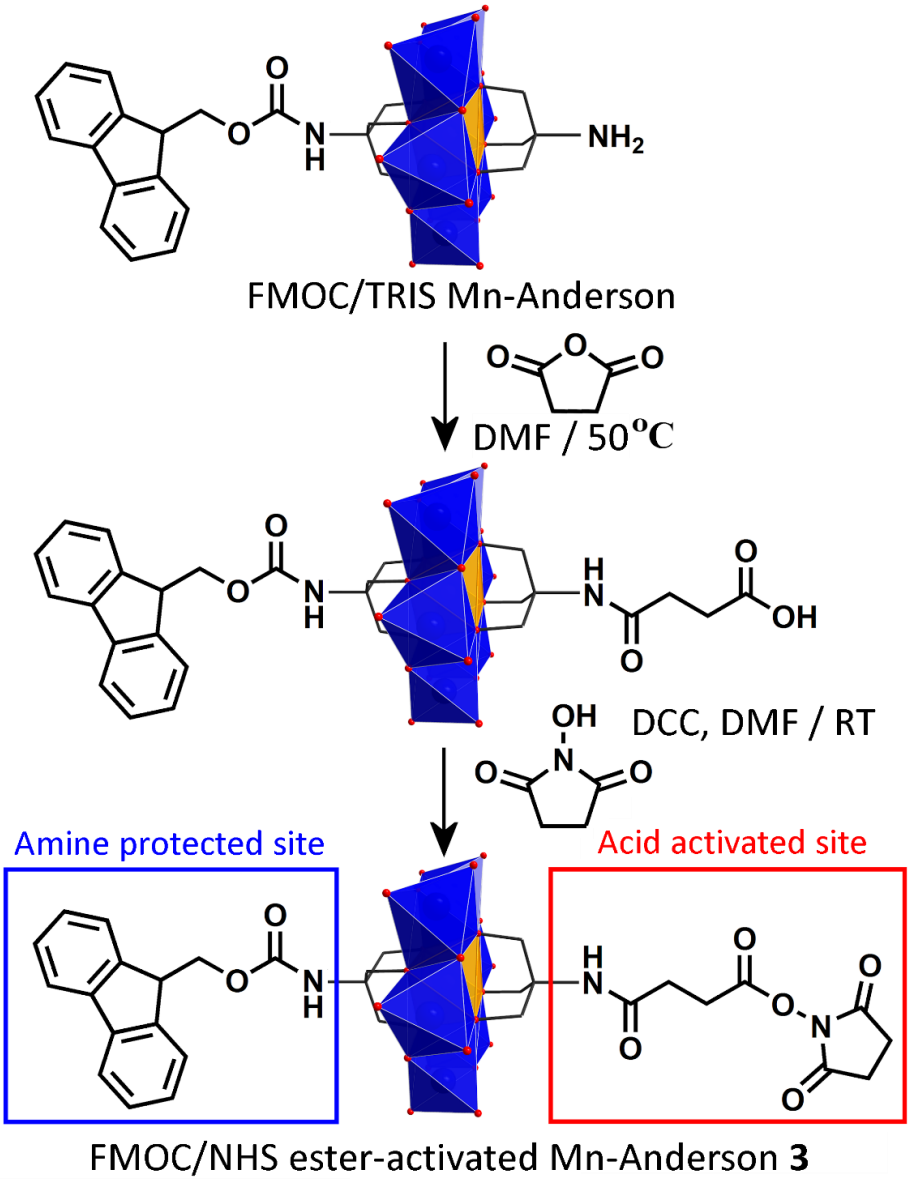

Figure 48 Reaction scheme for the synthesis of the "inorganic amino acid": an asymmetric Mn-Anderson with an FMOC-protected ligand and an acid activated site, made by functionalisation of the universal asymmetric precursor with succinic anhydride followed by NHS.

Solid phase peptide synthesis (SPPS) was then used to incorporate the FMOC/NHS ester-activated Mn-Anderson hybrid into a short peptide, forming a Mn-Anderson peptide hybrid. **Figure 49** shows how the individual amino acids and Mn-Anderson hybrid were added (using DIEA or DIC, respectively) and then deprotected (using piperidine/DMF), one at a time. The resulting chain was then cleaved from the resin using a cleavage cocktail of HFIP in DMF.

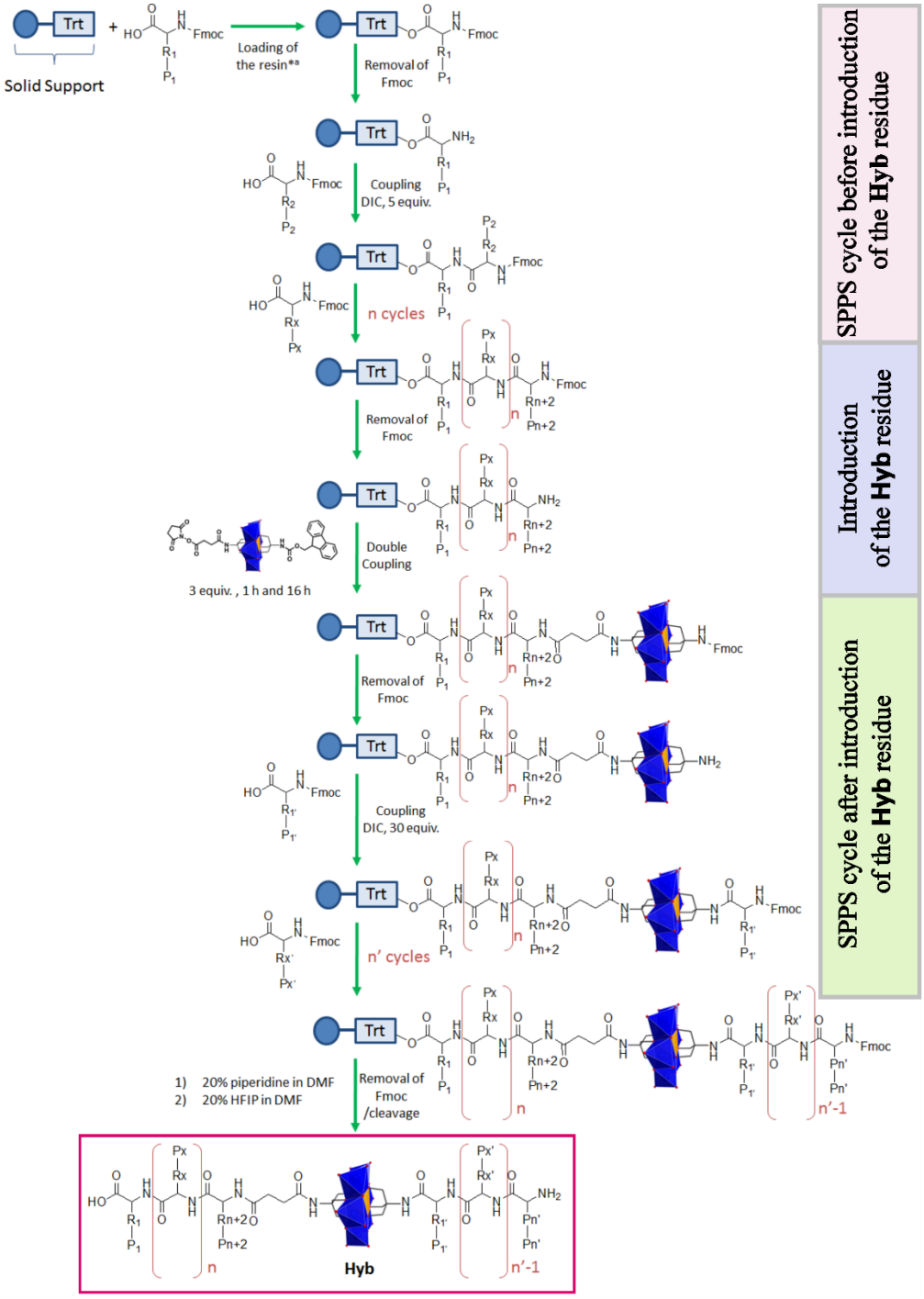

Figure 49 Reaction scheme outlining the solid-phase peptide synthesis approach taken for the incorporation of an asymmetric Mn-Anderson hybrid into a short peptide chain.

1.6.3 Theory of an Inorganic Origin to Life

The first parts of the introduction, section 1.1 introduced the concepts of polyoxometalates, a set of complex nanostructures that self-assemble from simple inorganic building blocks. The following sections discussed some other self-assembling macrostructures (section 1.5), mostly focusing on the configurable biopolymers: nucleic acids (1.6.1) and polypeptides (1.6.2), the molecules on which the *central dogma of biology* is built.[326,351] This final section neatly brings inorganic self-assembly and complex information-carrying biopolymers together by discussing a theory posed in 1966 by Alexander Graham Cairns-Smith that the origins of life stem from the spontaneous assembly of inorganic matter.

In his book "Seven Clues to the Origin of Life", Cairns-Smith breaks his argument down into seven concepts; analogies drawn from biology, biochemistry, the building trade, the nature of ropes, the history of technology, chemistry and geology.[352] He uses these ideas to argue that genetic information, a replicable *form* that outlasts *substance* must have been the initial component of life, but that the original "naked gene" could not have been a nucleic acid as these organic molecules are far too complex and not easily synthesizable by natural processes. He proceeds to make an analogy from (building) construction, where scaffolding is necessary to assemble structures such as arches and argues how likely it is that some elements, once part of the biological systems have since fallen away, leaving behind mutually dependent components, neither of which were the original structural piece, i.e. *a template*. In fact, the idea is taken to a greater extreme and it is suggested that not only could the initial scaffolding be missing, but the entire original system may have evolved so much that nothing of those first materials are still a component part today. Another comparison is then made, this time with the development of technology and the way primitive machines very rarely have the same design or use the same materials as the later versions. The first versions of a machine must be simple to assemble from easily accessible materials and result in an effective mechanism. Similarly, the first genetic information must have been easily assembled from simple readily available building blocks and capable of forming a functioning system. The hypothesis is then made that inorganic crystals would be biochemically available and reliable enough to replicate complex information, making them the most plausible

contestant as “low-tech genetic material” and so concluding that life originated from the crystal defects of mineral clay.

In further publications, Cairns-Smith argues the plausibility of an era predating the *RNA world*, centred around “inorganic enzymes”.[353] This period hypothetically would have allowed for the development of complex metabolic networks, characteristic of life as we know it and requiring well-tuned catalysts, but involving structures relatively less complex than those of proteins or nucleic acids which are nonetheless evolved enough to carry out specific roles. The key observation that holds this theory together is the manner in which imperfections of a crystal lattice can replicate themselves as part of the crystallisation process.[354] Under the right environmental conditions the replication of these crystal defects may have evolved into a complex process, containing an information density comparable to that of DNA. Over time, this primitive replication mechanism would have incorporated an increasing amount of organic materials: a “genetic metamorphosis” eventually leading to a complete transfer into complex organic molecules such as RNA.

Figure 50 There are many approaches and perspectives to origin of life research.

However compelling and elegant this theory may appear, it unfortunately lacks any experimental evidence and furthermore there are many other alternative and contrasting theories for the origin of life (**Figure 50**), which are beyond the scope of this thesis.[355–358]

2 Aims

Organic-inorganic polyoxometalate hybrids combine the unpredictable nature of polyoxometalate synthesis with the controlled certainty of organic chemistry. Not only does this result in hybrid clusters having a combination of interesting properties, but also results in two contrasting synthetic approaches; self-assembly and directed synthesis, both of which have benefits and drawbacks. Although the search for new self-assembling structures from basic starting materials does not guarantee results, it does allow for novel discoveries to be made from which deeper understanding of other spontaneous and complex systems, such as some biological processes, can be made. Directed synthesis on the other hand, is unlikely to produce insightful, unpredictable results but is extremely useful for the incorporation of POM hybrids into potential applications due to the level of control that can be obtained.

The overall aim of this thesis is to use these two opposing synthetic approaches to explore polymer-like structures that can form from organic-inorganic POM hybrids. This will be divided into three sections:

1) To start, the study of a self-assembled POM hybrid structure will be made. A biomolecule known to produce interesting supramolecular networks in solution will be reacted with a metal oxide to spontaneously produce a compound with multiple levels of complex structure in crystal form. Exploration of the properties and nature of this POM hybrid may provide some understanding to the behaviour of the biomolecule in its native system. The hybrid cluster in question is a Strandberg-type POM bi-functionalised with guanosine ligands which in solid form, stacks to form a double helix with dimensions comparable to those of the Z-form of DNA.

2) A contrasting approach will then follow, where a similar organic-inorganic POM hybrid monomer will be isolated and instead of forming an extended structure through spontaneous assembly the components will be strategically placed in order to demonstrate the level of control such hybrids allow. More specifically, a method for the controlled coupling of asymmetrically functionalised Mn-Anderson hybrids will be developed in order to form POM hybrid oligomers of specific lengths.

3) Once the methodology for controlled assembly of these POM hybrid structures is established, work will be carried out to further develop the technique for the incorporation of a wider variety of inorganic clusters. This will advance the strategy from allowing a remarkable level of control to additionally demonstrating a fine tuneability and ultimately leading to the design and synthesis of compounds with specific properties. To be exact, this final section involves working with the POM hybrids, Lindqvist, Fe- and Cr-Anderson in addition to the Mn-Andersons in order to form configurable mixed-POM oligomers.

3 Results and Discussion

3.1 A Self-Assembled Organic-Inorganic Hybrid Extended Structure

The work laid out in this next section is the study of the double helical extended structure formed when synthesising a bio-inorganic POM hybrid from a nucleoside and molybdate. Some of the work described here was carried out by former members of the Cronin group, namely the initial NMR, the gel inversion tests, (Dr Vladislav Kulikov), the MS (Dr Andrew Surman), the CD (Dr Sharon M. Kelly), the gel electrophoresis and the AFM (Dr Mohammed Hezwani). It is included here because further synthesis, experimentation and/or analysis of these techniques were later carried out by myself during compilation and completion of the resulting project.[359]

3.1.1 Guanosine Strandberg

The study of self-assembled extended POM hybrid structures is an important step towards the development of controlled synthesis of such systems. Bio-inorganic POM hybrids are additionally interesting as parallels and comparisons can be made with the self-assembly mechanisms found in biological systems.

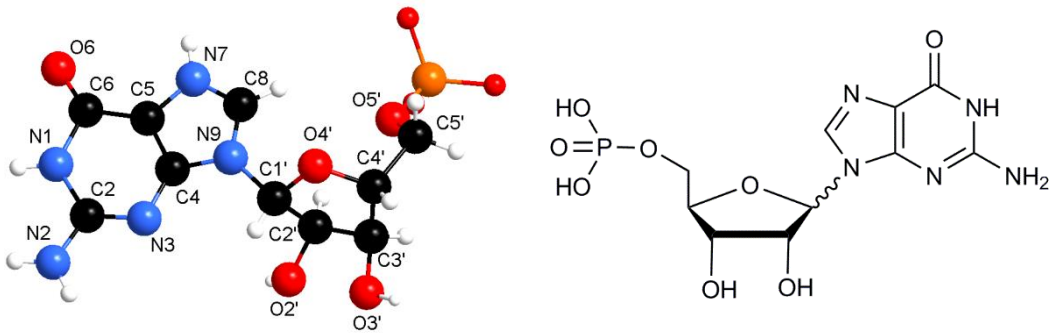

Figure 51 The atom numbering for the guanosine 5'-monophosphate (GMP) ligand Colour code – N (blue), O (red), P (orange), C (black).

It was with such a bio-inorganic POM hybrid target in mind that experimentation with simple inorganic materials and biomolecules was carried out. We chose to work under conditions favouring the formation of the Strandberg POM unit and with a guanine-based molecule because both systems are known to form interesting extended structures in solution, often resulting in gelation[214,304,360] and hybridisation of the Strandberg and adenosine (another nucleotide) had previously been reported.[361]

Table 1 Structural features of ideal B-, Z-DNA and guanosine Strandberg (**Compound 1**) *Guanine rings form H-bonded stacks as oppose to Watson-Crick base pairing.

	B-DNA[325]	**Z-DNA**[325]	**Compound 1**
Helical Sense	Right handed	Left handed	Left handed
Diameter	~20 Å	~18 Å	~32 Å
Base Pairs per Helical Turn	10	6	6*
Helical Twist per Base Pair	36°	60° per dimer	60° per dimer
Angle within Dimers		9°	4°
Rise per Turn	34 Å	45 Å	42 Å
Rise per Base Pair along the Central Axis	3.4 Å	7.4 Å per dimer	7.0 Å per dimer
Inter-planar Ring Distance	3.4 Å	3.4 Å within dimers	3.4 Å within dimers
Base Normal to the Helix Axis	6°	7°	7°
Sugar Pucker	C2'-*endo*	C2'-*endo* for pyrimidines; C3'-*endo* for purines	C2'-*endo*
Glycosidic Bond	Anti	Anti for pyrimidines; syn for purines	Anti

We found that on acidification of guanosine 5'-monophosphate (GMP) (**Figure 51**) and sodium molybdate in aqueous solution, a hydrogel spontaneously formed from which crystals grew after two weeks of slow methanol diffusion. Crystallographic data revealed the formation of an organic-inorganic POM hybrid, $Na_2[(HGMP)_2Mo_5O_{15}]\bullet 7H_2O$ (**Compound 1**) where two organic guanosine moieties connect via a phosphate group to the inorganic Strandberg-type core, a structure we termed the "guanosine Strandberg". As with other Strandberg-based POM hybrids (section 1.3.4), the discrete clusters come

together to form a complex intermolecular network, which in this case we found shared a strikingly large number of dimensions with those of the Z-form of DNA (**Figure 52**).

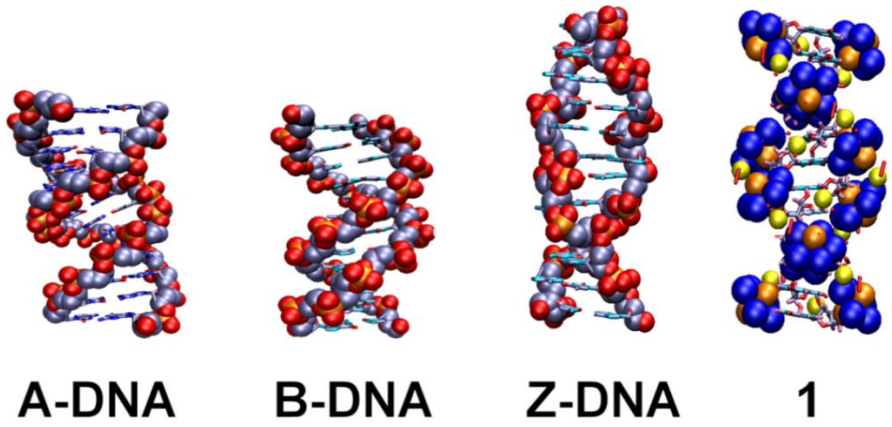

Figure 52 Comparison of the three forms of DNA with the guanosine Strandberg (**1**) double helix. The images were produced using VMD-software, using NDB-files pdb4okl (A-DNA), pdb4c64 (B-DNA), pdb1vty (Z-DNA).[362]

The similarity between the guanosine Strandberg (**Compound 1**) and the Z-DNA crystal structure is interesting to those familiar with Cairns-Smith's theory that biomolecules first formed by templating off self-assembled inorganic crystal structures (section 1.6.3), especially as there has yet to be any robust examples to back his hypotheses.[352–354] With this in mind, we set out to make a comprehensive comparison of the guanosine Strandberg (**Compound 1**) system with that of Z-DNA to explore the idea that such a system could behave as an inorganic template for DNA (**Figure 53**).

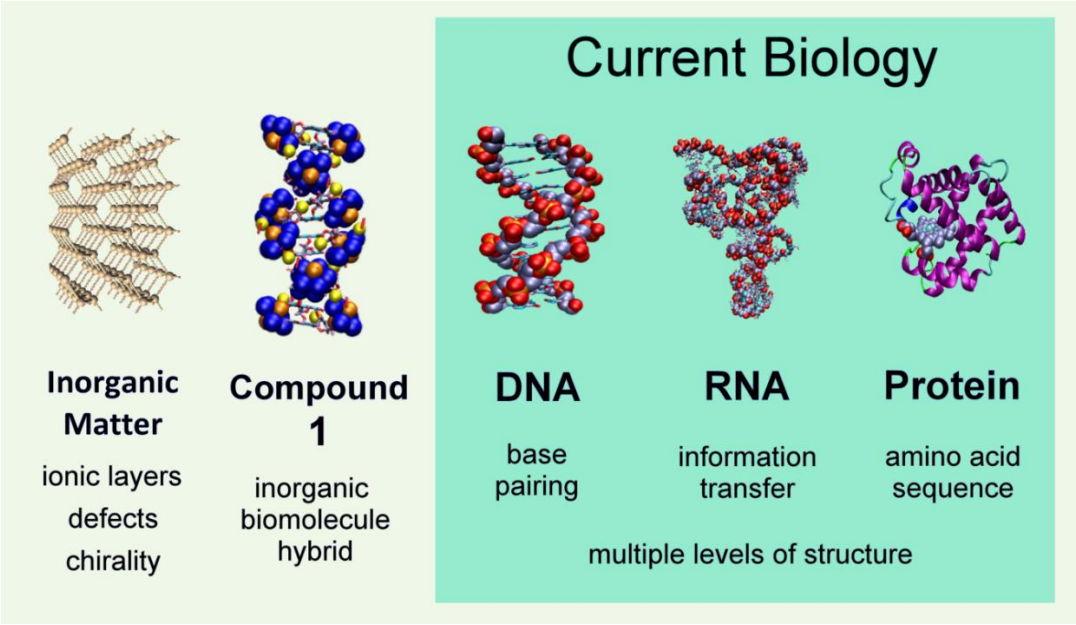

Figure 53 A suggestion that structures such as the guanosine Strandberg (**Compound 1**) could bridge the gap between the complex systems of the central dogma of biology and self-assembled inorganic materials.

3.1.2 Structure Description

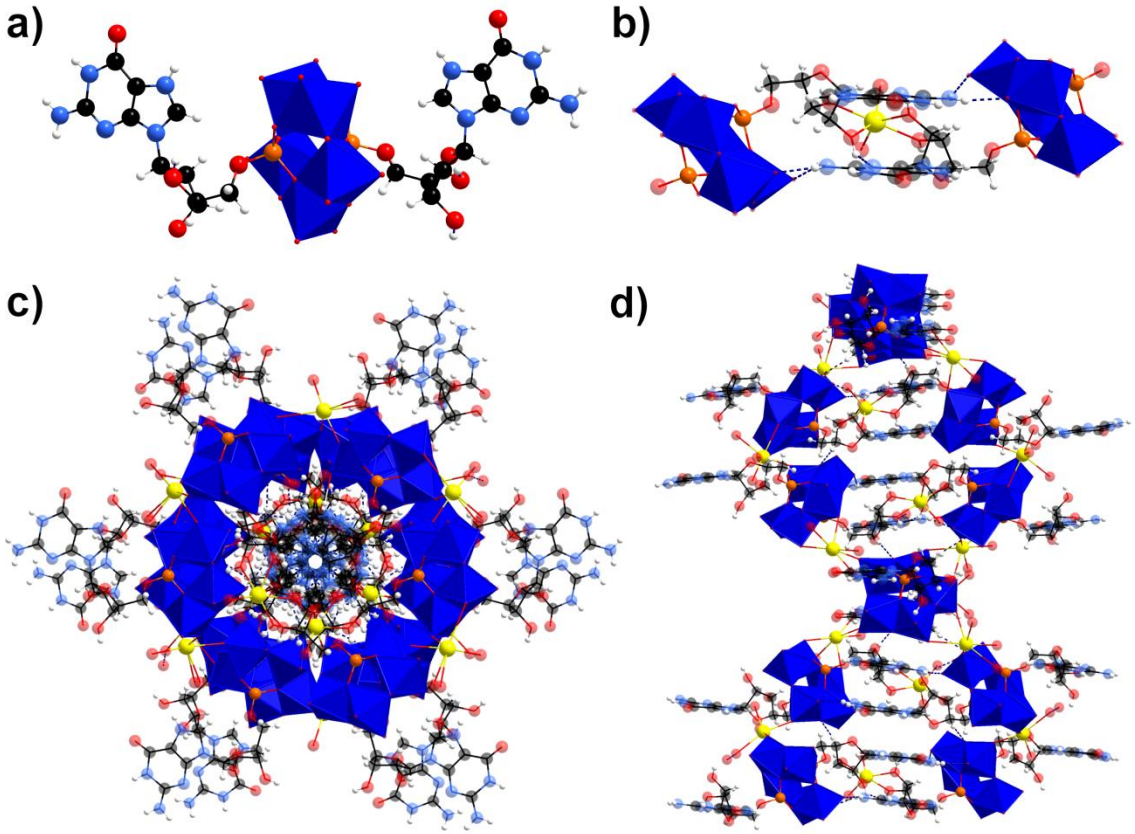

Figure 54 Crystal structure of the guanosine Strandberg: a) hybrid monomer, b) ligand interaction between monomer subunits and the double helix formation seen from c) above and d) side-on. Colour code – Strandberg POM cores (deep blue), N (light blue), O (red), P (orange), Na (yellow).

The guanosine Strandberg (**Compound 1**) assembly crystallises in the space group $P6_522$ forming a sixfold screw axis with a left-handed twist and two orthogonal twofold rotational axes as symmetry elements (**Figure 54**). As has already been mentioned, this network is constructed of monomers connected through intermolecular interactions. These molecular building blocks are bi-functionalised POM hybrids with a Strandberg-type inorganic core; an anionic ring of five condensed molybdate(VI) anions capped by phosphate groups above and below the ring plane. The two guanosine ligands connect to these phosphate atoms via the oxygen atom on the 5' carbon of the ribose ring.[363] The Z-DNA-like helical dimensions results from the arrangement formed by these monomers within the extended crystal structure. The GMP ligands aggregate together in a stacked arrangement held together through hydrogen bonding and π-π interactions (**Figure 55**) and the associated Strandberg POM cores mimic the sugar-phosphate backbone of DNA by forming double-helix spiral arrangement around the GMP core, through which the sixfold symmetry can be observed. Each individual monomer is therefore a component of

two adjacent double-helices as every GMP ligand is part of a different central stack. The distance from one purine ring plane to the next alternates between ~3.39 Å and ~3.54 Å, lengths characteristic of π-π interactions. Hydrogen bonds with distances of approx. 2.68-2.82 Å can be observed between the amines or imines of the guanosine residue and the solvent water molecules, oxo groups on the Strandberg cluster and the hydroxyl group of the ligand. Like the majority of polyoxometalate structures, the negatively charged clusters are balanced by counterions and in this case there are four Na^+, three of which are bound between cluster oxo ligands and solvent water molecules. More interestingly, the fourth Na^+ links guanosine ligands together via two hydroxyl groups from each moiety, with a typical distance of ~2.4 Å, and two solvent water molecules, completing the coordination sphere of a NaO_6 octahedron (**Figure 55**).

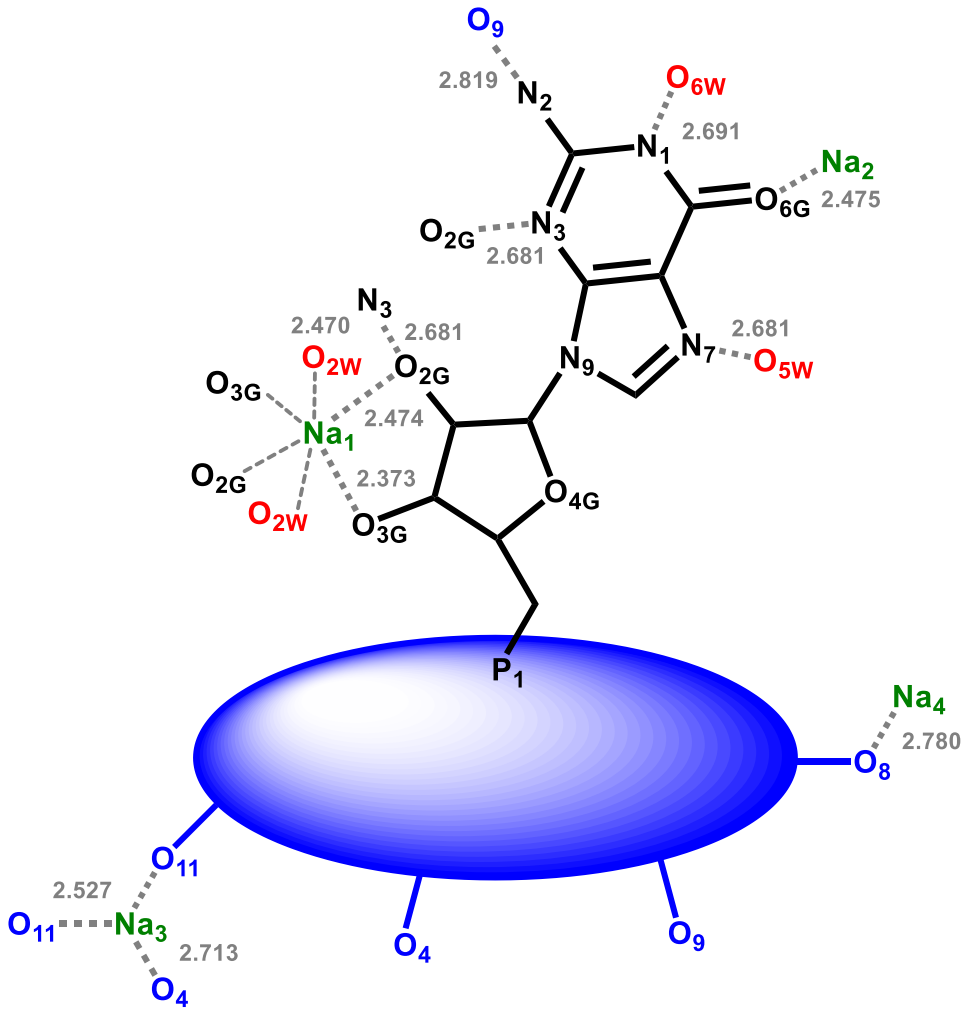

Figure 55 Schematic showing the Strandberg POM core (blue) and one guanosine ligand (black) of **Compound 1** and the intermolecular interactions (grey, units in Angastroms) they have with their surrounds, including the four sodium counterions (green) and solvent water molecules (red).

3.1.3 Gelation Studies

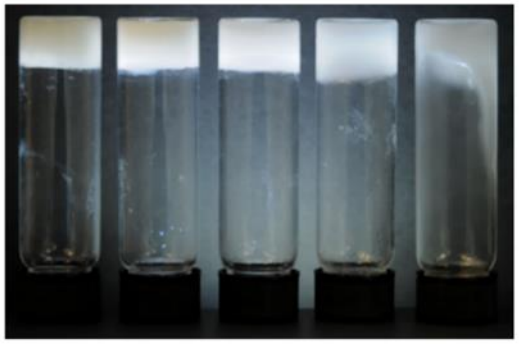

Figure 56 Tube inversion test was carried out after compound 1 solution was left for 20 minutes, pH = 1.2 and concentration from left to right (in mol/L): 0.025, 0.018, 0.014, 0.011, 0.009.

To further understand the physical properties of guanosine Strandberg (**Compound 1**), investigation of the low-molecular weight gelator (LMWG) properties in aqueous form was carried out using the tube inversion method (**Figure 56**), allowing for a comparison to be made between the compound and the gelation of the starting material, GMP.[173] When measured at room temperature and pH 1.2, the critical gelation concentration (CGC) was shown to be 0.009 M, corresponding to 1.28 wt % which, considering the molecular weight of **Compound 1** compared to other LMWG, is quite striking. Although there are some POM hybrids that can form gels, none of them are hydrogels. But in this case, the POM core must be contributing to the gelation properties as much as the ligands because the CGC of the guanosine Strandberg (**Compound 1**) at pH 1.2 is 50 times that of GMP alone (0.3M at pH 7).

3.1.4 Gel Electrophoresis

Interactions between POMs and biomolecules are not only of general interest but potentially useful for the development of POM-based drugs and chemical biology tools.[14] Gel electrophoresis studies were used to explore the interactions between guanosine Strandberg (**Compound 1**) and a functional biopolymer. Gel electrophoresis is a method used for the separation, identification and purification of biomolecules such as nucleic acids.

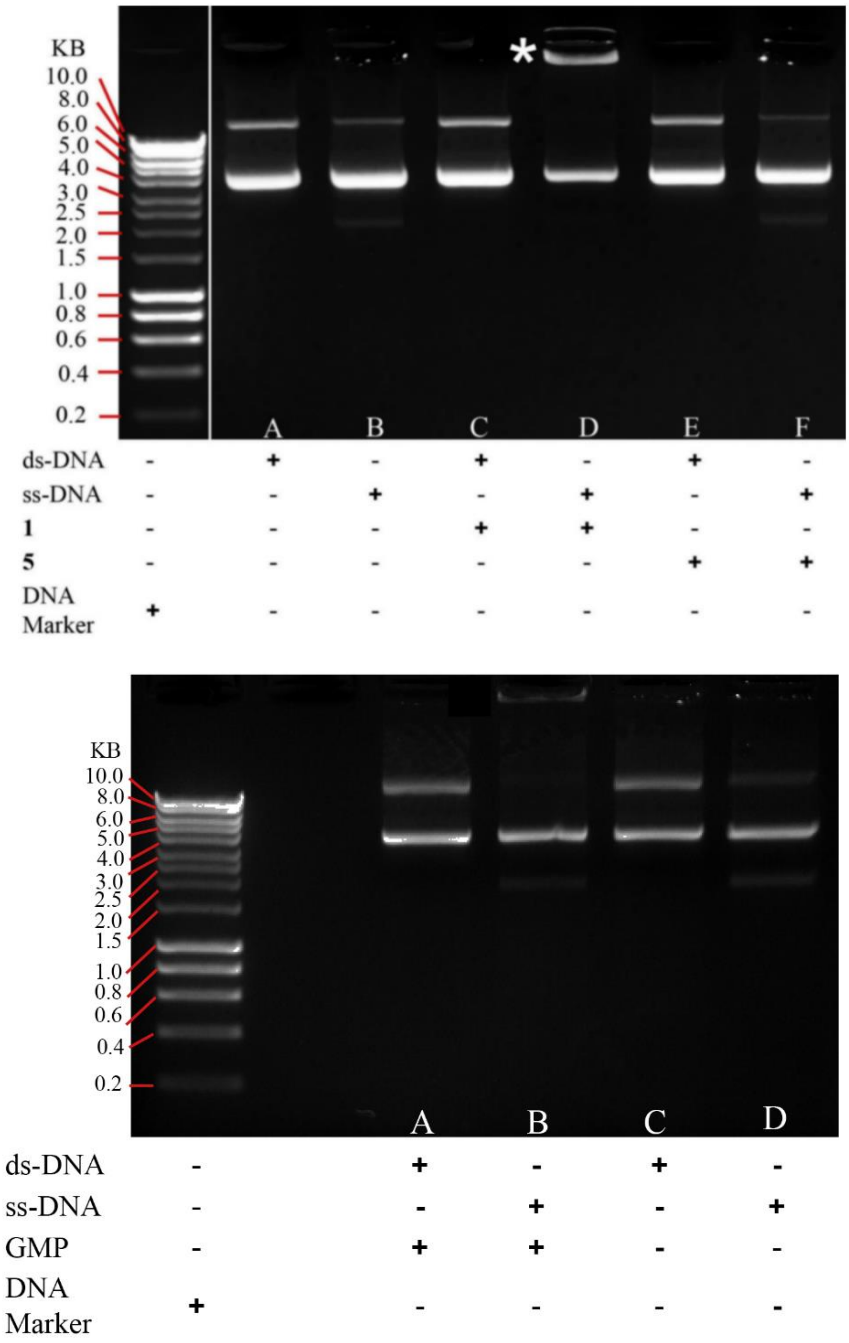

Figure 57 Gel electrophoresis results of interactions between ds-DNA = double stranded pGLO plasmid DNA, ss-DNA = single stranded pGLO plasmid DNA, guanosine Strandberg (1), Strandberg POM core and GMP = gunosine 5'-monophosphate. The star (*) highlights the new band formed by interaction between ss-DNA and the POM hybrid.

and proteins. It separates molecules out according to shape, size and charge by exposing them to an electric field in a solvent causing them to move through a porous support matrix, normally an agarose or polyacrylamide gel.[326,344] **Compound 1** was incubated with double-stranded (ds) and single-stranded (ss) plasmid DNA, pGLO. This plasmid is a short

loop of DNA engineered to act as a vector in biotechnology and contains three genes, including green fluorescent protein (GFP). **Figure 57** shows the results of the electrophoresis runs on these incubations. Migration was seen with ss-DNA demonstrating the formation of non-covalent adducts with pGLO, but not the double-sided version of the plasmid. The same experiment was repeated using the inorganic Strandberg anion, $Na_6Mo_5P_2O_{23}$ and no interactions were observed between the POM cluster and either DNA strand, suggesting that it is the free guanosine ligands of the hybrid POM that are facilitating the interaction with ss-DNA.

3.1.5 Comparison with Z-DNA

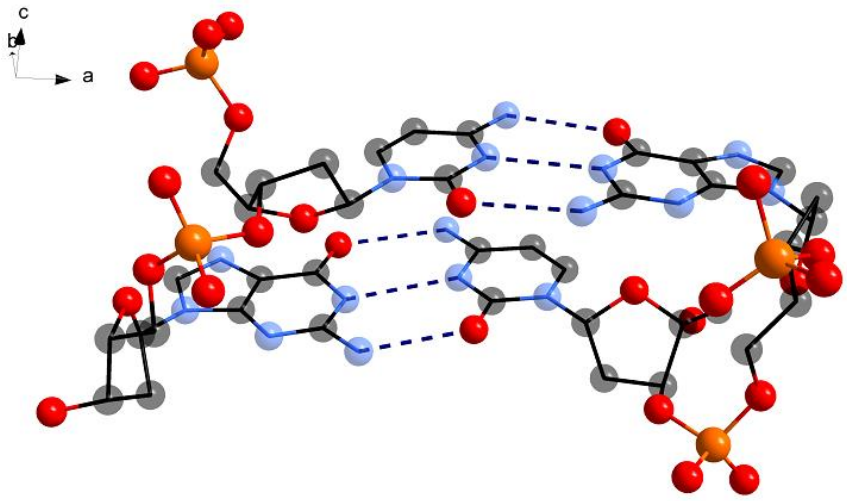

Figure 58 Dimer of Z-DNA displaying Watson-Crick base-paring. N (blue), O (red), P (orange).

Although the guanosine Strandberg (**Compound 1**) network shares much of its dimensions and symmetry with Z-DNA, there are some key differences. The nucleobase interactions for instance, in DNA are Watson-Crick base-pairs where a purine is hydrogen bonded to its complimentary pyrimidine partner and these interactions are further stabilised by the intermolecular bonding between each rigid base pair, resulting in a stack (see Section 1.5.1). In contrast, the interactions between the guanine moieties in **Compound 1** are of course, not complementary base-pair interactions and so each ligand pair relies more heavily on the surrounding ligands for structural support.

Without this archetype Watson-Crick base-pairing occurring in the guanosine Strandberg (**1**), it is perhaps surprising that such a double helix structure is forming (**Figure 58**). An explanation for this comes when the nature of the organic ligand is considered: the Z-

form of DNA is known most easily to form in guanosine-rich DNA strands.[325] The significance of

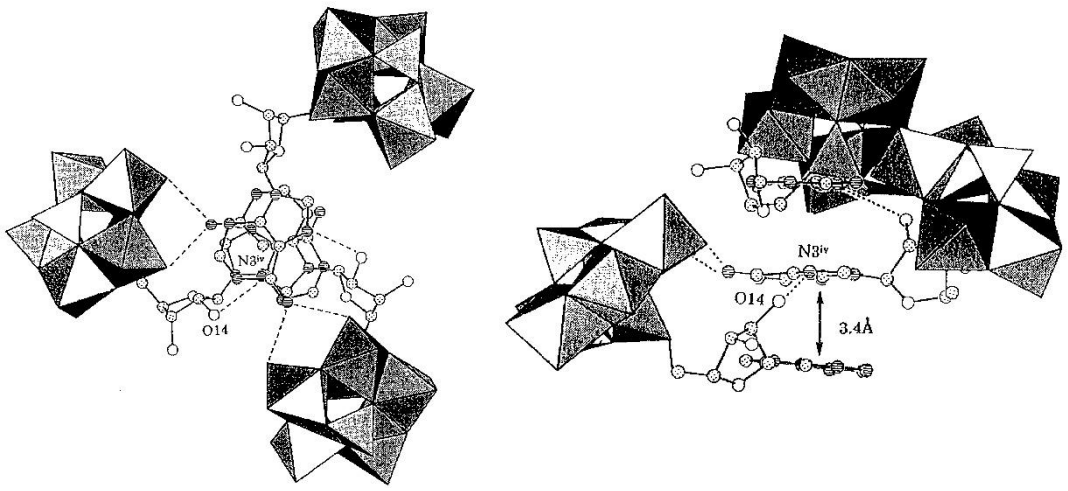

Figure 59 Structure of the adenosine Strandberg hybrid POM, an analogue to **Compound 1.** Reproduced with permission.[361]

the guanine group is further confirmed when observing how the adenosine analogue of **Compound 1**, synthesised by Yamase and Inoue in 1996, does not form a double helix but instead has a space group of $P3_121$ with a threefold twist going through the middle of the adenine ring (**Figure 59**).[360,361] Together these points highlight the key role that guanosine itself must play in the formation of the characteristic Z-DNA helical shape.

Another difference to be considered between the POM hybrid and DNA is the nature of the extended assembly. Although both materials contain a molecular component whose interactions result in a secondary structure, the size of the molecular unit is not the same: a polymer in the case of deoxyribose nucleic acid and a monomer for **Compound 1**. There is also an added level of complexity to these nucleic acid polymers that is non-existent for the guanosine Strandberg (**Compound 1**) and that is the "configurability" of the polymer strands: the order of the pendent nucleobases can vary and the self-assembly of the double helix relies on two strands being complementary. There is no configurability within the POM hybrid structure as all monomers are identical to one another, self-assembling into a network that extends out in all directions where the double helix nature is observable only in one direction (**Figure 60**). The assembly of Z-DNA on the other hand is linear and any greater network formations are a result of environmental factors influencing the folding tendencies of the double-helix strand. Environmental factors also influence **Compound 1** and the ionic nature of the crystal structure with its polyanions

and sodium cations, results in dissolution of the material and loss of the regular network in solid form. Having said this, complete loss of intermolecular structure is highly unlikely due to the gelation that occurs when the POM hybrid is dissolved.

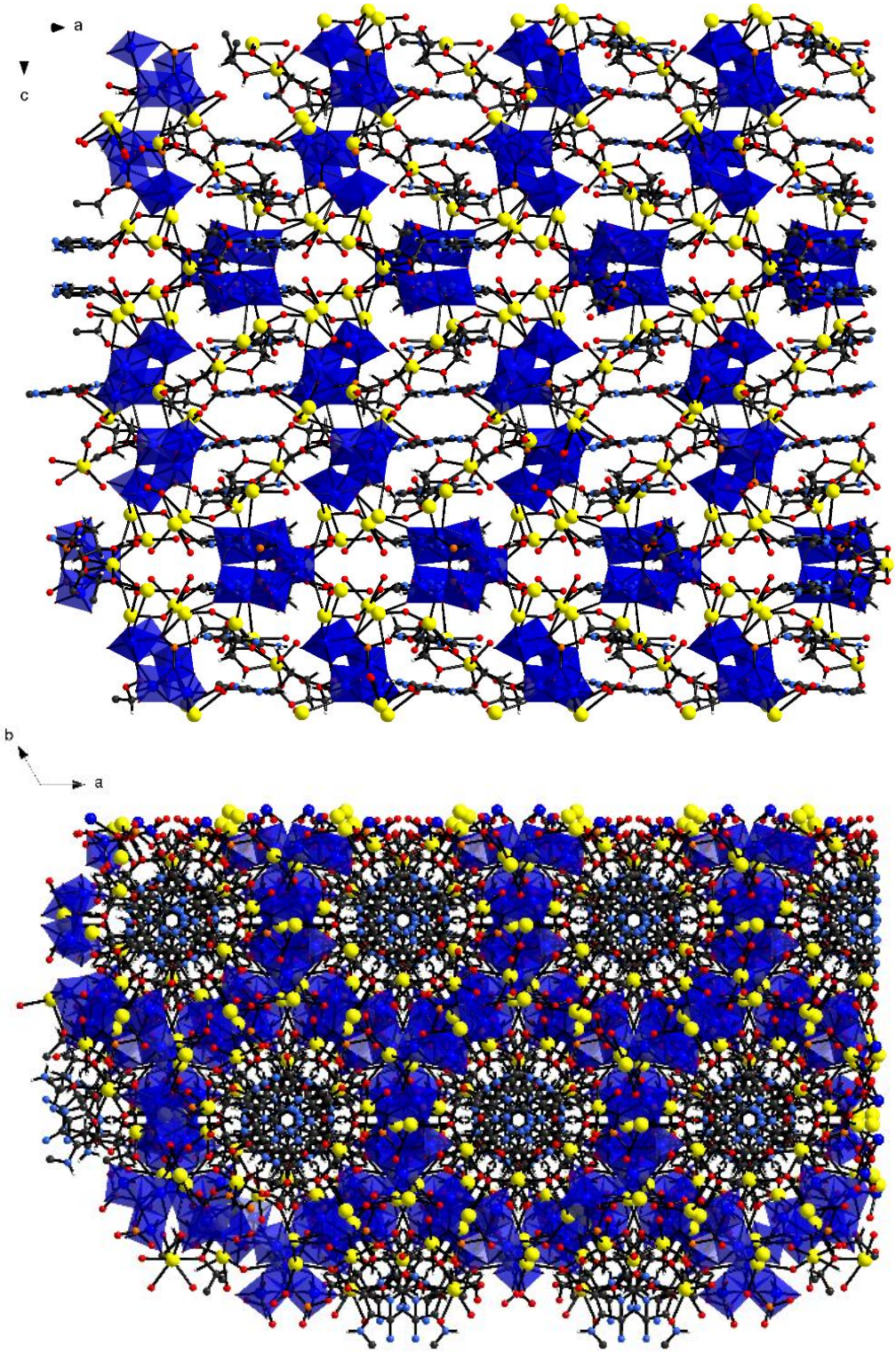

Figure 60 The extended crystal structure of compound 1 from the top and the side shows the connection and dependency of one helix with those adjacent to it. The significance of the Na^+ ions in holding the structure together is also evident. Colour code - Strandberg POM cores (deep blue), N (light blue), O (red), P (orange), Na (yellow) and C (black).

The nature of this gelation was considered intriguing and speculation made over how the tendency of guanine-derivatives to form extended structures such as G-wires, G4-quartetes and G-quadruplexes (see section 1.5.2) would be influenced by the presence of inorganic cores: is it possible for instance, that the helical polymer element of the solid structure might remain present in solution?

3.1.6 Solution Studies

To investigate this key question about what structures formed in a solution of the guanosine Strandberg (**Compound 1**), a number of analytical techniques were used. Unless otherwise stated, all the measurements were carried out under acidic conditions to prevent hydrolysis of the compound, which takes place at pH 7. The precision of the pH readings should however be put into question for two reasons, firstly the diffusion of protons in very viscous mixtures and gels is not the same as standard solutions and secondly the use of deuterated solvents during the NMR experiments also impact the measurement accuracy. This proved problematic as it became clear just how sensitive the aqueous system was to small changes.

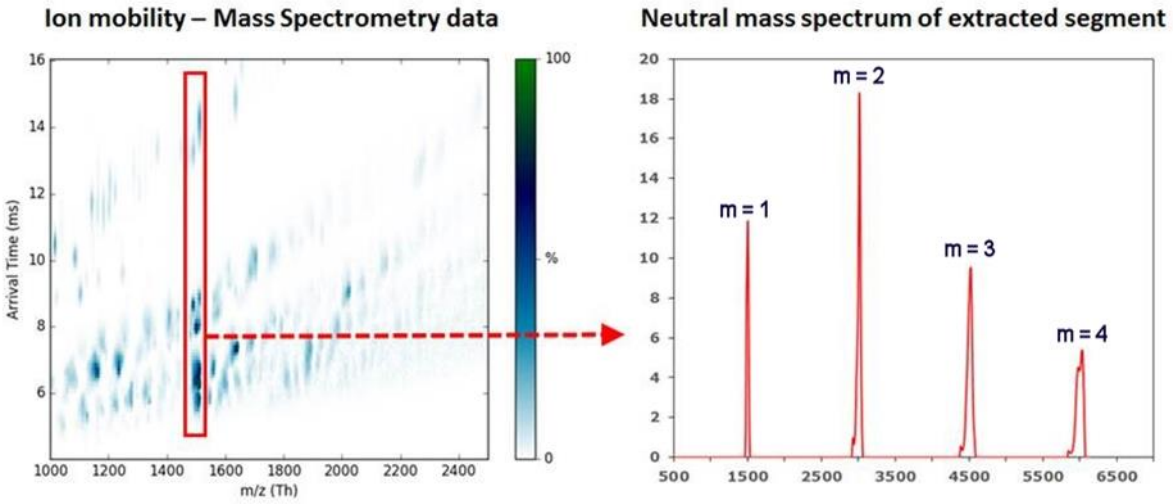

Figure 61 IMS-MS spectrum and interpretation as a neutral mass spectrum. This reveals a series of oligomeric peaks which may be assigned to a $[(C_{10}H_{13}N_5O_8P)_2(Mo_5O_{15})_1(K)W(Na)_X(H)_Y(H_2O)_Z]_m$, suggeting the cluster to be intact in aqueous solution and demonstrating its propensity to aggregate.

To begin with confirmation that the simple monomer unit of a Strandberg core with a pair of guanosine 5’-monophosphate ligands remained intact in solution was made to a satisfactory level using ion-mobility spectroscopy-mass spectroscopy (IMS-MS) and phosphorus NMR. IMS-MS is a technique that separates ions out based on their surface

area as well as their mass to charge ratio (explained in more detail in section 3.2.5) and made it possible to isolate a peak envelope assignable to a $[(GMP)_2(Mo_5O_{15})(K)_W(Na)_X(H)Y(H_2O)_Z]_m$ series where (GMP = $C_{10}H_{13}N_5O_8P$), see **Figure 61**. Presence of the P-O-R bond between POM core and ligand was demonstrated using ^{31}P NMR with a doublet of a doublet at 0.98 ppm (**Figure 62**).

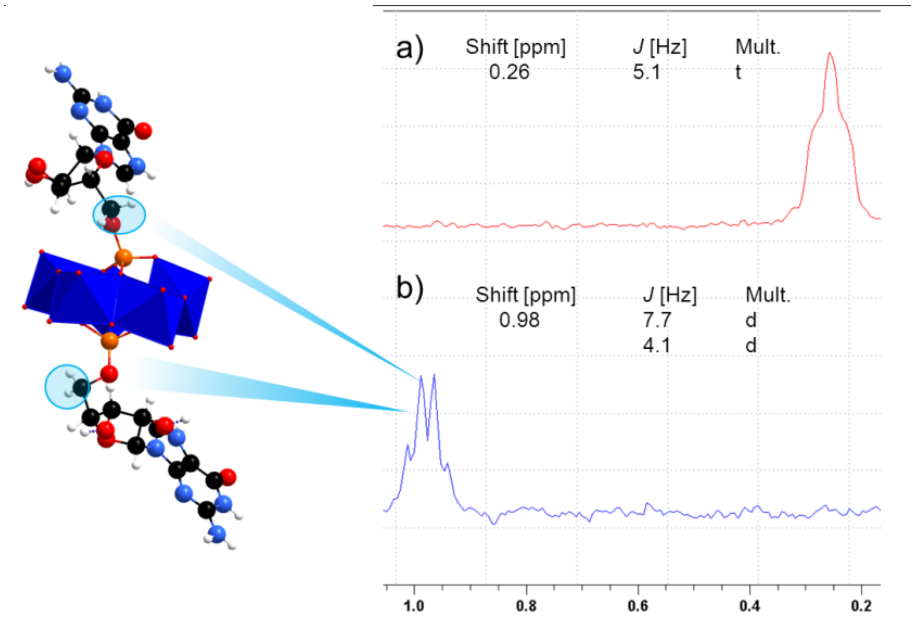

Figure 62 a) ^{31}P-NMR-Spectrum of GMP (c = 2.4 mg/ml; pD = 2.92); b) ^{31}P-NMR-Spectrum of compound 1 (c = 5.6 mg/ml ; pD = 2.92).The protons coupling to the P-nucleus are indicated by blue circles. Colour code - Strandberg POM cores (deep blue), N (light blue), O (red), P (orange), Na (yellow) and C (black).

Further analysis was made using NMR, this time in an attempt to understand more about the extended structure forming in the solution by collecting ^1H NMR data at varying conditions and also making diffusion order spectroscopy (DOSY) NMR measurements.[364] However, a plot of the peak integrations over the concentration measured demonstrated that the secondary structures were too big to be detected using this technique. NMR was also limited by the LMWG properties as using solutions of the compound at concentrations detectable for NMR resulted in a gel too viscous for the measurements to be made.

To continue investigating the nature of the structures in solution, dynamic light scattering (DLS) measurements were made. DLS is a method that allows determination of the particle size distribution of colloidal-type formations by measuring the scattering angle θ of a laser beam shone through a sample.[365] This technique will only give an accurate

reading in very homogenous solutions which unfortunately was not the case with the guanosine Strandberg (**Compound 1**) measurements.

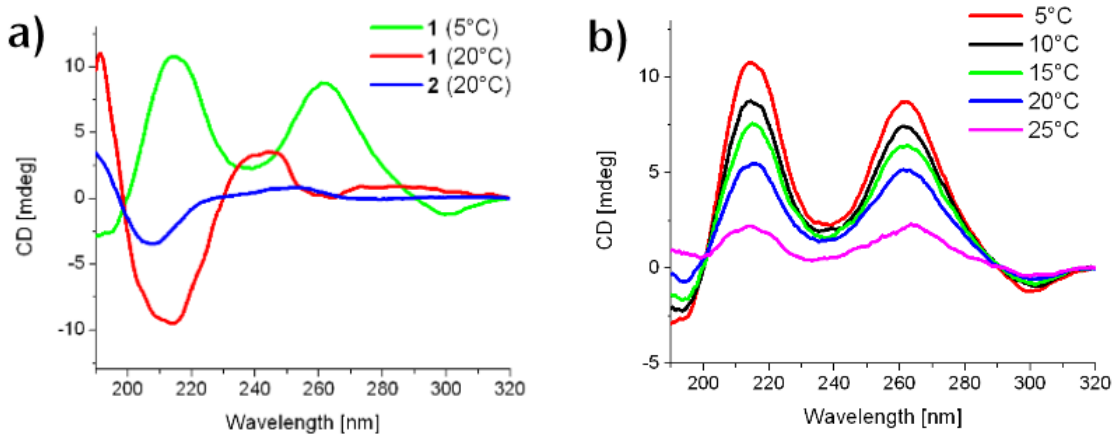

Figure 63 a) CD spectra of guanosine Strandberg (1) in a 0.01cm cell at 20°C and a 0.001cm cell at 5°C and GMP reference spectrum (2) in a 0.01cm pathlength cell. b) Temperature dependence of CD spectrum of 1 after cooling down to 5°C. All spectra were measured at concentration of 4mM and pH 1.2.

More information on the extended structure was obtained using circular dichroism (CD) spectroscopy, a technique commonly used to analyse the solution-based secondary structures of biomolecules, by detecting whether any left- or right-circularly polarized light passing through a compound has been absorbed.[366] The remaining proportions of the polarized light, indicates the proportions of chiral enantiomers present because d- and l-enantiomers absorb light rotating in opposing directions. Apart from high-resolution X-ray diffraction, circular dichroism is the only technique that can determine absolute stereostructure, independent of the physical form of a substance and unlike XRD, CD does not rely on the availability of high quality single crystals. In fact, CD measurements can be taken in a variety of forms, including solution, gas phase, solid dispersions (CD of randomly oriented molecules), films, gels, liquid crystals, and even on monocrystals (CD of oriented systems). The reason this makes CD so useful is because complex chiral systems are commonly observed in biomolecular systems, which are generally systems that take place in solutions and so a measurement of a crystal of such a system could give deceptive results as the structure is likely to be altered in its different environments. The biomolecules most commonly measured by such techniques are proteins, RNA and DNA and the CD measurements result in spectra with characteristic patterns which are associated with various types of folding, whether it be the α-helices and β-sheets of a peptide or the double helix and G-quadruplexes formed by nucleic acids.

By comparing the CD measurements of the guanosine Strandberg (**Compound 1**) and the GMP starting material, it was evident that the POM hybrid was forming an extended ordered structure different in nature to guanosine 5'-monophosphate alone, and ruled out disassociation of GMP and the POM core (**Figure 63a**). These signals were also different to that of the Z-DNA CD measurement which has a negative minimum at 290 nm and positive maximum at 260 nm. Results of CD measurements for the guanosine Strandberg (**1**) at varying temperatures indicate that the structure is more ordered when cooler. **Figure 63b** shows how **Compound 1** at 20°C has a weak, but distinct signal that strengthens on cooling to 5 °C and suggesting that a greater level of structure has formed. Interestingly on reheating the cooled sample back up to 25°C, the original signal does not reform, suggesting the presence of a secondary structure.

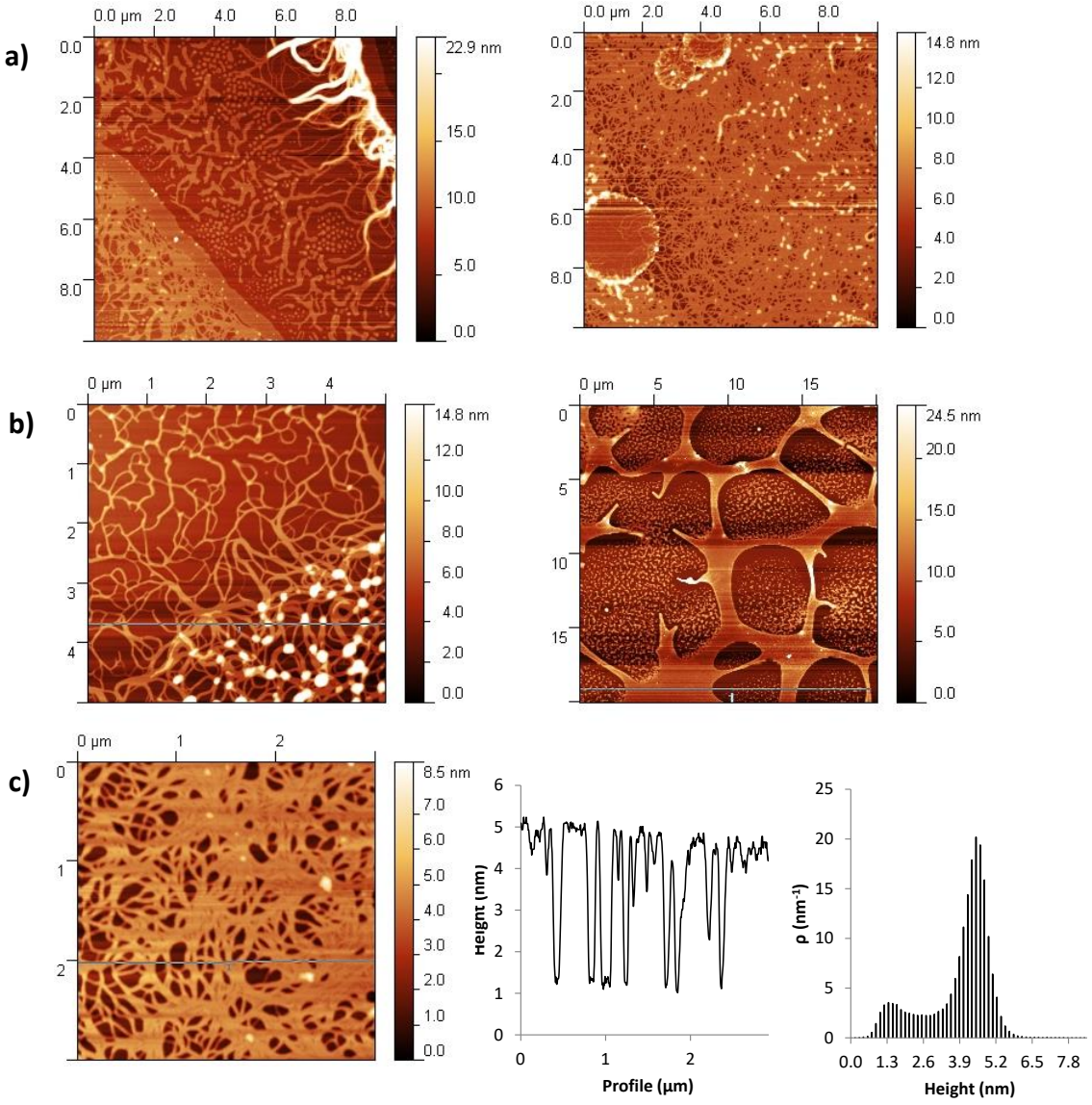

Figure 64 AFM height pictures: a) taken after 3 days of aging, b) taken after 5 days of aging and c) taken after 3 days with corresponding profile extract (middle) and height distribution (right).

The final technique used on the guanosine-Strandberg (**Compound 1**) solution was atomic force microscopy (AFM). This technique is a form of scanning probe microscopy (SPM) where surface forces are explored using a mechanical probe resulting in imaging on nanometre scale.[367] AFM pictures were taken in semi-contact mode, 3 to 5 days after drop casting 10 µL of guanosine Strandberg (**Compound 1**) solution on a freshly cleaved mica surface (**Figure 64**). The resulting fibres displayed a noticeable helical twist which did not change with age although this varied dependent on local concentration. Despite this, the diameter of the fibres were systematically between 3.5 and 4.0 nm which is wider than the fibres that form when GMP self-assembles on its own, known to between 1.5-2.0 nm.[306,310] Although the 10 nm tip of the cantilever limited measurements of greater precision, this result indicated that the compound in solution might form fibres made from GMP with an inorganic core, which would have a diameter of 3.85 nm. Any interactions or aggregation taking place on the slightly negatively charged mica surface would be unlikely to be a result of the anionic POM hybrid and would instead be due to either the Na^+ cations or any free guanosine moieties.

3.1.7 Guanosine Enantiomer

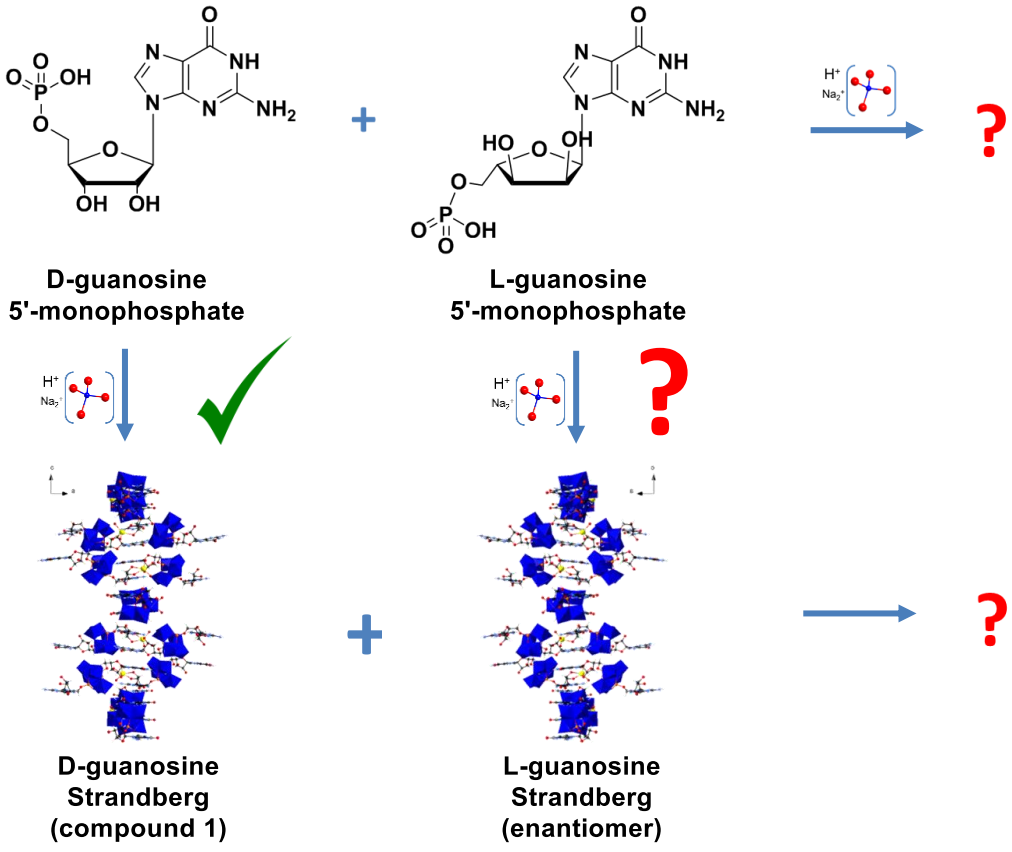

Figure 65 Speculation over possible outcomes of using one enantiomer of guanosine 5'-monophospate or a mixture of both under conditions that form the guanosine Strandberg

The double-helix element of the guanosine Strandberg (**Compound 1**) crystal structure has a left-handed screw axis, the direction of which is thought to be caused by the chiral nature of the nucleobase moiety. It is the D-enantiomer of guanosine 5'-monophosphate that is used in the synthesis of **Compound 1** and so it was hypothesised that using the L-enantiomer during the reaction instead would result in a product with a double helix that turns in the opposite direction (**Figure 65**).

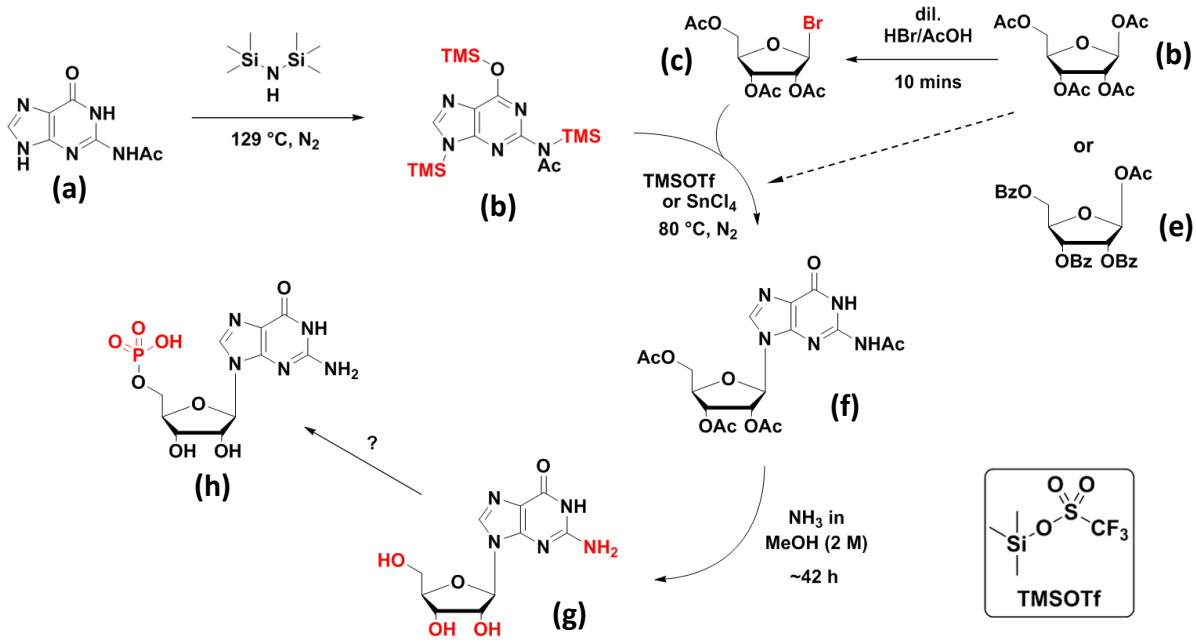

Figure 66 Scheme showing Method A for the synthesis of guanosine '5-monophosphate (h). acetylguanine (a) is silylated to give intermediate (b). (f) is formed through the addition of an activated sugar (c) or protected sugar (d)/(e) to (b) in the presence of a Lewis base. (f) is deprotected to give guanosine (g) and finally phosphorylated to give (h).

In order to test this hypothesis, it was necessary to synthesise the L-enantiomer of GMP (**Compound 2**) as only the D-enantiomer was commercially available. The ribose sugar was used as a starting material and although it was the L-ribose that would lead to the L-enantiomer, it was significantly more expensive to obtain than the R-ribose. For this reason, R-ribose was used during the development of the synthetic route which once established would be easily substituted with L-ribose leading to the desired chiral product. The chosen synthetic route began by binding the sugar to the guanine and followed on with a phosphorylation. The basic steps consisted of activating a protected sugar, protecting the guanine ring, connecting the guanine and sugar together, deprotecting the resulting molecule (to make guanosine) and finally phosphorylate it.[368–370] This rough outline was refined down to a couple of different procedures, based on syntheses found in the literature: Method A (**Figure 66**) and Method B (**Figure 67**) both of

which were completed through to the deprotection stage where trace amounts of the product, guanosine was detected. The level of yield and purity obtained was, unfortunately not sufficient to allow for completion of the last step and as a result this aspect of the project was set aside as future work.

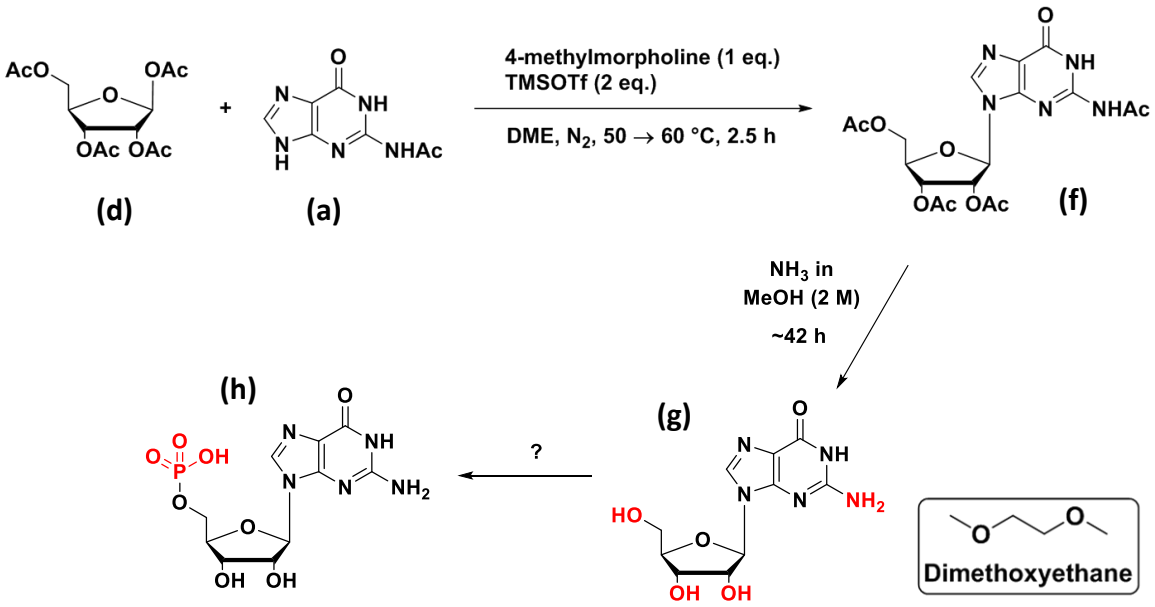

Figure 67 A scheme showing Method B for the synthesis of guanosine '5-monophosphate (H). A protected sugar (d) and acetylguanine (a) are left to react in the presence of base. (f) is deprotected to give guanosine (g) and finally phosphorylated to give (h).

3.1.8 Section Summary

This section described how on acidification of an aqueous solution of sodium molybdate and guanosine 5'-monophosphate, an organic-inorganic POM hybrid (**Compound 1**) forms, the crystal structure of which has a striking resemblance to that of the Z-DNA double helix. The crystal structure of guanosine Strandberg (**Compound 1**) is composed of discrete doubly functionalised organic-inorganic POM hybrid monomers: two guanosine 5'-monophosphate (GMP) ligands covalently bonded to a Strandberg-type POM core. The GMP ligands of these monomers aggregate together, resulting in stacks around which the POM cores spiral, forming a recognisable double helix shape. Simple inorganic and biomolecular building blocks self-assembling into a structure comparable to DNA was considered very interesting to those familiar to the work of Cairn-Smith, who theorised that biomolecules first formed by templating off information-containing, self-replicating inorganic structures. As a result some studies were carried out on **Compound 1** to further compare its structure with Z-DNA.

Although the guanosine Strandberg (**Compound 1**) was shown to have almost identical structural dimensions to the Z-DNA double helix, some key differences between the structures were highlighted. The POM hybrid double helix structure is itself a component of a larger crystalline network and not a polymer like the nucleic acid. It is made up of monomers, the two individual GMP ligands of which are each central to adjacent double helices. The GMP ligands are not neatly "base-paired" in the same way as the purine-pyrimidine H-bonded pairs are in Z-DNA, but rather stacked and interacting with every other surrounding ligand. Also, unlike Z-DNA the organic-inorganic POM hybrid monomers are negatively charged ions and the resulting Na^+ counterions play a crucial role in the bonding of the structure. These ionic and intermolecular interactions holding the structure together in solid form will of course function differently when the compound is dissolved. Interactions of some form however were clearly occurring due to the gelation of the aqueous mixture and so various techniques were used in order to explore the characteristics of **Compound 1** in solution as an attempt to discern its structural nature and whether the double helix strands remain intact.

To begin with the stability of the POM hybrid monomers themselves was confirmed using IMS-MS and ^{31}P NMR. Further NMR experiments were then carried out to detect

secondary structure, but unfortunately neither ^{1}H NMR nor DOSY could provide any information due to the viscosity of the samples. Study of the gelation itself was however interesting as the critical gelation concentration (CGC) of the hydrogel was shown to be 50 times higher than GMP alone, a well-known LMWG. DLS measurements were also taken but the solutions were not uniform enough to give reliable results. CD suggested that an ordered structure was formed in solution different to that of GMP alone, indicating that the GMP had remained associated to the POM core in solution. The CD spectrum was also shown to vary with temperature demonstrating how cooling from 20°C to 5°C and back again resulted in an irreversible structural change. AFM showed evidence of strands of appropriate dimensions to account for the guanosine Strandberg (**Compound 1**) double helix. Gel electrophoresis was used to probe the bioactivity of **Compound 1** and demonstrated the ability of the POM hybrid to form non-covalent adducts with natural plasmids.

The nature of the left-handed screw-axis was thought to be caused by the chirality of the guanosine 5'-monophosphate moieties. It was hypothesised that by using the other enantiomer of GMP as a starting a material, a helix turning in the opposite direction would form. However, these ideas were never explored as synthesis of the necessary GMP enantiomer in large enough quantities was not achieved.

In conclusion, a bio-inorganic POM hybrid was synthesised and its crystal and solution phase structures explored. In its crystal form the guanosine Strandberg (**Compound 1**) assembled into a structure almost identical to that of Z-DNA and evidence suggested that an ordered macrostructure also formed in solution.

3.2 Extended POM Hybrid Structure: Directed Synthesis

In contrast to the previous section (3.1), this chapter explores a POM hybrid extended system using an alternative approach. As detailed in the introduction, unlike purely inorganic POM clusters whose synthesis is often difficult to predict, organic-inorganic POM hybrids can be manipulated with a higher level of tuneablity and control. Specifically, instead of relying on the self-assembly process for structure formation, as with the guanosine Strandberg double helix, the functionality of organic chemistry is used to direct and control the formation of the structure. The inorganic compounds used for this exploration are the asymmetric Mn-Anderson hybrids, for which a robust isolation method has previously been developed by Cronin et al. in 2013 (see section 1.3.9.2). Straightforward access to such compounds in large quantities allows for the development of more complex POM hybrid architectures such as their use as side chains in polymers and surfaces or in the formation of vesicles, oligomers or dendrimers (**Figure 68**). Here, it is the design and synthesis of discrete oligomers that is investigated and developed.

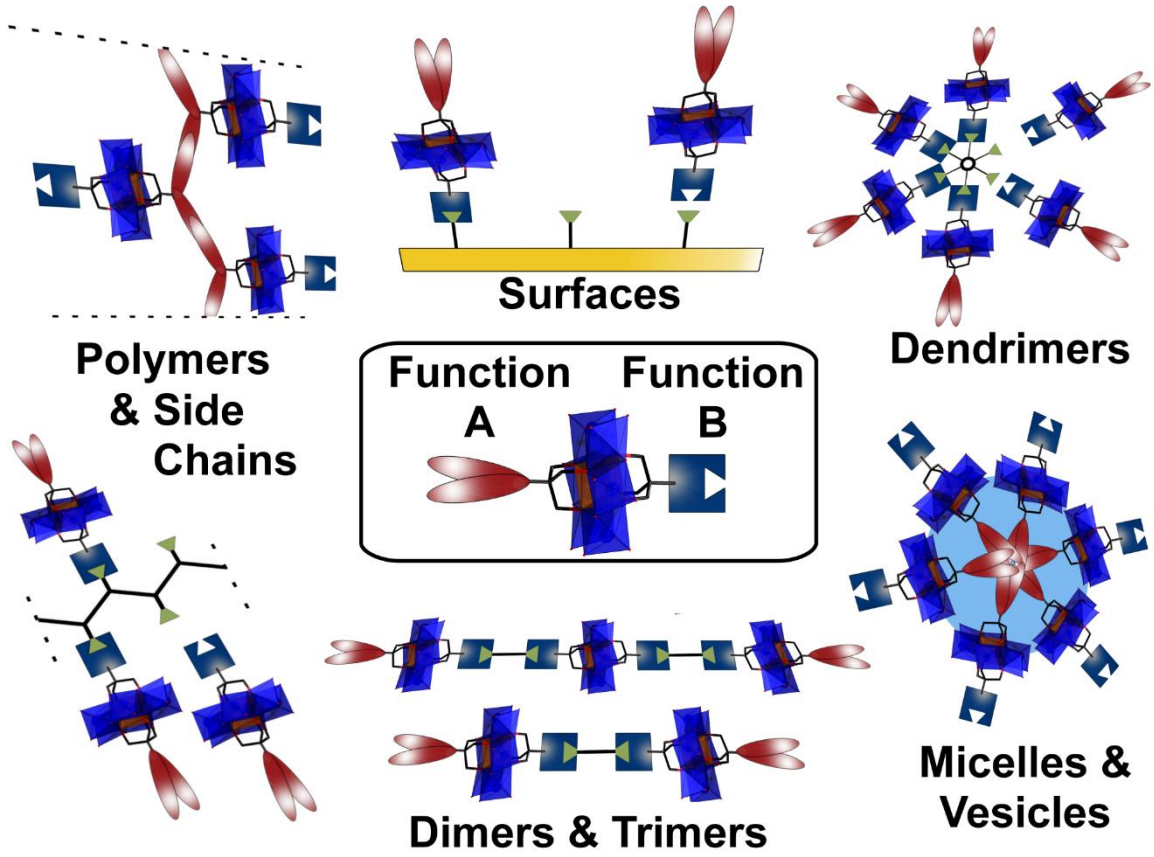

Figure 68 Examples of the use of the now easily isolatable asymmetric Mn-Anderson hybrids including dendrimer, oligomer and vesicle formation as well as incorporation onto surfaces and polymers. (Central blue polyhedral are the Anderson POM core).

3.2.1 Coupling of Asymmetric POM Hybrids

Although section 1.4 has shown that polymerisation of POM hybrids is not uncommon, it has so far had major restrictions. Polymerisation is only possible for the bi-functionalised clusters, generally Anderson hybrids, as mono-functionalised clusters are limited to the formation of dimers. Using bi-functionalised POM hybrids in this way is however problematic due to the monomers reacting with themselves and resulting in polymers of "infinite" or undeterminable lengths. **Figure 69** demonstrates dimer and uncontrolled polymer formations for an AA coupling mechanism where a functional group is able to form a link with itself and an AB coupling mechanism where two different functional groups (A and B) react to form a bond.

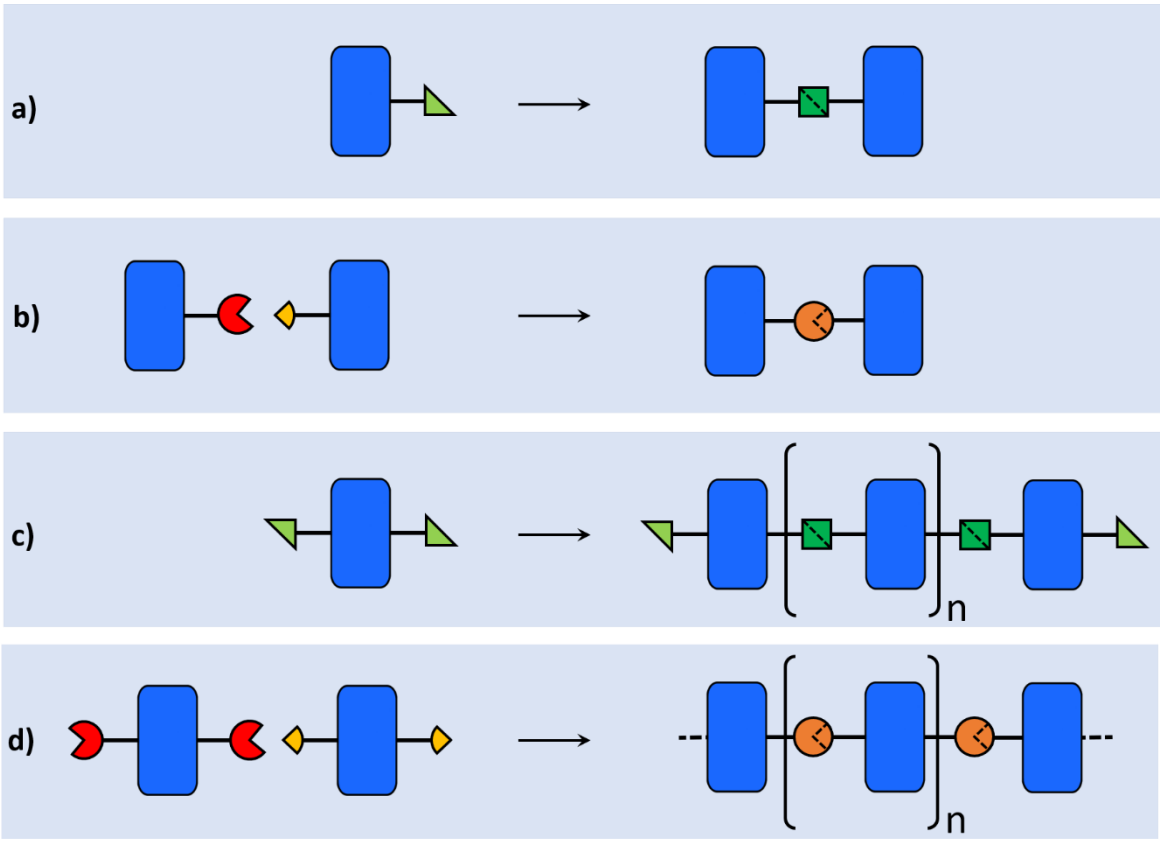

Figure 69 Reaction of mono-functionalised POM hybrids result in dimer formation (a & b) whereas reaction of bi-functionalised POM hybrids results in uncontrolled polymerisation (c & d). This is the case for both AA coupling mechanisms (a & c) and AB coupling mechanisms (b & d).

Introduction of the asymmetric (bi-)functionalised POM hybrid allows for two different types of functional group to be connected to the same cluster. Chain formation using such asymmetric clusters will however still result in uncontrolled proliferation if there are two active moieties on a cluster at the same time (**Figure 70a**). To have complete control over the polymerisation of this system it is essential for clusters to have only one active

functional group at any given time, which means functionalising an asymmetric cluster with one active group and one blocking group. This blocking group can later be activated allowing for controlled build-up of the chain, two POM cores at a time. This begins with formation of a dimer the blocking groups of which, once activated, are able to react with asymmetric monomers, one at each end, forming a tetramer and so on, making a chain of any length containing an even number of POM cores (**Figure 70b**). This oligomerisation method cannot take place in a controlled manner using AA coupling as the monomer and dimer units will react together in a number of ways giving a mixture of products (**Figure 70c**).

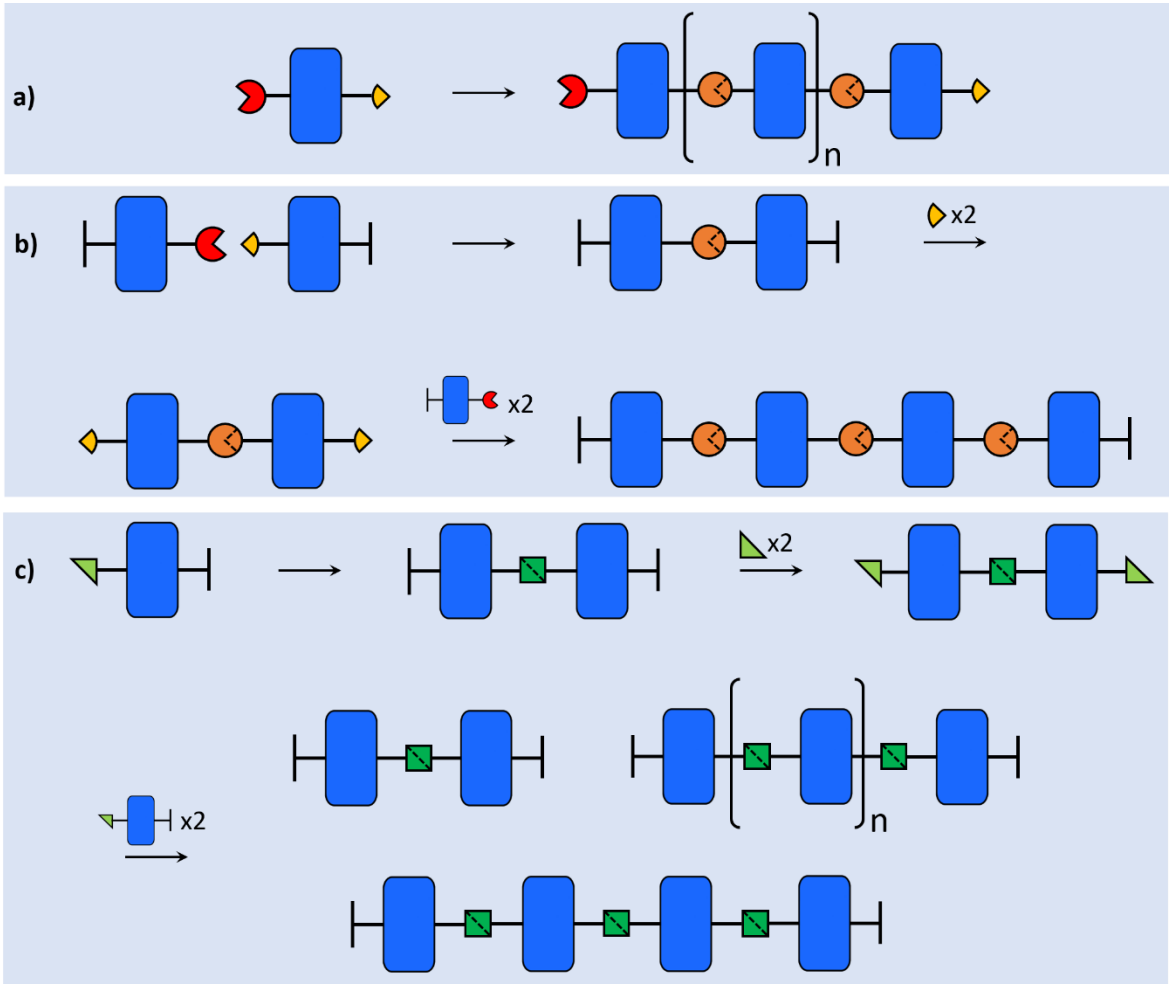

Figure 70 a) Uncontrolled polymerisation via AB coupling of an asymmetric POM hybrid. b) Sequence demonstrating controlled oligomerisation using AB coupling, firstly the formation of a dimer from asymmetric POM hybrids each containing a single functional group and a blocking group which is then functionalised allowing for the addition of two more monomers. c) Scheme highlighting how such a sequence using an AA coupling mechanism results in a mixture of products.

Now in order to also obtain the odd-numbered POM hybrid oligomer series, it is necessary to begin with a trimer which has to be made from two asymmetric monomers connecting to one symmetric monomer and, like in the previous example, is only

controllable when an AB coupling mechanism is applied (**Figure 71**). This approach, just like with the even-numbered POM core series, allows for the controlled and systematic build-up of an oligomer sequence two clusters at a time: trimer, pentamer, heptamer etc.

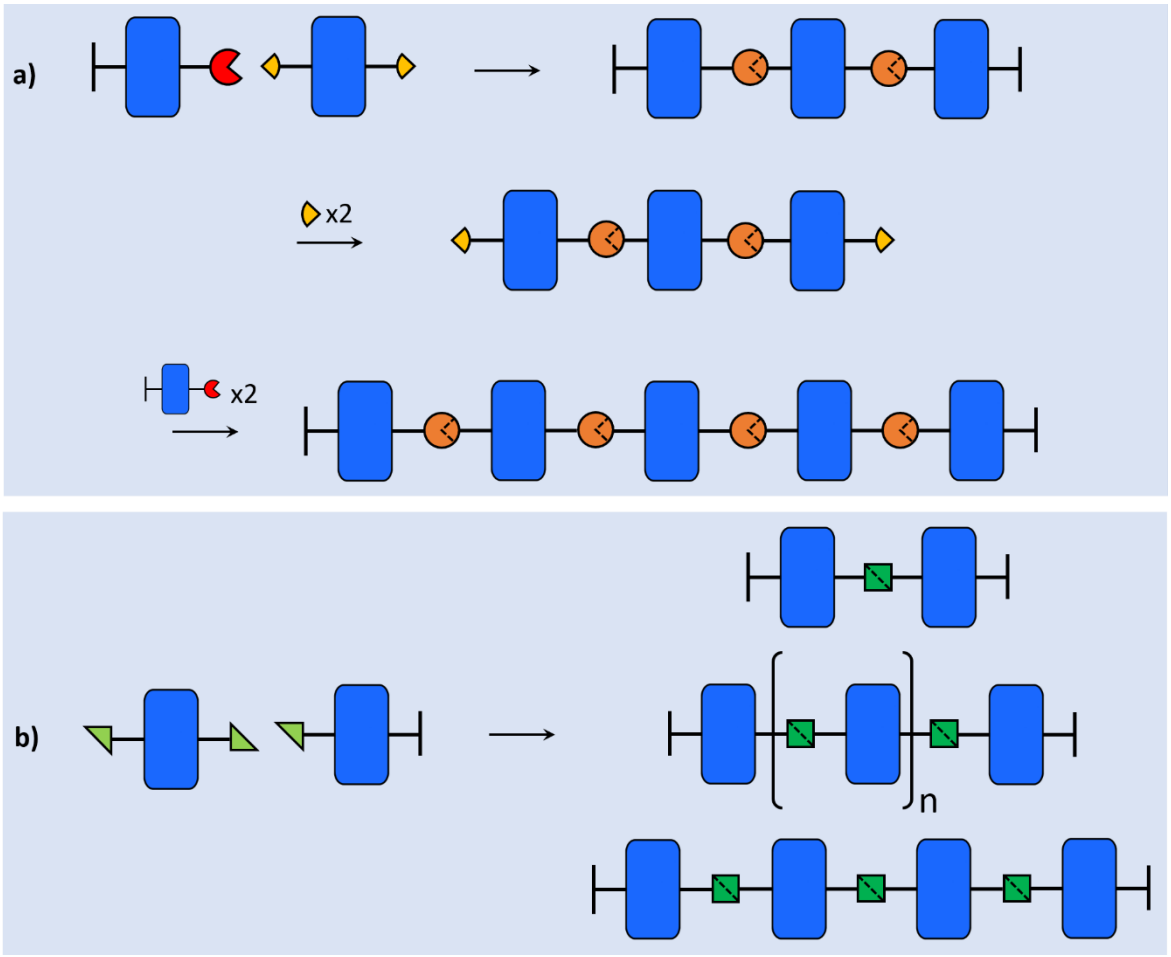

Figure 71 a) Scheme showing how formation of a trimer from symmetric and asymmetric POM hybrid monomers using AA coupling results in a mixture of products whereas b) using an AB coupling mechanism instead gives the necessary amount of control for only the trimer to form, which can then be activated, and another two monomers added to form a pentamer.

This therefore explains that for successful oligomer formation an asymmetric POM hybrid with an AB coupling mechanism is necessary. Working within a POM hybrid system however, adds some constraints to what specific AB coupling mechanisms can be used. Firstly, pH needs to be controlled so that the POM cluster, in this case the Mn-Anderson hybrid, is not destroyed. POMs generally decompose in basic conditions therefore a mechanism which utilizes acidic conditions is preferred. In addition to this, finding a solvent compatible both with the organic moieties and the inorganic core could prove challenging as the majority of POM systems are formed in aqueous conditions. In general however, POM hybrid anions will be soluble in organic solvents such as acetonitrile or DMF when coupled with large organic counterions such as TBA^{+}.[1] These reaction

specifications could be met by the "Click" chemistry discussed in sections 1.2.3 and 1.2.4 and especially the Cu-catalysed azide-alkyne cycloaddition (CuAAC) reaction (**Figure 72**) that has already been shown to be effective in the coupling of a Keggin [$PW_{11}O_{39}Sn$] and a Dawson [$P_2W_{17}O_{16}Sn$] cluster (**Figure 15**).[115] In this previously published method, the reaction took place in the presence of copper sulfate ($CuSO_4$) and sodium ascorbate in a water/MeCN mixture. Attempting this method exactly however, led to the decomposition of the Mn-Anderson hybrid system, and so an adapted version of the reaction was developed. After it was found that copper powder and heating under microwave also produced the blue insoluble compound that suggested Mn-Anderson decomposition, CuI was tried in catalytic amounts and found not to decompose the POM. However, only the starting materials were observed by mass spectroscopy which could be explained by the observation made by Micoine et al[115] that small amounts of copper may adsorb onto the POM surface and so the quantity of CuI was increased to a molar equivalent. Although this time the reaction was shown to take place, the mixture would occasionally turn green, suggesting oxidation of the copper. To overcome this issue the reaction was carried out under inert conditions. Finally, using CuI as the catalytic copper source, DIEA (N,N-diisopropylethylamine) as a base, excluding oxygen and water from the reaction by using nitrogen gas and either MeCN or DMF proved an effective combination.

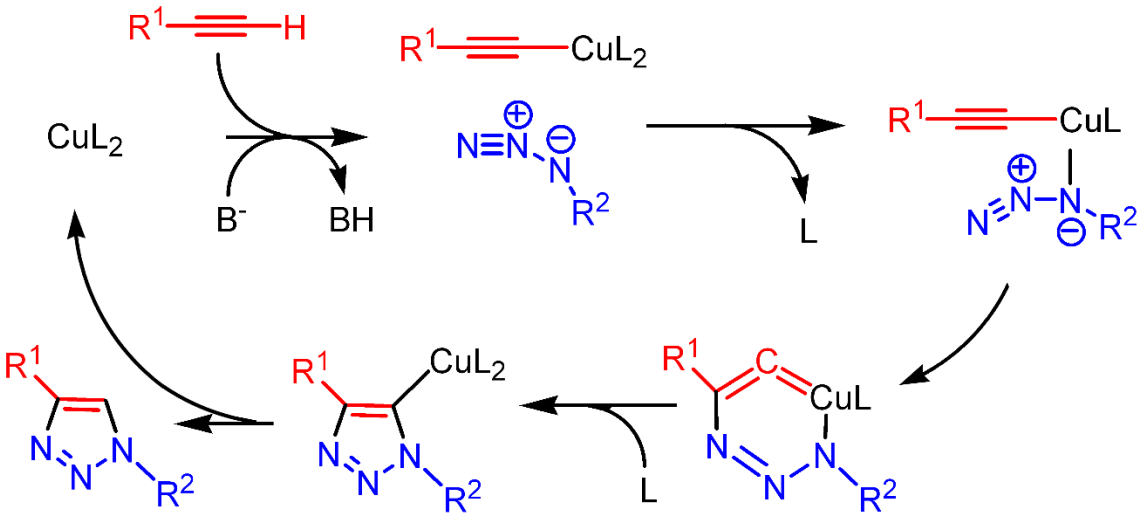

Figure 72 Reaction scheme showing the proposed intermediates in the Cu-catalysed azide-alkyne cycloaddition based on DFT calculations. L = MeCN or H_2O.

3.2.2 Building Block Synthesis

Having established a coupling mechanism appropriate for Mn-Anderson oligomerisation, the necessary POM hybrid building blocks had to be constructed, two asymmetric Mn-Andersons and one symmetric Mn-Anderson. Suitable azide and alkyne compounds needed to be selected with which to functionalise the asymmetric Mn-Anderson hybrids, with commercially availability and, in the case of the azide reactant, limited reactivity. These compounds also required the ability to bind to the Mn-Anderson hybrid in the first place, whether through pre- or post-functionalisation. 4-azidobenzoic acid and 5-hexynoic acid were considered suitable choices because it is generally straightforward to react a carboxylic acid with an amine group, allowing for direct functionalisation of the classic TRIS ligands that hybridise an Anderson cluster.

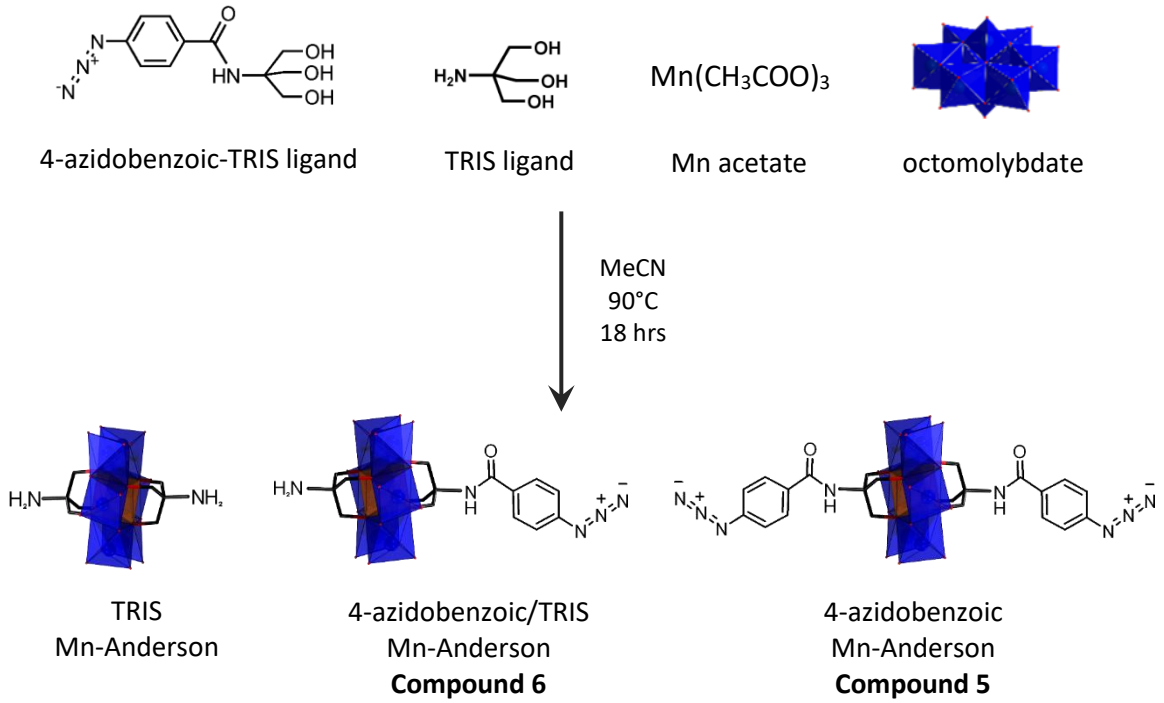

Figure 73 The pre-functionalisation approach used for the synthesis of the 4-azidobenzoic Mn-Anderson **(5)** and 4-azidobenzoic/TRIS Mn-Anderson **(6)** building blocks.

In order to attach these compounds asymmetrically onto the POM, pre-functionalisation or post-functionalisation approaches can be taken. Pre-functionalisation involves a one-pot reaction similar the synthesis of the asymmetric Mn-Anderson synthesis described in section 1.3.9.2, where two variations of the TRIS ligand, a molybdenum source and a manganese source are reacted together forming an asymmetric and two symmetric Mn-Anderson products which are then separated out using RP-LC. Post-functionalisation makes use of the “Universal” asymmetric Mn-Anderson (**Compound 3**, also discussed in

section 1.3.9.2) which allows for functionalisation of the two ligands separately due to the presence of a protecting group on one side. The first side has an amine group immediately available for functionalisation and the second side a protecting FMOC-group which when removed reveals another amine group that can either be further functionalised or left alone (**Figure 34**). Choosing between which of these two approaches to use depends not only on the reactivity of the specific compounds used but also on the difference in polarity between the ligands: two ligands of comparable hydrophilicity will not separate out distinctly using chromatography and so in these cases it is vital to use the "Universal" asymmetric Mn-Anderson Compound **3**) as the asymmetric aspect of the molecule can be obtained before specific functionalisation occurs.

For the azide starting material, the pre-functionalisation approach was used as the polarity of the azide group was significantly different from the amine of the classic TRIS ligand and the necessary 4-azidobenzoic-TRIS ligand (**Compound 4**) starting material could easily be made overnight in good yield. Synthesis of this involved firstly the formation of a carbonic anhydride precursor using ethyl chloroformate with N-methylmorpholine as a base followed by addition of TRIS ligand and tiethylamine (TEA). The product was then extracted using a water/ethyl acetate separation as the TRIS ligand was more soluble in water than the product (**Compound 4**). This azide ligand, along with TRIS ligand was used to synthesise a mixture of symmetric (**Compound 5**) and asymmetric (**Compound 6**) 4-azidobenzoic Mn-Anderson hybrids (**Figure 73**). These compounds were isolated using the RP-LC separation method described in section 1.3.9.2 with a mobile phase of MeCN and TBA^+ buffer. They were then purified through crystallisation under slow Et_2O diffusion usually forming a fine orange powder and occasionally larger crystals, but never of diffractable quality.

In contrast, a post-functionalisation method was used to synthesise the alkyne starting material because synthesising an alkyne-TRIS ligand in quantities large enough for pre-functionalisation proved challenging. Asymmetric 5-hexynoic/TRIS Mn-Anderson hybrid (**Compound 7**) was synthesised by functionalising the "Universal" asymmetric Mn-Anderson precursor (**Compound 3**) with 5-hexynoic acid followed by deprotection of the FMOC group, leaving an amine group behind (**Figure 74**).

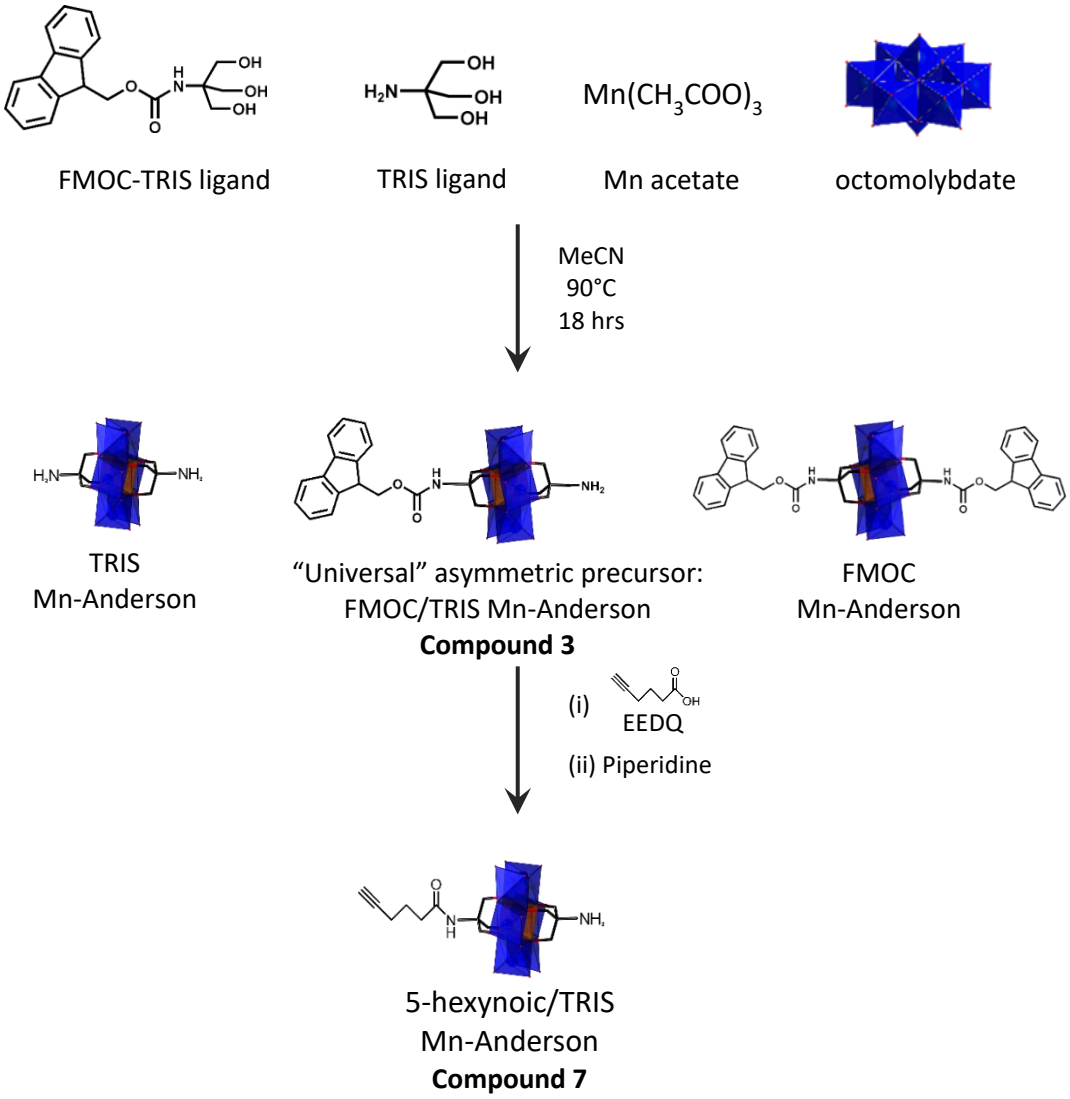

Figure 74 The post-functionalisation method used for the synthesis of the 5-hexynoic Mn-Anderson **(7)** building block is an adaptation of the method described in section 1.3.9.2.

3.2.3 Mn-Anderson Oligomer Synthesis

Having successfully synthesised and isolated the building blocks (**Table 2**), they could then be used to assemble oligomers, a task which involved several stages of synthesis, isolation and purification. To begin with (see **Figure 75**), a Mn-Anderson hybrid dimer (**Compound 8**) was synthesised by reacting an asymmetric 5-hexynoic/TRIS Mn-Anderson hybrid (**Compound 7**) and an asymmetric 4-azidobenzoic/TRIS Mn-Anderson hybrid (**Compound 6**) together, in the presence of a copper catalyst in a nitrogen atmosphere for the CuAAC reaction described in section 3.2.1. In a similar manner, a Mn-Anderson hybrid trimer (**Compound 9**) was synthesised by reacting an asymmetric 5-hexynoic/TRIS Mn-Anderson hybrid (**Compound 7**) and a symmetric 4-azidobenzoic Mn-Anderson hybrid (**Compound 5**) together.

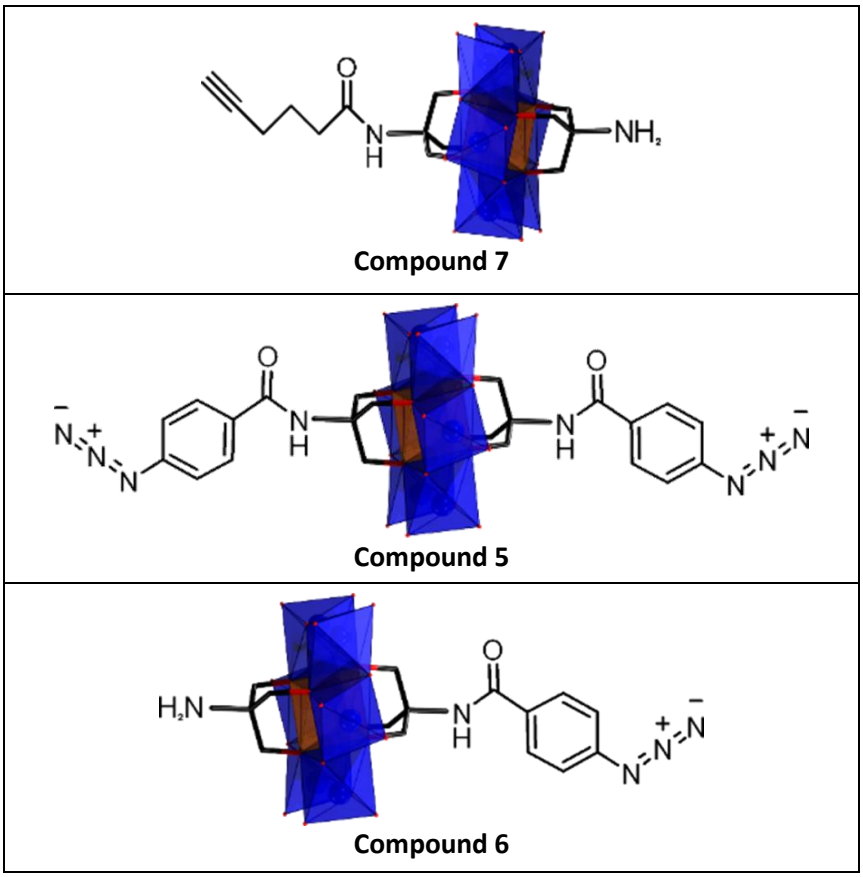

Table 2 A table showing the POM hybrid starting materials prepared for the CuAAC couplings: 5-hexynoic/TRIS Mn-Anderson (top) **(7)**, symmetric 4-azidobenzoic Mn-Anderson hybrid (middle) **(5)** and asymmetric 4-azidobenzoic/TRIS Mn-Anderson hybrid (bottom) **(6)**.

In order to make oligomers of a greater length, it was necessary to functionalise the end groups (TRIS moieties) of the dimer (**Compound 8**) and trimer (**Compound 9**) with 5-hexynoic acid to give a Mn-Anderson dimer (5-hexynoic) (**Compound 10**) and a Mn-Anderson trimer (5-hexynoic) (**Compound 11**). The reaction occurred with an overnight MeCN reflux in the presence of EEDQ (2-ethoxy-ethoxycarbonyl-1,2-dihydroquinoline). This allowed the previously unreactive groups to react with asymmetric 4-azidobenzoic/TRIS Mn-Anderson hybrid (**Compound 7**) (**Figure 76**) adding two new POM cores to the chain, one on each end. In this way, it was possible to extend from a dimer (**Compound 8**) to a tetramer (**Compound 12**) and from a trimer (**Compound 9**) to a pentamer (**Compound 13**) lengthening the chain symmetrically in both directions (**Figure 77**).

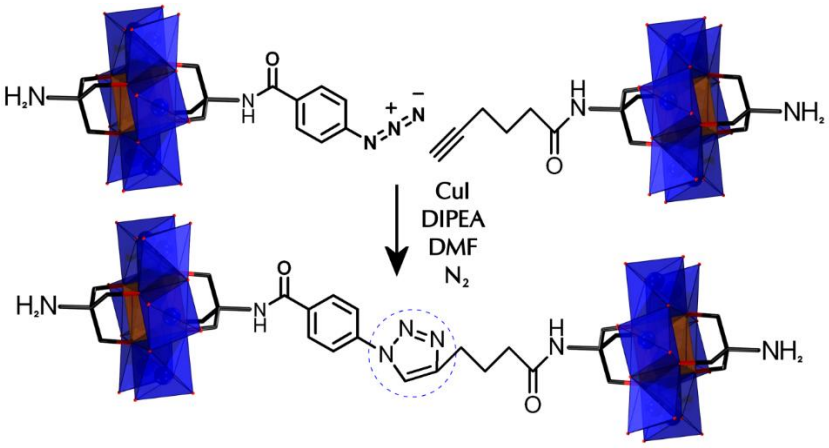

Figure 75 Scheme showing the formation of the Mn-Anderson dimer **(8)** via the copper catalysed azide-alkyne coupling of the building blocks 4-azidobenzoic/TRIS **(6)** and 5-hexynoic/TRIS Mn-Anderson **(7)**. Formation of the timer is similar but uses symmetric 4-azidobenzoic Mn-Anderson instead of the asymmetric version.

All the crude oligomer mixtures were separated from the excess monomer using RP-LC in similar conditions to the building block syntheses themselves. Again, crystallisation for single-crystal X-ray diffraction was not successful, but slow Et_2O diffusion at 18°C allowed for precipitation of a fine orange-brown powder (longer chains were darker in colour) of good purity.

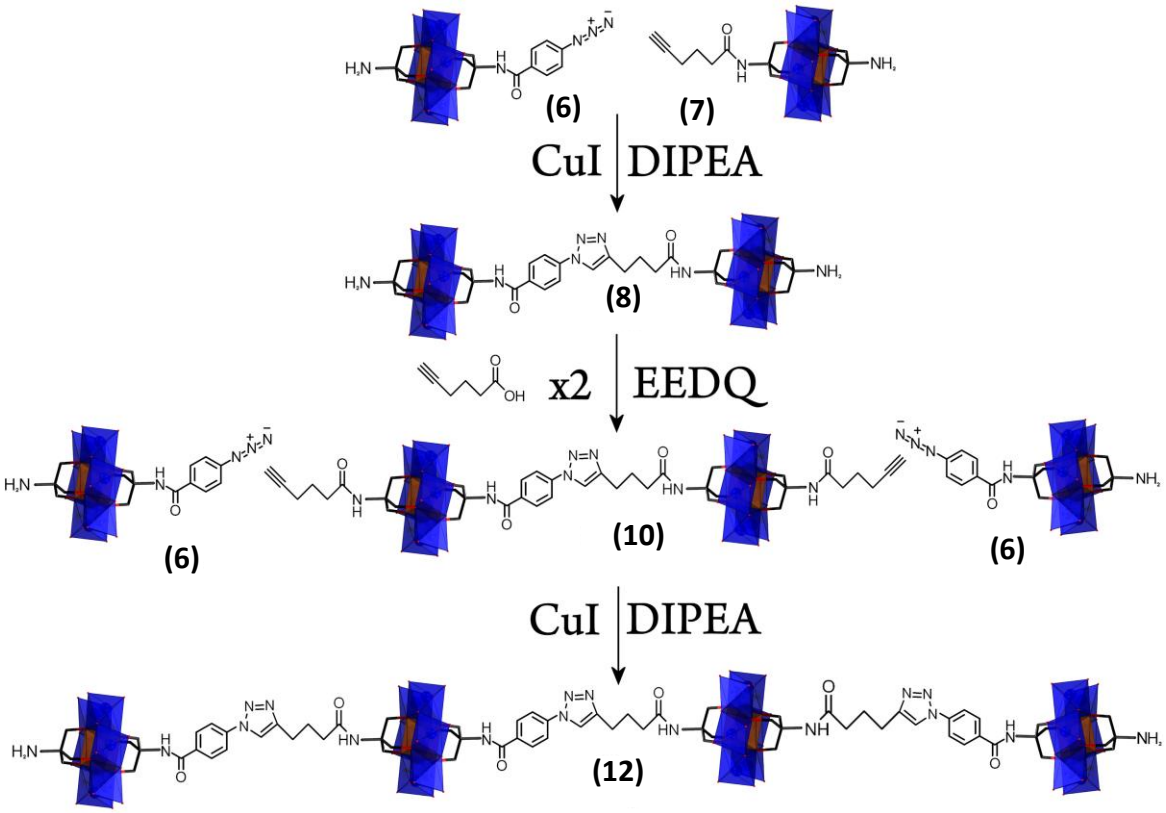

Figure 76 By functionalisation of the dimer with 5-hexynoic acid, it becomes possible to form a tetramer by adding 4-azidobenzoic/TRIS Mn-Anderson **(6)** building blocks. Formation of the trimer **(9)** and pentamer **(13)** are similar but starts from a symmetric building block **(5)**.

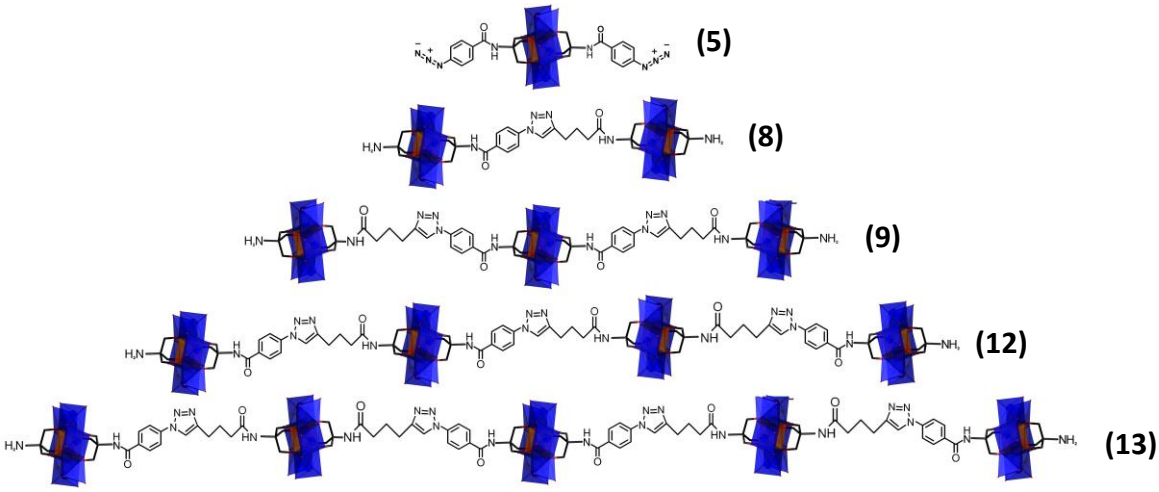

Figure 77 Representation of the four oligomers and a monomer **(5)**: dimer **(8)**, trimer **(9)**, tetramer **(12)** and pentamer **(13)** Mn-Andersons synthesised via CuAAC.

3.2.4 Validation of Oligomer Formation

Typically, single-crystal X-ray crystallography is the primary form of analysis used to validate the formation of POMs. However as has now been mentioned several times, in the case of these POM hybrid oligomers and their precursors, single-crystal XRD was very rarely possible due to the poor quality of the crystals formed. This is most likely due to the speed at which the crystals were grown resulting in less well-ordered packing and the choice of solvent used for the diffusion technique: the rapid evaporation of diethyl ether from the crystals during crystallography measurements are likely to damage the crystals.

Therefore electrospray ionisation mass spectrometry (ESI-MS) was the form of analysis used to initially verify the reactions had successfully gone to completion (**Figure 78**). This was found to be the simplest approach because peak envelopes were reproducible, immediately recognisable, assignable and the spectra where generally simple and clear of side products. Mass spectrometry (MS) relies on the detection of ionic fragments of materials and so would not be typically considered a good analytical tool in the case of reactions where the product can be broken down into fragments identical to the starting material components. In these cases, there would generally be no clear indication of whether a product, and its fragmentation patterns, or starting material was being observed because even in cases where a product peak is seemingly visible, it might in fact be two starting material ions flying together in the instrument resulting in a peak that resembles the product.

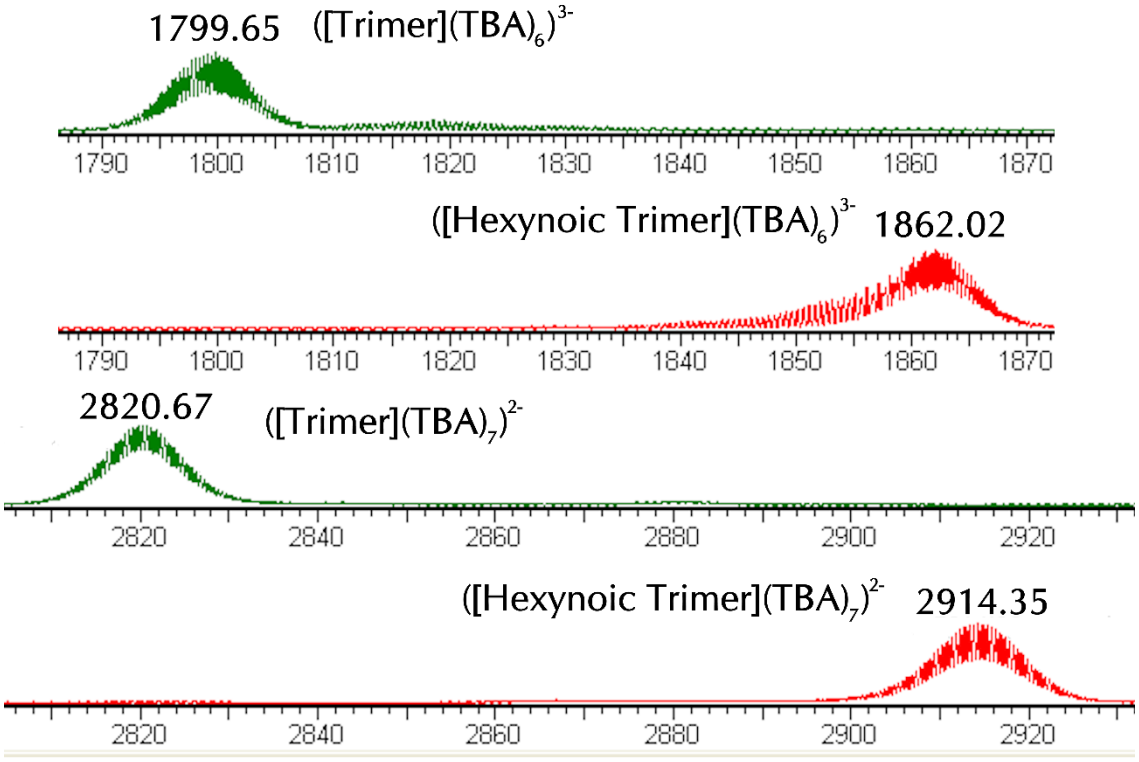

Figure 78 A comparison of two mass spectra: the Mn-Anderson trimer (TRIS) **(9)** in green (expected m/z = 1799.33 and 2820.14) and the Mn-Anderson trimer (5-hexynoic) **(11)** in red (expected m/z = 1862.02 and 2914.19). The number of mass units the peak has shifted by 187.2, within error of the 188.1 corresponding to two 5-hexynoic groups coupling to the terminal TRIS groups. Complete disappearance of the Mn-Anderson trimer (TRIS) in the red spectra strongly suggests that all the starting material has been converted.

With this potential ambiguity in mind, analysis of these spectra was approached with care. Multiple comparisons were made of the reaction mixtures as they progressed in order to familiarise ourselves with variations within the spectra. The addition of one building block in excess allowed for the reaction progress to be tracked by following the disappearance of the other reactant's peak as opposed to the formation of the product itself. In addition, the products were analysed once more after separation using the reverse-phase liquid chromatography (RP-LC) system which significantly increased the certainty that the purified product peaks observed were not a combination of starting materials flying together. The RP-LC flash column separation method was arguably also a qualitative indicator of success due to the reproducible elution times of the different fractions, not dissimilar to high-performance liquid chromatography (HPLC). Once compounds reached a satisfactory purification level, other methods of analysis were used: infrared (IR) measurements, elemental analysis (EA) and most notably nuclear magnetic resonance (NMR) to verify the formation of the triazole group.

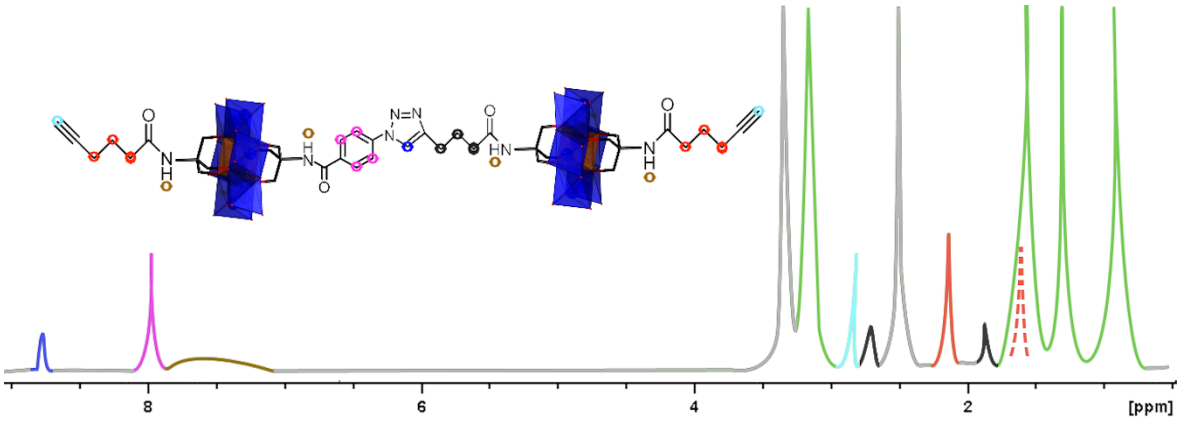

Figure 79 Diagram representing the ^{1}H NMR of a Mn-Anderson dimer (5-hexynoic) **(10)** and proton correspondence, assigned by peak colour. Very similar peak positions are observed for the other oligomers. Colour code: Light blue – alkyne proton, red – exterior hexynoic CH_2 groups (including peak obscured by larger TBA peak), gold – NH protons, pink – 4-azidobenzoic aromatic protons, dark blue – triazole proton, black – interior hexynoic CH_2 groups and green – TBA protons. The grey peaks are for water and DMSO.

Standard ^{1}H and ^{13}C NMR are not generally used in pure POM chemistry, but in the case of organic-inorganic POM hybrids they are a useful tool for the inspection of the organic ligands.[76] ^{1}H NMR in particular helped to confirm the formation of the azide-alkyne with confidence. Unlike with ESI-MS, where chemical compounds can easily be confused if they contain identical motifs, the precise local environment of molecules affects the NMR response of their nuclei, which manifests in the observed chemical shifts, allowing for resolution of structurally similar moieties. This means that the same atom in an azide functional group will be seen in a different position to when it is in an azide-alkyne coupling and so the difference between crude starting material and product should be easily observable. **Figure 79** demonstrates where the different ligand functional groups and connections can be expected to be found.

3.2.5 Oligomer Characterisation and Comparison

In addition to validation of compound formation, other analytical techniques were used to compare the oligomers with one another in order to explore how their characteristics might be affected by chain extension. The longer the length of an oligomer, the more the chain can fold in on itself and have individual components of the sequence interact with one another. This concept is especially clear in the case of peptides where the secondary and tertiary structures of these biomolecules rely on the interaction of different functional groups along the amino acid string (section 1.6.2).

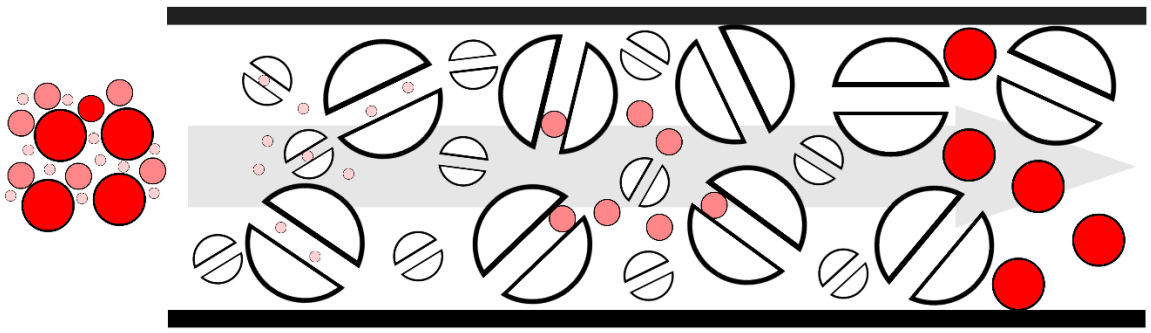

Figure 80 Diagram demonstrating how size-exclusion chromatography is able to separate mixtures according to size as smaller components are exposed to a larger surafce area of the porous beads and so have an increased elution time compared to the larger substances which pass more rapidly through the column.

The oligomers were passed through a size exclusion HPLC column (**Figure 80**). Unlike the C18 reverse phase separation system used for the purification of these compounds that differentiates between chemicals based on their polarity (**Figure 32**), a size exclusion system separates compounds out based purely on size. The method works by using a stationary phase of porous beads through which smaller molecules take longer to pass due to the access they have to a larger surface area.

Number of Mn-Anderson Cores	Calculated Molecular Mass (Da)	Retention Time (s)
1	1882.13	18.48
2	4003.32	16.16
3	6124.59	15.32
4	8245.85	15.13
5	10367.12	15.10

Table 3 A table showing the relationship between the number of Mn-Anderson cores and the observed retention time by SE-HPLC. The molar mass calculated for each of the oligomers is also included to show how close it is to the limit of the column used (100 to 10000 Da).

As hypothesised, we found that the shorter oligomers passed through the column more slowly than the longer ones. However, on inspection of the retention times (**Table 3** and **Figure 81**), it can be noted that the retention time difference between the compounds decreases with the larger oligomers. This is due to the limited range of the column, which is not normally an issue for its typical use of peptide separation where the different sequences are much closer in size to one another.

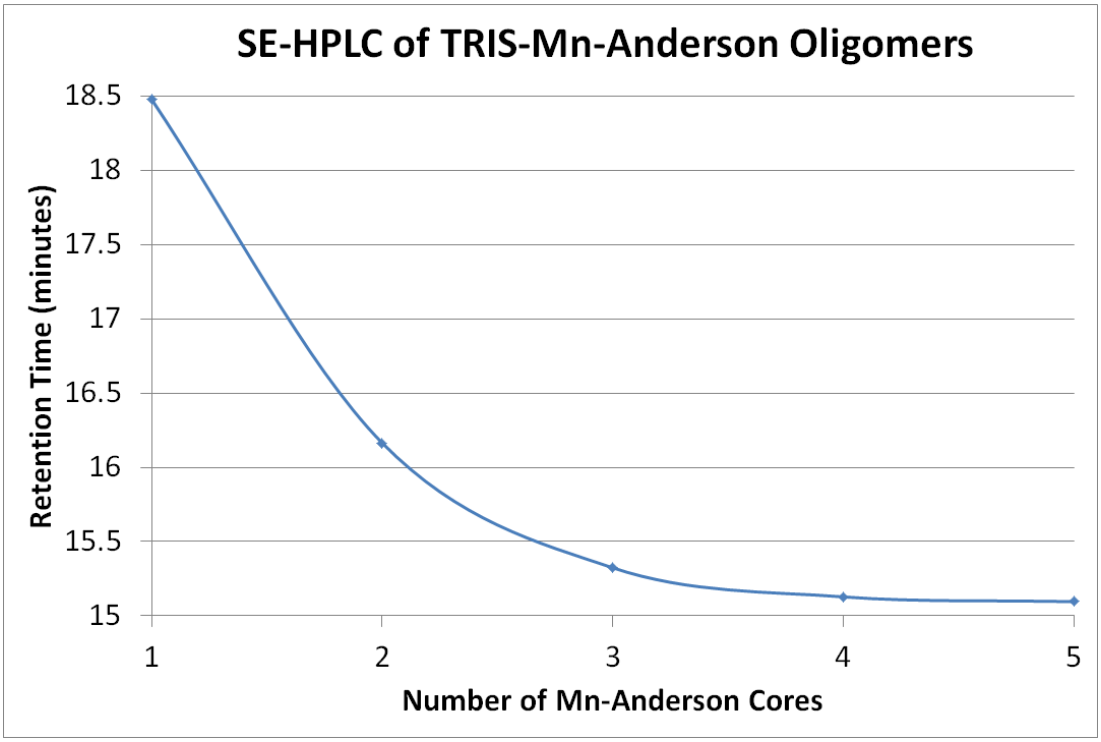

Figure 81 A graph showing the change in SE-HPLC retention time with increasing numbers of Mn-Anderson cores in the oligomer. The difference in retention time reduces sharply as the molecular mass approaches the column size limit (10000 Daltons), but shows a definite increase in size across the range.

Ion-mobility spectrometry–mass spectrometry (IMS-MS) is a form of spectrometry which separates ions out according to physical size as well as the mass to charge ratio (m/z), creating a 2D spectrum that allows for the differentiation of different conformers that have the same mass. Ion mobility can calculate the size of ions by measuring the time it takes for them to drift through a tube of inert gas. Ions with a larger cross-sectional area take longer to pass through as they collide with a greater number of gas atoms.

IMS-MS was used to measure the surface area of the oligomers as well as look for multiple conformers the chains might form. The data chosen for the measurement were the 3- ion fragments as they gave the best resolution spectra for the larger oligomers. This did however result in exclusion of the monomer data as the 3- charged ion flies without any TBA^+ counterions and cannot therefore be fairly compared with the others. Measurements for the 3- ions were plotted against the drift-times of standard compounds (**Figure 82**) and this calibration graph allowed the cross-sectional area of the oligomers to be determined (**Figure 83** and **Table 4**).[266,371] The IMS-MS data and the cross-sectional area calculation suggests that the tetramer (**Compound 12**) may form two different conformers, differing in cross-sectional area by 22 $Å^2$.

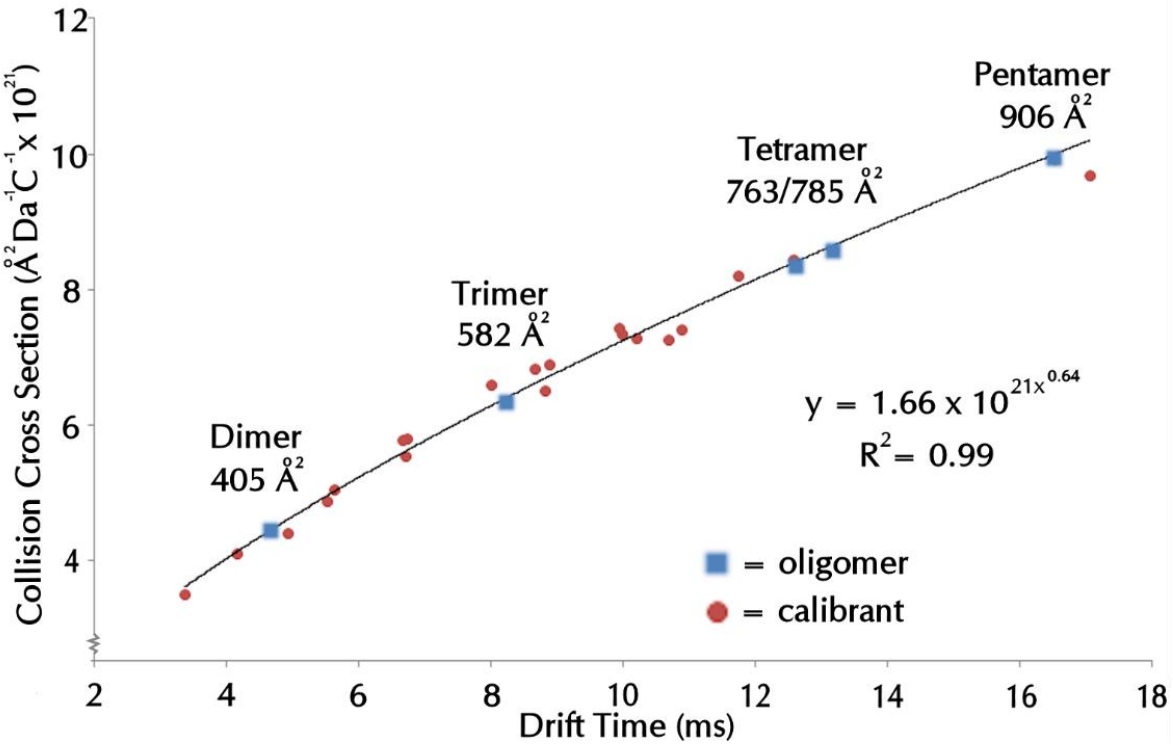

Figure 82 A graph showing the drift time measured for a series of calibrant samples plotted against the literature values for their collision cross section (adjusted for charge and molecular mass) as red circles. A line of best fit is then plotted through these points and this is used to obtain collision cross sections from the drift times measured for the hybrid Mn-Anderson oligomers, shown as blue squares

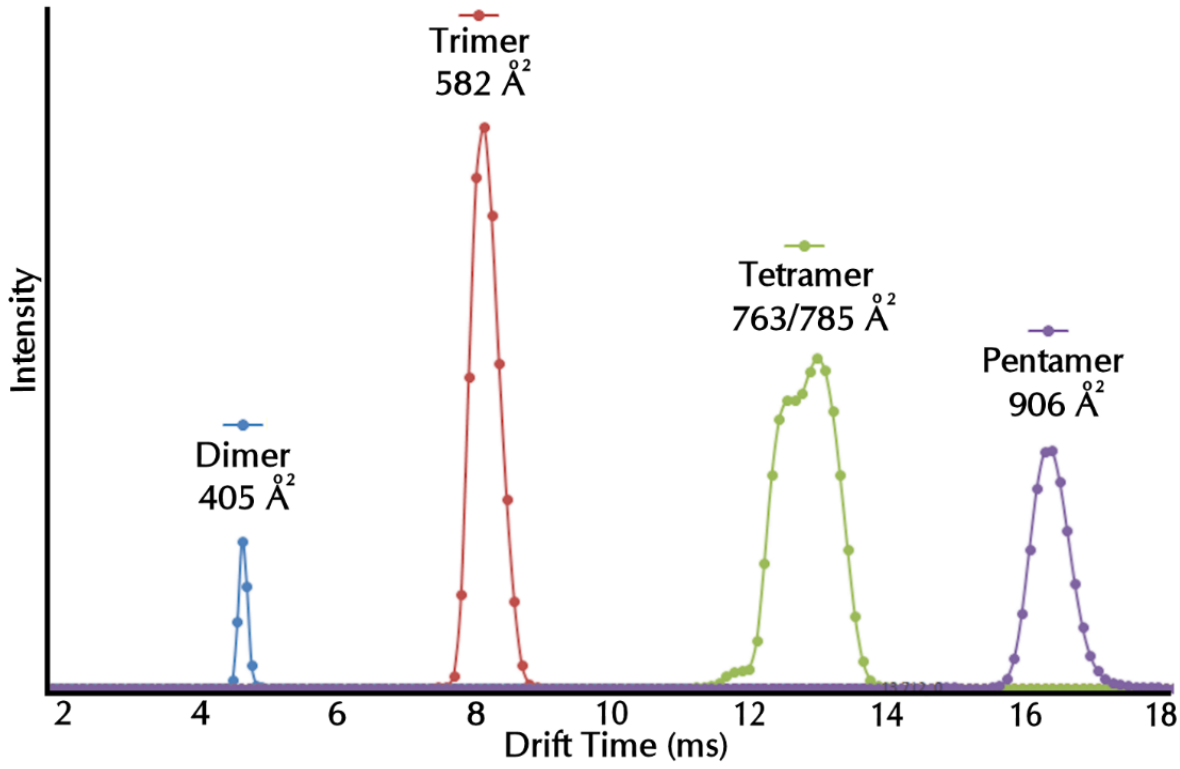

Figure 83 A simplified graph showing only the drift times observed for the 3- peaks of the four oligomers, including the two separate drift times observed for the tetramer.

Number of Mn-Anderson Cores	Drift Time of 3- Peak (ms)	Cross-Sectional Area (Å^2)
2	4.65	405
3	8.20	582
4	12.55	763
4’	13.12	785
5	16.42	906

Table 4 A table showing the drift times measured for the 3- peaks of each of the Mn-Anderson oligomers and the cross-sectional area attained by comparison with a series of calibrants. The tetramer (4 and 4') showed two drift times for the 3- peak, possibly suggesting that the molecule assumes one of two different configurations in the gas phase.

3.2.6 Section Summary

This section has shown how a series of POM hybrid oligomers were built from the Cu-catalysed azide-alkyne coupling of asymmetric Mn-Anderson hybrids. The AB coupling mechanism and the asymmetry of the building blocks is key for the controlled formation of oligomers without resulting in uncontrolled polymerisation. Two equivalent synthetic pathways were followed, with one producing oligomers with an even number of POM cores and the other producing oligomers with an odd number of POM cores. Specifically, the tetramer (**Compound 12**) was formed from the dimer (**Compound 8**) and similarly, the pentamer (**Compound 13**) from trimer (**Compound 9**). For both of these pathways, a set of building blocks had to be synthesised. A pre-functionalisation approach was used for the formation of 4-azidobenzoic/TRIS Mn-Anderson (**Compound 6**) and 4-azidobenzoic Mn-Anderson (**Compound 5**) where a one-pot reaction containing 4-azidobenzoic-TRIS ligand (**Compound 4**) and TRIS ligand formed both compounds which could then be isolated using flash chromatography. 5-hexynoic/TRIS Mn-Anderson (**Compound 7**) on the other hand was post-functionalised with 5-hexynoic acid from the "Universal" asymmetric precursor: FMOC/TRIS Mn-Anderson (**Compound 3**). The dimer (**Compound 8**) and trimer (**Compound 9**) were formed, by reacting the necessary building blocks in the presence of CuI and DIEA under inert conditions. The protruding amine groups were then functionalised with 5-hexynoic acid allowing for another two asymmetric Mn-Anderson hybrids to be coupled, one on either side of the chain, forming a tetramer (**Compound 12**) and a pentamer (**Compound 13**).

All of the compounds, both building blocks and oligomers were separated from their crude reaction mixtures using the RP-LC system and then purified in MeCN through slow diethyl ether diffusion. Unfortunately, this system did not produce good quality crystals, so IMS-MS was used initially to confirm reactions had gone to competition by looking for the disappearance of the starting material. Once purified, the azide-alkyne coupling was verified with ^{1}H and ^{13}C NMR. Two analytical techniques were then used to quantify the physical shape and size of the oligomers from one another. SE-HPLC was used to derive molecular mass from retention time although the size range of the column was a limiting factor. IMS-MS was used to calculate the cross-sectional area and identify any potential conformers resulting from folding of the POM hybrid chain. With this we determined that the tetramer (**Compound 12**) may have two different possible conformations.

3.3 Expansion of the POM hybrid Oligomerisation Method

This final part builds directly from the work carried out in section 3.2 by attempting to extend the method for the controlled coupling of Mn-Anderson hybrids via "Click" chemistry to other organic-inorganic clusters. This project was considered interesting because, although Mn-Andersons are some of the most stable and versatile POM hybrids available, they do not exhibit particularly interesting properties, nor do they show much realistic potential for application.[283] For the developed controlled coupling method to be of more general interest, it is necessary to demonstrate its adaptability. A straightforward way of doing this would be to create a number of other asymmetrically functionalised POM hybrids, or indeed any organic-inorganic hybrid clusters, suitable for use in azide-alkyne cycloadditions leading to the formation of POM hybrid oligomers (**Figure 84**). Ideally, these POM hybrids would display some interesting properties or at least demonstrate how feasible it is to work with compounds of a more challenging nature in such systems.

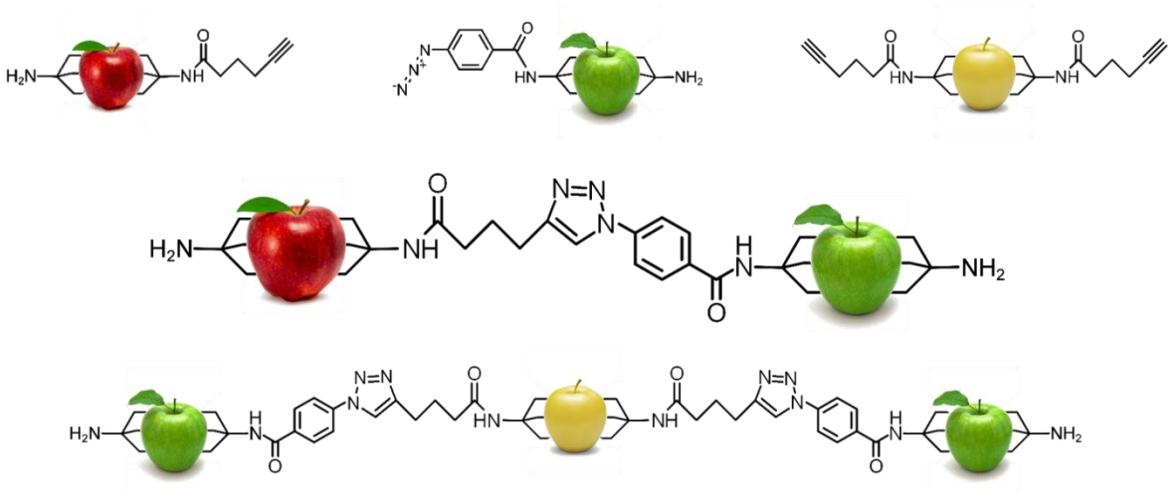

Figure 84 A cartoon illustrating the aim of this project which was to create a set of azide and alkyne functionalised organic-inorganic hybrids that can be used as building blocks for the configurable assembly of oligomers. The apples ("pommes" in French) represent inorganic cores.

To further highlight the tuneability of this method, it was considered worthwhile to demonstrate how POM cores of different natures could be chained together. Adaptation of this method from *controlled* polymer formation to *configurable* polymer formation would expand the interest of such a system. Configuration of polymers is a level of control that allows for the fine tuning of systems and is clearly demonstrated with the biological structures described in section 1.6, namely nucleic acids and peptides, where

polymers are built up from a pool of available building blocks that all share common functional groups to enable coupling, but also contain sufficiently different component parts to give each building block unique characteristics to bring to the system. Such an approach has the potential to produce compounds with a wide variety of finely tuneable properties.

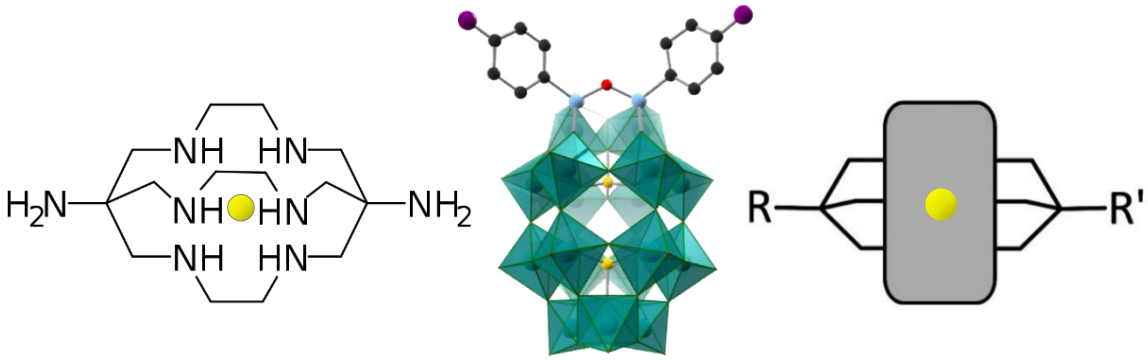

Figure 85 An illustration of the variety of compounds potentially adaptable to the CuAAC oligomerisation; simply an Anderson with a different metal centre (right), another POM hybrid (such as a two-branched Si-substituted Dawson, middle) or use cage-like structure which is not a POM (sarcophogine, left). The yellow circles represent a central metal atom.

As a starting point for the development of usable building blocks, the range of diversity of inorganic structures had to be considered, from the extremes of selecting organic-inorganic hybrids from outside the POM-realm with wildly different properties (for example, sarcophagine, a bicyclic cage-like metal chelator molecule[372]), to focusing solely on Anderson hybrids with different metal-centres whose chemistry would likely be easily adaptable to the already existing coupling system (**Figure 85**). A middle ground approach was considered the best place to start working, allowing for the incorporation of new properties while remaining in the familiar territory of polyoxometalate systems that easily adapt to the “Click” coupling method.

3.3.1 The Criteria of a Building Block

For a material to function effectively as a building block it must: 1) be producible in high yields, 2) be clearly detectable, 3) be stable in a variety of environments and 4) have the appropriate solubility and functionability. If the material fails to meet one of these 4 requirements, it will be very difficult to incorporate it into a configurable chain. POM chemists frequently work with compounds that are difficult to make quickly and in large quantities. This is because a lot of POM chemistry is focused on the search for more interesting, generally larger clusters, where all that is needed is enough pure material for

full characterisation (a few milligrams is usually sufficient).[1] Often, the synthesis process for obtaining these incredible structures is long, laborious and very low yielding: sometimes involving the preparation of hundreds of reactions, months of waiting for crystals to grow and occasionally even the separation of individual crystals by hand. Going through this process is reasonable when the aim of the task is simply to produce the cluster itself, but when working to create starting materials for other reactions, a very different attitude has to be taken. As described in section 3.2, the azide-alkyne coupling method for building up oligomers involves a number of stages of synthesis and purification, during which material is lost. This loss accumulates as progress along the steps is made and therefore results in only a tiny fraction of material remaining relative to what was originally started with. For this reason, it is vital for building blocks to be synthesisable on a "grams" scale if the target molecules are ever to be reached. This yield should ideally be obtainable with relative speed and ease in order not to waste too much time working solely on creating starting material. In conjunction with this, purity of the starting material is also important, as impurities are likely to, at best, accumulate as the synthesis pathway progresses and, at worst, interfere with reactions.

As the complexity of the compounds built up, characterisation becomes increasingly more challenging. Already the existing asymmetric Mn-Anderson building blocks (**Compound 6** and **Compound 7**) are exceptionally difficult to crystallise to a high enough standard for X-ray diffraction and the hybrid oligomers themselves are even more so. The same issue is likely to be encountered when working with other POM cores and similar challenges may also be encountered for other analytical techniques such as NMR and MS. For this reason, it is crucial for the simple building blocks to be easily detectable using a number of techniques in monomer form in order for characterisation of the hybrid oligomers to be at all possible. Considering how many synthesis stages and varying reaction conditions building blocks need to withstand, these starting materials need to be robust. POM clusters are very sensitive to pH and are also likely to have unreliable stability over time. This may limit the pool of usable POM clusters, as the "Click" coupled oligomerisation method takes time and the pH varies throughout the stages.

The solubility of the clusters is also important as the use of a variety of different solvents throughout the process is key to successful synthesis, isolation and purification of the compounds. With the Mn-Anderson hybrids for example, the initial synthesis of the

building blocks takes place in acetonitrile, with purification and crystallisation relying on its insolubility in diethyl ether, the azide-alkyne cycloaddition is in DMF and the reverse phase chromatography relies on partial solubility with water/acetonitrile mixes. Finding another compound with exactly the same solubility properties is improbable and an adaptation of some of these stages would no doubt be necessary, which could for example involve tuning the cluster solubility using cation exchange. But overall, a compound with varying solubility over a range of organic solvents and partial solubility in water would be ideal: good solubility is essential for reactions to take place and insolubility with other solvents allows for purification of the material.

In order for the incorporation of the hybrid building block into "Click" coupled oligomerisation, it needs to have the appropriate functional groups, namely ligands with an alkyne or an azide for the coupling reaction itself, or an unreactive group that is available for later functionalisation, ideally an amine. This is the minimum requirement; hybrid building blocks that can be functionalised asymmetrically are preferable as this allows for their full configurability, whereas symmetric building blocks can only be used as the initial, central monomer of a chain.

3.3.2 Building Block Candidates

The fulfilment of all the requirements mentioned in the previous section (3.3.1) is not immediately evident when first starting to work with a building block candidate because many of the characteristics of the material can be greatly improved with optimisation. Equally, issues that are not immediately obvious are likely to arise part-way through the building block development. This section demonstrates, with examples, how this building block trial and error development can take place.

3.3.2.1 Lindqvist Hybrid Work

As mentioned previously in Section 1.3.2, Lindqvist hybrids have been successfully functionalised with azide or alkyne groups and used in reactions and the ligands modified via "Click" reactions (**Figure 86** and **Figure 87**).[373] Modification of these pre-existing methods for the formation of an asymmetric POM hybrid seemed an obvious move forward to further diversify the building block pool with a vanadium-based hybrid cluster. On closer investigation of the synthetic method used, the length of time and number of

synthetic steps required to obtain the alkyne ligand used was noted. To add another 3 organic synthesis reactions[374,375] to what was already a lengthy process was considered unwise due to the additional yield and time losses this could introduce, and so an attempt to obtain similar compounds through a more direct route was made.

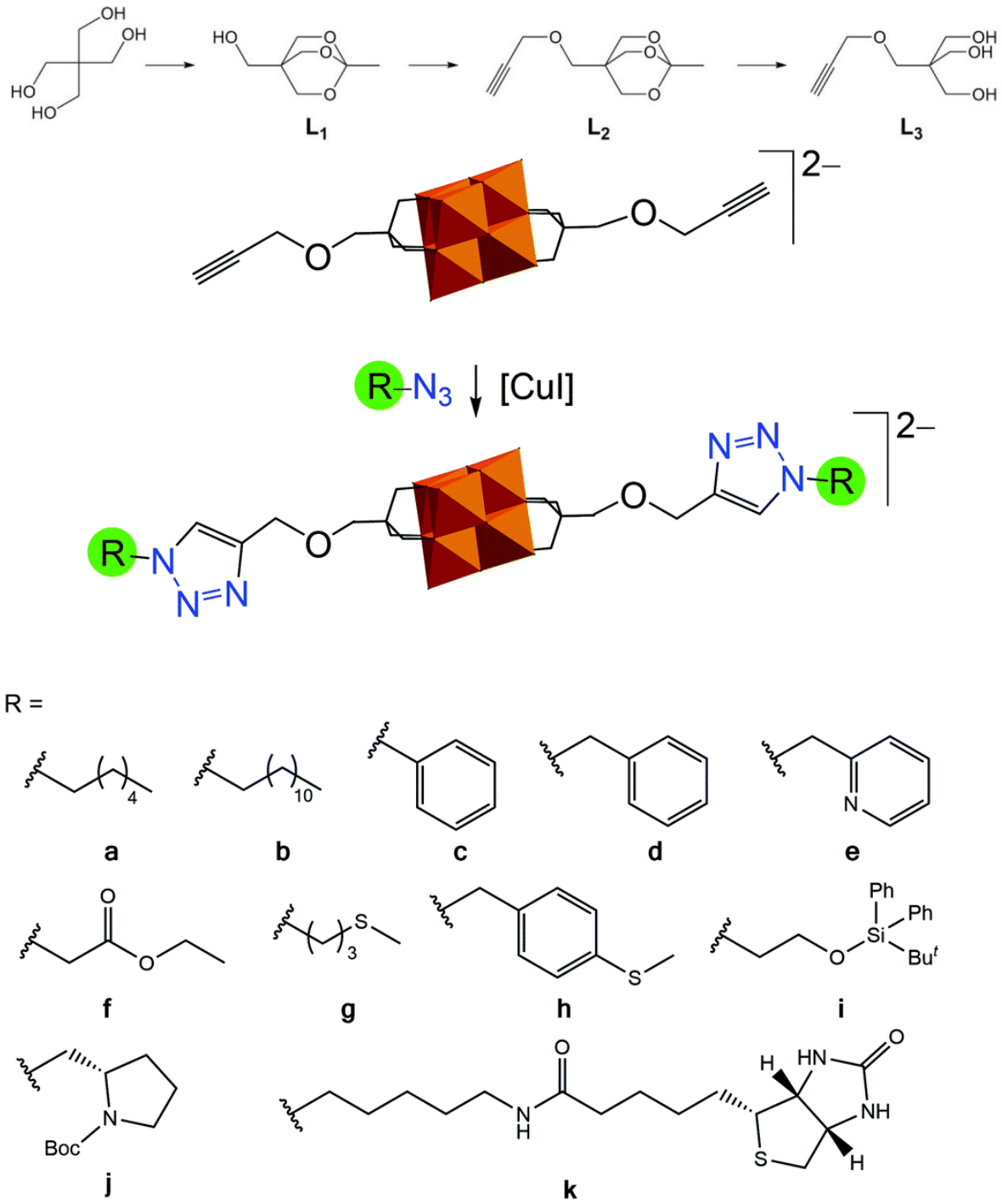

Figure 86 Scheme outlining the procedure by Monakhov et al for the synthesis of alkyne-TRIS ligand (L_3) used to form a Lindqvist hybrid and the moieties post-functionalised with a series of ligands (a-k) via azide-alkyne cycloaddition. Reproduced with permission.[376] Colour code: orange – vanadium polyhedra.

To begin with, decavanadate (**Compound 14**) was synthesised as a precursor to the Lindqvist cluster, the synthetic methods of which were only roughly outlined in the literature.[377] After some optimisation, acidification of Na_3VO_4 followed by addition of TBABr, washing and recrystallization resulted in the expected yellow solid forming in satisfactory quantities (**Figure 88**).

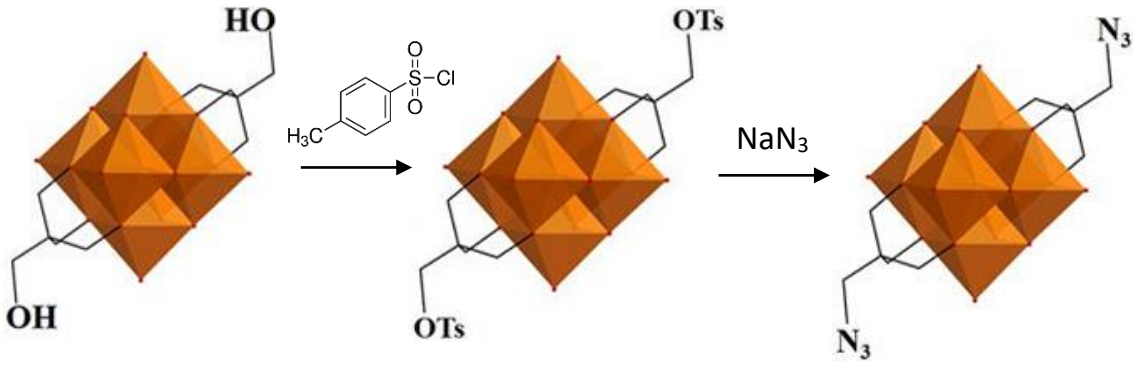

Figure 87 A reaction scheme outlining a procedure by Wei et al for the synthesis of an azide-functtionalised Lindqvist via Tosylation of an alcohol. Reproduced with permission.[373] Colour code: orange – vanadium polyhedra.

There are a number of different procedures outlining the conversion of decavanadate to Lindqvist hybrid and variations on these methods were adopted to try and synthesise the desired compound.[373,376,378,379] This included refluxing decavanadate with the ligands TRIS, HCl.TRIS and FMOC-TRIS in acetonitrile, DMF and DMA for between 12 to 60 hours and sometimes under dry, inert conditions (**Figure 89**). The resulting crude solid was generally redissolved in MeCN or DMF and left to crystallise via diethyl ether diffusion, sometimes with the addition of TBAOH or HCl. Peak envelopes corresponding to symmetric FMOC Lindqvist hybrid (**Compound 15**) and asymmetric FMOC/TRIS Lindqvist hybrid (**Compound 16**) were observed via ESI-MS for a synthesis involving a 3 day DMA reflux and about 10 mg of TRIS Lindqvist hybrid (**Compound 17**), was isolated on a couple of occasions, once from a reaction where FMOC-TRIS and TRIS were heated in dry DMF for 24 hours and the second time overnight in dry DMA but using only the FMOC-TRIS ligand, which must get deprotected in situ.

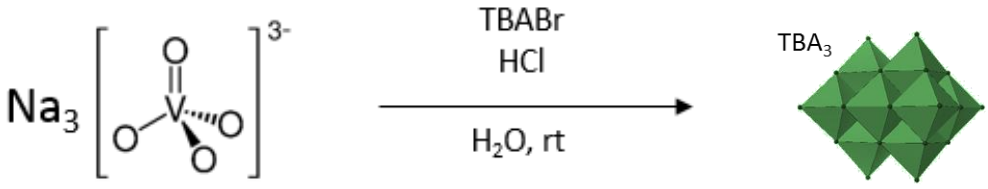

Figure 88 A diagram showing how decavanadate **(14)** can be synthesised by acidification of aqueous Na_3VO_4, a method adapted from the literature. Colour code: green – vanadium polyhedra.

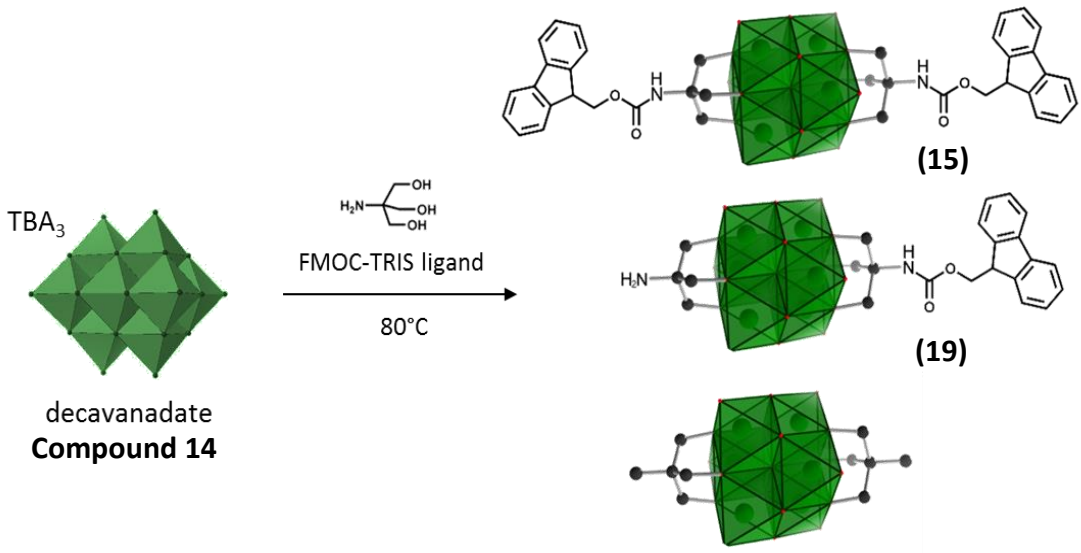

Figure 89 A scheme outlining some approaches to the conversion of decavanadate **(14)** to symmetric **(15)** and asymmetric Lindqvist hybrid **(19)**. Colour code: green – vanadium polyhedra.

Replication of these successes proved challenging and it was eventually acknowledged that such yields would not be sufficient to allow for a continuation along the synthetic pathway towards oligomer formation. Other POM hybrid clusters were therefore considered as potential oligomer building blocks.

3.3.2.2 Fe-Anderson Hybrid Work

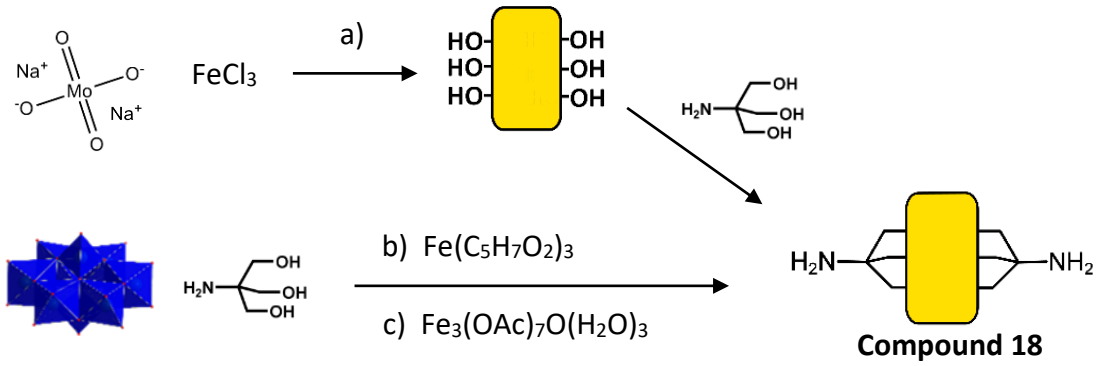

Figure 90 Different methods for the synthesis of a Fe-Anderson hybrid: a) a two-step synthesis where the Fe-Anderson POM is made followed by hybridisation, b) a one-pot involving iron (III) acetylacetonate and c) a one-pot involving iron (III) acetate. Colour code: blue – molybdenum polyhedra and yellow squares - Fe-Anderson cores.

Having experienced difficulties working with another classic POM hybrid cluster, a step back was taken and focus narrowed down to working with alternative Anderson hybrid clusters. The Fe-Anderson hybrid is a cluster that is frequently used in a similar way to Mn-Anderson hybrids, suggesting it is likely to be reliable to synthesise and functionalise.[282] A number of different synthetic routes are described in the literature for

the synthesis of Fe-Anderson hybrids. One method involves the initial formation of the Fe-Anderson POM from $FeCl_3$ and addition of the desired ligand in a subsequent reaction (**Figure 90a**).[40] It is also possible to form Fe-Anderson hybrids in a one-pot reaction comparable to that of the Mn-Anderson hybrid synthesis where iron (III) acetylacetonate, $Fe(acac)_3$ is substituted for Mn acetate and the other reaction materials and conditions remained identical, namely $\{Mo_8\}$ and the TRIS-based ligands in an acetonitrile overnight reflux (**Figure 90b**).[379] As well as simple symmetric TRIS Fe-Anderson hybrid (**Compound 18**) and symmetric FMOC Fe-Anderson hybrid syntheses, the asymmetric FMOC/TRIS Fe-Anderson hybrid (**Compound 19**) reaction was also carried out (**Figure 91**). Although evidence of the expected compounds was seen via ESI-MS (**Figure 94a**), a high number of impurities were also observed, in particular $(TBA)_2[Mo_6O_{19}]$ which can be easily confused with Fe-Anderson as it has a similar solubility and forms yellow crystals. This also manifested itself as an issue during purification using the reverse-phase flash chromatography method from Section 3.2 where unclear, complex and irreproducible separations caused confusion (**Figure 91**).

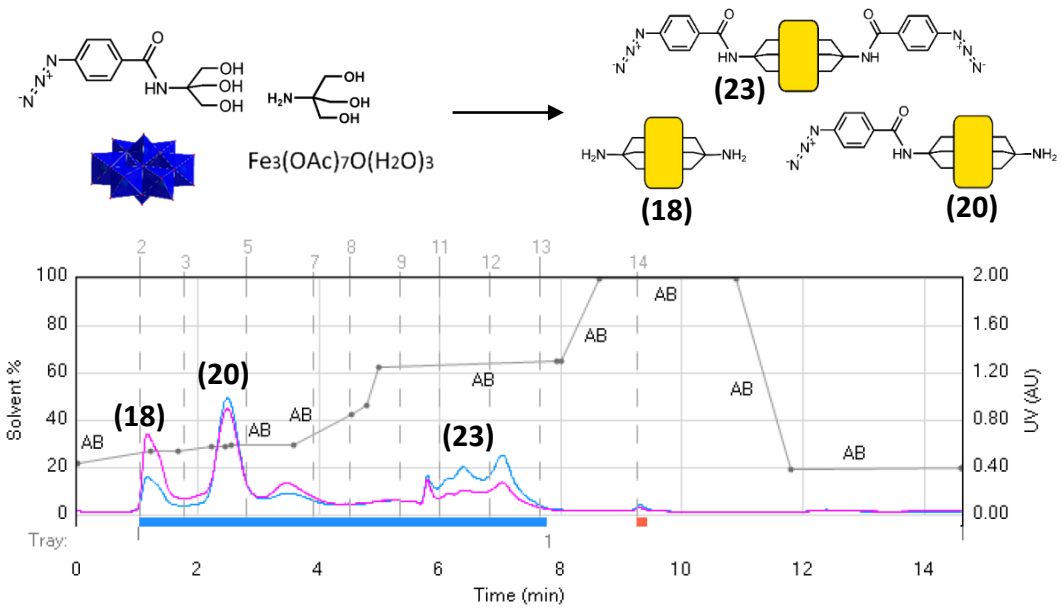

Figure 91 The synthesis of FMOC/TRIS Fe-Anderson **(20)** using octomolybdate, TRIS ligand, FMOC-TRIS ligand and $Fe(acac)_3$, resulted in side products such a $(TBA)_2[Mo_6O_{19}]$, observed in the ESI-MS data and leading to difficulties with purification using the RP-LC system, the UV trace of which is shown. Colour code: blue – molybdenum polyhedra and yellow squares - Fe-Anderson cores.

To overcome this difficulty, the procedure was modified to resemble more closely that of the Mn-Anderson hybrid synthesis, by using iron (III) acetate instead of $Fe(acac)_3$ (**Figure 90c**). Although this method has been previously reported, iron acetate is not commercially available and so had to be synthesised using a modification of a published procedure.[264] As hoped, the ESI-MS of the resulting reaction mixture contained no detectable $\{Mo_6\}$ species, although there were still more unrecognised peak envelopes than on the equivalent Mn-Anderson spectrum (**Figure 94b**). Some of these uncharacterised species were eliminated on discontinuing the use of the standard TRIS ligand, that contains a basic amine group which is likely to interfere with the Anderson hybrid cluster formation and potentially also be causing the breakdown of the hybrids once formed. On replacing the standard TRIS ligand with FMOC-TRIS ligand, an extra deprotection step had to be introduced in order to obtain the azide-functionalised symmetric and asymmetric Fe-Andersons which simply involved stirring the material at room temperature for one hour in a solution of acetonitrile, 20% piperidine (**Figure 92**). The reduction of side products and decomposition can be observed in the ESI-MS spectrum of the crude reaction mixture, where only peaks assignable to the three expected products are observed (**Figure 94c**).

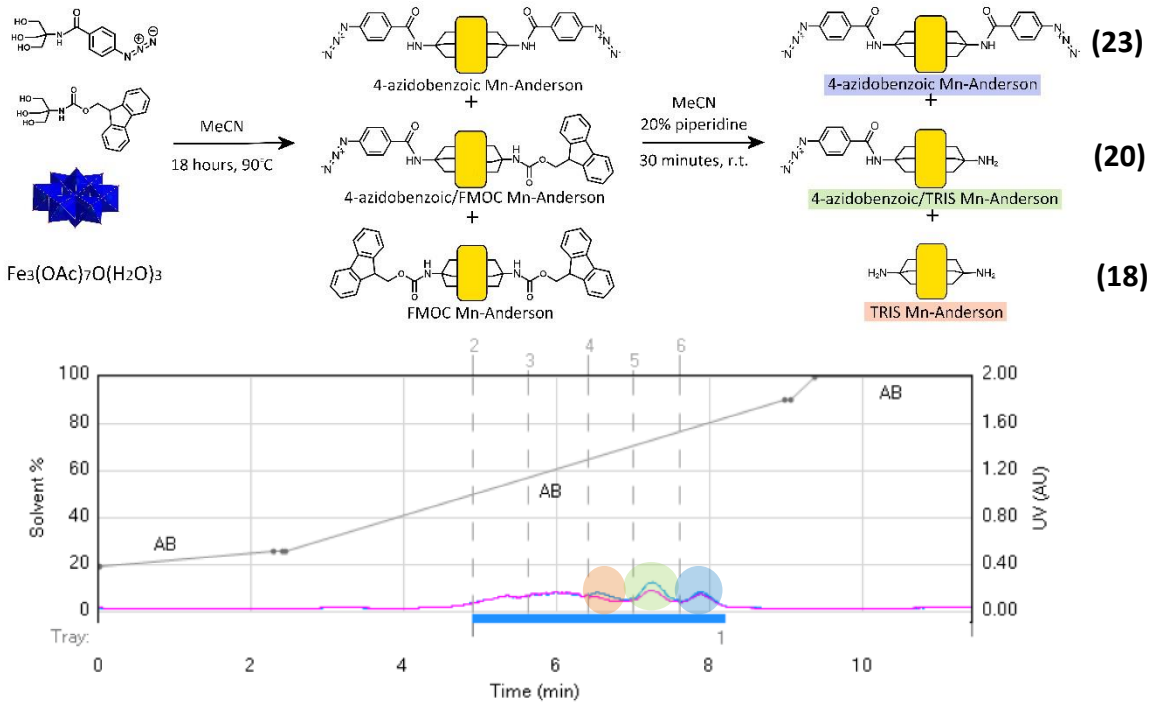

Figure 92 Synthetic procedure for the formation of asymmetric Fe-Anderson involving an additional FMOC deprotection step in order to avoid use of the basic TRIS ligand. The UV trace for the purification of this method gives a much simpler separation (peak height relates to sample size). Colour code: mauve – 4-azidobenzoic Mn-Anderson **(23)**, green – 4-azidobenzoic/TRIS Mn-Anderson **(20)**, orange – TRIS Mn-Anderson **(18)**. Colour code: blue – molybdenum polyhedra and yellow squares - Fe-Anderson cores.

Obtaining pure asymmetric hybrid compound at a desired scale however still proved challenging because the Fe-Anderson hybrid is at least partially soluble in most solvents. This resulted in samples being very difficult to purify because addition of diethyl ether, either rapidly to initiate immediate precipitation or slowly when crystallising through diffusion, would not lower the solubility threshold enough for solid to form. Similarly, separation of the desired material from the side products using the flash chromatography method developed for the Mn-Anderson hybrids (Section 3.2) also continued to be challenging due to the ease of solubility in water, meaning the varying gradient of water to acetonitrile resulted in much poorer fraction separation (**Figure 93**).

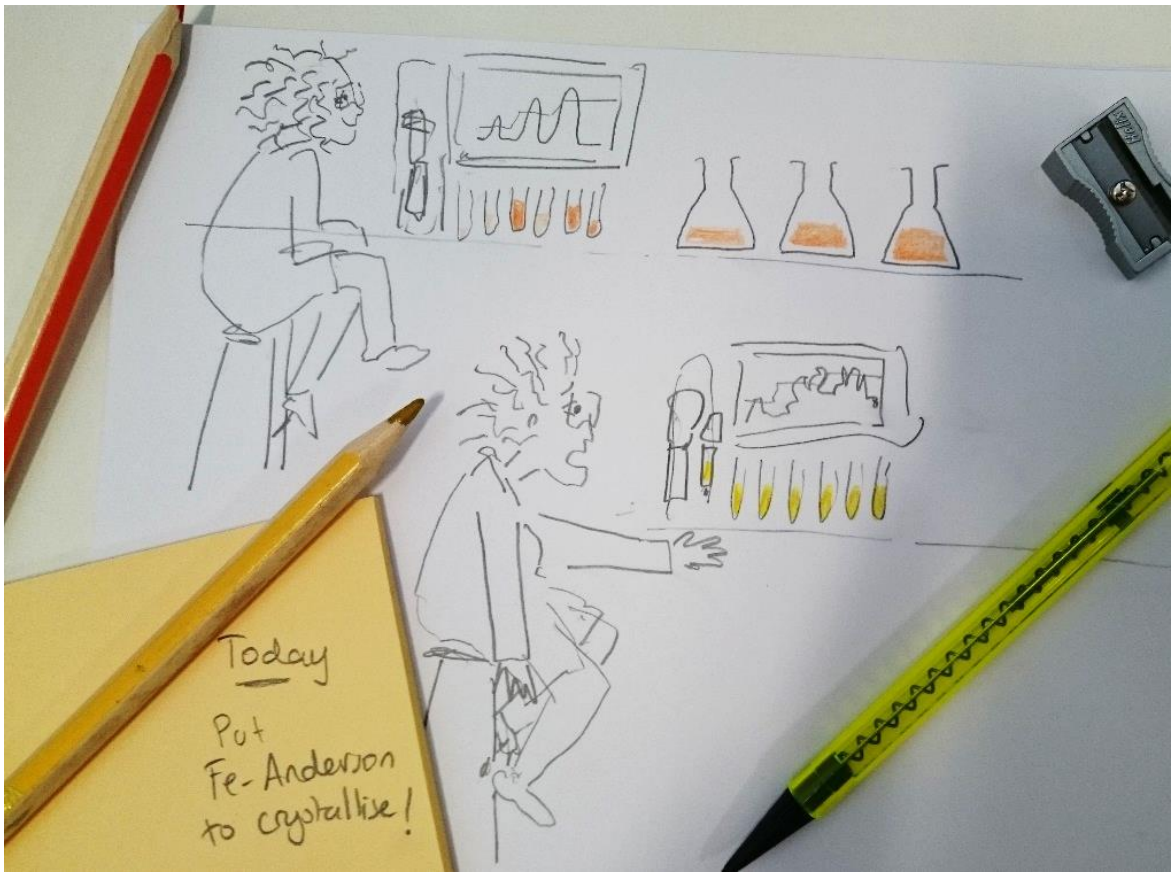

Figure 93 A cartoon illustrating the confusion resulting from initial attempts to purify asymmetric Fe-Anderson hybrids (yellow solution) using the RP-LC system developed for the Mn-Anderson hybrids (orange solution).

The result of these modifications led to a small amount of asymmetric 4-azidobenzoic/TRIS Fe-Anderson hybrid (**Compound 20**) being made and larger quantities of symmetric 4-azidobenzoic Fe-Anderson hybrid (**Compound 23**) and 5-hexynoic Fe-Anderson hybrid (**Compound 21**) being synthesised, all three of which were considered suitable as building blocks for POM hybrid oligomer formation.

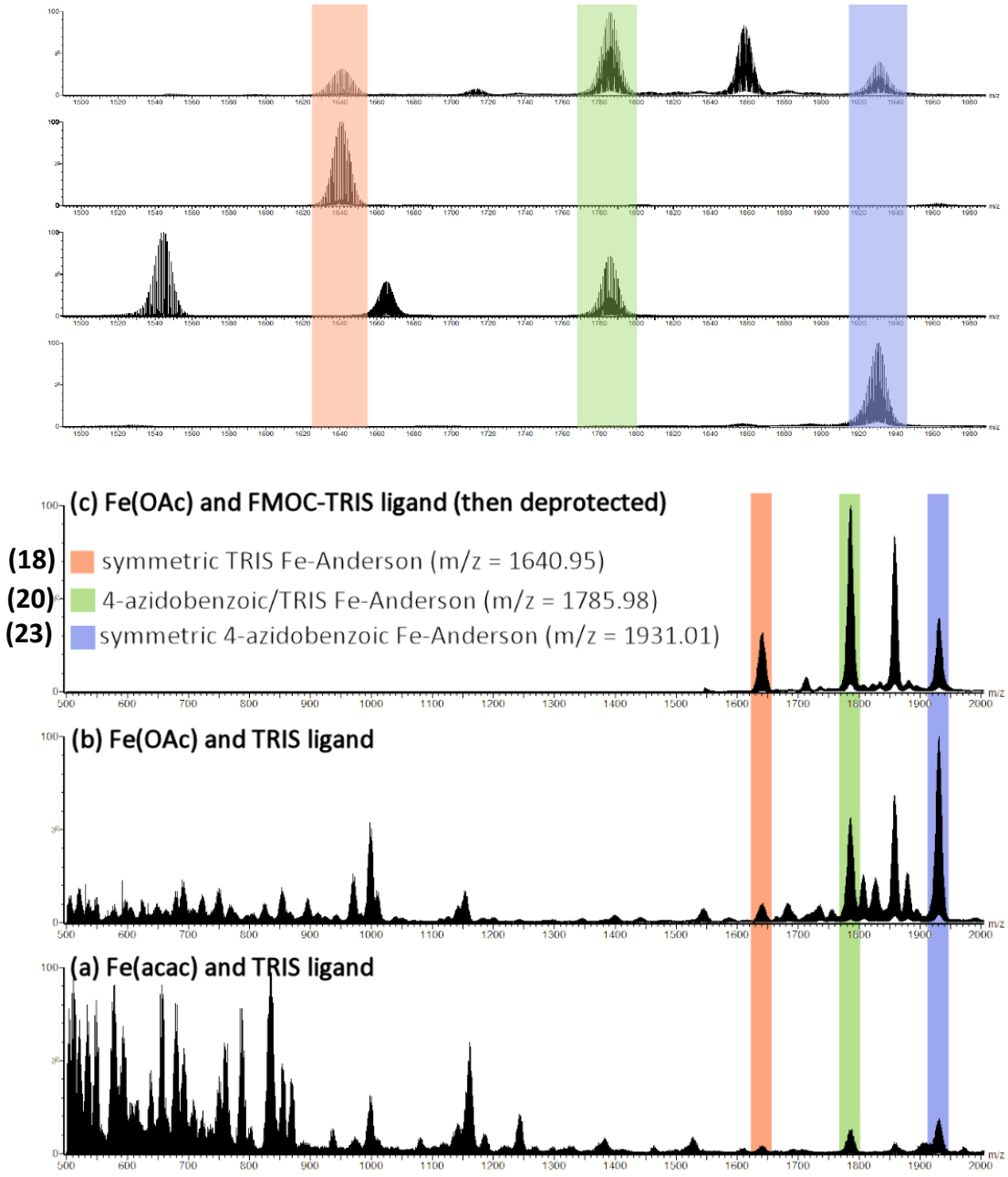

Figure 94 ESI-MS spectra of crude reaction mixtures for three versions (a), (b) and (c) of the 4-azidobenzoic/TRIS Fe-Anderson hybrid. Close-ups correspond to (c) compared to purified materials. Peak envelope colour code: mauve – 4-azidobenzoic Mn-Anderson **(23)**, green – 4-azidobenzoic/TRIS Mn-Anderson **(20)**, orange – TRIS Mn-Anderson **(18)**.

3.3.2.3 {$CoMo_3$} Hybrid Exploration

Having realised (in section 3.3.2.2) that Fe-Anderson could be more reliably synthesised using iron (III) acetate as a starting material as oppose to the $Fe(acac)_3$ compound, the same procedure was applied using a selection of readily available metal-acetates to investigate whether any other metal-centred Anderson hybrid structures might result (**Figure 95**). The selection included metals which have already been observed as the central atom of an Anderson POM or hybrid, namely acetates of nickel, zinc and aluminium (Section 1.3.9) but also some metals which have not: cobalt, cadmium and copper. It was noted that Anderson hybrid traces were more frequently observed with the experiments involving the FMOC-TRIS ligand as opposed to the TRIS ligand itself, likely due to basicity of the amine group. As an alternative to FMOC protection, the hydrochloride salt of the TRIS ligand was also used. Although a number of metal-acetate reactions did show traces of Anderson hybrid formation when analysing the reaction mixtures using ESI-MS, none showed reliable enough results to continue development.

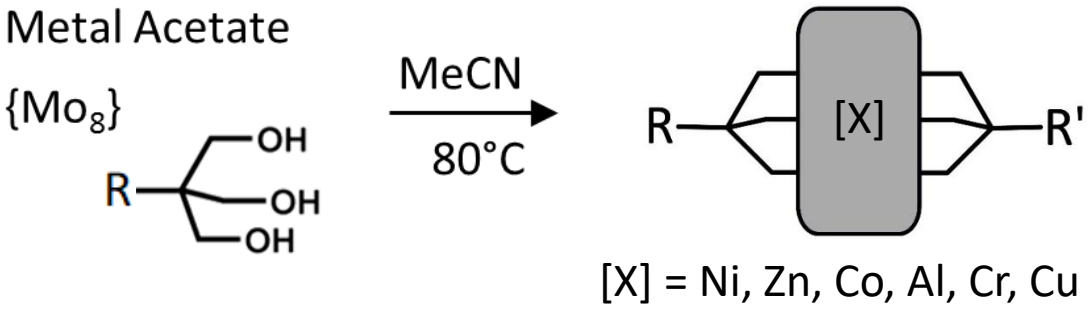

Figure 95 Reaction scheme of the exploration of one-pot reactions using a selection of metal [X] acetates from which an Anderson hybrid might form, where R and R' = $-NH_2$, -FMOC or $-NH_2$.HCl.

One reaction however, did yield crystals under slow diethyl ether diffusion but unexpectedly of a completely different POM hybrid cluster. These violet crystals formed after 3 days from a blue DMF solution of cobalt acetate, {Mo_8} and HCl.TRIS ligand which was heated to 85°C overnight (**Figure 96a**). The solved crystal structure revealed a very small cluster of three molybdate units and a central cobalt atom coordinated to three TRIS ligands: {$CoMo_3$} (**Compound 24**). Unlike with most TRIS-functionalised POM hybrids, the ligands coordinate to the POM core not via the three hydroxyl groups but rather via two of the hydroxyl groups and the amine group, leaving a hydroxyl group as the free functional group (**Figure 96b**).

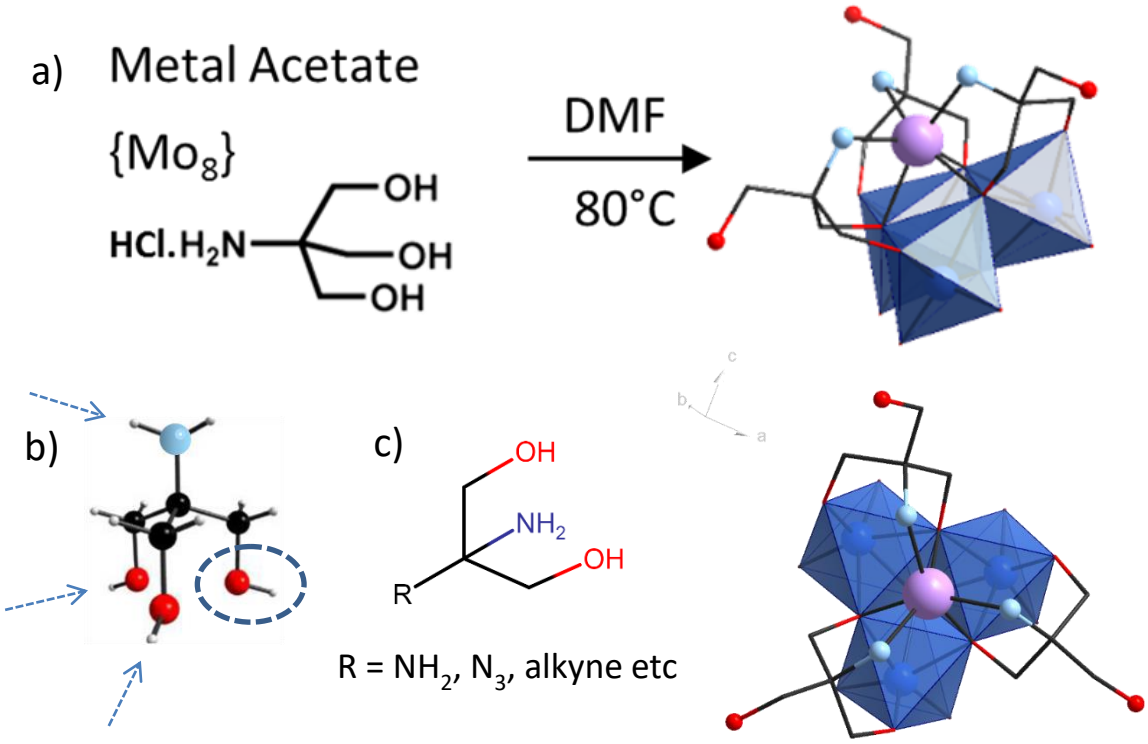

Figure 96 a) The reaction conditions for the formation of the {$CoMo_3$} cluster (**Compound 24**) which, b) binds to TRIS ligands via two hydroxyl groups and the amine group, leaving one -OH (circled) free. The pre-functionalisation approach to modification of these free hydroxyl groups would involve using molecule c) which is not commercially available, most likely due to reactivity of all the different groups.

In contrast to the Fe-Anderson hybrids, this compound was not readily soluble in water or the majority of common organic solvents but the synthesis was robust and the yield high. The ease with which large quantities of this material could be accumulated sparked interest and so a little time was dedicated to exploring its suitability as a POM hybrid building block. Naturally this {$CoMo_3$} hybrid (**Compound 24**), with three functional groups instead of two, does not lend itself to the formation of oligomers unless modification of the separate ligands was possible. In the case of all three ligands being modifiable only in unison, then this building block would not behave as a component of the chain itself, instead a centre point from which three individual, identical chains would extend (**Figure 97**).

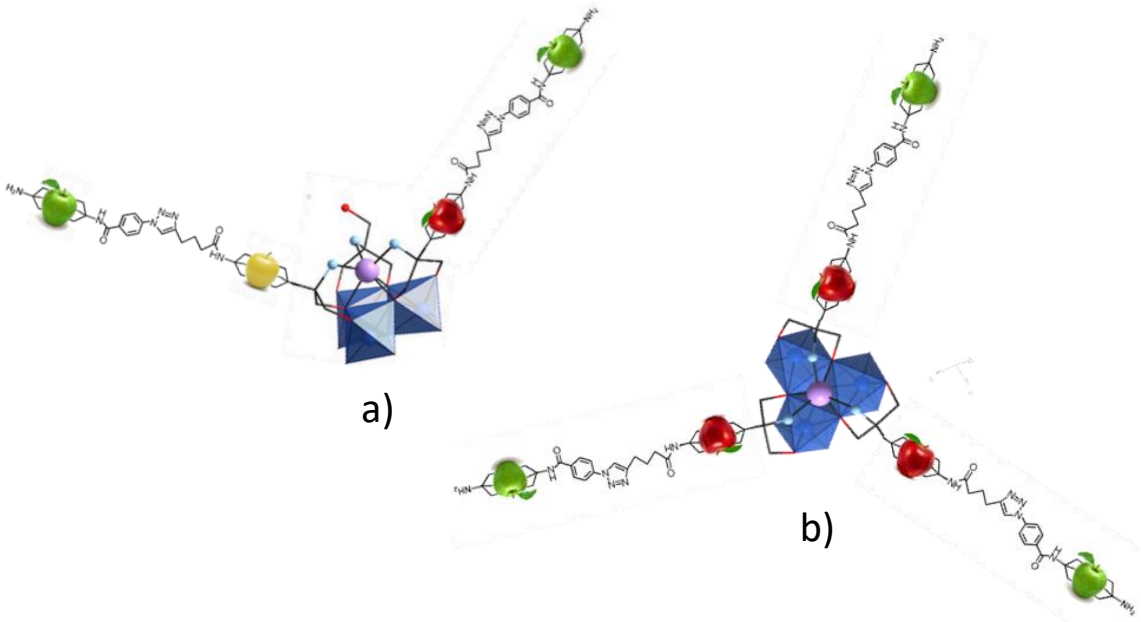

Figure 97 Cartoon demonstrating that for incorporation within a chain a), individual functionalisation of each ligand would have to be possible otherwise b) the three identical functional groups the hybrid would behave as a centre point for three-way oligomer extension. The apples ("pommes" in French) represent organic-inorganic cores.

In order to achieve this, conversion of the hydroxyl groups to alkyne or azide functionality was necessary which was somewhat more challenging than starting from an amine because the hydroxyl groups are less reactive. There are examples in the literature however of hydroxyl-functionalised ligands on POM hybrids that have been successfully modified, the reaction scheme followed by Wei et al[373] is particularly relevant because the target compound contains an azide group (**Figure 87**). The first step of this approach was attempted with the {$CoMo_3$} hybrid to try and replace the hydroxyl groups with 4-toluenesulfonyl groups via a 4-day reaction with TEA and DMAP. Due to the solubility restrictions of the hybrid, DMF at 70°C was used instead of acetonitrile at 50°C (**Figure 98**). An adaptation of the Mitsonobu reaction was also tried[380,381] using diethylazodicarboxylate (DEAD), DPPA, PPh_3 in DMF at 25°C for 2 hours and then again in THF at room temperature.

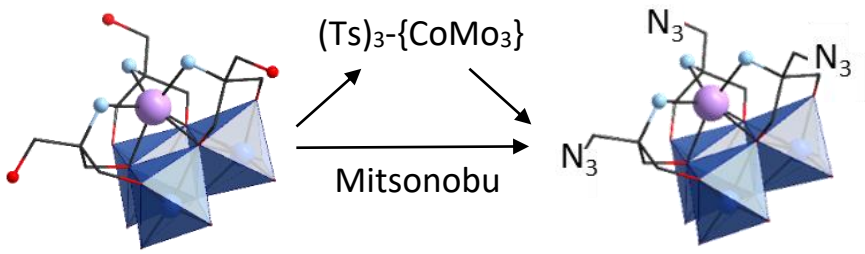

Figure 98 Approaches used to attempt functionalisation of the hydroxyl moieties of the {$CoMo_3$} hybrid (**Compound 24**) involved a Mitsonobu reaction or going via a 4-toluenesulfonyl intermediate.

Pre-functionalisation of the hybrid was also considered but quickly dismissed as this would require using a small organic molecule containing two hydroxyl group, an amine and another functional group (**Figure 96c**). This was not commercially available and the synthesis of such a molecule would have been difficult. After these attempts at functionalisation revealed the level of challenge hydroxyl group modification posed with the solubility and POM-compatibility limitations of {$CoMo_3$}, it was deemed wise to refocus the project and go back to working with the bi-functionalised Anderson hybrids.

3.3.2.4 Cr-Anderson Hybrid Work

As with Mn- and Fe-Anderson hybrids, Cr-Anderson hybrid clusters have also been modified and worked with frequently, suggesting they have a level of robustness that could be of interest as a potential building block.[282,382] In this case however, a different synthetic route for asymmetric Cr-Anderson hybrid synthesis was used, compared to the method used previously in this research, closely resembling how Cr-Anderson hybrids are commonly made in the literature.[109,281,383] With the synthesis of both the asymmetric Mn-Anderson and Fe-Anderson hybrids, a one-pot reaction was used where the desired compound was synthesised alongside two symmetric Anderson hybrid side-products, from which the target molecule had to be isolated using RP-LC. Although this approach had the benefit of being completed in a single step, purification, as seen with the Fe-Anderson hybrid building blocks, could prove challenging. The synthetic route toward an asymmetric Cr-Anderson hybrid compound in contrast, involved three consecutive reactions but resulted in a product requiring little purification (**Figure 99** and **Figure 100**).

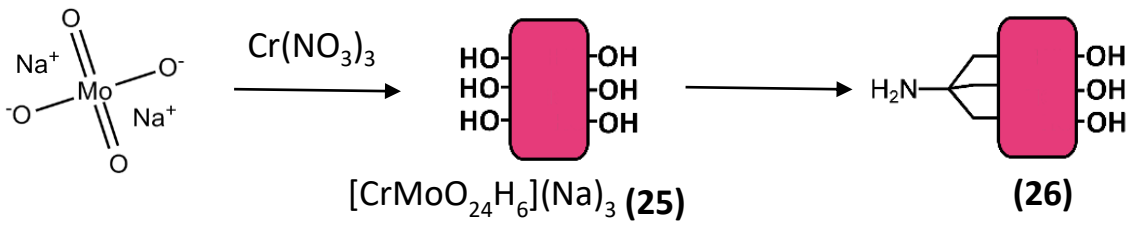

Figure 99 Scheme showing how the formation of the Cr-Anderson POM **(25)** is followed by single-sided functionalisation **(26)** with a HCl.TRIS ligand. Pink squares represent the Cr-Anderson core.

This approach involved the initial formation of pure Cr-Anderson POM (**Compound 25**) in aqueous conditions using $Na_2MoO_4.2H_2O$ and $Cr(NO_3)_3.9H_2O$ as starting materials. Large quantities of pink crystals formed in H_2O through slow evaporation. The pure POM core could then be directly functionalised with a TRIS ligand on one side only, leaving the other

side as before containing only the hydroxyl groups of the inorganic cluster (**Figure 99**). This single-sided TRIS Cr-Anderson hybrid (**Compound 26**) was synthesised based off a previously described method that was modified slightly by changing the ligand used.[382] In order to circumvent the previously mentioned issue of the TRIS ligand basicity, the hydrochloride salt of this TRIS-group was used where the HCl associated with the ligand would act as a protecting group and counter the basic properties.

The formation of single-sided TRIS Cr-Anderson hybrid (**Compound 26**), was a straightforward reaction involving only the HCl.TRIS ligand and the pure POM core (**Compound 25**) itself and took place under hydrothermal aqueous conditions. Once cooled, TBABr was added to the pink solution and crystals that formed from evaporation after a couple of days were pure enough to use for the next step, after a quick wash with isopropanol and vacuum drying. Attempts at adapting this method to form single-sided 4-azidobenzoic Cr-Anderson hybrid and single-sided FMOC Cr-Anderson hybrid were also made, but both resulted in the breakdown of the POM or the modified ligand.

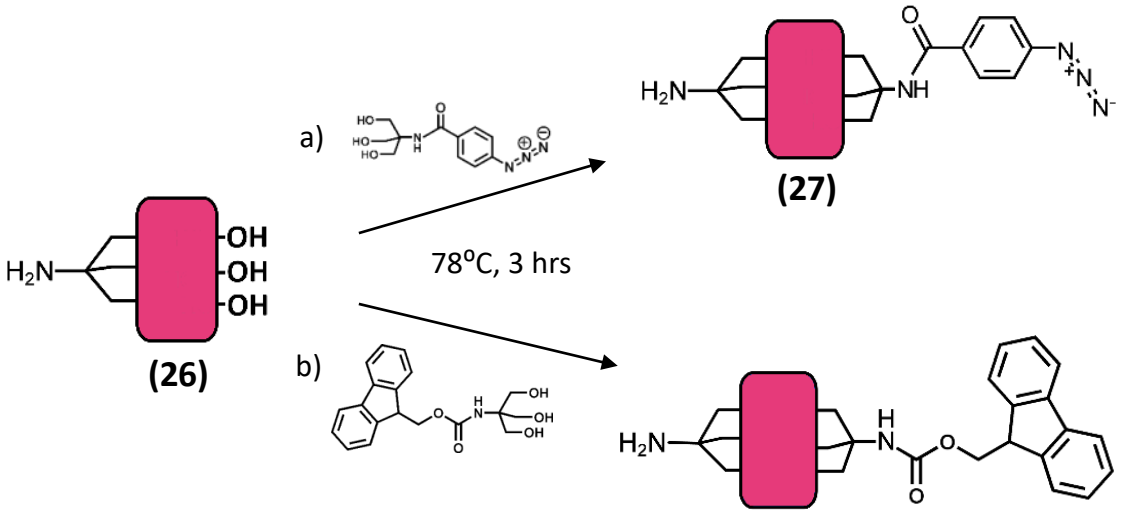

Figure 100 Reaction scheme for the formation of asymmetric Cr-Anderson hybrids by functionalisation using (a) 4-azidobenzoic TRIS ligand **(4)** and (b) FMOC-TRIS ligand. Pink squares represent Cr-Anderson cores.

The synthesis of the building block itself took several attempts, but the reaction conditions found to be most effective were in fact, very straightforward. A number of conditions and solvents were used in attempts to fuse the single-sided TRIS Cr-Anderson hybrid (**Compound 26**) with a series of different ligands: HCl.TRIS ligand, FMOC-TRIS ligand and 4-azidobenzoic-TRIS ligands (**Compound 4**). Eventually, 4-azidobenzoic/TRIS Cr-Anderson hybrid **(Compound 27)** was successfully formed from a three-hour ethanol

reflux containing the 4-azidobenzoic TRIS ligand and the single-sided hybrid cluster (**Compound 26**) (**Figure 100a**). Preliminary ^{1}H NMR data showed the formation of this compound and the same result was also seen to form FMOC/TRIS Cr-Anderson when the FMOC-TRIS ligand was used (**Figure 100b**).

3.3.3 Mixed-Anderson "Click" Coupling

Having now successfully developed an additional two building blocks (**Table 5**), the assembly of mixed-Anderson oligomers could begin. The asymmetric Cr-Anderson hybrid (**Compound 27**) and the Fe-Anderson hybrids (**Compound 20, Compound 21, Compound 22** and **Compound 23**) alongside the original Mn-Anderson hybrids (**Compound 5, Compound 6** and **Compound 7**) have the potential to be arranged in a variety of sequences. In order to demonstrate the configurability of the system, it was necessary to show at the very least two different oligomers containing Anderson cores linked in different orders.

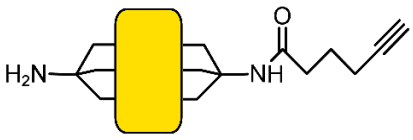	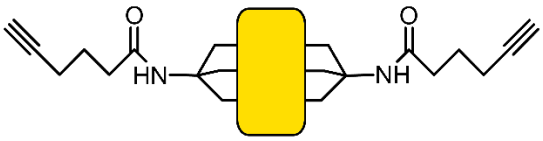
5-hexynoic/TRIS Fe-Anderson (22)	**5-hexynoic Fe-Anderson (21)**
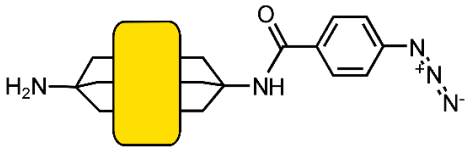	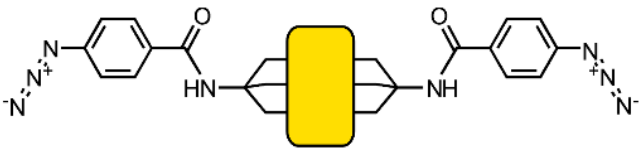
4-azidobenzoic/TRIS Fe-Andrsn. (20)	**4-azidobenzoic Fe-Anderson (23)**
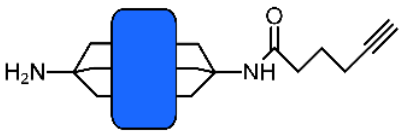	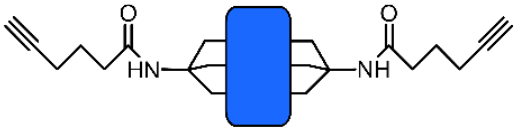
5-hexynoic/TRIS Mn-Anderson (7)	**5-hexynoic Mn-Anderson**
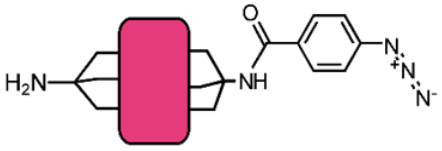	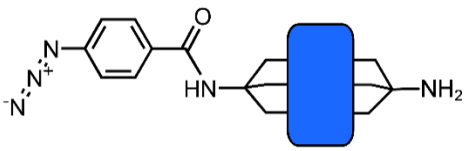
4-azidobenzoic/TRIS Cr-Andrsn. (27)	**4-azidobenzoic/TRIS Mn-Anderson (6)**

Table 5 Successfully isolated POM hybrid building blocks, available for coupling to form oligomers. Coloured square represents the Anderson cluster with metal centers: Mn (blue), Fe (yellow) and Cr (pink). Synthesis and isolation of the Mn-Anderson hybrids are described in an earlier chapter (Section 3.2.2).

3.3.3.1 Mixed-Anderson Trimer Formation

The first mixed-Anderson oligomer to be synthesised was a Mn/Fe/Mn-Anderson trimer (**Compound 28**) because the necessary starting materials, 5-hexynoic/TRIS Mn-Anderson (**Compound 7**) and 4-azidobenzoic Fe-Anderson (**Compound 23**) were the compounds most reliable to make and easiest to work with (**Figure 101**). As with the azide-alkyne couplings described in section 1.2.3 the reaction took place in dry, inert conditions with DIEA and CuI (s) in catalytic amounts. ESI-MS of the reaction mixture showed an expected trimer peak at m/z = 2821 (-1), suggesting probable success of the reaction. The crude material was then purified using the reverse phase flash chromatography system and method from section 1.3.9.2 and ESI-MS of the isolated fraction showed a simpler spectrum containing the trimer peaks and no starting materials present.

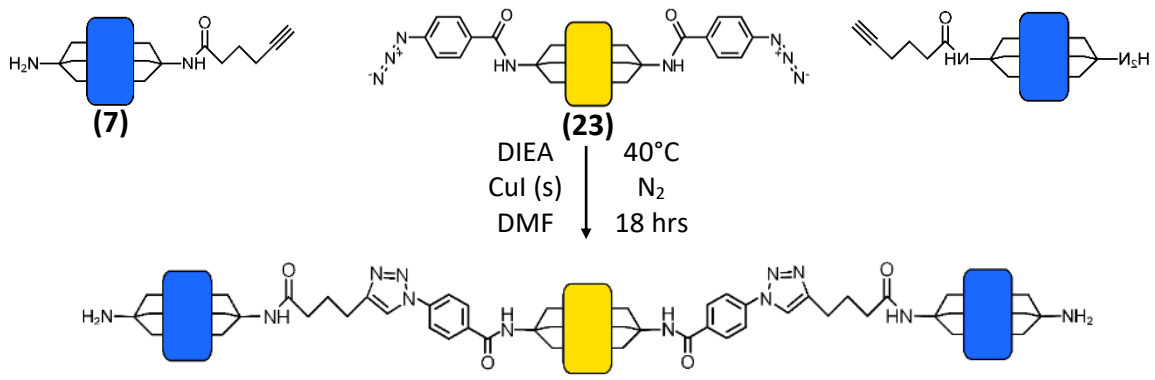

Figure 101 Reaction scheme for the synthesis of the Mn/Fe/Mn-Anderson (**Compound 28**) via azide-alkyne cycloaddition. Coloured squares represent Anderson cores with Mn (blue) and Fe (yellow) metal centres.

Similarly, 4-azidobenzoic/TRIS Cr-Anderson (**Compound 27**) and 5-hexynoic Fe-Anderson (**Compound 21**) were combined in an attempt to synthesise Cr/Fe/Cr-Anderson timer (**Compound 29**) (**Figure 102**). In this instance, a symmetrical alkyne POM hybrid was used instead of an azide-functionalised core like the one used for **Compound 28** because the only Cr-Anderson hybrid building block available was an asymmetric azide/TRIS hybrid. The initial ESI-MS measurement of the crude reaction mixture showed no clear indication of the outcome and separation of the products through RP-LC revealed 4 major fractions, most of which could themselves be subdivided. An attempt to purify the fractions through diethyl ether diffusion was made followed by some ESI-MS and ^{1}H NMR measurements and although there was some indication of starting material still present, the identity of the other fractions is still under investigation: whether expected product, unexpected product or building block breakdown has occurred remains unclear.

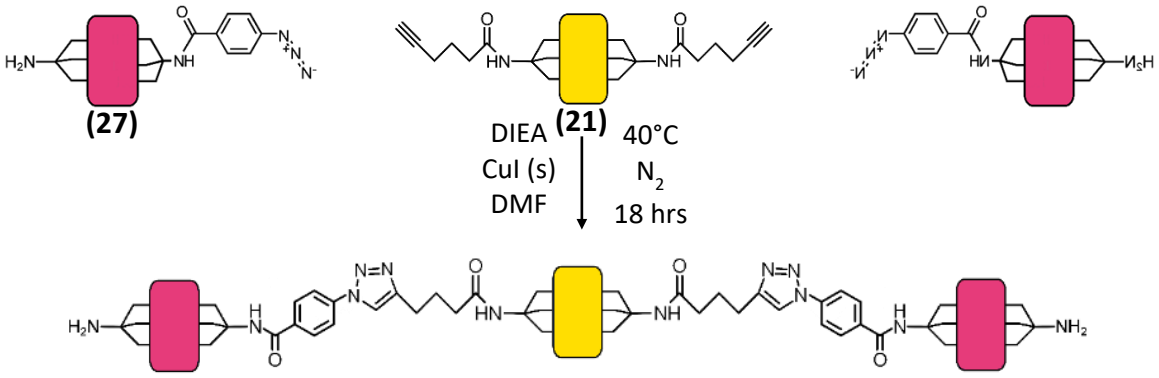

Figure 102 Reaction scheme for the synthesis of Cr/Fe/Cr-Anderson (**Compound 29**) via azide-alkyne cycloaddition. Coloured squares represent Anderson cores with Cr (pink) and Fe (yellow) metal centres.

A reaction for the formation of Cr/Mn/Cr-Anderson trimer (**Compound 30**) was then attempted using 4-azidobenzoic/TRIS Cr-Anderson (**Compound 27**) and 5-hexynoic Mn-Anderson as building blocks (**Figure 103**). This was carried out after speculation that the reactivity of the asymmetric Cr-Anderson compound could be verifiable when coupled to the most reliable and familiar building block, the Mn-Anderson hybrid. Again, initial ESI-MS measurements of the crude reaction mixture revealed no clear result and the purification step is currently under way.

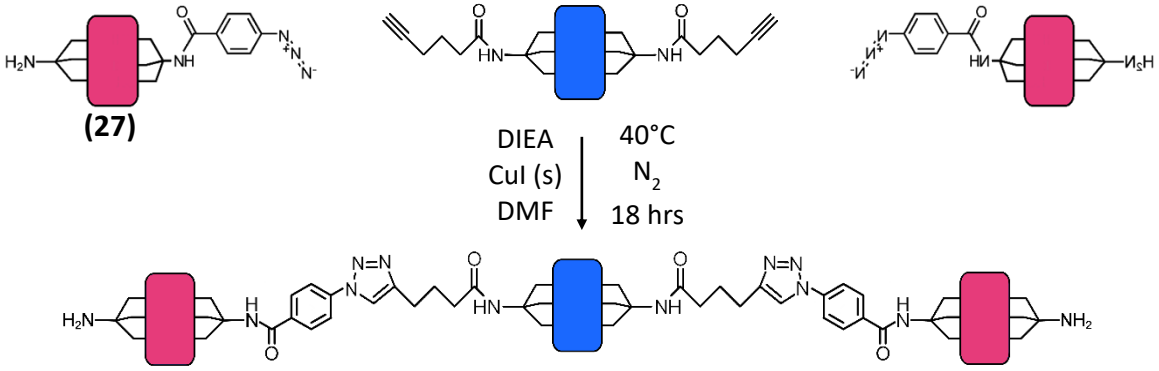

Figure 103 Reaction scheme for the synthesis of Cr/Mn/Cr-Anderson (**Compound 30**) via azide-alkyne cycloaddition. Coloured squares represent Anderson cores with Cr (pink) and Mn (blue) metal centres.

After two attempts at synthesis of a trimer-containing the Cr-Anderson hybrid, the reactivity of this 4-azidobenzoic/TRIS building block (**Compound 6**) was questioned. As a result, an Fe/Mn/Fe-Anderson trimer (**Compound 31**), was synthesised in order to form at least two different POM hybrid oligomers of varying sequence (**Figure 104**). Unfortunately, due to the challenging nature of the asymmetric Fe-Anderson hybrid synthesis described in section 3.3.2.2, this reaction was only possible on a small scale and resulting product was not in large enough quantities to make further extension of this

particular POM cluster chain possible. This coupling reaction used 5-hexynoic/TRIS Fe-Anderson (**Compound 22**) as the asymmetric building block and 4-azidobenzoic Mn-Anderson (**Compound 5**) as the symmetric central POM core. As with **Compound 29**, the chromatography purification step is currently under way.

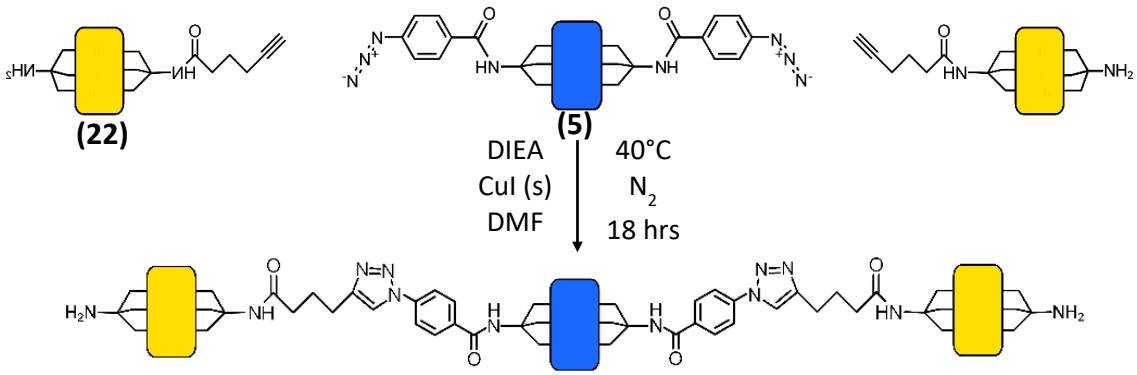

Figure 104 Reaction scheme for the synthesis of Fe/Mn/Fe-Anderson (**Compound 31**) via azide-alkyne cycloaddition. Coloured squares represent Anderson cores with Mn (blue) and Fe (yellow) metal centres.

3.3.3.2 Mixed-Anderson Pentamer Formation

Mn/Fe/Mn-Anderson trimer (**Compound 28**) was the only material synthesised in large enough quantities to allow for further extension of the oligomer chain to be attempted. Similarly to the method described in section 3.2.3, the Mn/Fe/Mn-Anderson trimer had to first be functionalised using two equivalents of 5-hexynoic acid in order for the "Click" coupling to be again possible (**Figure 105a**). This transformation of **Compound 28** to 5-hexynoic Mn/Fe/Mn-Anderson trimer (**Compound 32**) took place successfully without need for any modifications from the original method and the product to starting material ratio clearly traceable through ESI-MS with a total disappearance of the m/z = 2821 (-1) TRIS-trimer and conversion into m/z = 2915 (-1) 5-hexynoic-trimer.

In order to fully demonstrate the configurability of the oligomer-forming system, an attempt to add the third successfully isolated building block, 4-azidobenzoic/TRIS Cr-Anderson (**Compound 27**) to the trimer was made. Excess of the asymmetric Cr-Anderson monomer (**Compound 27**) and 5-hexynoic Mn/Fe/Mn-Anderson trimer (**Compound 32**) were reacted together under the same azide-alkyne cycloaddition conditions as with the previous couplings in an attempt to form a Cr/Mn/Fe/Mn/Cr-Anderson pentamer (**Compound 33**) (**Figure 105b**). Analysis of the initial reaction mixture with ESI-MS proved uninformative with no observable peaks of either starting materials or the expected

product and as with the separation of **Compound 33**, a large number of fractions were isolated, many of which are still unidentified.

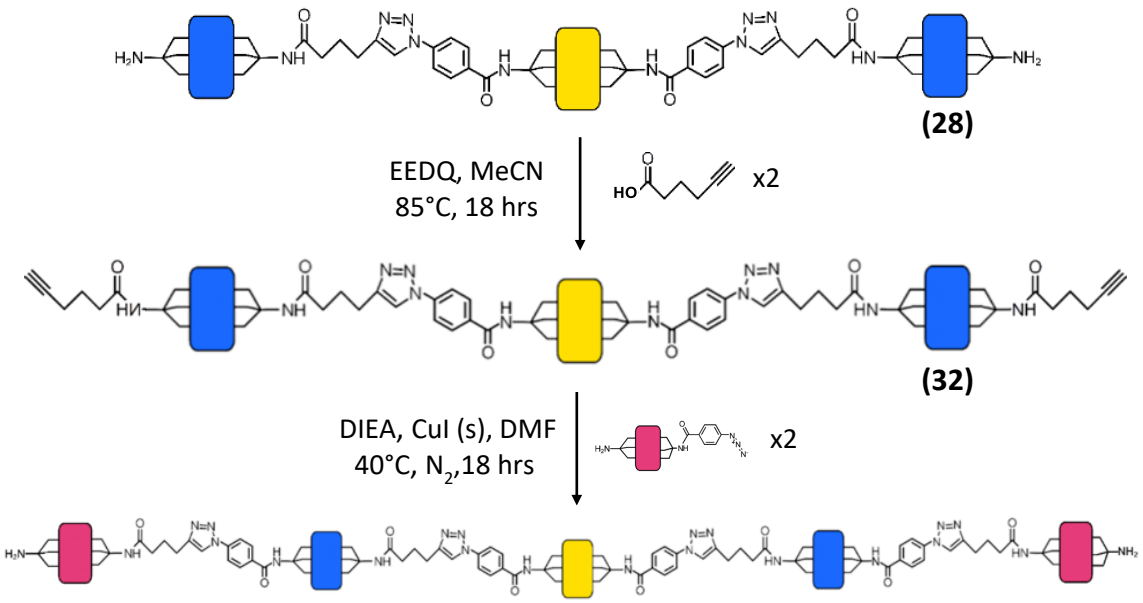

Figure 105 Reaction scheme for the synthesis of (a) 5-hexynoic Mn/Fe/Mn-Anderson followed by (b) Cr/Mn/Fe/Mn/Cr-Anderson (**Compound 33**) via azide-alkyne cycloaddition of 4-azidobenzoic/TRIS Cr-Anderson (**Compound 27**). Coloured squares represent Anderson cores with Mn (blue), Cr (pink) and Fe (yellow) metal centres.

3.3.4 Section Summary

This section builds directly on the previous project (3.2) which demonstrated how asymmetric Mn-Anderson hybrids could be coupled together through azide-alkyne cycloaddition to form oligomers of specific lengths. One way of expanding this work involved not only adapting the system for other POM hybrid monomers, but doing it in such a way that the different POM cores could be linked together in any order as a single chain. Development of such a system takes inspiration from the already existing configurable polymer systems that exist in biology, in particular peptide chains.

To begin with, a selection of monomer building blocks had to be developed that met a set of criteria which made them reliable starting materials. These, ideally asymmetric, POM hybrids needed to be stable, modifiable and high yielding in order to survive the varied and numerous steps needed to form “Click” coupled oligomers. A number of different building block candidates were worked with to explore how well they met the criteria required. The bi-functionalised Lindqvist hybrid **(Compound 17)** has previously been used in azide-alkyne cycloadditions and so was considered a promising candidate. Unfortunately, the yield of the hybrid formation reactions was too low to be useful as starting material.

Asymmetric Fe-Anderson hybrids **(Compound 20 and Compound 22)** were successfully synthesised using the same method as the one-pot Mn-Anderson hybrids but yielded products of much lower purity with by-products such as $\{Mo_6\}$ forming. This was greatly improved by the substitution of $Fe(acac)_3$ for FeOAc and the discontinuation of the use of the classic TRIS ligand whose basicity was altering the reaction conditions. Despite these improvements, purification of the asymmetric compounds still proved challenging due to the unfavourable solubility properties of the compound and so only small amounts of the asymmetric building blocks were isolated. The symmetric Fe-Anderson hybrids **(Compound 21 and Compound 23)** on the other hand, could be made in satisfactory quantities.

Attempts were made to form other metal-centred Anderson hybrids from one-pot organic reactions and during that process an entirely new POM hybrid **(Compound 24)** was found. On heating cobalt acetate, $\{Mo_8\}$ and HCl.TRIS ligand in DMF overnight a small

cobalt-centred cluster formed to which three TRIS ligands were grafted, but unexpectedly coordinated through the amine group and two of the hydroxyl groups, leaving a total of three hydroxyl groups free for functionalisation. Functionalisation of hydroxyl groups in the presence of a POM cluster however, proved challenging and so despite the ease of synthesis and high yields of the compound, it was not used as an oligomer building block.

An asymmetric Cr-Anderson hybrid **(Compound 27)** was synthesised through a set of aqueous and organic reactions where the POM core itself was made and then functionalised one ligand at a time. Firstly, the pure Cr-Anderson POM **(Compound 25)** was functionalised with a single HCl.TRIS group in aqueous hydrothermal conditions and then this single-sided TRIS Cr-Anderson **(Compound 26)** was refluxed in ethanol with the 4-azideobenzoic ligand for 3 hours.

Having successfully made three different types of metal-centred Anderson hybrid **(Compound 5, Compound 6, Compound 7, Compound 20, Compound 21, Compound 22, Compound 23, Compound 27)**: Mn, Fe and Cr, the concept of configurable mixed-POM oligomers could now be demonstrated. To begin with a symmetric Fe-Anderson **(Compound 23)** and an asymmetric Mn-Anderson **(Compound 7)** were coupled together forming a trimer **(Compound 28)**. This was functionalised **(Compound 32)** with 5-hexynoic acid and an attempt to add the asymmetric Cr-Anderson building block to both ends, forming a pentamer was made. The success of this Cr/Fe/Mn/Fe/Cr-Anderson pentamer **(Compound 33)** is still under determination as are the other three trimers which were also attempted: Cr/Fe/Cr-Anderson **(Compound 29)**, Cr/Mn/Cr-Anderson **(Compound 30)** and Fe/Mn/Fe-Anderson **(Compound 31)**.

4 Conclusions and Future Work

4.1 Guanosine Strandberg Structure

4.1.1 Solution-Phase Characterisation

As described in section 3.1.6, circular dichroism (CD) and atomic force microscopy (AFM) gave some indications that the guanosine Strandberg hybrid **(Compound 1)** forms an ordered structure in solution. However, the nature of this structure was not determined and remains a question to be answered. Finding a characterisation technique suitable to continue exploring this subject matter is not immediately obvious, as analysis of the system must be carried out in a viscous liquid or gel phase. Characterisation methods that are carried out in either solid or liquid phase would require dilution of the gel and as a result change the nature of the structure. Nonetheless, such solid or liquid analysis is still likely to continue shedding some light on the nature of the system: perhaps recrystallization under a variety of conditions would result in alternative packing, for example.

4.1.2 Guanosine Strandberg Analogues

Further study of other similar compounds may also prove helpful in developing an understanding of the guanosine Strandberg extended structure in various phases. An existing example of this is the previously mentioned "adenosine Strandberg" $Na_2[(HAMP)_2Mo_5O_{15}]$ (where AMP = adenosine 5'-monophosphate) which demonstrates how use of a different nucleotide results in crystal packing with a different helical axis (section 3.1.5).[360,361] Although it does share the same rise per turn as B-DNA (3.4Å), it forms a threefold twist with a 120°C rotation between each monomer. ^{1}H and ^{31}P NMR studies suggest that complexation occurs between AMP and molybdate in solution, but a specific structure has not been determined. Preliminary experiments using cytidine and thymidine monophosphates have not indicated the formation of any similar structures; nonetheless even if further reactions confirm this, measurements of these mixtures may still prove valuable as comparative data. Varying the metal oxide starting material and experimental conditions is also an option which could lead to a variety of other POM hybrid structures, however, although such clusters could be interesting in their own right, they are less likely

to be relevant to further understanding of the inorganic DNA-type structure as the variation of POM structures that could potentially form is very broad.

More notably, directions of study which could provide information of greater value are experiments involving a variety of guanosine 5'-monophosphate derivatives and experiments involving mixtures of nucleotides. As explained in section 1.5.2, guanosine has a much higher tendency to interact with itself and form gels than the other nucleotides.[292] As a result, one way to alter reaction conditions while trying to remain in the territory of viscous solution and gel analysis would be to use a variety of derivatives of guanosine 5'-monophosphate and observe how this effects the properties of the resulting gels and of course any crystal structures that happen to form.

A key characteristic of nucleotide chemistry is the variety of hydrogen bonding interactions available between the various purine and pyrimidine structures, some of which can be seen in **Figure 38**. The most well-known of these are the Watson-Crick base pairs between, cytosine with guanine and adenine with thymine, which are a key feature of the DNA double helix structure. These planar hydrogen bonded connections are one of the biggest differences between the Z-DNA structure and the guanosine Strandberg helix where the stacking of ligands is the most important interaction. It would be interesting to see whether altering the guanosine Strandberg reaction mixture to contain equal amounts of complimentary nucleotides, such as guanosine 5'-monophosphate and cytidine 5'-monophosphate could lead helical POM hybrid structures containing moieties that are Watson-Crick base paired, or otherwise interacting. Such a result would be stronger evidence to support Cairns-Smith's inorganic origin of life theory (section 1.6.3) as a POM hybrid containing paired nucleotides, especially if the order of these base pairs was shown to be adjustable demonstrating *configurability* of the structure, would be much stronger evidence of information-containing organic-inorganic systems.[352–354]

4.1.3 Polymerisation

The remarkable double helix motif found in the crystal form of the guanosine Strandberg compound is part of a greater supramolecular structure that extends out in all directions; it is not a stand-alone polymer strand as is seen with DNA molecules themselves. One possible area of further study could involve developing a method for isolation and

condensation of the POM hybrid forming individual double-helix strands. To achieve this it would be necessary to have one organic moiety of each guanosine Strandberg monomer incorporated into the core of the helical structure while the other moiety remains free around the outer rim (resembling the structure seen in **Figure 54c & d**). Finding conditions in which some of the guanine ligands behave and arrange themselves differently to the others could prove challenging and might involve finding the right equilibrium and working with dilute solutions. Another issue with this approach is that elimination of surrounding monomers and sodium cations would remove a lot of the stability of the extended structure and so it is questionable as to whether such a material would be able to stay intact. Despite all these complications, formation of individual strands is perhaps not impossible as the AFM results described in section 3.1.6 show how guanosine Strandberg arranges itself into fibres of 3.5 to 4.0 nm in width when the solution is dropped onto mica and this project is another reason why better understanding of the compound's structure in solution would be useful.

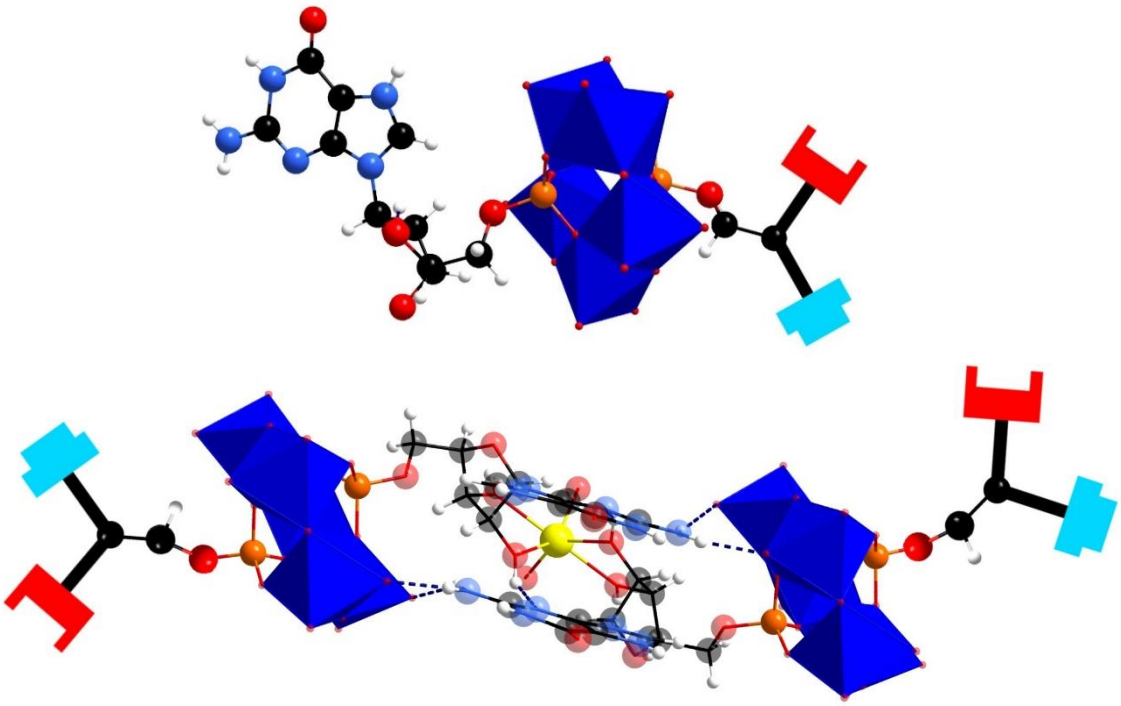

Figure 106 A cartoon representation of a hypothetical asymmetric guanosine Strandberg monomer (top) where the ball and socket mechanism represents a ligand allowing for formation of a polymerised backbone to the double helix structure. As with the standard guanosine Strandberg compound, the guanine-based ligand would stack in the core of the helical structure as displayed in with the dimer (bottom).

One approach could involve the synthesis and isolation of asymmetrically hybridised guanosine Strandberg monomers with a guanosine moiety on one side and a different

organic ligand on the other, so that the central stacked core of the double helix would only be able to form on one side of the monomer building blocks (**Figure 106**). This concept could be further developed if the second organic ligand was engineered to polymerise with itself, forming a covalently connected backbone to the outside of the strand and mimicking the phosphate-sugar backbone seen in nucleic acids themselves.

4.1.4 Enantiomer Work

The challenging nature of the D-guanosine 5'-monophosphate enantiomer synthesis prevented any further work in this part of the project from taking place (section 3.1.7). However, were a successful synthetic route for the GMP enantiomer developed, a number of experiments could then be completed with outcomes of variable predictability. Carrying out the standard guanosine Strandberg synthesis but using D-GMP for example, would most likely lead to formation of the same crystal structure except with a right-handed helical twist and an inverted CD spectrum. It should also be possible to try experiments combining both L- and D-GMP enantiomers to investigate whether the two opposingly twisted structures form in stoichiometric amounts, or whether one is favoured over the other with helical structures that remain separated, growing in different crystals or combine resulting in a structure containing twists going in both directions. It may also be possible for an entirely different structure to form, especially in the case where the proportions of starting material is varied and where small quantities of the opposite enantiomer could lead to the disruption of the crystallisation. The formation of crystal defects is a key concept used in Cairns-Smith's theories (section 1.6.3) and so exploring how it affects the guanosine Strandberg system could be interesting.

4.2 Mn-Anderson Oligomers

4.2.1 Limitations of the "Click" Chemistry Method

Now that the Mn-Anderson oligomer formation has been demonstrated, there are several clear directions for development that could lead to its improvement. The main limitation of the current method is the number of synthetic steps resulting in loss of yields and time. Whenever another two POM cores are added to the chain, the sample is purified using RP-LC and then crystallised under slow Et_2O diffusion. Making an oligomer longer in length becomes increasingly difficult with every additional step and requires an increasingly larger amount of material to be synthesised during the initial stages. Another limitation of the current method is the dependence on symmetry as it is only possible to build the chains up by adding identical POM cores to each end. Being able to create asymmetrical oligomers would add a useful additional level of control.

4.2.2 Solid Phase Anderson Oligomers

Solid phase (resin beads) could be used to synthesise oligomers at a faster pace as well as allowing the Mn-Anderson hybrids to be joined one POM core at a time providing more control over the oligomer's sequence (**Figure 107**). This concept is not dissimilar to the solid phase peptide synthesis (SPPS) method, were a resin-bound peptide is built up one amino acid at a time.[347] Such a method should be faster because the purification steps in the original method are eliminated: oligomers bound to resin beads are not soluble so after the addition of a new POM core, the unreacted material can simply be washed off with solvent. The resin-bound oligomers can then be used for the next reaction without the need for RP-LC separation or crystallisation.

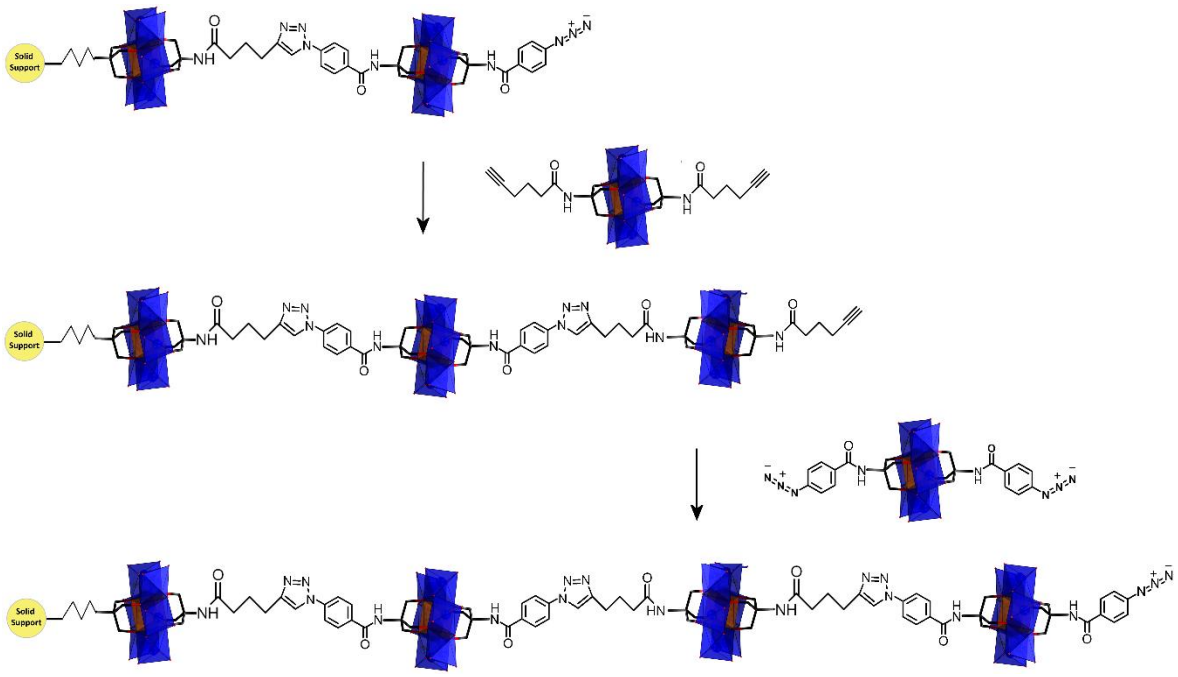

Figure 107 A simple schematic demonstrating how a Mn-Anderson hybrid tetramer could be formed using a solid phases synthetic protocol. In this diagram, use of symmetric Mn-Anderson monomers is proposed as they would be easier to obtain, if however this method proved ineffective, asymmetric versions could also be used.

Preliminary results have indicated that finding a suitable resin for binding to a POM may require some work as much of the solid phase literature focuses on protein synthesis and the methods would require a fair amount of change for adaptation to POM hybrids. Challenges involve overcoming the potential steric hindrance between the Mn-Anderson hybrids and the resin bead as well as testing the limits of the CuAAC reaction, which up till now has been carried out under inert atmosphere. Overcoming these issues with relative ease might be possible by altering the Mn-Anderson oligomerisation method to resemble peptide synthesis even more closely and using NHS Mn-Anderson compounds developed in the Cronin group for incorporation of a POM into a peptide chain (section 1.6.2.1, **Figure 108**).[384]

Finding appropriate analytical methods for tracking the synthesis is also essential, ideally a technique which allows samples to be measured while they are still bound to the solid phase. Mass spectrometry is the technique used to track oligomer synthesis using the current method which would be a bit more complicated when using a solid phase-based synthesis as some material would have to be cleaved from the resin bead in order to be used for the MS analysis. A method such as IR can be used initially to verify the bonding of the first Mn-Anderson with the resin but may not be qualitative enough to be used for further build-up of the chain.

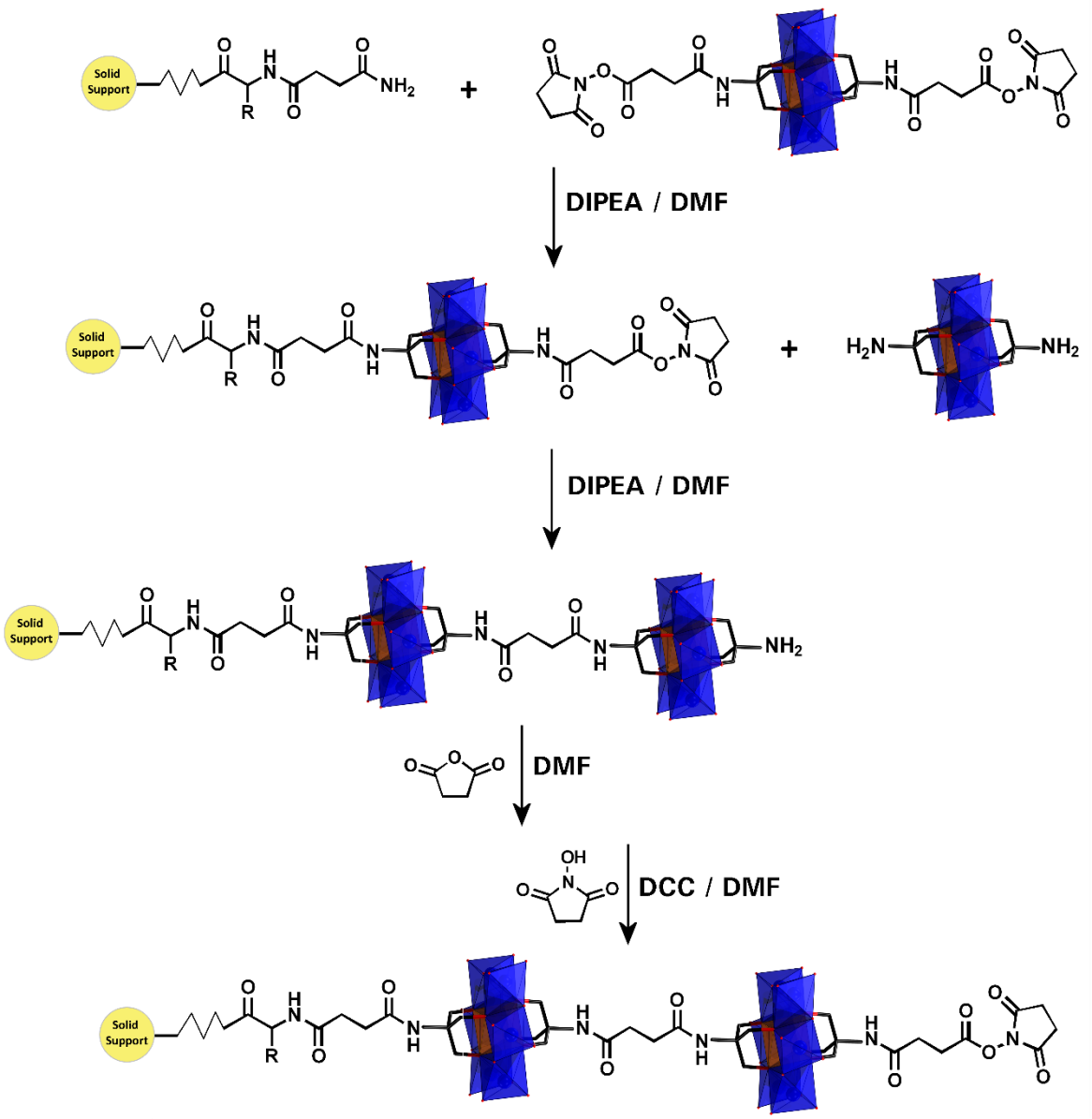

Figure 108 Reaction scheme demonstrating an oligomerisation method inspired by peptide synthesis and using NHS-functionalised ligands to form activated acid groups.

Continuing to draw parallels between POM hybrid oligomer synthesis and SPPS, once a system for solid phase POM hybrid oligomer synthesis is developed, automation of such a method would be an evident next step. This would allow for faster and more reliable formation of oligomers of any given length and access to greater quantities of the product which could then be used in further applications. As with the solid-phase development, automation of POM hybrid synthesis may be more rapidly achievable due to the "inorganic amino acid" work being undertaken in our lab, in parallel to this project (section 1.6.2.1). This complimentary work is currently focused on automation of inorganic SPPS and as this work continues to develop, adaptation of the Mn-Anderson oligomerisation in a similar manner should be possible.

4.3 Configured POM Hybrid Oligomers

4.3.1 Optimising Oligomer Formation

Configurability of the POM hybrid oligomerisation method described in section 3.2 and 3.3 has been demonstrated only tentatively and so in order to solidify these results, further work is necessary. To achieve this, several oligomers containing a mixture of POM hybrid building blocks in a variety of orders must be isolated and fully characterised. Firstly, larger quantities of starting material need to be obtained, either by continuing to optimise the synthesis and isolation of the current building blocks, Fe- and Cr-Anderson, or by working to develop several other organic-inorganic hybrid building blocks (and is discussed in the next section).

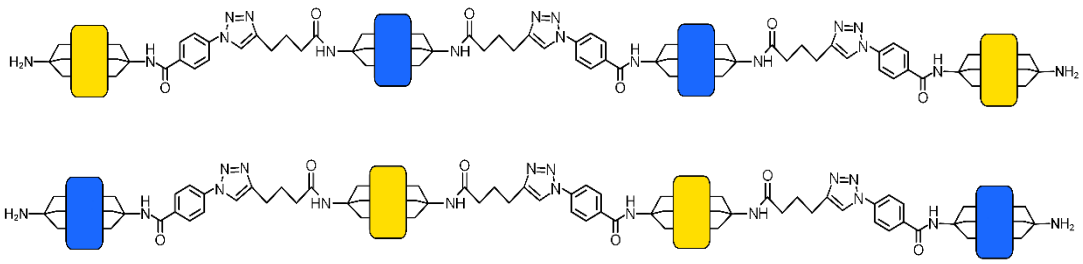

Figure 109 A representation of two POM hybrid oligomer isomers where only the central heteroatom differs (yellow – Fe, blue – Mn): Mn/Fe/Fe/Mn-Anderson hybrid tetramer and Fe/Mn/Mn/Fe-Anderson hybrid tetramer.

The other main challenge this project faces is analysis of the finished products. As the complexity of the configurable oligomer chains rises, characterisation will become increasingly difficult. This is especially the case with the different metal-centred Andersons who vary one from another by a single atom meaning they are unlikely to be easily differentiable in conjunction with identifying their position along a chain. Techniques such as mass spectrometry or elemental analysis, inductively coupled plasma atomic emission spectroscopy for example, would help with the determination of the building blocks present but not their order. X-ray diffraction on the other hand, would show the order and overall structure, but not reveal the identity of the central metal ions. In the case of chains formed of several metal-centered Andersons such as the sequences Fe/Mn/Mn/Fe and Mn/Fe/Fe/Mn, even a combination of MS, NMR, ICP and XRD would not be enough to fully confirm the identity of one sequence verses the other (**Figure 109**). The ideal form of analysis would allow for identification of each individual building block

as it moves along the chain, much like the biological molecules involved in the reading of nucleic acids, a concept adopted by nanopore technology (**Figure 110**).[385,386]

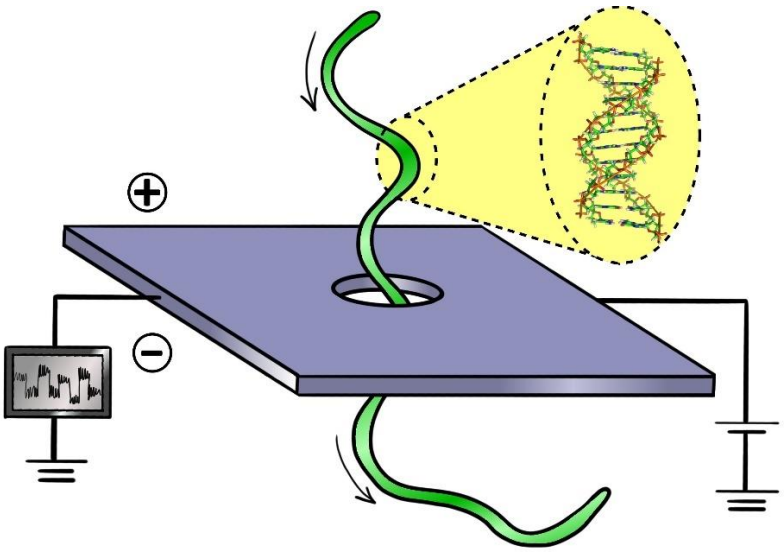

Figure 110 Cartoon demonstrating the basic concept behind nanopore technology.

Development of a more reliable purification system would make characterisation easier, successfully growing crystals for example, would be a challenging breakthrough to make. As has been discussed in section 4.2.2, another possible way to form purer compounds in fewer steps would be to once again follow in the footsteps of synthetic biochemistry and use solid-phase to make the oligomer chains. Not only would this build-up of the chain from a resin bead break the symmetry of the system, but it would also remove the chromatography separation step.

4.3.2 Continued Building Block Development

To fully complete the Cr-Anderson hybrid series, the preliminary synthesis of the FMOC/TRIS Cr-Anderson hybrid (section 3.3.2.4) should be followed up as it could be used to make both the symmetric and asymmetric 5-hexynoic Cr-Anderson building blocks, which would give the hybrid a fuller range of options, for example use as the centre cluster of a trimer.

For the Fe-Anderson hybrid and Cr-Anderson hybrid building blocks to be more reliably isolated, further optimisation of their separation and purification is necessary. Using and adapting methods already established for the isolation of the asymmetric Mn-Anderson hybrids has resulted in lengthening of the synthetic process as steps were added to

accommodate for the property differences of these other building blocks. Even with adjustments, the efficiency and reliability of the separation technique is not so well adapted for the Fe- and Cr-Andersons and taking an altogether different approach might result in quicker and simpler purification method being developed. This could involve a radical change in the chromatography technique using different types of columns and solvent mixes or exploring other purification techniques such as gel electrophoresis or fractional crystallisation.

Other metal-centred Anderson hybrids could of course be adapted in similar ways to either the Fe- or Cr-Anderson. The Al-Anderson for instance, is often used in hybrid research and follows the same synthetic step-wise pathway as the Cr-Anderson where the pure POM is synthesised initially followed by sequential addition of organic moieties.[387]

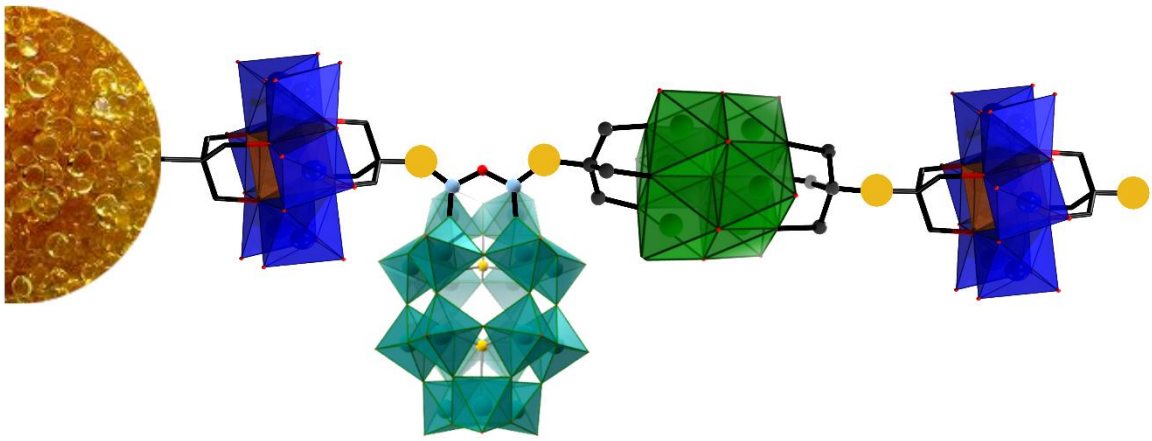

Figure 111 Representation of a POM hybrid oligomer linking together Anderson (blue), Dawson (teal) and Lindqvist (green) POM cores starting from a solid support. Here the binding mechanism is left ambiguous.

As discussed in section 3.3.2.1, the major limitation of the Lindqvist hybrid is its yield: without larger amounts of material it is unsuitable as a building blocks for the start of a multi-step synthesis. With further work optimising the synthesis of the [V_6] Lindqvist cluster, the incorporation of the cluster into a configurable oligomer should be possible and it would be a simple way of adding more variety to POM oligomers which up till now only contain molybdenum-based Anderson clusters. Another POM that can be TRIS functionalised and is often used in organic-inorganic hybrid systems is the Dawson. Exploration of this cluster as a building block cluster would be worthwhile due to the versatility of the Dawson POM although it should be noted that as with the Lindqvist hybrid, yield is likely to be a major limiting factor (**Figure 111**).

4.3.3 {$CoMo_3$} Hybrid Development

If the solubility restrictions and the reactivity of the hydroxyl groups on the {$CoMo_3$} hybrid (section 3.3.2.3, **Compound 24**) were resolved, then this could potentially lead to a number of interesting structures. A capsule made from three chains or linkers capped at either end, or even a more complex composition of this nature could be created (**Figure 112**). The angles of the three ligands one from another is key in determining the number of possibilities: the larger the angle, the longer the chains would need to be to make joining up again at the other end possible. In these large angle cases, bigger capsule or cage-like structures would probably be preferred.

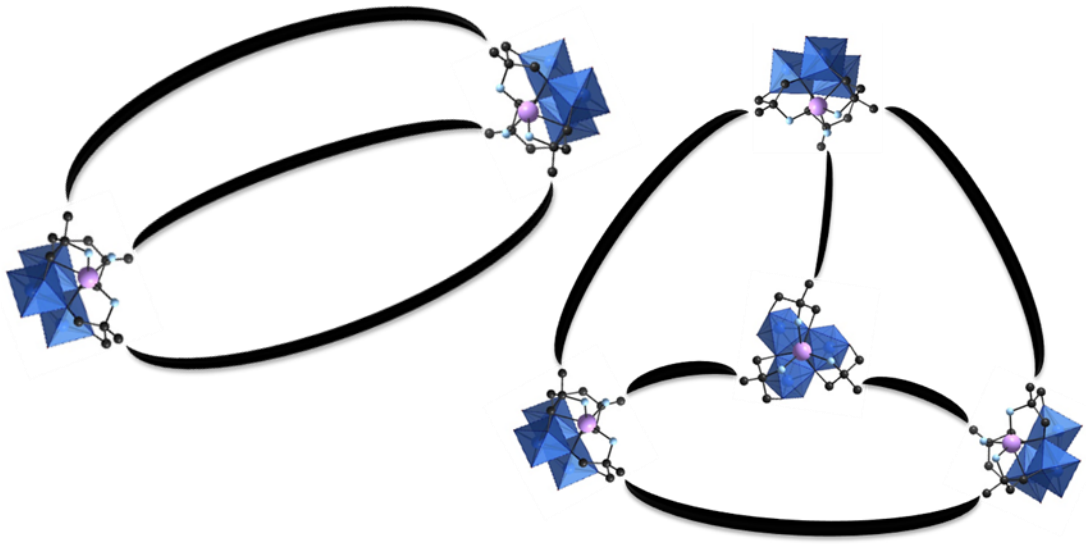

Figure 112 Visual speculation over what a capsule (left) and pyramid (right) made from connecting {$CoMo_3$} hybrids together via an appropriate linker would look like. Colour code: dark blue - Mo, pale blue - N and lilac - Co.

Formation of asymmetric versions of the {$CoMo_3$} hybrid by functionalisation of the individual ligands separately would increase the potential of the cluster. To achieve this, a pre-functionalisation method like the one used for the synthesis of asymmetric Mn-Andersons where several different ligands are included in the reaction mixture and the resulting products are separated through chromatography would have to be used. The two main challenges this approach would face are the adaptation of the RP-LC separation method to suit this compound and finding TRIS based ligands containing two hydroxyl groups, one amine and a different functional group. Another potential option would be post-functionalisation using a very diluted quantity of reactive species in an attempt to modify only one or two out of the three identical ligands of the {$CoMo_3$} hybrid.

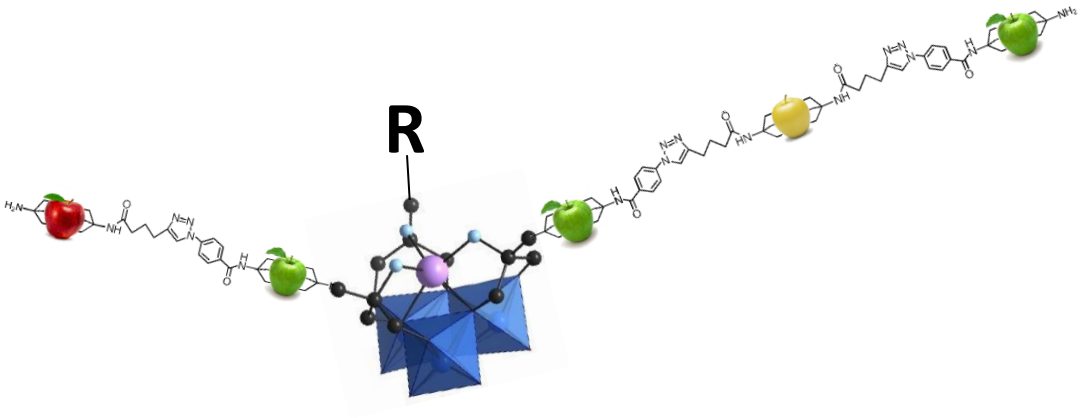

Figure 113 Cartoon representation of a POM hybrid oligomer chain containing an {$CoMo_3$} hybrid where the spare ligand, R could act as a pendent group available for surface binging or further extension of the chain in a third direction. Dark blue - Mo, pale blue - N, lilac - Co and the apples ("pommes" in French) represent unspecified organic-inorganic cores.

Assuming these challenges were overcome, the resulting asymmetric species could have a variety of unreactive and reactive ligands and would increase the number of possibilities the compound could be used for. If only two of the three ligands were functionalised with reactive species, for example, the compound could be used as an ordinary bi-functionalised hybrid building block and could be positioned somewhere along the length of the oligomer chain. This would leave a pendant group available for post-functionalisation such as binding to a surface, addition of side-branch oligomer chain or incorporation into a biological system (**Figure 113**).

5 Experimental

5.1 Materials

Unless otherwise mentioned, all solvents and reagents were purchased from commercial sources (primarily Sigma Aldrich and Tokyo Chemical Industry UK) and were used without further purification. TBA octamolybdate ($((C_4H_9)_4N)_4[\alpha\text{-}Mo_8O_{26}]$)[41] and TBA TRIS Mn-Anderson ($((C_4H_9)_4N)_3[Mo_6O_{24}\text{-}(C_4H_8N)_2]$)[267] starting materials were synthesised following the published procedures.

5.2 Instrumentation

5.2.1 Elemental Analysis (Microanalysis)

Carbon, hydrogen and nitrogen content were determined by the University of Glasgow School of Chemistry microanalysis services using an EA 1110 CHNS CE-440 Elemental Analyser.

5.2.2 ICP-OES

30mg of **Compound 1** was submitted to the *Institut für Festkörperforschung in Jülich*, Germany, for analysis of Mo, Na and P. Sample was digested in a 3:1 mixture of HNO_3 and H_2O_2. A TJA-IRIS-Advantage spectrometer with echelle optics and CID semiconductor was used to observe in the wavelength range 170 – 900 nm.

5.2.3 Fourier-transform infrared (FT-IR) spectroscopy

The compound was prepared as a powdered sample and measured using a Shimadzu FTIR 8400S Fourier Transformer Infrared Spectrophotometer with attenuated diffraction diamond cell (“golden gate”). Wavenumbers (ν) are given in cm^{-1}; intensities are denoted as w = weak, sh = sharp, m = medium, b = broad, s = strong.

5.2.4 NMR Spectroscopy

NMR data for compounds **1-13** was recorded on a Bruker Avance 400 MHz at T = 300 K and compounds **14-32** recorded on a Bruker Advance 600 MHz. ^1H NMR at 600 MHz and ^{13}C NMR at 150.9 MHz; deuterated solvents were purchased at Goss Scientific. The

samples were prepared from D_2O/H_2O (1/10) solutions, the pD/pH adjusted by DCl/D_2O (0.2 M). The NMR spectra are referenced to the peaks of 3-(Trimethylsilyl)propionic-2,2,3,3-d_4 acid (87 mM, δ (H, C of the TMS-group) = 0.0 ppm) and D_3PO_4 (1 mM, δ = 0.0 ppm) in D_2O. The peaks are denoted s = singlet, d = doublet, m = multiplet, br = broad and all coupling constants (J) are given in Hz.

5.2.5 CD-Spectroscopy

CD Spectra were recorded in a JASCO J-810 spectropolarimeter in quartz cells using pathlengths ranging from of 0.001 cm to 0.01cm.

5.2.6 AFM

The AFM pictures were taken in semi-contact mode using the NTEGRA Spectra platform of NTMDT. The cantilevers used were purchased from NTMDT (NSG10, resonant frequency 140-390 kHz, force constant 3.1-37.6 N/m). The samples were prepared by drop cast 10 µl of the solution of 1 (0.1 mg/mL, pH = 1.95 adjusted by 1 M HCl, matured for 6 days) on a freshly cleaved mica surface.

5.2.7 Tube Inversion Tests

The samples for inversion test were prepared by addition of HCl (1M) to the solutions of $Na_2MoO_4 \bullet 2H_2O$ and $Na_2GMP \bullet H_2O$ after which the purity of **compound 1** was verified by ^{31}P NMR. Each sample was left standing for 20 min every time before conducting the inversion test.

5.2.8 Differential Thermoanalysis / Thermogravimetric Analysis

DTA/TG-measurements were performed on a Netzsch STA 409 thermal analyser with a heating rate of 10°C/min.

5.2.9 DNA-Annealing Experiments

The interaction of **compound 1** with DNA was assessed by incubating of 9 µg of each compound with double stranded (ds) and single stranded (ss) plasmid DNA (pGLO, 500µg

in each case; in 12.6 mM acetate buffer at pH = 4.0) and resolving the complex formation on a 1% agarose TAE gel adjusted to contain 0.5 µg/mL ethidium bromide.

5.2.10 Electrophoresis

The electrophoresis studies were performed using a commercially available submarine-type electrophoresis system (Pt-wire electrodes set at a distance of 13 cm).

5.2.11 Electrospray Ionisation Mass Spectroscopic Measurements

Measurements for compounds **1-33** were carried out at 180 °C in MeCN using a Bruker MaXis Impact instrument. Standard tuning mix was used, enabling calibration between approximately 50 - 2000 m/z. Samples were dissolved in MeCN and introduced into the MS at a dry gas temperature of 180°C. The ion polarity for all MS scans recorded was negative, with the voltage of the capillary tip set at 4500 V, the end plate offset at -500 V, the funnel 1 RF at 400 Vpp, the funnel 2 RF at 400 Vpp, the hexapole RF at 400 Vpp, the ion energy at 5.0 eV, the collision energy at 15 eV, the collision cell RF at 2100 Vpp, the transfer time at 120.0 µs, and the pre-pulse storage time at 20.0 µs. Each spectrum was collected for 2 min using an AD scientific syringe pump. Analysis of these MS spectra was carried out using Data Analysis 4.0 software supplied by Bruker Daltonics.

Measurements for all Ion-Mobility Spectrometry - Mass Spectrometry (IMS-MS) was performed on a Waters Synapt-G2 instrument equipped with Quadropole and Time of Flight modules (Q/TOF). The standard tuning mix used allowed calibration between 500 – 5000 m/z and the samples were intruduced using a Harvard syringe pump. For compounds (guan) the following parameters were used: ESI capillary voltage, 2.7 kV; sample cone voltage, 30 V; extraction cone voltage, 4.0 V; source temperature, 80 ˚C; desolvation temperature, 180 ˚C; cone gas (N_2) flow, 15 L/h; desolvation gas (N_2) flow, 750 L/h; source gas flow, 0 mL/min; trap gas flow, 2 mL/min; helium cell gas flow, 180 mL/min; IMS gas flow, 90 mL/min; IMS wave velocity, 1000 m/s; IMS wave height, 40 V. For compounds **1-13** the settings were a capillary voltage of 2.7 kV, a sampling cone voltage of 94 kV and an extraction cone voltage of 4.0 kV, a source temperature of 80°C and a desolvation temperature of 180 °C and a cone gas flow of 15 Lh^{-1} and a desolvation gas flow of 750 Lh^{-1}. For the IMS-MS mode, MS conditions were as described for the

negative mode ESI-MS measurements above. The IMS facility is provided by a travelling-wave drift cell located between the quadropole and time-of-flight sections and consists of a trap-, an ion-mobility- and a transfer-cell. Analysis of IMS-MS spectra was conducted using the DriftScope v2.1 software included in the MassLynx v.4.1 software provided.

IMS-MS spectra were further processed using UniDec[216] to allow clear visualisation and produce mass distribution spectra (i.e. deconvoluted "neutral mass spectra"). Briefly, the data processing workflow ran as follows (i) raw data files were loaded into UniDec; (ii) some filtering/processing was carried out – primarily subtraction of a curved background and gaussian smoothing in the m/z domain and application of a 5-10% minimum intensity threshold; (iii) peak width and shape was assigned using the UniDec GUI's dedicated tool; (iv) manual assignment of peak charge was made in most cases, where charge was clearly observable; (v) deconvolution was run, yielding 'cube' figures of the IMS-MS data, and deconvoluted "neutral mass" spectrum.

5.2.12 Single Crystal X-ray Diffraction

Single crystal X-ray diffraction was performed on a Bruker Apex II Quasar charge-coupled device (CCD) detector (λ (MoKα) = 0.71073Å) at 150(2) K, with the data reduction and structure solution performed using the Apex2 software package. Corrections for incident and diffracted beam absorption effects were applied utilising analytical numeric absorption correction with a multifaceted crystal model,[388] or using empirical absorption correction.[389] Refinement was carried out with SHELXS-97 or -2013[35] and SHELXL-97 or -2013[35] using WinGX[390] via a full matrix least-squares on F2 method.

5.2.13 HPLC Measurements

RP-HPLC measurements were performed on an Agilent 1100 Series (Agilent Technologies) equipped with a vacuum degasser, a binary pump (G1312A), a thermostated column compartment (G1316A), a standard autosampler (G1313A) and a variable wavelength detector (VWD) (G1314A). 5 µL of the samples were injected on a Phenomenex Luna® 3 µm C18(2) 100 Å, 150 x 2 mm column and eluted at 0.5 mL/min with a gradient of 0.05 M ammonium acetate (pH = 6.7 - 6.9) (A)/MeCN (B) (solvent gradient given in Table 2). The oven temperature was set to 25 °C and elution was detected by UV (λ = 254 nm). The data recorded was processed using Bruker compass Hystar 3.2 (Bruker Daltonics) and

Hyphenation Star PP software. SE-HPLC Measurements were performed on the same instrument and processed in the same manner, but used a Phenomenex PolySep GFP-P 2000 size-exclusion column and a constant solvent composition of 50% A and 50% B, with a flow rate of 0.5 $mLmin_{-1}$ and a runlength of 30 min.

Time (min)	**A** (%)	**B** (%)
0.0	95	5
3.0	95	5
15.0	5	95
17.0	5	95

Table 6 Eluent composition for RP-HPLC measurements. Runlength 17.0 min.

5.2.14 Flash Chromatography

Flash chromatography separations were performed on a Reveleris® iES Flash chromatography system using the Reveleris® NavigatorTM software. Before injection, columns were equilibrated for 4 min with 65:35 of A/B solvents at 18 mL/min. Samples were injected dry on Pre-packed Reveleris® C18 4 g columns (two in series), adsorbed on celite (20 wt%, maximum total weight 1.8 g (i.e. 300 mg of compound adsorbed on 1.5 g of celite® 535 coarse)). Columns were eluted at 18 mL/min with a gradient of solvent A and B (see Table 3) and elution was detected by UV (at λUV1 = 254 nm and λUV2 = 350 nm) and an ELSD (carrier solvent: isopropanol).

Time (min)	**A** (%)	**B** (%)
0.0	65.0	35.0
2.2	65.0	35.0
11.8	5.0	95.0
12.9	5.0	95.0

Table 7 Eluent composition for flash chromatography. Run length 12.9 min.

After the separations performed for compounds, solvent A was replaced with a 0.01 M TBABr solution with the pH adjusted to 7 by addition of TBAOH and the two 4 g columns were replaced with one 12 g column from the same series. This system was used for all other separations.

5.3 Compound Synthesis

Compound 1 Guanosine Strandberg

$Na_2[(HGMP)_2Mo_5O_{15}]\bullet 7H_2O$

$Na_2MoO_4\bullet 2H_2O$ (0.72 g, 3.04 mmol, Merck, Darmstadt, Germany, p.a.) and $Na_2GMP\bullet H_2O$ (**13**, 0.61 g, 1.44 mmol, ABCR, Karlsruhe, Germany, 98%) were dissolved in H_2O (10 ml). 1.0 M HCl (7.2 ml) was added upon vigorous stirring over the course of 15 min adjusting the pH to 3.24. H_2O (6 ml) was added after further 50 min of stirring to the reaction mixture. The stirring was continued for further 30 min. A white solid was obtained upon MeOH-vapour diffusion after a week. The white product was separated from the gelatinous reaction mixture via centrifugation (1600 rpm, 1 hr) and washed 3 times with 20 ml portions of MeOH. 0.70 g (0.43 mmol, 58%) of the product was obtained after drying it for two days in air and two hours under dynamic vacuum (0.02 mbar).

^{1}H NMR (400 MHz, c = 28 mg/ml, pD = 2.60, ppm): 4.48 (m, 1H, $H^{4'}$), 4.53 (m, 1H, $H^{5'}$), 4.60 (m, 1H, $H^{5'}$), 4.72 (m, 1H, $H^{3'}$), 4.96 (m, 1H, $H^{2'}$), 6.00 (d, $^3J_{H1'H2'} \approx 6.3$ Hz, 1H, $H^{1'}$), 8.68 (s, 1H, H^8). **^{13}C NMR** (101 MHz, c = 28 mg/ml, pD = 2.60, ppm): 68.0 (d, $^2J_{C5'P} \approx 4.4$ Hz, $C^{5'}$), 73.9 ($C^{3'}$), 77.0 ($C^{2'}$), 87.6 (d, $^3J_{C4'P} \approx 9.7$ Hz, C^{4R}), 90.3 ($C^{1'}$), 140.2 (C^8), 154.0, 157.3, 160.3 (C^2, C^4, C^6). ^{31}P NMR (162 MHz, c = 5.6 mg/ml, pD = 2.92, ppm): 0.97 (dd, $^3J_{PH5'} \approx 3.9$ Hz, $^3J_{PH5'} \approx 7.8$ Hz). **IR** (KBr): v (cm^{-1}) = 3350 (very broad, vs, 2938 (w), 1696 (s), 1635 (s), 1599 (s), 1533 (m), 1480 (w), 1411 (w), 1361 (m), 1250 (w), 1139 (s), 1073 (s), 993 (s), 932 (s), 907 (s), 798 (w), 681 (broad, vs), 526 (w), 496 (w). **Elemental Analysis** (%): Calc. for $C_{20}H_{40}Mo_5N_{10}Na_2O_{38}P_2$: C 14.86, H 2.49, N 8.67, Mo 29.68, Na 2.84, P 3.83; found: C 15.05, H 2.31, N 8.77, Mo 28.8, Na 3.38, P 3.63.

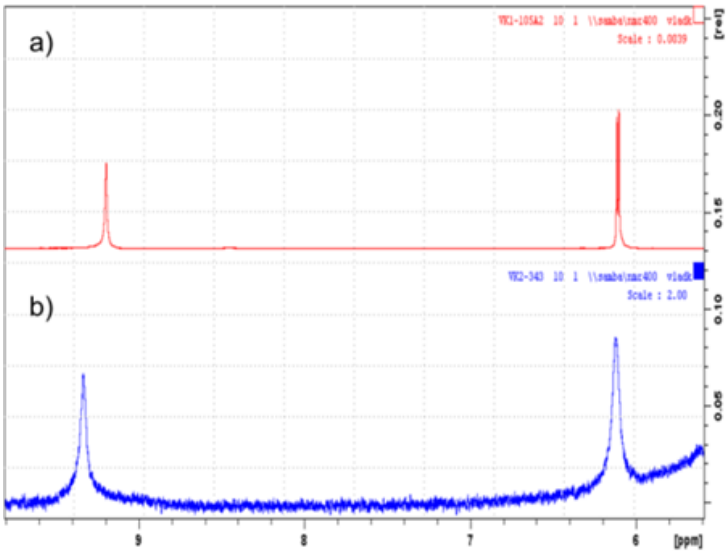

Low field region of the ^{1}H-NMR spectrum of **1**: a) c = 5.6 mg/ml; pD = 2.92; b) c = 35.9 mg/ml; pD = 2.15.

Compound 2 Guanosine 5'-Monophosphate

$C_{10}H_{12}N_5Na_2O_8P \cdot xH_2O$

Method A

Method adapted from existing procedure.[364]

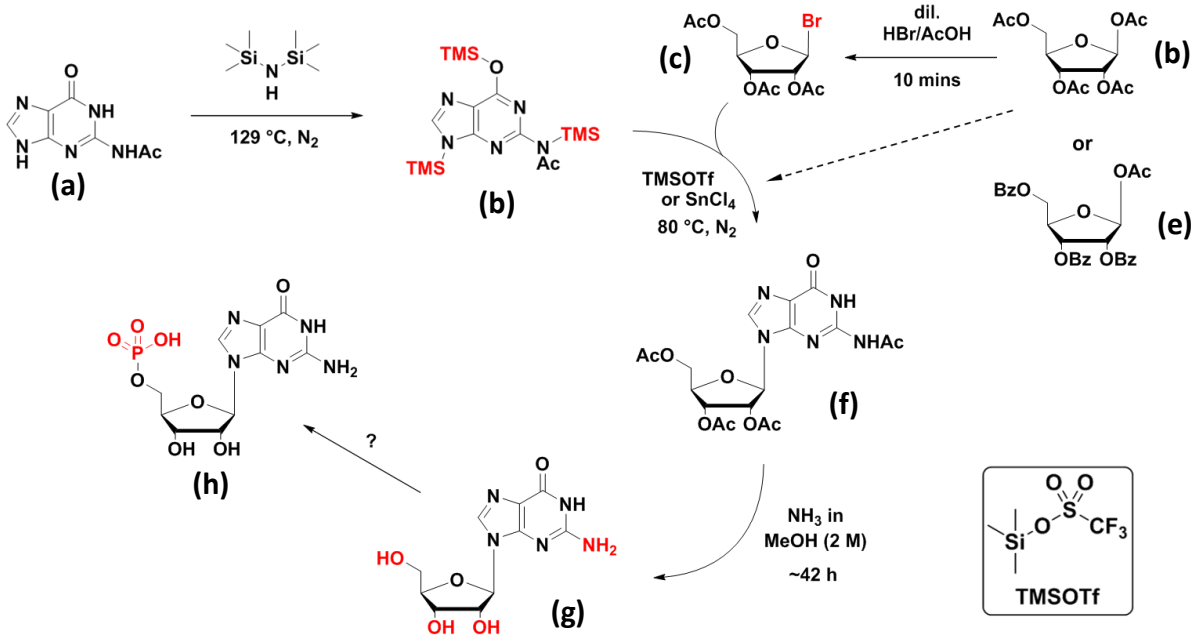

A mixture of N^2-acetylguanine (**a**) (0.777 mmol, 150 mg), hexamethyldisilazane and timethylchlorosilane (1.553 mmol, 169 mg, 197uL) was left to reflux at 145°C under nitrogen for 18 hours. The excess HMDS was removed by co-distillation with xylenes and the mixture dried under vacuum. ß-D-Ribofuranose 1-acetate 2,3,5-tribenzoate (**e**) (0.396 mmol, 200mg) was added to the crude mixture and 35mL of dry DCE was added. $SNCl_4$ (5.726 mmol, 1.491 g, 670 µL) was added and the mixture heated under nitrogen protection under reflux at 80°C for 2-3 hours until no starting material remained. 2mL of fridge-cooled $NaHCO_3$ solution was added followed by 20mL DCM. Precipitate filtered off and the aqueous and organic phases separated. The organic phase was dried over Na_2SO_4, filtered and dried under vacuum until crystals (**f**) formed in the flask.

Crude product (**f**) was dissolved in 4mL dry 2M NH_3/MeOH solution and left to stir at room temperature for 24 hours. The volatiles were removed under vacuum and the

remaining solid redissolved in 10mL MeOH:DCM 1:1. The solution was stirred for 1 hour and the solvents then removed under vacuum leaving crude product, (**g**). Results inconclusive.

Method B

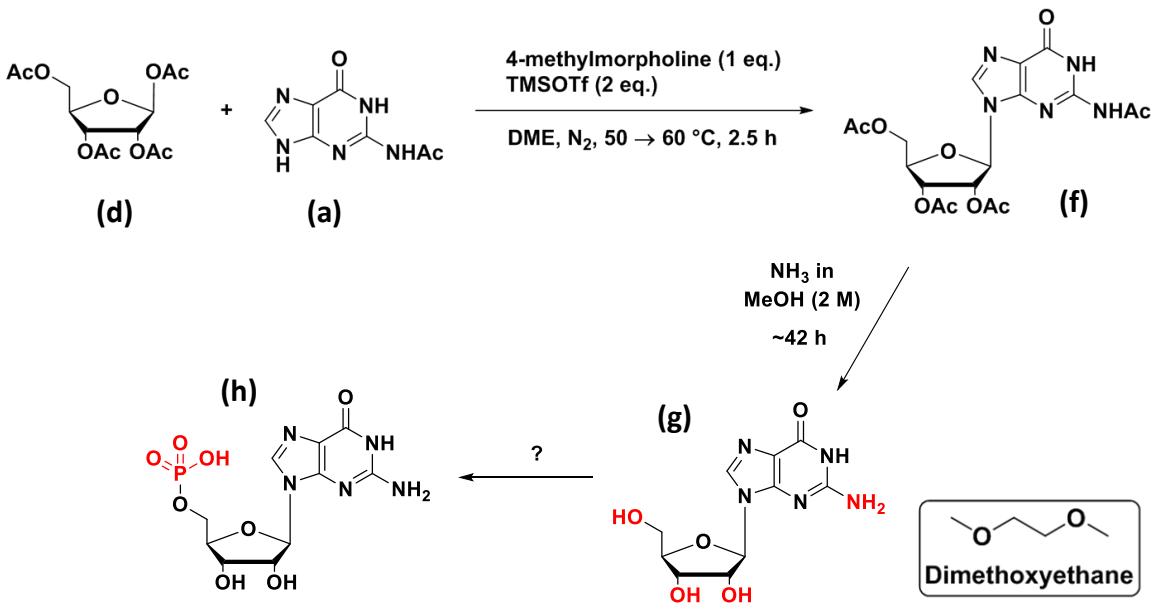

First part adapted from existing procedure.[368]

ß-D-Ribofuranose 1,2,3,5-tetraacetate (**d**) (3.7 mmol, 1.178 g) and 7mL acetic acid were combined and left to cool to 0°C. 7mL of 30 percent HBr:AcOH was added to the mixture dropwise and left to stir at room temperature for 10 minutes. The reaction mixture was poured into a 50mL ice-water mixture and the aqueous layer was extracted with CH_2Cl_2 and organic layers washed with cold saturated sodium bicarbonate solution, dried over sodium sulfate and concentrated under reduced pressure. Crude mixture (**c**) dissolved in 4.5mL DME and used immediately.

Second part adapted from existing procedure.[369]

N-methylmorpholine (3.55 mmol, 4.04 mL) was added to N^2-acetylguanine (**a**) (3.905 mmol, 754 mg) dissolved in 4mL DME. Mixture heated to 50°C and TMSOTf (4.19 mmol, 0.76 mL) added. The temperature was raised to 65°C and crude solution of (**c**) was added over the course of 15 minutes. Reaction mixture stirred at 65°C for 90 minutes and upon completion was quenched at 65°C over a period of 15 minutes with an aqueous solution

of trisoduim citrate monohydrate (522 mg, 1.78 mmol) and citric acid (342 mg, 1.78 mmol) in water (5mL). Reaction mixture diluted in MeOH and solid filtered off. Phases were separate, aqueous layer washed with DCM and organic layer washed with water. Organic layer concentrated down and purified using flash chromatography, column 35cm x 16cm, DCM/MeOH 20:1.

Crude product (**f**) was dissolved in 4mL dry 2M NH_3/MeOH solution and left to stir at room temperature for 24 hours. The volatiles were removed under vacuum and the remaining solid redissolved in 10mL MeOH:DCM 1:1. The solution was stirred for 1 hour and the solvents then removed under vacuum leaving crude product, (**g**). Results inconclusive.

Compound 3 FMOC/TRIS Mn-Anderson Hybrid

$((C_4H_9)_4N)_3[MnMo_6O_{24}(C_{19}H_{18}NO_2)(C_4H_6N)]$

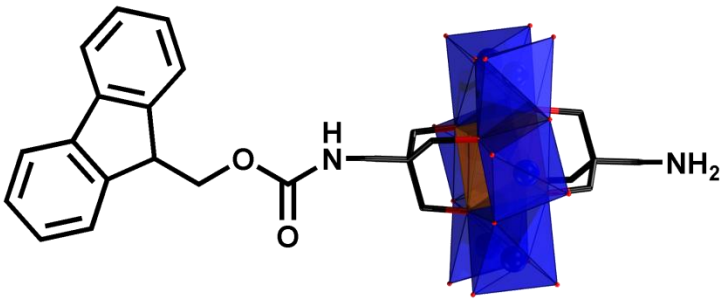

A mixture of $((C_4H_9)_4N)_4[\alpha\text{-}Mo_8O_{26}]$ (1.53 g, 0.71 mmol), $Mn(OAc)_3{\cdot}2H_2O$ (0.44 g, 1.62 mmol), TRIS (0.28 g, 1.87 mmol) and FMOC-TRIS[391]($FMOC\text{-}NHC(CH_2OH)_3$, 0.64 g, 1.87 mmol) was refluxed in MeCN (45 mL) for 18 h. The resulting brown mixture was cooled down to room temperature and the precipitate removed by centrifugation to lead to a bright orange solution. The crude mixture was isolated by crystallisation by Et_2O diffusion, giving orange crystals after three days, which were isolated (crude mixture yield: 1.40 g). 300 mg of the crude mixture was combined with celite (1.5 g) in 20 mL of MeCN then evaporated under vacuum to obtain a powder. The crude material adsorbed on celite was purified by flash chromatography and the pure fractions (purity checked by RP-HPLC with a retention time of 12.84 min) were combined and a large excess of TBA bromide (0.5 g, 1.55 mmol) was added to the resulting light orange solution. The MeCN was evaporated under vacuum causing a white/orange powder to precipitate from the remaining water. This precipitate was isolated by centrifugation then dissolved in MeCN then set up for crystallisation with Et_2O diffusion. Within 3 days, crystals were formed, dried and analysed.

Yield: 588 mg, 0.28 mmol, 30 % based on Mo (based on the purification of a 300 mg sample - a 60 % recovery of the asymmetric product); **^{1}H NMR** (DMSO-d_6, 400 MHz): δ = 0.93 (m, 36H, CH_3 from TBA), 1.31 (m, 24H, CH_2 from TBA), 1.56 (m, 24H, CH_2 from TBA), 3.16 (m, 24H, CH_2 from TBA), 3.55 (s, br, 2H, NH_2), 4.23 (m, 3H, CH_2 + CH), 7.67 - 7.25 (m, 5H, 4CH + NH), 7.75 (m, 2H, 2CH), 7.88 (d, 2H, 2CH, J = 7.4 Hz), 60.00 - 65.00 ppm (s, br, $6CH_2$); **^{13}C DEPTQ NMR** (DMSO-d_6, 100 MHz): δ = 174.0 (CO), 147.9 (C), 138.7 (C), 138.3 (C), 131.2 (C), 129.6 (CH), 120.3 (CH), 118.4 (CH), 113.5 (CH), 57.5 (CH_2), 33.17 (CH_2),

25.86 (CH_2), 24.06 (CH_2), 23.06 (CH_2), 19.31 (CH_2), 13.58 (CH_3); **Elemental analysis:** Calc. for $C_{71}H_{134}MnMo_6N_5O_{26}$ (2104.42 g.mol^{-1}): C 40.52, H 6.42, N 3.33; Found: C 40.52, H 6.45, N 3.41; **ESI-MS:** Peak envelopes were observed with central peaks at *m/z* 1620.73 (z = -1) and 1862.02 (z = -1) were assigned to $[((C_4H_9)_4N)H\ [MnMo_6O_{24}(C_{19}H_{18}NO_2)(C_4H_8N)]]^{1-}$ (predicted: 1620.74) and $[((C_4H_9)_4N)_2[MnMo_6O_{24}\text{-}(C_{19}H_{18}NO_2)(C_4H_8N)]]^{1-}$ (predicted: 1862.02), respectively.

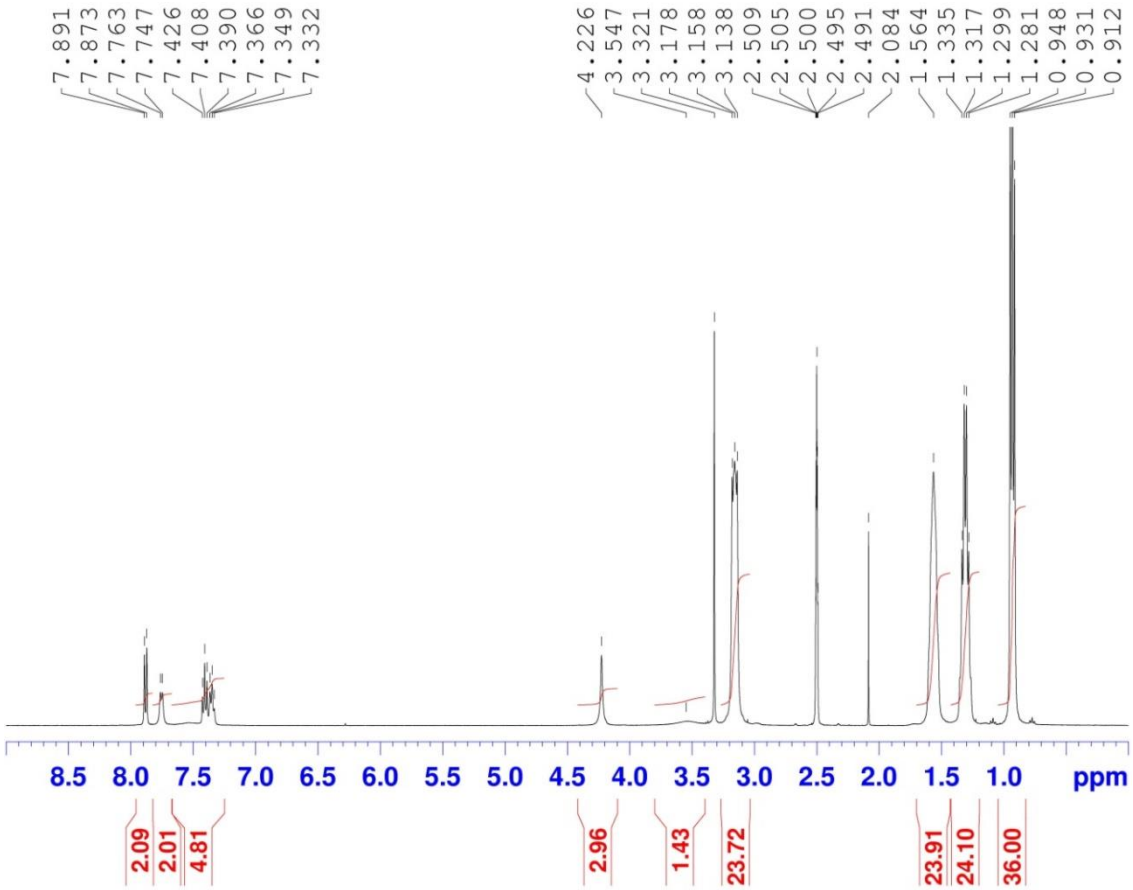

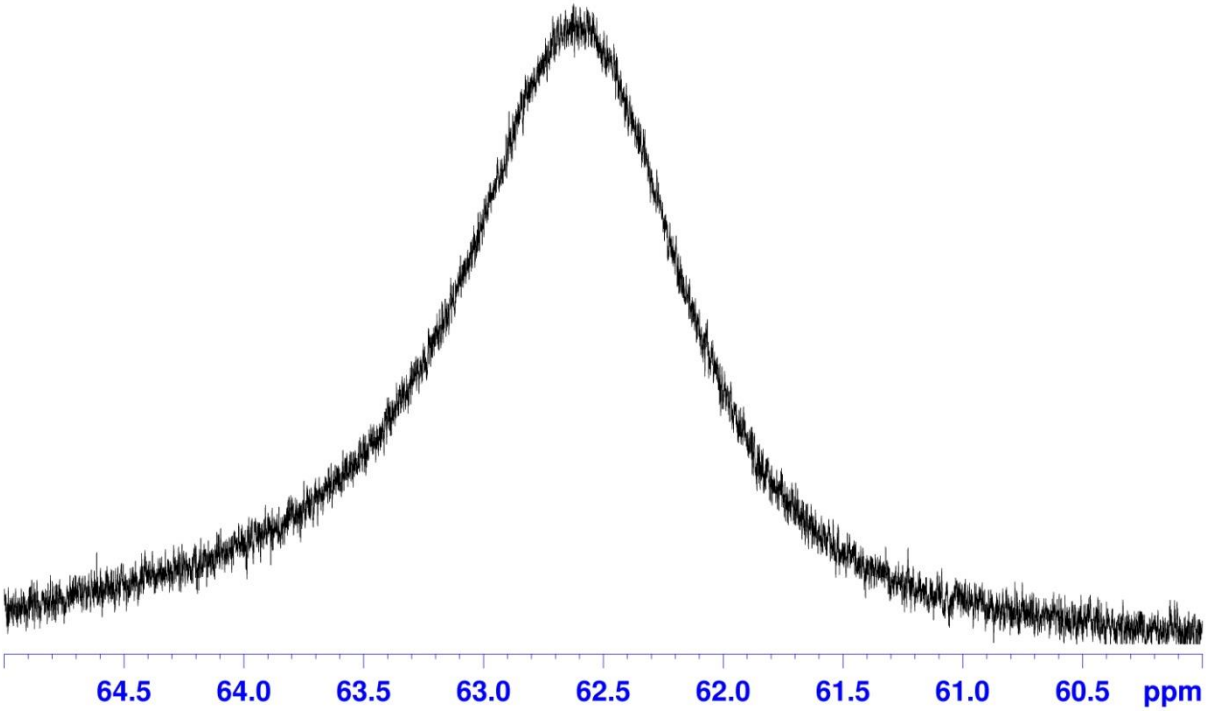

^{1}H NMR of the FMOC/TRIS Mn-Anderson (3) in DMSO-d_6 at 400 MHz

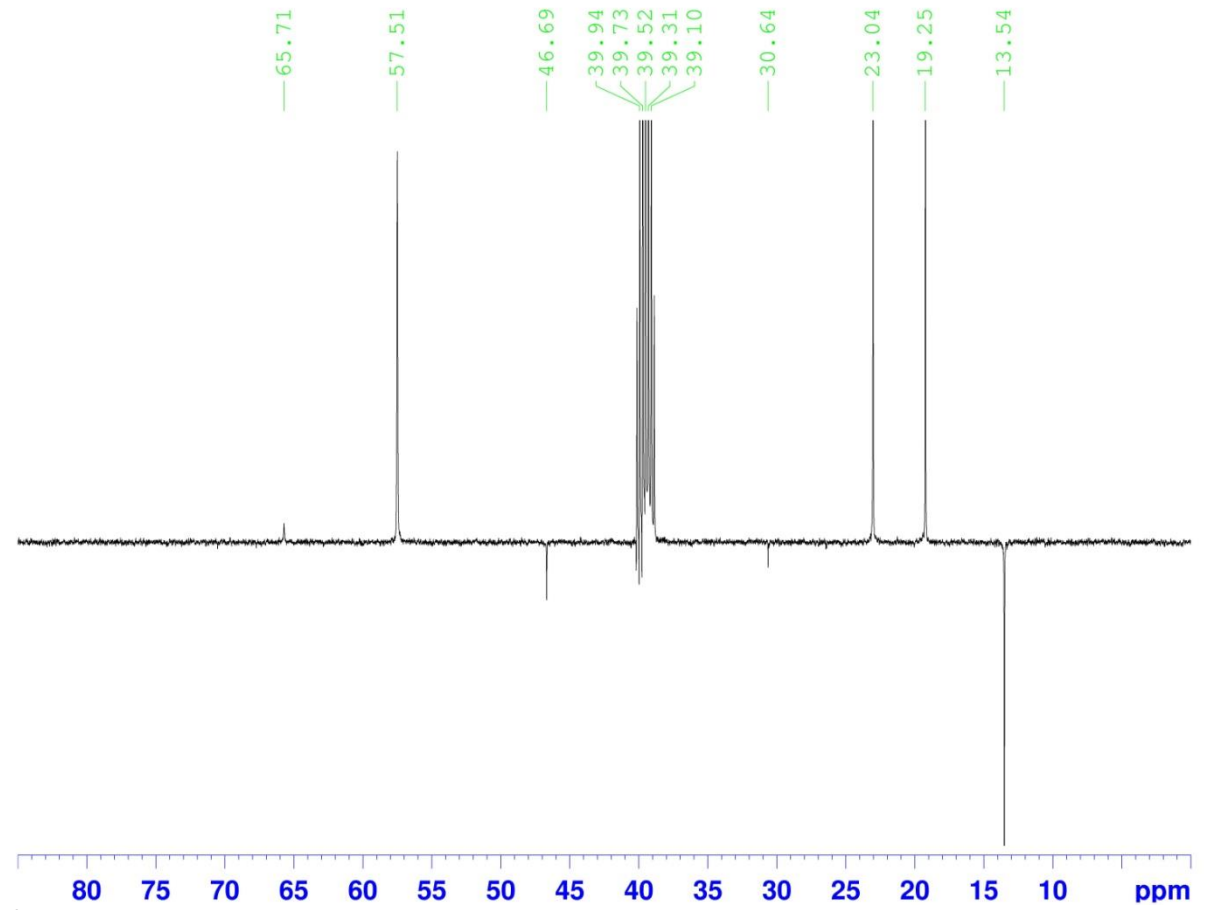

^{13}C DEPTQ NMR of the FMOC/TRIS Mn-Anderson (**1**) in DMSO-d_6 at 100 MHz

Compound 4 4-Azidobenzoic TRIS Ligand

$C_{11}H_{14}N_4O_4$

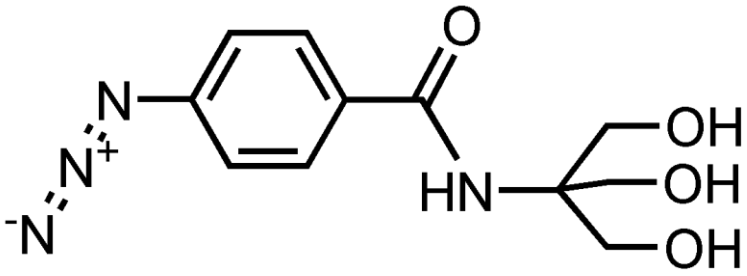

To a solution of 4-azidobenzoic acid (1.31 g, 8 mmol) and N-methylmorpholine (1.00 mL, 8.8 mmol) in tetrahydrofuran (20 mL) at 0 °C, ethylchloroformate (0.88 mL, 8.8 mmol) was added dropwise, causing a white precipitate to form. The reaction mixture was then stirred for 30 min at 0 °C, then filtered into a solution of tris(hydroxymethyl)aminomethane (TRIS, $((HOCH_2)_3CNH_2)$, 0.97 g, 8 mmol) and triethylamine (TEA, 1.21 mL, 8.8 mmol) in N,N-dimethylformamide (DMF, 10 mL) which had been stirring for 10 min. The reaction mixture was then stirred overnight, after which solvents were removed under reduced pressure until only a small amount of DMF remained. 50 mL of water was added to this and the product extracted with 2x40 mL of ethyl acetate, using a small quantity of brine to aid phase separation. The organic layers were assembled, washed with water then brine then dried with $MgSO_4$**.** The solvents were removed under vacuum and the remaining yellow powder was washed with diethyl ether and dried.

Yield: 0.780 g, 2.93 mmol, 36.6 %; **^{1}H NMR** (DMSO-d_6, 400 MHz)**:** δ = 3.68 (d = 5.9 Hz, 6H, CH_2), 4.75 (t = 5.85, 3H, OH), 7.19 (m, 2H, CH), 7.29 (bs, 1H, NH), 7.85 (m, 2H, CH). **^{13}C DEPTQ NMR (DMSO-d6, 100 MHz)**: δ = 60.3(CH_2), 62.7 (C), 118.8 (CH), 129.3 (CH), 131.7 (C), 142.2 (C), 166.3 ppm (CO); **Elemental analysis:** Calc. for $C_{11}H_{14}N_4O_4$ (266.22 g.mol-1): C 49.63 H 5.30 N 21.04; Found C 49.53 H 5.30 N 20.92.

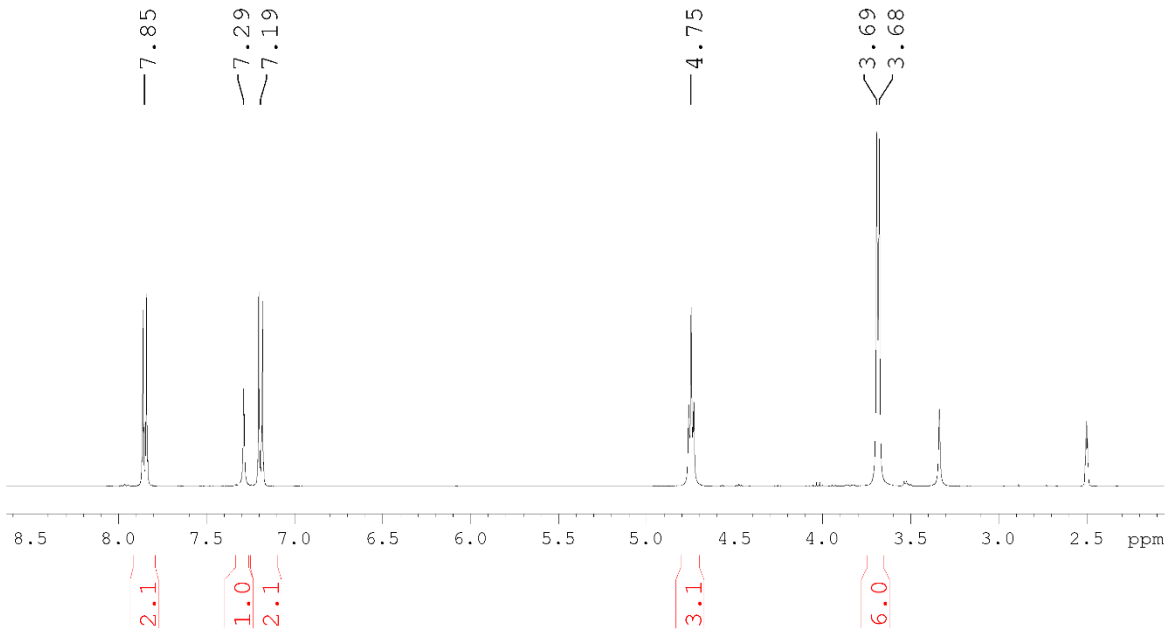

^{1}H NMR of the 4-Azidobenzoic TRIS Ligand (**4**) in DMSO-d_6 at 500 MHz.

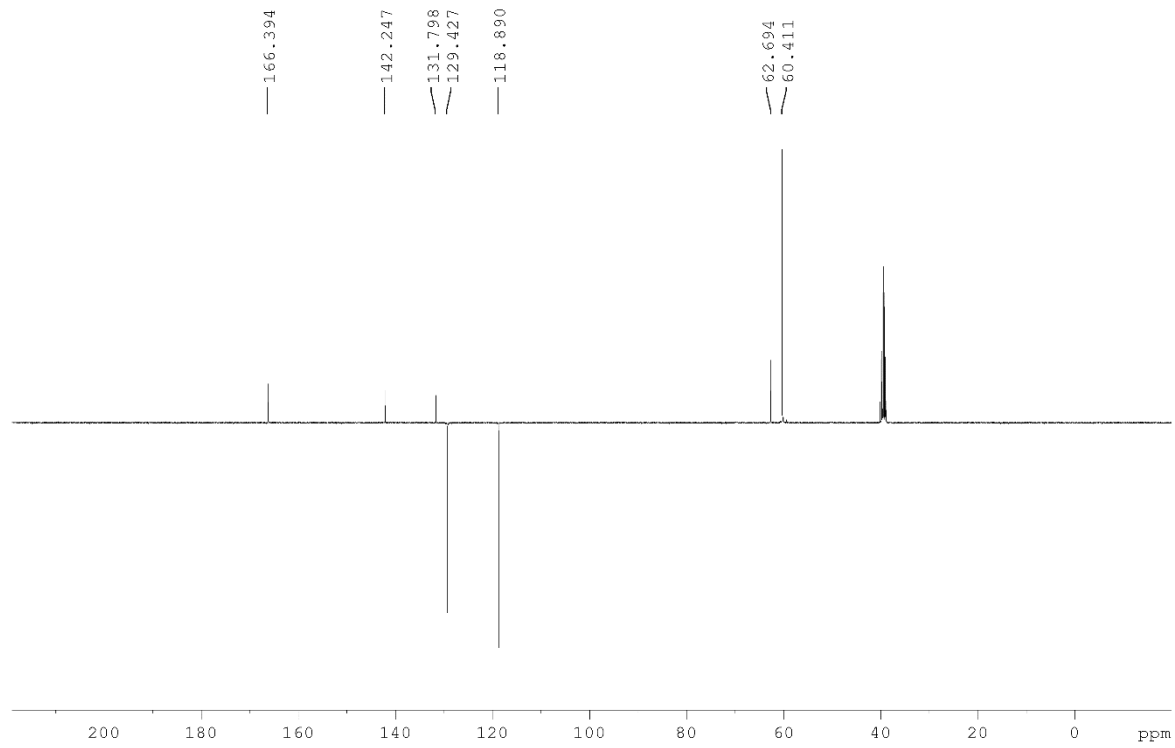

^{13}C DEPTQ NMR of the 4-Azidobenzoic TRIS Ligand (**4**) in DMSO-d_6 at 125 MHz.

Compound 5 4-Azidobenzoic Mn-Anderson Hybrid

$(C_{16}H_{36}N)_3[MnMo_6O_{24}(C_{11}H_{11}N_4O)_2]$

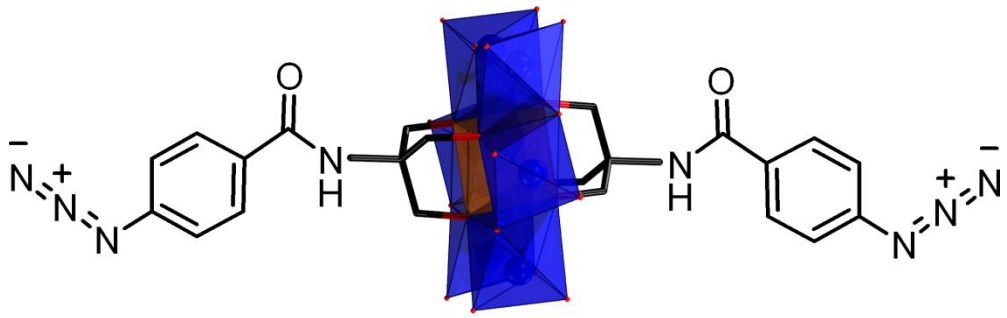

Adapted from a published procedure.[103]

A mixture of $(TBA)_4[\alpha\text{-}Mo_8O_{26}]$[11] (945 mg, 0.44 mmol), $Mn(OAc)_3{\cdot}2H_2O$ (174 mg, 0.65 mmol) and 4-azidobenzoic-TRIS ligand (414 mg; 1.56 mmol) was refluxed in MeCN (20 mL) for 16 h. The resulting bright orange solution was allowed to cool to room temperature. This crude mixture was purified via crystallisation by Et_2O diffusion. After a day, orange crystals were formed, isolated and analysed. Single crystals suitable for X-ray diffraction were grown from MeCN by slow Et_2O diffusion.

Yield: 1.035 g, 0.476 mmol, 81.1 % based on Mo; **^{1}H NMR** (DMSO-d_6, 500 MHz): δ = 0.93 (m, 36H, CH_3 from TBA^+), 1.30 (m, 24H, CH_2 from TBA^+), 1.56 (m, 24H, CH_2 from TBA^+), 3.16 (m, 24H, CH_2 from TBA^+), 7.16 (bs, 4H, 4CH), 7.54 (bs, 2H, 2NH), 7.84 (bs, 4H, 4CH), 65.00 ppm (s, br, 12H, CH_2). **^{13}C DEPTQ NMR** (DMSO-d_6, 100 MHz): δ = 13.6 (CH_3), 19.3 (CH_2), 23.0 (CH_2), 57.5 (CH_2), 118.2 (CH), 128.4 (C), 130.0 (CH), 142.4 (C), 166.3 ppm (CO), peaks for missing (C) and (CH) ambiguous due to signal-to-noise ratio; **Elemental analysis:** Calc. for $C_{70}H_{130}MnMo_6N_{11}O_{26}$ (2172.26 g.mol^{-1}): C 38.70, H 6.03, N 7.09 Found: C 38.62, H 6.03, N 7.09. **ESI-MS:** Peak envelopes were observed with central peaks at *m/z* 1930.20 (z = -1), 3016.45 (z = -2) and 4102.73 (z = -1) were assigned as $[((C_4H_9)_4N)_2[MnMo_6O_{24}(C_{11}H_{11}N_4O)_2]]^-$ (predicted: 1930.01), $[((C_4H_9)_4N)_7[MnMo_6O_{24}(C_{11}H_{11}N_4O)_2]_3]^{2-}$ (predicted: 3016.16) and $[((C_4H_9)_4N)_5[MnMo_6O_{24}(C_{11}H_{11}N_4O)_2]_2]^-$ (predicted: 4102.30), respectively.

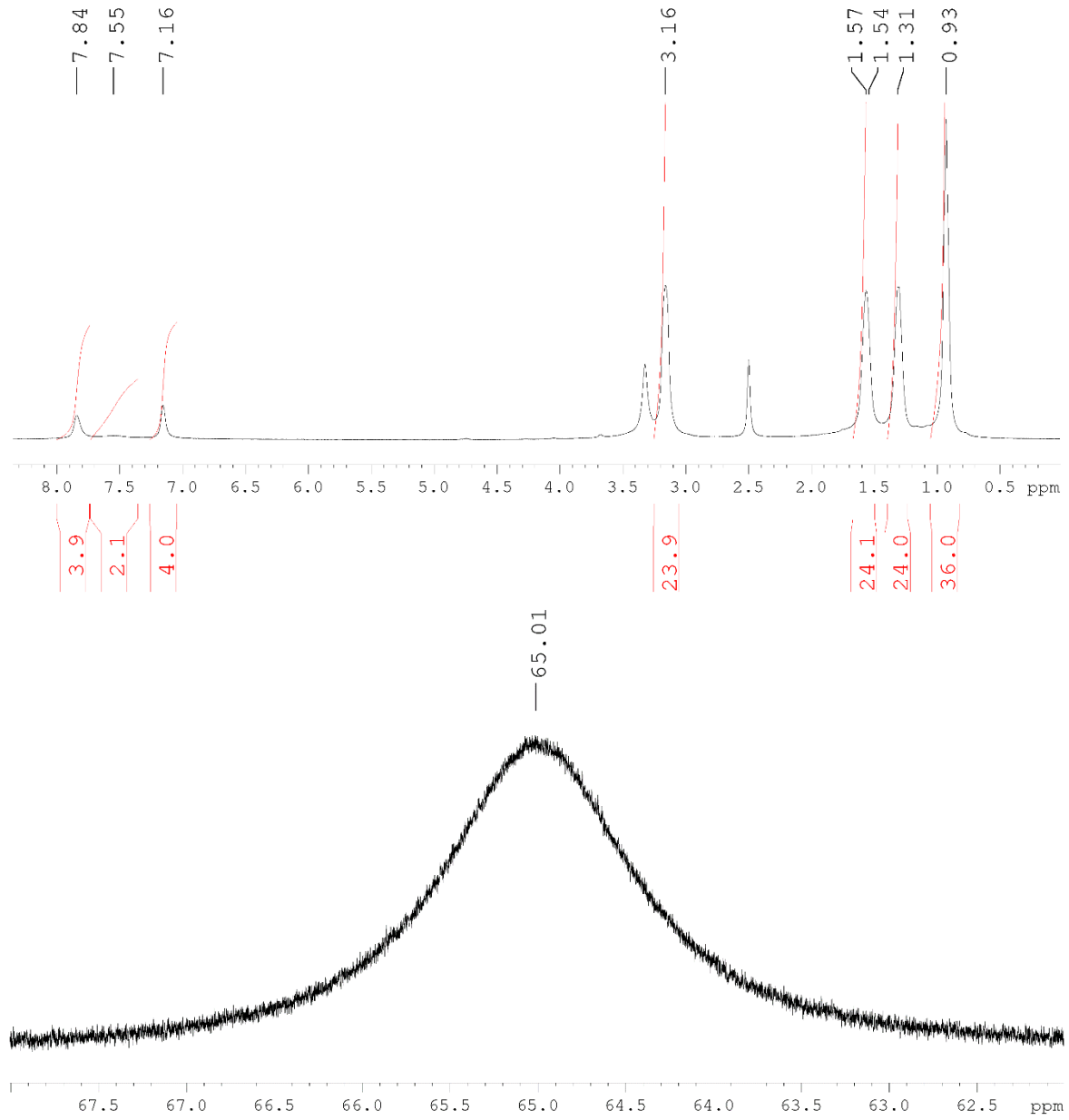

^{1}H NMR of the 4-Azidobenzoic Mn-Anderson (**5**) in DMSO-d_6 at 500 MHz.

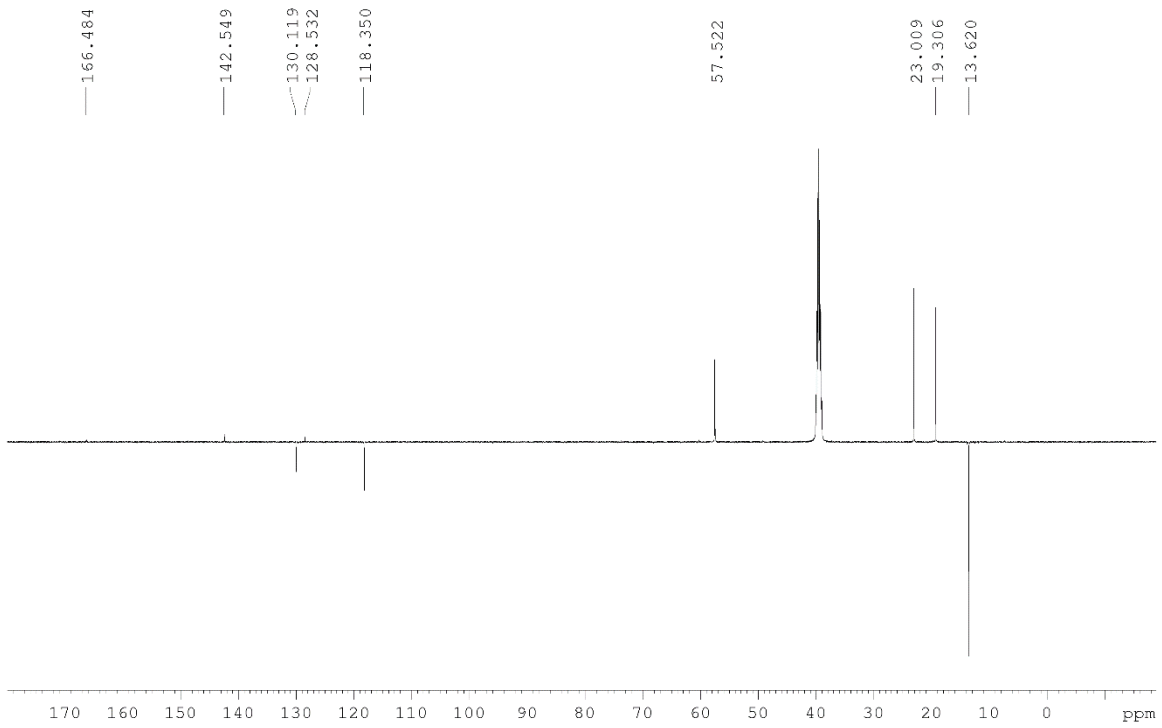

^{13}C DEPTQ NMR of the 4-Azidobenzoic Mn-Anderson (**5**) in DMSO-d_6 at 125 MHz.

Compound 6 4-Azidobenzoic/TRIS Mn-Anderson Hybrid

$((C_4H_9)_4N)_3[MnMo_6O_{24}(C_{11}H_{11}N_4O)\ (C_4H_8N)]$

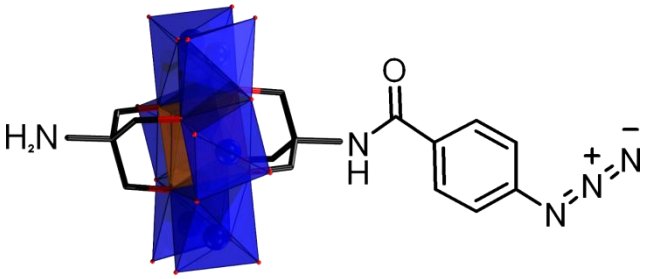

A mixture of $(TBA)_4[\alpha\text{-}Mo_8O_{26}]$[11] (3.22 g, 1.50 mmol), $Mn(OAc)_3{\cdot}2H_2O$ (592 mg, 2.21 mmol), 4-azidobenzoic-TRIS ligand (706 mg; 2.65 mmol) and TRIS ligand (321 mg, 2.65 mmol) was refluxed in MeCN (60 mL) for 16 h. The resulting bright orange solution was allowed to cool to room temperature then filtered. This crude mixture was purified via crystallisation by Et_2O diffusion, giving a mixture of symmetric and asymmetric products. These were separated using a Reveleris flash chromatography system with a C-18 column with MeCN and a 10 mM aqueous solution of TBABr as eluents. The samples corresponding to the central peak as shown by the UV trace were combined and the MeCN was removed under vacuum, giving an orange precipitate. This was separated by centrifugation then dissolved in MeCN and set up for crystallisation by Et_2O diffusion. After a day, orange crystals were formed, isolated and analysed.

Yield: 854 mg, 0.421 mmol, 21.1 % based on Mo (42.2 % based on 50% asymmetric product) **^{1}H NMR** (DMSO-d_6, 500 MHz): δ = 0.93 (t, 36H, CH_3 from TBA^+, *J = 7.24 Hz*), 1.31 (m, 24H, CH_2 from TBA^+), 1.56 (m, 24H, CH_2 from TBA^+), 3.16 (m, 24H, CH_2 from TBA^+), 7.14 (m, 2H, CH), 7.57 (bs, 1H, NH), 7.83 (bs, 2H, CH), 62.90 ppm (s, br, 12H, CH_2). **^{13}C DEPTQ NMR** (DMSO-d_6, 100 MHz): δ = 13.5 (CH_3), 19.3 (CH_2), 23.0 (CH_2), 57.5 (CH_2), 59.8 (CH_2), 64.9 (C), 111.0 (C), 118.2 (CH), 128.5 (C), 130.0 (CH), 142.4 (C), 166.5 ppm (CO); **Elemental analysis:** Calc. for $C_{63}H_{127}MnMo_6N_8O_{25}$ (2027.16 g.mol^{-1}): C 37.33, H 6.31, N 5.53 Found: C 36.56, H 6.23, N 5.32. **ESI-MS:** Peak envelopes were observed with central peaks at *m/z* 1785.09 (z = -1), 2798.84 (z = -2) and 3812.47 (z = -1) were assigned as $[((C_4H_9)_4N)_2\ [MnMo_6O_{24}(C_{11}H_{11}N_4O)(C_4H_8N)]]^-$ (predicted: 1784.98), $[((C_4H_9)_4N)_7[MnMo_6O_{24}(C_{11}H_{11}N_4O)\ (C_4H_8N)]_3]^{2-}$ (predicted: 2798.61) and $[((C_4H_9)_4N)_5[MnMo_6O_{24}(C_{11}H_{11}N_4O)(C_4H_8N)]_2]^-$ (predicted: 3812.25), respectively.

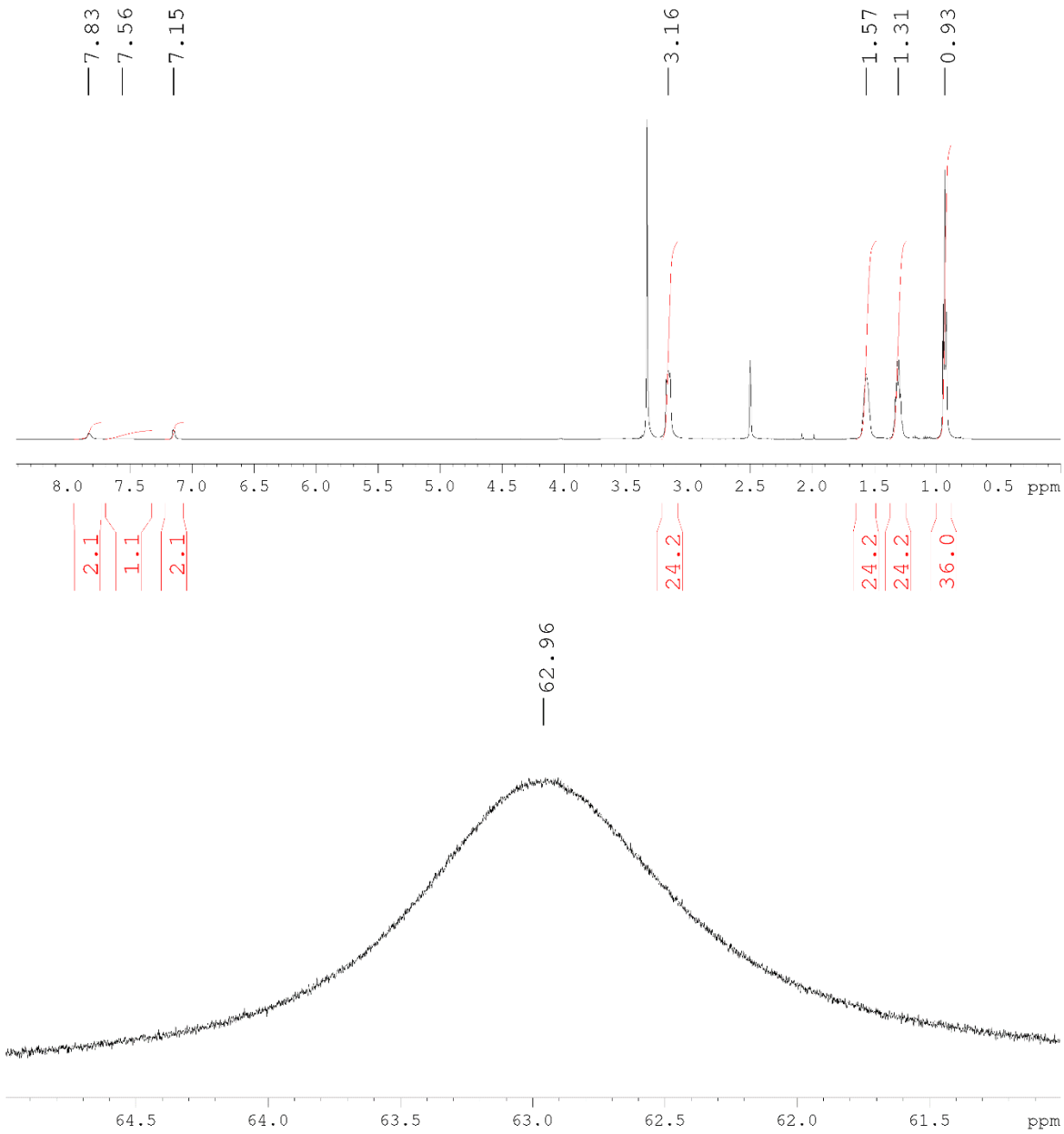

^{1}H NMR of the Asymmetric 4-Azidobenzoic/TRIS Mn-Anderson (**6**) in DMSO-d_6 at 500 MHz.

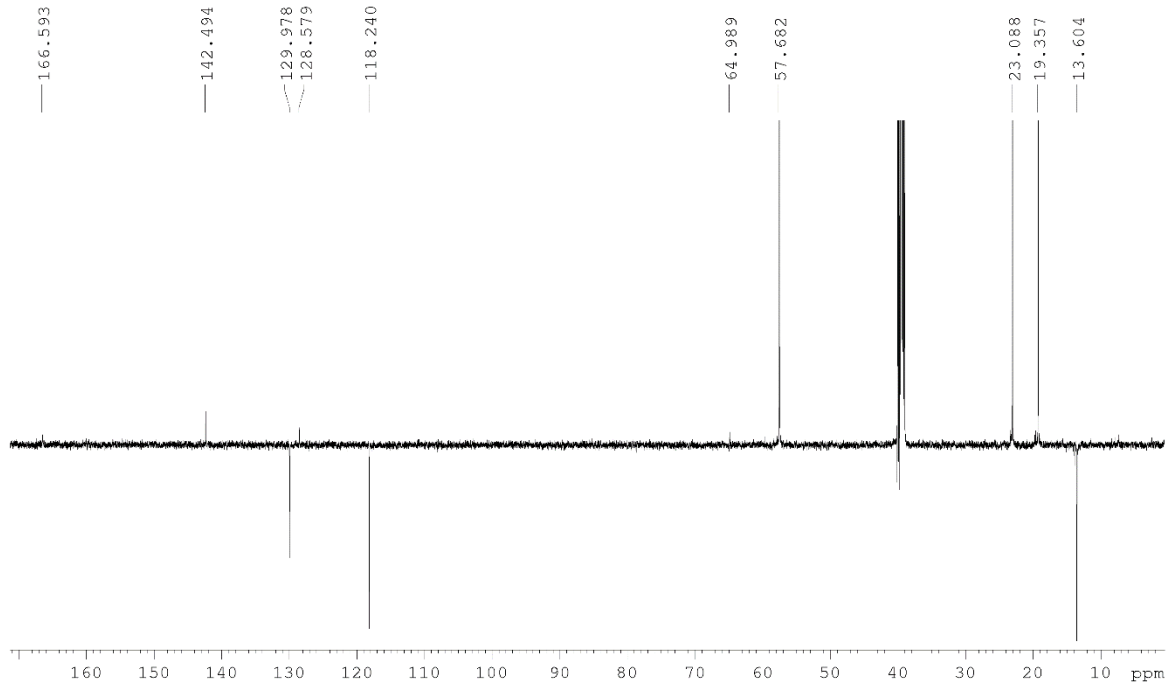

^{13}C DEPTQ NMR of the Asymmetric 4-Azidobenzoic/TRIS Mn-Anderson (**6**) in DMSO-d_6 at 125 MHz.

Compound 7 5-Hexynoic/TRIS Mn-Anderson Hybrid

$((C_4H_9)_4N)_3[MnMo_6O_{24}(C_{10}H_{14}NO)(C_4H_8N)]$

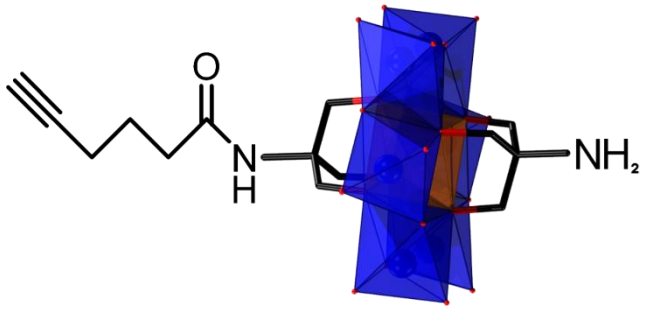

5-hexynoic acid (63 µL, 64 mg, 0.54 mmol), EEDQ (207 mg, 0.84 mmol) and asymmetric FMOC/TRIS Mn-Anderson (900 mg, 0.42 mmol) were combined in 20 mL of MeCN and this was stirred under reflux overnight. The bright orange solution was then allowed to cool to room temperature and this crude mixture was purified via crystallisation by Et_2O diffusion. After one day, orange crystals were formed, isolated and analysed. Single crystals suitable for X-ray diffraction were grown from MeCN by slow Et_2O diffusion.

Yield: 781 mg, 0.395 mmol, 94.1 %; **^{1}H NMR** (DMSO-d_6, 500 MHz): δ = 0.93 (t, 36H, CH_3 from TBA^+, J = 7.20 Hz), 1.31 (m, 24H, CH_2 from TBA^+), 1.57 (m, 24H, CH_2 from TBA^+), 1.63 (bs, 4H, CH_2), 2.13 (bs, 2H, CH_2), 2.75 (bs, 1H, CH), 3.16 (m, 24H, CH_2 from TBA^+), 7.47 (bs, H, NH), 64.90 ppm (s, br, 12H, CH_2) **^{13}C DEPTQ NMR** (DMSO-d_6, 125 MHz): δ = 13.6 (CH_3), 17.6 (CH_2), 19.3 (CH_2), 23.1 (CH_2), 25.1 (CH_2), 32.4 (CH_2), 57.5 (CH_2), 84.0 (CH), 173.4 ppm (CO) peaks for missing (C) and (CH) ambiguous due to signal-to-noise ratio; **Elemental analysis:** Calc. for $C_{62}H_{130}MnMo_6N_5O_{25}$ (1976.16 g.mol^{-1}): C 37.68, H 6.63, N 3.54 Found: C 36.86, H 6.55, N 3.52. **ESI-MS:** Peak envelopes were observed with central peaks at *m/z* 745.89 (z = -2), 1075.29 (z = -3) and 1734.09 (z = -1) were assigned as $[((C_4H_9)_4N)[MnMo_6O_{24}(C_{10}H_{14}NO)(C_4H_8N)]]^{2-}$ (predicted: 745.35), $[((C_4H_9)_4N)_3[MnMo_6O_{24}(C_{10}H_{14}NO)(C_4H_8N)]_2]^{3-}$ (predicted: 1075.24) and $[((C_4H_9)_4N)_2[MnMo_6O_{24}(C_{10}H_{14}NO)(C_4H_8N)]]^{1-}$ (predicted: 1734.00), respectively.

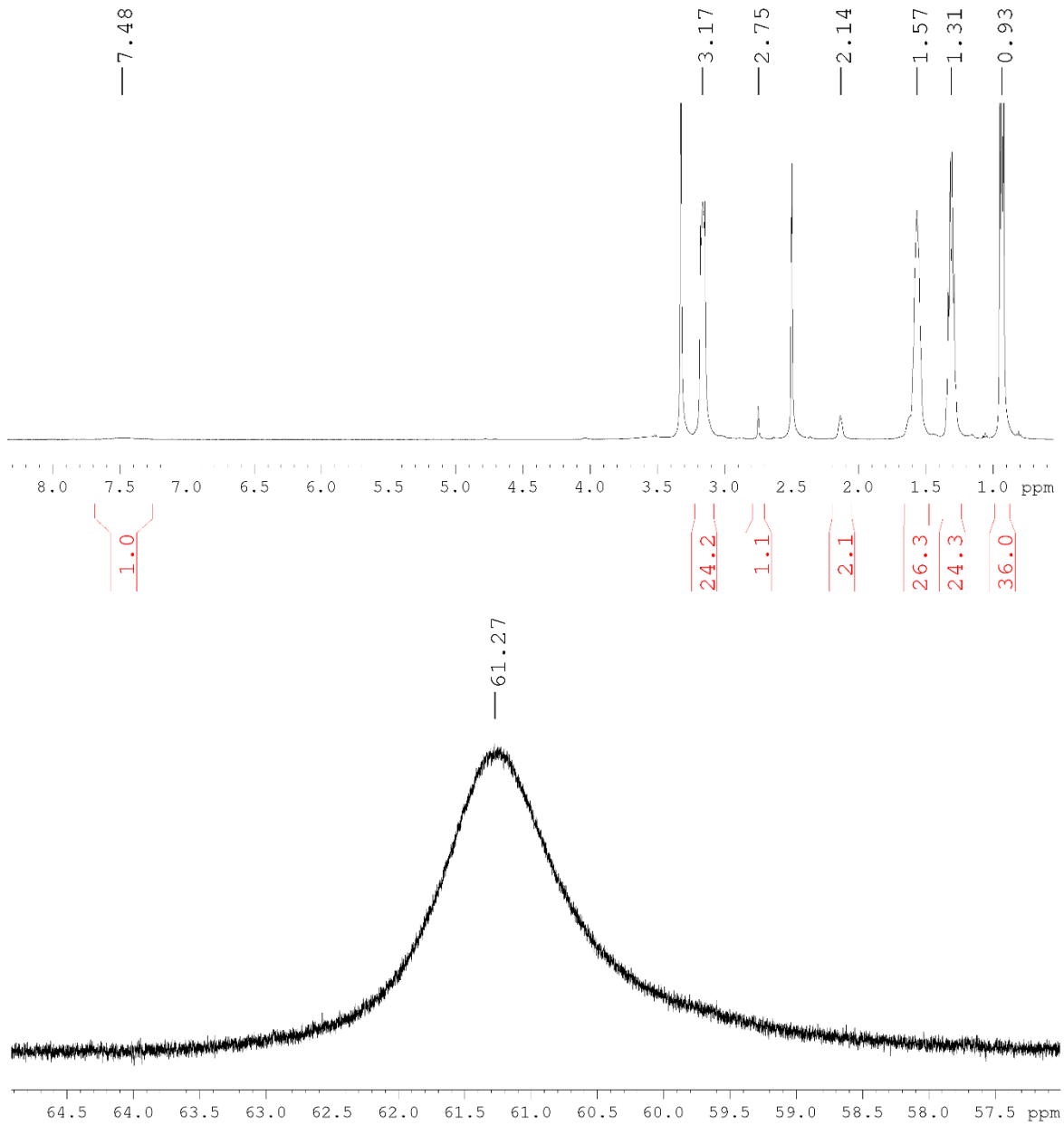

^{1}H NMR of the asymmetric 5-Hexynoic/TRIS Mn-Anderson (**7**) in DMSO-d_6 at 500 MHz.

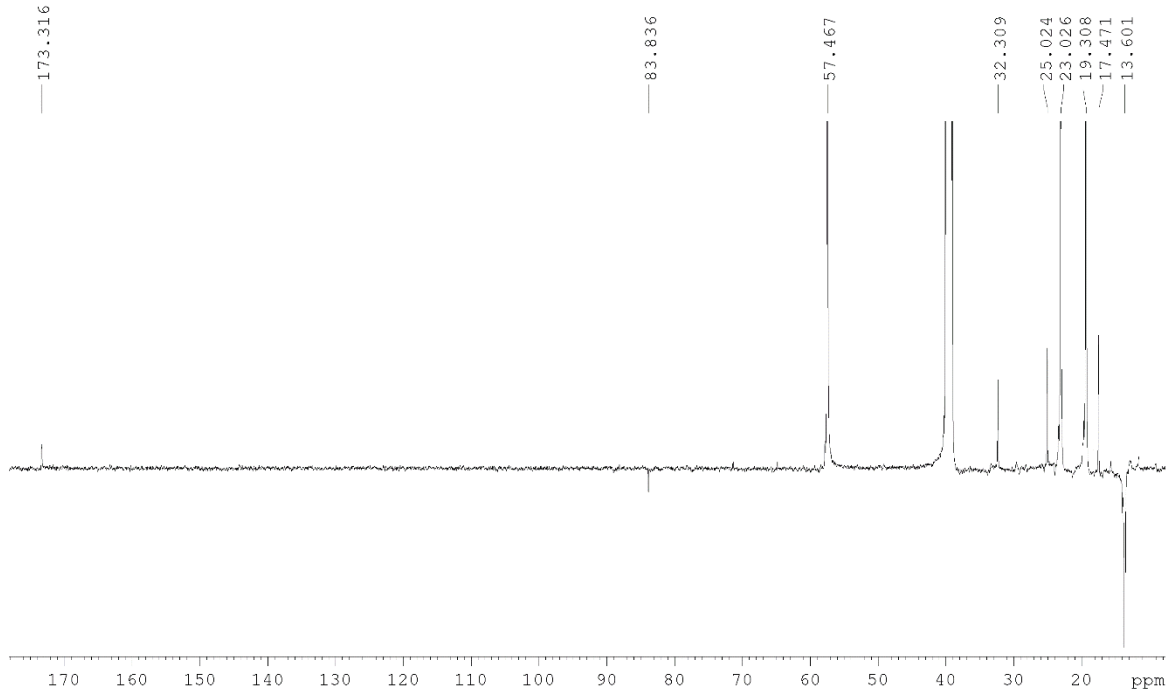

^{13}C DEPTQ NMR of the asymmetric 5-hexynoic/TRIS Mn-Anderson (**7**) in DMSO-d_6 at 125 MHz.

Compound 8 Mn-Anderson Dimer (TRIS)

$((C_4H_9)_4N)_6[MnMo_6O_{24}(C_{11}H_{11}N_4O)\ (C_4H_8N)]$-$[MnMo_6O_{24}(C_{10}H_{14}NO)(C_4H_8N)]$

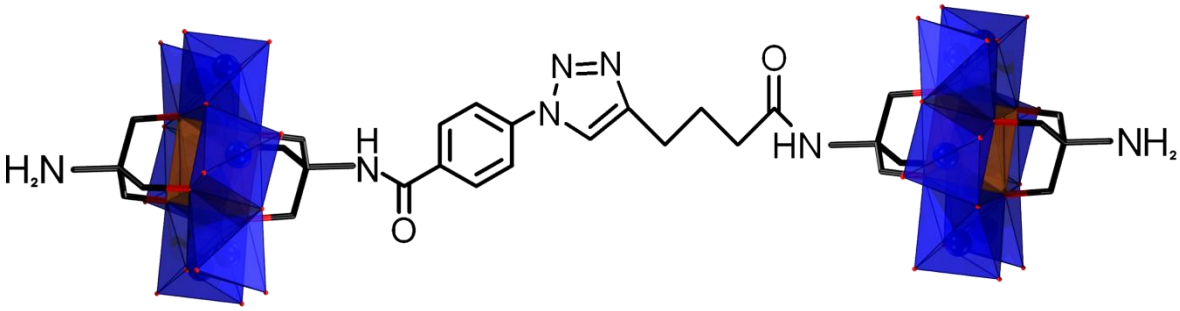

A mixture of asymmetric 5-hexynoic/TRIS Mn-Anderson (**7**) (1.18 g, 0.60 mmol) and asymmetric 4-azidobenzoic/TRIS Mn-Anderson (**6**) (816 mg, 0.40 mmol) was dissolved in a Schlenk tube in 1 mL of DMF, to which DIEA was added (160 µL, 0.32 mmol). The solution was then degassed by bubbling nitrogen through it for 5 minutes, then CuI (32 mg, 0.16 mmol) was added and the tube was sealed under nitrogen. The mixture was then stirred at 40°C for 16h. The product was then precipitated from the DMF with diethyl ether, redissolved in MeCN and loaded onto silica. The product was then separated from the remaining starting material using a Reveleris flash chromatography system with a C-18 column with MeCN and a 10 mM aqueous solution of TBABr as eluents. Fractions were combined, MeCN was removed and the precipitate was collected by centrifugation. The residue was then recrystallised from MeCN with diethyl ether diffusion.

Yield: 721 mg, 0.18 mmol, 45.0%; **^{1}H NMR** (DMSO-d_6, 500 MHz): δ = 0.93 (m, 72H, CH_3 from TBA^+), 1.31 (m, 48H, CH_2 from TBA^+), 1.56 (m, 48H, CH_2 from TBA^+), 1.87 (bs, 2H, CH_2), 2.70 (bs, 2H, CH_2), 3.16 (m, 48H, CH_2 from TBA^+), 7.53 (bs, 2H, NH), 7.96 (s, 4H, CH), 8.76 (s, H, Triazole-H), 63.11 ppm (bs, 24H, CH_2). **^{13}C DEPTQ NMR** (DMSO-d_6, 125 MHz): δ = 13.6 (CH_3), 19.3 (CH_2), 23.1 (CH_2), 25.0 (CH_2), 26.0 (CH_2), 33.2 (CH_2), 57.6 (CH_2), 118.5 (CH), 120.3 (CH), 129.8 (CH), 131.3 (C), 138.8 (C), 147.9 ppm (C) peaks for missing (CO), 2 (C)s and (CH) ambiguous due to signal-to-noise ratio; **Elemental analysis:** Calc. for $C_{125}H_{257}Mn_2Mo_{12}N_{13}O_{50}$ (4003.32 g.mol^{-1}): C 37.50, H 6.47, N 4.55 Found: C 36.96, H 6.31, N 4.55. **ESI-MS:** Peak envelopes were observed with central peaks at *m/z* 1092.20 (z = -3), 1293.35 (z = -6) , 1759.46 (z = -2), 2159.84 (z = -5) , 2427.05 (z = -3) , 2761.07 (z = -4) and

2960.65 (z = -5) were assigned as $[((C_4H_9)_4N)_3[(MnMo_6O_{24})_2(C_{11}H_{11}N_4O)(C_{10}H_{14}NO)(C_4H_8N)_2]]^{3-}$ (predicted: 1092.23), $[((C_4H_9)_4N)_4[(MnMo_6O_{24})_2(C_{11}H_{11}N_4O)(C_{10}H_{14}NO)(C_4H_8N)_2]]^{2-}$ (predicted: 1759.49), $[((C_4H_9)_4N)_{13}[(MnMo_6O_{24})_2(C_{11}H_{11}N_4O)(C_{10}H_{14}NO)(C_4H_8N)_2]_3]^{5-}$ (predicted: 2159.64), $[((C_4H_9)_4N)_9[(MnMo_6O_{24})_2(C_{11}H_{11}N_4O)(C_{10}H_{14}NO)(C_4H_8N)_2]_2]^{3-}$ (predicted: 2426.74), $[((C_4H_9)_4N)_{14}[(MnMo_6O_{24})_2(C_{11}H_{11}N_4O)(C_{10}H_{14}NO)(C_4H_8N)_2]_3]^{4-}$ (predicted: 2760.13) and $[((C_4H_9)_4N)_{19}[(MnMo_6O_{24})_2(C_{11}H_{11}N_4O)(C_{10}H_{14}NO)\text{-}(C_4H_8N)_2]_4]^{5-}$ (predicted: 2960.35), respectively.

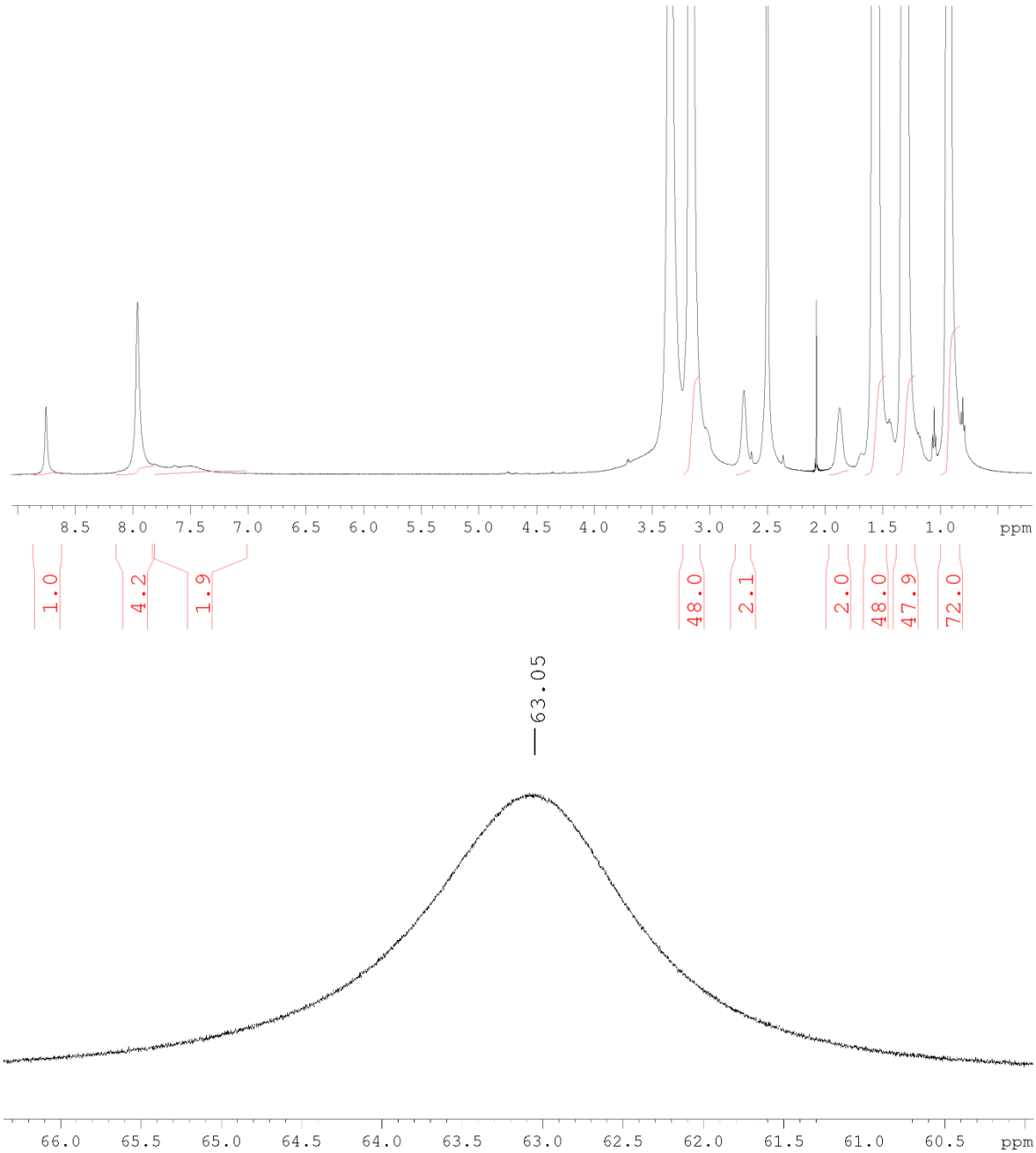

^{1}H NMR of the Mn-Anderson dimer (TRIS) (**8**) in DMSO-d_6 at 500 MHz.

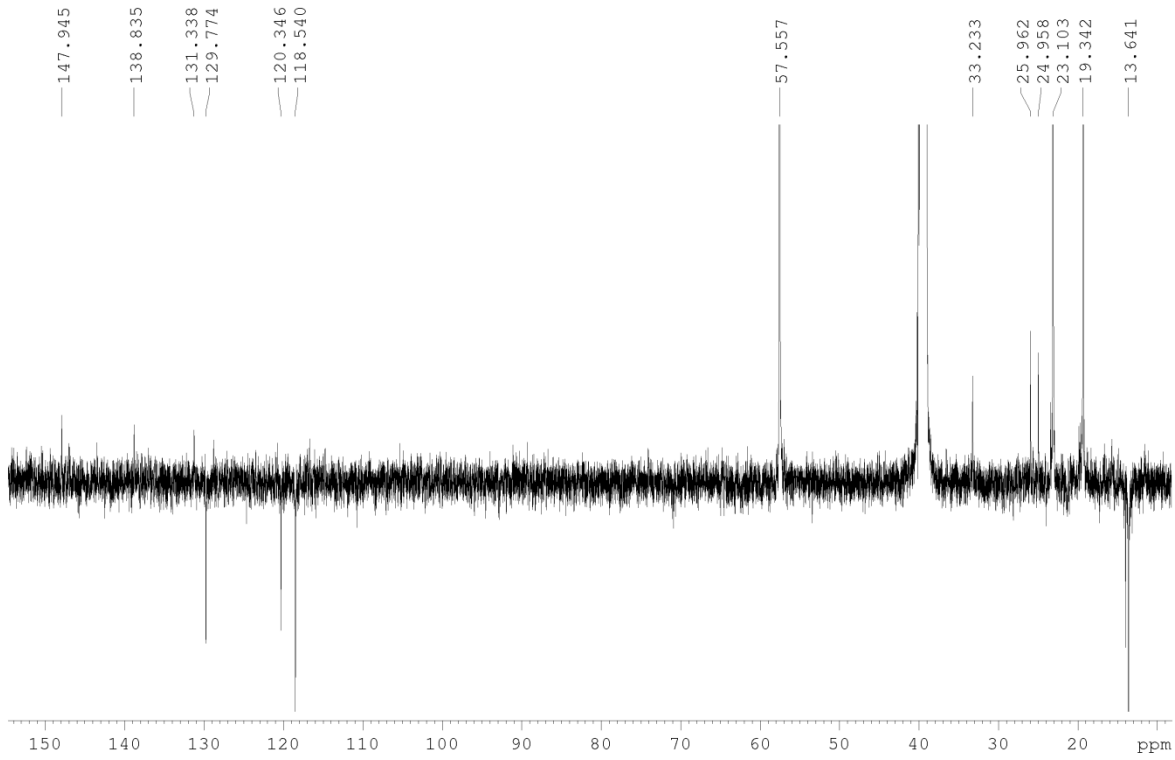

^{13}C DEPTQ NMR of the Mn-Anderson dimer (TRIS) (**8**) in DMSO-d_6 at 125 MHz.

Compound 9 Mn-Anderson Trimer (TRIS)

$((C_4H_9)_4N)_9[MnMo_6O_{24}(C_{11}H_{11}N_4O)_2]$-$[MnMo_6O_{24}(C_{10}H_{14}NO)(C_4H_8N)]_2$

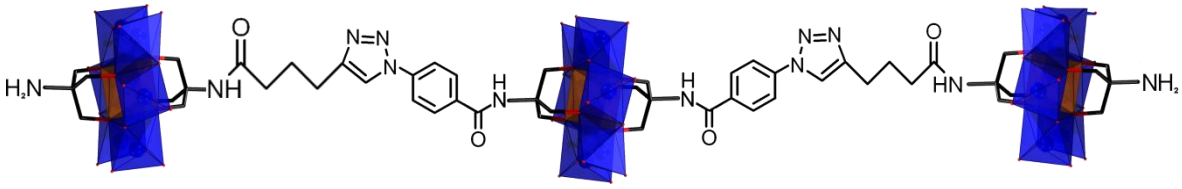

A mixture of asymmetric 5-hexynoic/TRIS Mn-Anderson (**7**) (3.23 g, 1.64 mmol) and symmetric 4-azidobenzoic Mn-Anderson (**5**) (1.18 g, 0.55 mmol) was dissolved in a Schlenk tube in 10 mL of DMF, to which DIEA was added (153 µL, 0.88 mmol). The solution was then degassed by bubbling nitrogen through it for 5 minutes, then CuI (84 mg, 0.44 mmol) was added and the tube was sealed under nitrogen. The mixture was then stirred at 40°C for 16h. The product was then precipitated from the DMF with diethyl ether, redissolved in MeCN and loaded onto silica. The product was then separated from the remaining starting material using a Reveleris flash chromatography system with a C-18 column with MeCN and a 10 mM aqueous solution of TBABr as eluents. Fractions were combined, MeCN was removed and the precipitate was collected by centrifugation. The residue was then recrystallised from MeCN with diethyl ether diffusion.

Yield: 2.00 g, 0.33 mmol, 59.8%; **^{1}H NMR** (DMSO-d_6, 500 MHz): δ = 0.93 (t, 108H, CH_3 from TBA^+, J = 6.95 Hz), 1.31 (m, 72H, CH_2 from TBA^+), 1.57 (m, 72H, CH_2 from TBA^+), 1.88 (bs, 4H, CH_2), 2.71 (bs, 4H, CH_2), 3.16 (m, 72H, CH_2 from TBA^+), 7.98 (s, 8H, CH), 8.76 (s, 2H, Triazole-H), 64.25 ppm (m, br, 36H, CH_2) **^{13}C DEPTQ NMR** (DMSO-d_6, 125 MHz): δ = 13.6 (CH_3), 19.3 (CH_2), 23.1 (CH_2), 24.9 (CH_2), 25.9 (CH_2), 33.3 (CH_2), 57.5 (CH_2), 118.5 (CH), 120.4 (CH), 129.8 (CH), 147.9 ppm (C), peaks for missing (C) ambiguous due to signal-to-noise ratio, but tentative suggest 138.7, 131.5, 114.1 and 113.3; **Elemental analysis:** Calc. for $C_{194}H_{390}Mn_3Mo_{18}N_{21}O_{76}$ (6124.59 g.mol^{-1}): C 38.05, H 6.42, N 4.80 Found: C 37.18, H 6.33, N 4.58. **ESI-MS:** Peak envelopes were observed with central peaks at *m/z* 1288.64 (z = -4), 1799.65 (z = -3) , 2207.16 (z = -5) and 2820.67 (z = -2) were assigned as $[((C_4H_9)_4N)_5[(MnMo_6O_{24})_3(C_{11}H_{11}N_4O)_2(C_{10}H_{14}NO)_2(C_4H_8N)_2]]^{4-}$ (predicted: 1288.93), $[((C_4H_9)_4N)_6[(MnMo_6O_{24})_3(C_{11}H_{11}N_4O)_2(C_{10}H_{14}NO)_2(C_4H_8N)_2]]^{3-}$ (predicted: 1799.33),

$[((C_4H_9)_4N)_{13}[(MnMo_6O_{24})_3(C_{11}H_{11}N_4O)_2(C_{10}H_{14}NO)_2(C_4H_8N)_2]_2]^{5-}$ (predicted: 2207.46), and $[((C_4H_9)_4N)_7[(MnMo_6O_{24})_2(C_{11}H_{11}N_4O)_2(C_{10}H_{14}NO)_2(C_4H_8N)_2]_4]^{2-}$ (predicted: 2820.14), respectively.

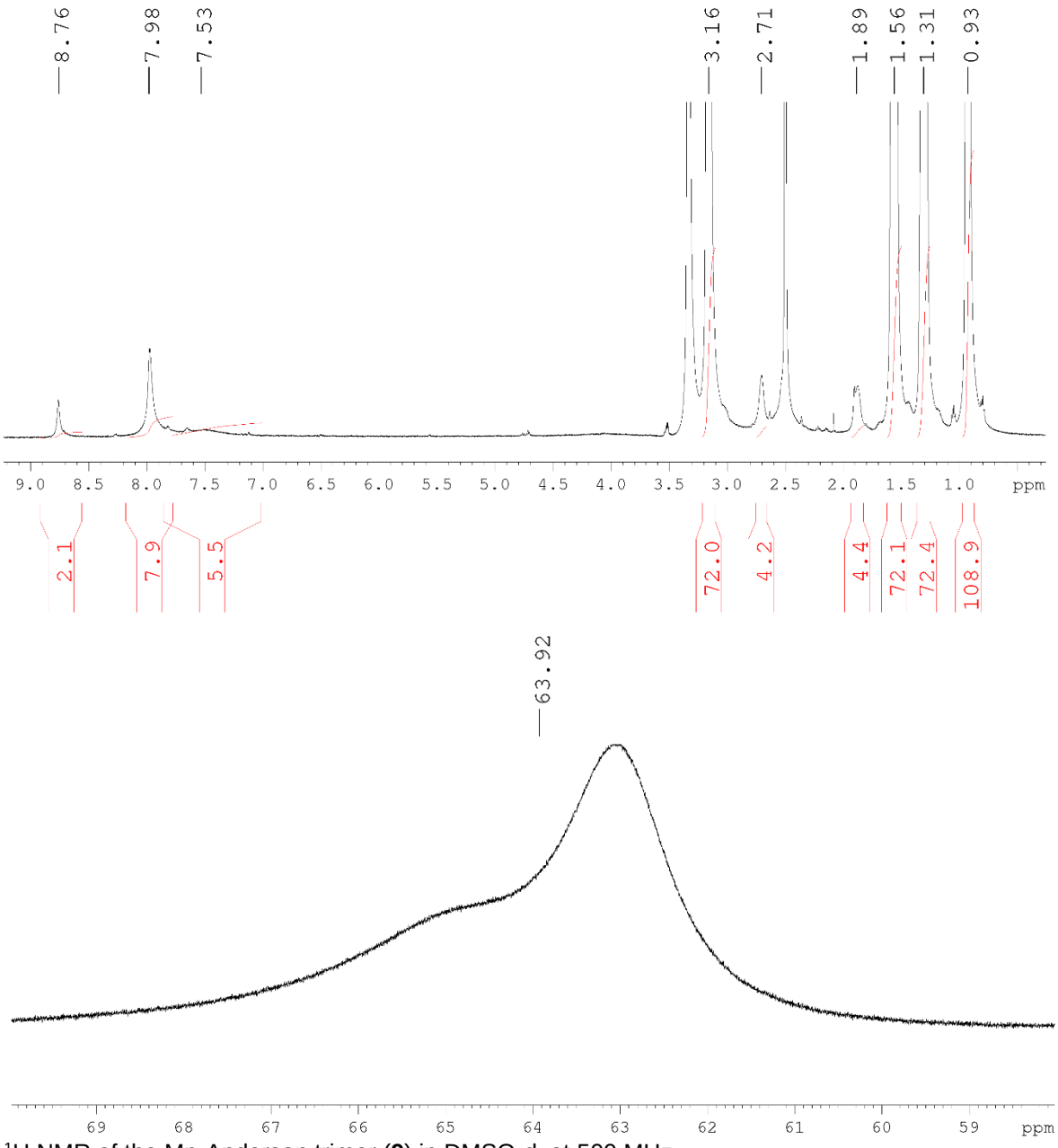

^{1}H NMR of the Mn-Anderson trimer (**9**) in DMSO-d_6 at 500 MHz.

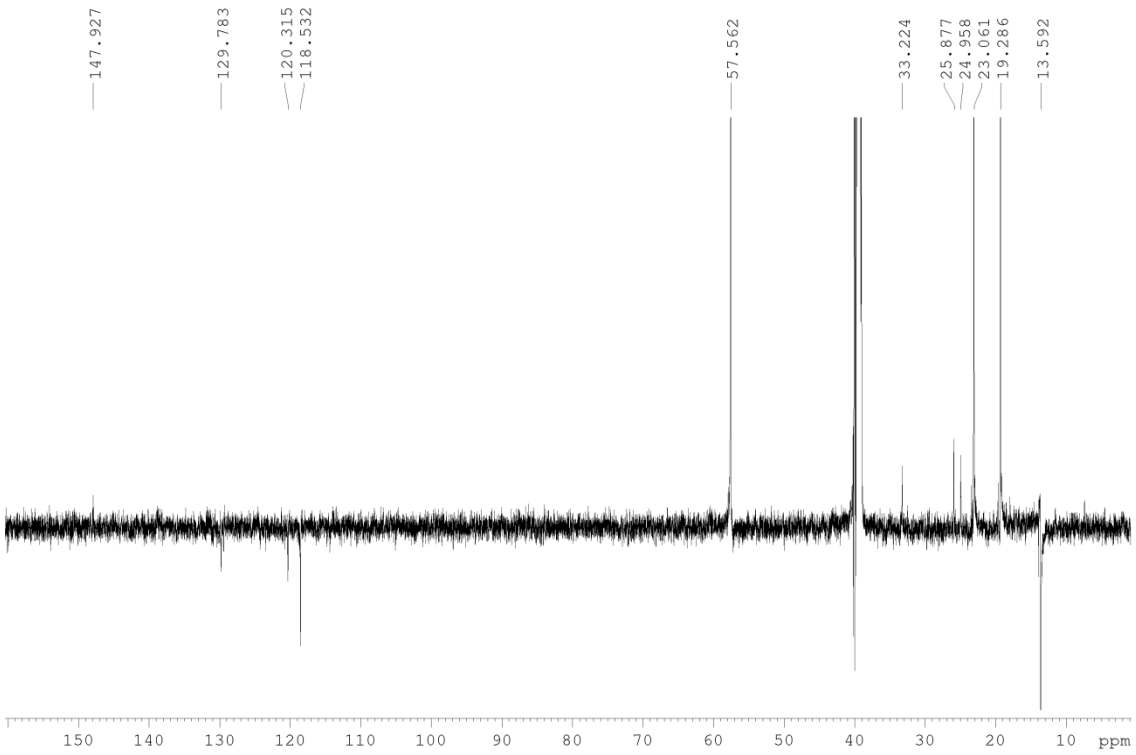

^{13}C DEPTQ NMR of the Mn-Anderson trimer (**9**) in DMSO-d_6 at 125 MHz.

Compound 10 Mn-Anderson Dimer (5-hexynoic)

$((C_4H_9)_4N)_6[MnMo_6O_{24}(C_{11}H_{11}N_4O)\ (C_4H_8N)]$-$[MnMo_6O_{24}(C_{10}H_{14}NO)(C_4H_8N)]$

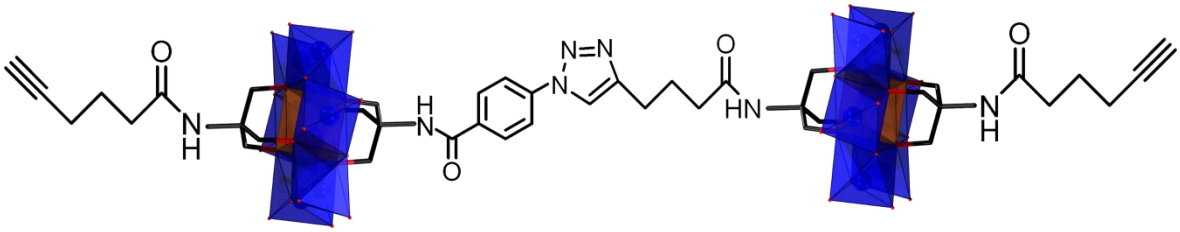

5-hexynoic acid (21 µL, 21 mg, 0.18 mmol), EEDQ (46 mg, 0.19 mmol) and Mn-Anderson dimer (TRIS) (**8**) (300 mg, 0.08 mmol) were combined in 20 mL of MeCN and this was stirred under reflux overnight. The bright orange solution was then allowed to cool to room temperature and this crude mixture was purified via crystallisation by Et_2O diffusion. After three days, orange crystals were formed, isolated and analysed. Single crystals suitable for X-ray diffraction were grown from MeCN by slow Et_2O diffusion.

Yield: 250 mg, 0.06 mmol, 79.5 %; **^{1}H NMR** (DMSO-d_6, 500 MHz): δ = 0.93 (t, 72H, CH_3 from TBA^+, *J = 6.95 Hz*), 1.31 (m, 48H, CH_2 from TBA^+), 1.56 (m, 4 + 48H, CH_2 + CH_2 from TBA^+), 1.87 (bs, 2H, CH_2), 2.14 (bs, 4H, CH_2), 2.70 (bs, 2H, CH_2), 2.75 (s, 2H, CH), 3.16 (m, 48H, CH_2 from TBA^+), 7.50 (bs, 4H, NH), 7.97 (s, 4H, CH), 8.76 (s, H, Triazole-H), 64.68 ppm (bs, 24H, CH_2). **^{13}C DEPTQ NMR** (DMSO-d_6, 125 MHz): δ = 13.6 (CH_3), 17.5 (CH_2), 19.3 (CH_2), 23.1 (CH_2), 24.9 (CH_2), 25.1 (CH_2), 25.9 (CH_2), 32.5 (CH_2), 33.2 (CH_2), 57.5 (CH_2), 71.4 (CH_3), 83.9 (CH), 118.5 (CH), 120.3 (CH), 129.7 (CH), 130.5 (C), 131.3 (C), 131.5 (C), 138.8 (C), 147.9 (C), 173.8 ppm (CO); **Elemental analysis:** Calc. for $C_{137}H_{269}Mn_2Mo_{12}N_{13}O_{52}$ (4191.54 g.mol^{-1}): C 39.26, H 6.47, N 4.34 Found: C 37.74, H 6.24, N 4.19. **ESI-MS:** Peak envelopes were observed with central peaks at *m/z* 1853.62 (z = -2), 3111.08 (z = -5) , 3949.58 (z = -1) were assigned as $[((C_4H_9)_4N)_4\ [(MnMo_6O_{24})_2(C_{11}H_{11}N_4O)(C_{10}H_{14}NO)_3]]^{2-}$ (predicted: 1853.53), $[((C_4H_9)_4N)_{19}[(MnMo_6O_{24})_2\ (C_{11}H_{11}N_4O)(C_{10}H_{14}NO_3]_4]^{5-}$ (predicted: 3111.02), and $[((C_4H_9)_4N)_5[(MnMo_6O_{24})_2(C_{11}H_{11}N_4O)\ (C_{10}H_{14}NO)_3]]^-$ (predicted: 3949.35), respectively.

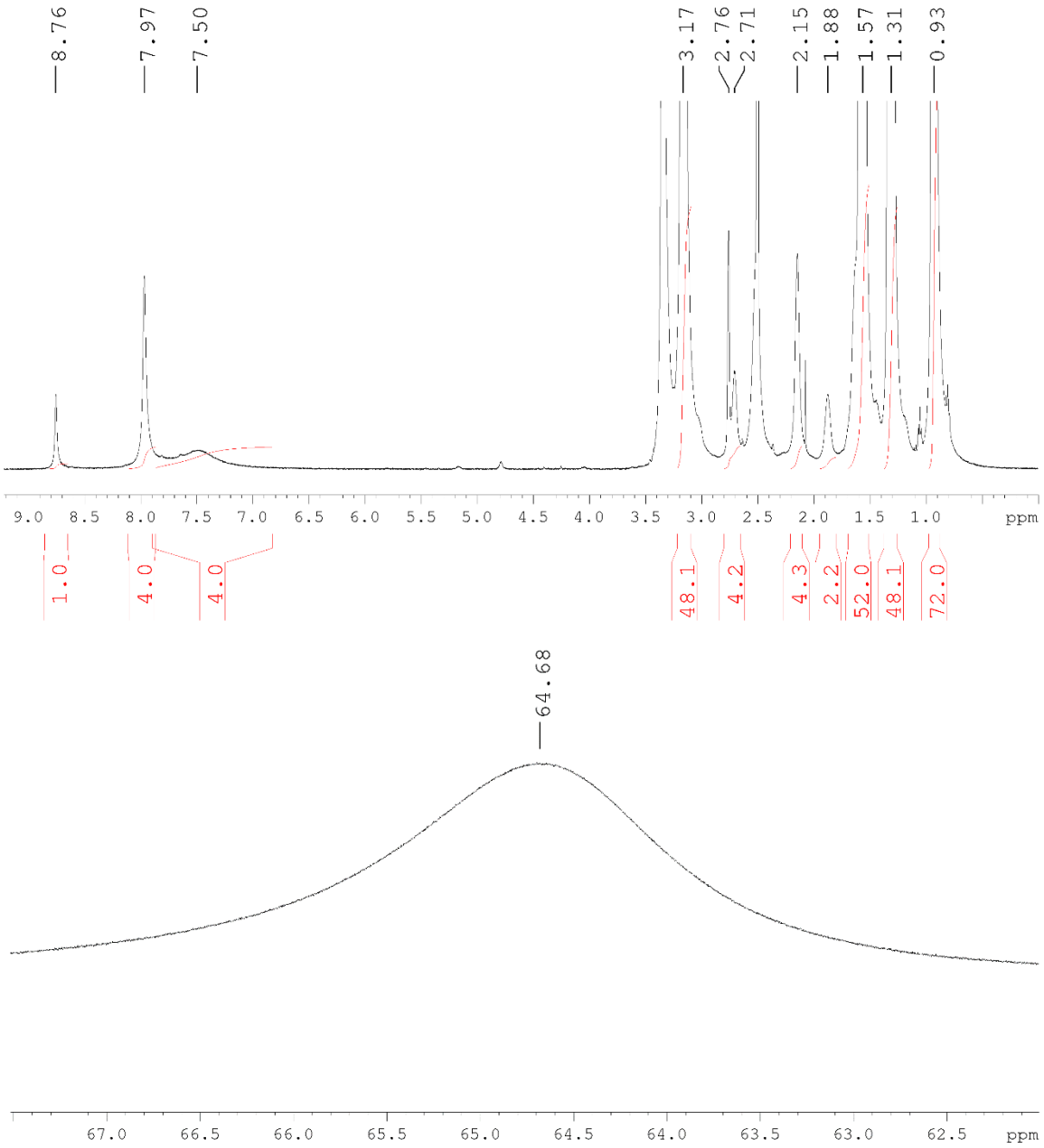

^{1}H NMR of the Mn-Anderson dimer (5-hexynoic) (**10**) in DMSO-d_6 at 500 MHz.

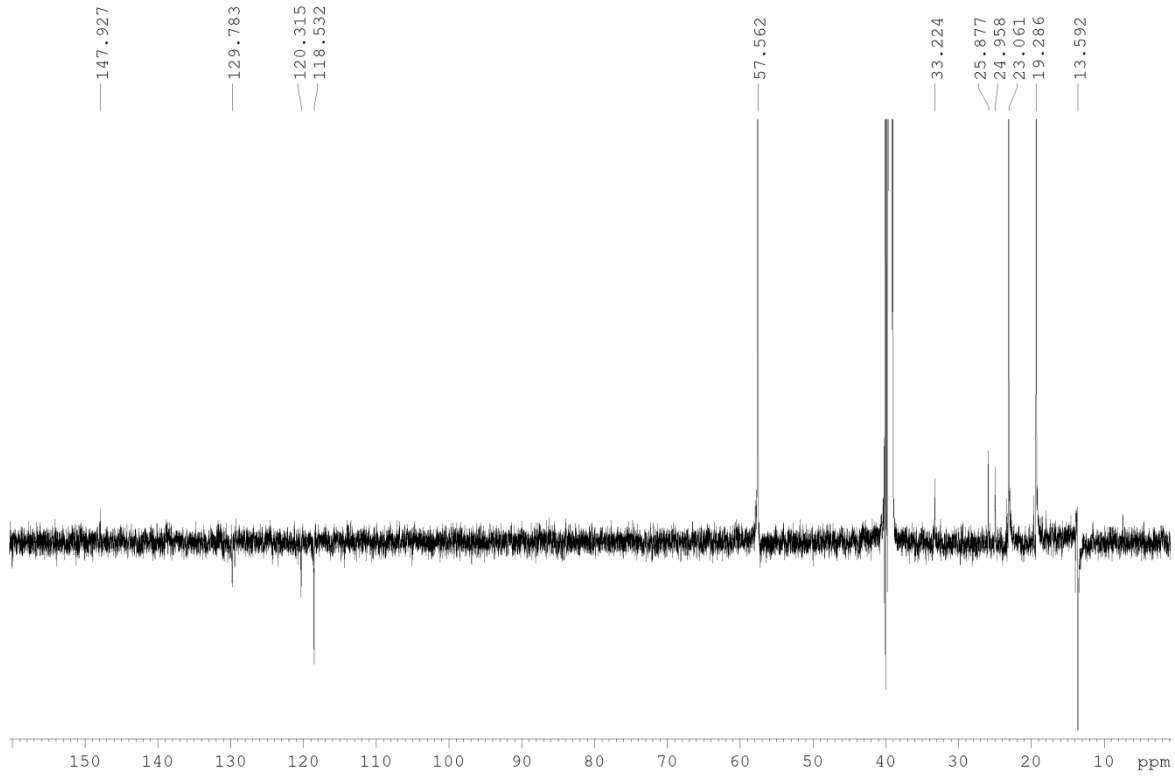

^{13}C DEPTQ NMR of the Mn-Anderson dimer (5-hexynoic) (**10**) in DMSO-d_6 at 125 MHz.

Compound 11 Mn-Anderson Trimer (5-hexynoic)

$((C_4H_9)_4N)_9[MnMo_6O_{24}(C_{11}H_{11}N_4O)_2]$-$[MnMo_6O_{24}(C_{10}H_{14}NO)(C_4H_8N)]_2$

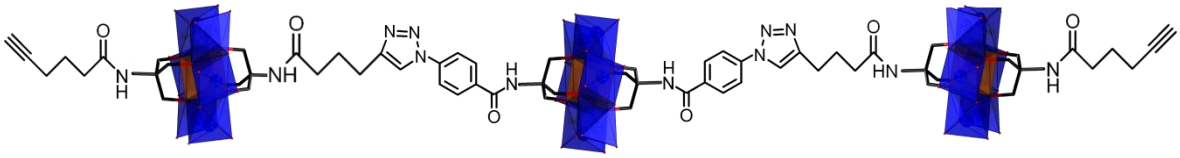

5-hexynoic acid (65 µL, 66 mg, 0.59 mmol), EEDQ (145 mg, 0.59 mmol) and Mn-Anderson trimer (TRIS) (**9**) (600 mg, 0.10 mmol) were combined in 80 mL of MeCN and this was stirred under reflux overnight. The bright orange solution was then allowed to cool to room temperature and this crude mixture was purified via crystallisation by Et_2O diffusion. After three days, orange crystals were formed, isolated and analysed. Single crystals suitable for X-ray diffraction were grown from MeCN by slow Et_2O diffusion.

Yield: 536 mg, 0.09 mmol, 86.6 %; **^{1}H NMR** (DMSO-d_6, 500 MHz): δ = 0.93 (t, 108H, CH_3 from TBA^+, J = 6.95 Hz), 1.31 (m, 72H, CH_2 from TBA^+), 1.57 (m, 72H, CH_2 from TBA^+), 1.88 (bs, 4H, CH_2), 2.71 (bs, 4H, CH_2), 3.16 (m, 72H, CH_2 from TBA^+), 6.7 – 7.7 (m, 6H, NH), 7.98 (s, 8H, CH), 8.76 (s, 2H, Triazole-H), 64.25 ppm (m, br, 36H, CH_2) **^{13}C DEPTQ NMR** (DMSO-d_6, 125 MHz): δ = 13.6 (CH_3), 17.6 (CH_2), 19.3 (CH_2), 23.1 (CH_2), 24.9 (CH_2), 25.1 (CH_2), 25.9 (CH_2), 32.5 (CH_2), 33.3 (CH_2), 57.5 (CH_2), 118.5 (CH), 120.3 (CH), 129.8 (CH), 147.9 ppm (C), missing peaks left ambiguous due to signal-to-noise ratio, but tentative suggest 178.4 and 173.2 for (CO) and 147.9, 135.4, 129.0 and 121.0 for (C); **Elemental analysis:** Calc. for $C_{206}H_{402}Mn_3Mo_{18}N_{21}O_{78}$ (6312.80 g.mol^{-1}): C 39.19, H 6.42, N 4.66 Found: C 37.56, H 6.20, N 4.47. **ESI-MS:** Peak envelopes were observed with central peaks at *m/z* 1862.11 (z = -3), 2914.35 (z = -2) and 3966.46 (z = -5) were assigned as $[((C_4H_9)_4N)_6[(MnMo_6O_{24})_3(C_{11}H_{11}N_4O)_2(C_{10}H_{14}NO)_4]]^{3-}$ (predicted: 1862.02), $[((C_4H_9)_4N)_7[(MnMo_6O_{24})_3(C_{11}H_{11}N_4O)_2(C_{10}H_{14}NO)_4]]^{2-}$ (predicted: 2914.19) and $[((C_4H_9)_4N)_{15}[(MnMo_6O_{24})_3(C_{11}H_{11}N_4O)_2(C_{10}H_{14}NO)_4]_2]^{3-}$ (predicted: 3966.34), respectively.

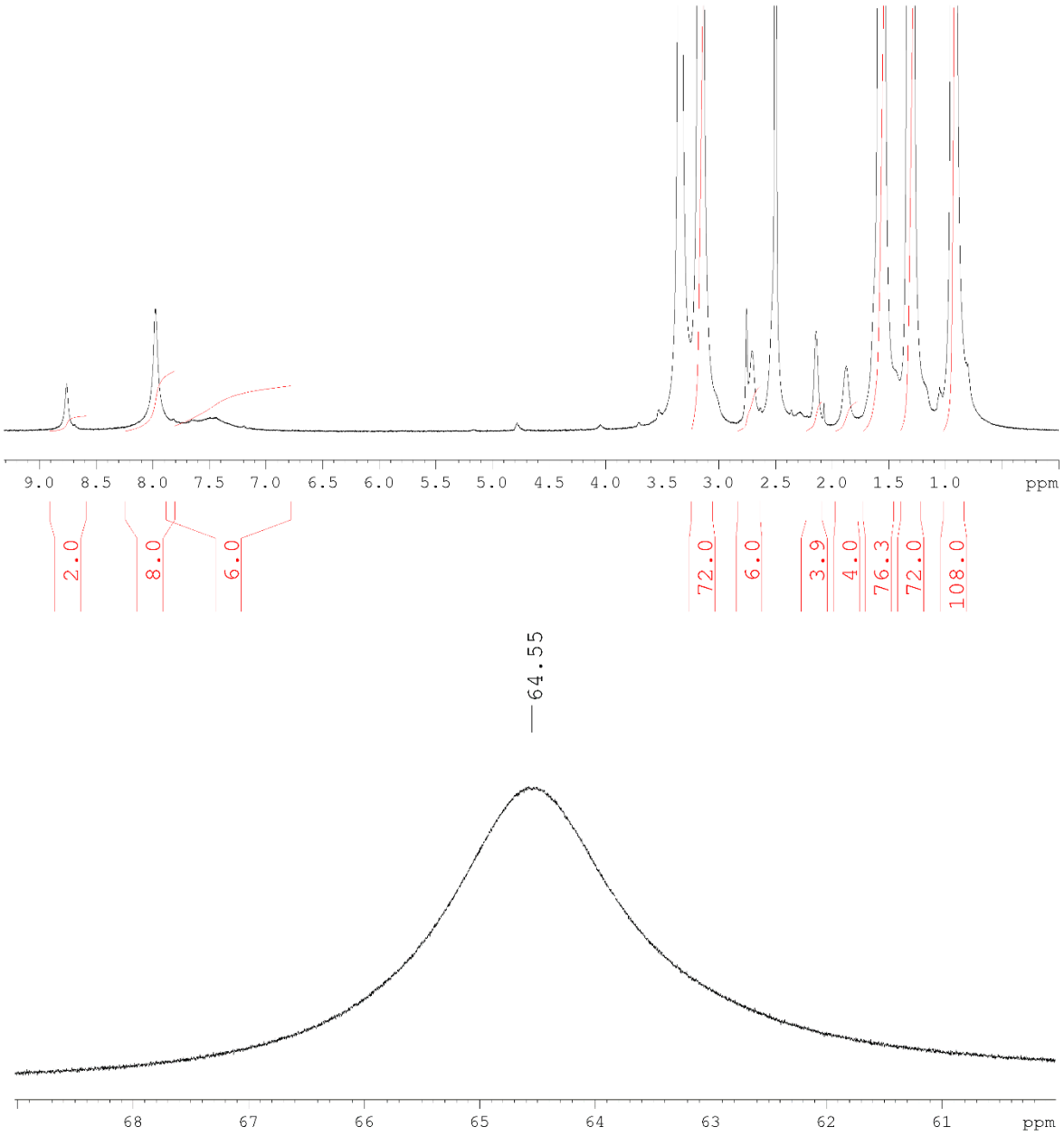

^{1}H NMR of the Mn-Anderson trimer (5-hexynoic) (**11**) in DMSO-d_6 at 500 MHz.

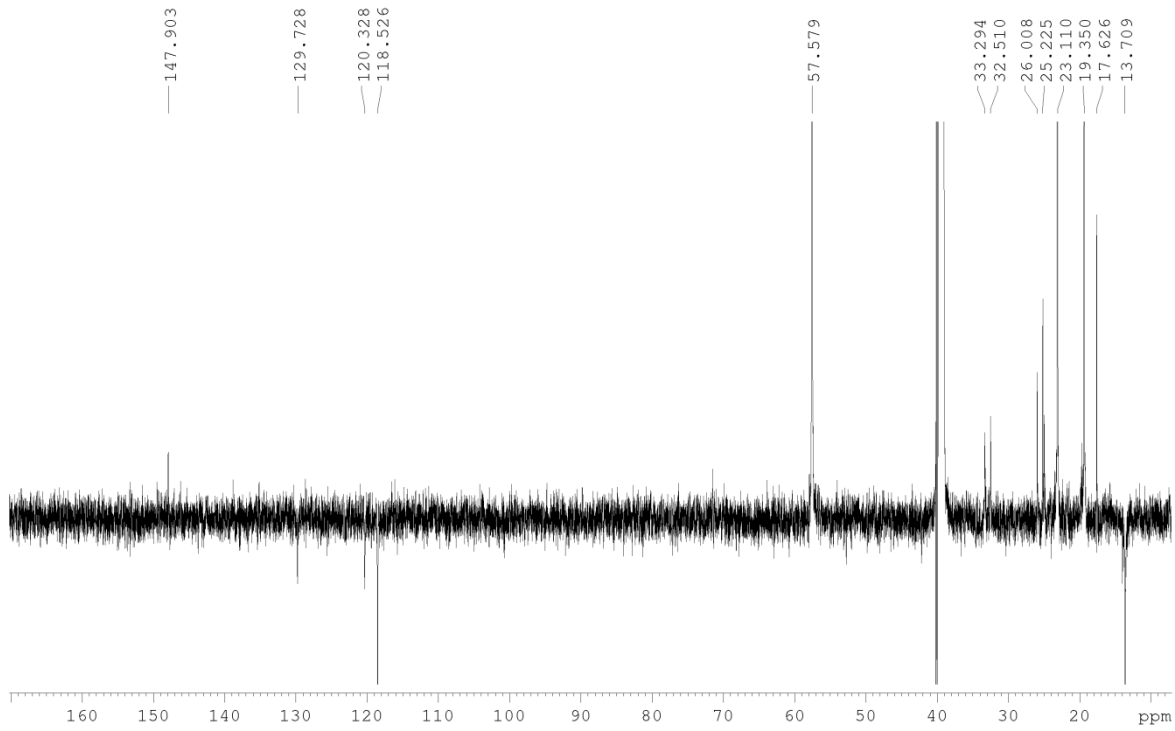

^{13}C DEPTQ NMR of the Mn-Anderson trimer (5-hexynoic) (**11**) in DMSO-d_6 at 125 MHz.

Compound 12 Mn-Anderson Tetramer

$((C_4H_9)_4N)_{12}[MnMo_6O_{24}(C_{11}H_{11}N_4O)\text{-}(C_{10}H_{14}NO)][MnMo_6O_{24}(C_{10}H_{14}NO)_2][MnMo_6O_{24}(C_{11}H_{11}N_4O)\ (C_4H_8N)]_2$

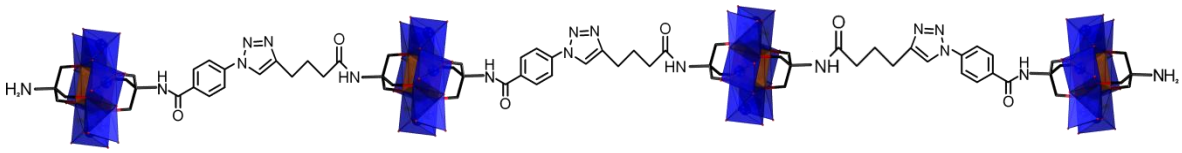

A mixture of asymmetric 4-azidobenzoic/TRIS Mn-Anderson (**6**) (181 mg, 0.09 mmol) and Mn-Anderson dimer (5-hexynoic) (**10**) (150 mg, 0.04 mmol) was dissolved in a Schlenk tube in 6 mL of DMF, to which DIEA was added (12 µL, 0.07 mmol). The solution was then degassed by bubbling nitrogen through it for 5 minutes, then CuI (7 mg, 0.04 mmol) was added and the tube was sealed under nitrogen. The mixture was then stirred at 40°C for 16h. The product was then precipitated from the DMF with diethyl ether, redissolved in MeCN and loaded onto silica. The product was then separated from the remaining starting material using a Reveleris flash chromatography system with a C-18 column with MeCN and a 10 mM aqueous solution of TBABr as eluents. Fractions were combined, MeCN was removed and the precipitate was collected by centrifugation. The residue was then recrystallised from MeCN with diethyl ether diffusion.

Yield: 126 mg, 0.02 mmol, 41.7%; **^{1}H NMR** (DMSO-d_6, 500 MHz): δ = 0.93 (t, 144H, CH_3 from TBA^+, J = 6.61 Hz), 1.31 (m, 96H, CH_2 from TBA^+), 1.57 (m, 96H, CH_2 from TBA^+), 1.88 (bs, 6H, $2CH_2$), 2.71 (bs, 6H, $2CH_2$), 3.16 (m, 96H, CH_2 from TBA^+), 6.7 – 7.7 (m, 6H, NH), 7.97 (s, 12H, CH), 8.76 (s, 3H, Triazole-H), 63.84 ppm (m, br, 36H, CH_2) **^{13}C DEPTQ NMR** (DMSO-d_6, 125 MHz): δ = 13.6 (CH_3), 19.3 (CH_2), 23.1 (CH_2), 24.9 (CH_2), 25.9 (CH_2), 33.3 (CH_2), 57.5, 59.7 (C), 81.2 (C), (CH_2), 118.4 (CH), 120.3 (CH), 129.7 (CH), 131.1 (C), 138.7 (C), 147.9 ppm (CO); **Elemental analysis:** Calc. for $C_{263}H_{523}Mn_4Mo_{24}N_{29}O_{102}$ (8245.85 $g.mol^{-1}$): C 38.31, H 6.39, N 4.92 Found: C 38.25, H 6.38, N 4.86. **ESI-MS:** Peak envelopes were observed with central peaks at *m/z* 1819.28 (z = -4), 2506.49 (z = -2), 3056.01 (z = -2) and 3880.40 (z = -1) were assigned as $[((C_4H_9)_4N)_8[(MnMo_6O_{24})_4(C_{11}H_{11}N_4O)_3(C_{10}H_{14}NO)_3(C_4H_8N)_2]]^{4-}$ (predicted: 1819.26), $[((C_4H_9)_4N)_9[(MnMo_6O_{24})_4(C_{11}H_{11}N_4O)_3(C_{10}H_{14}NO)_3(C_4H_8N)_2]]^{3-}$ (predicted: 2506.44),

$[((C_4H_9)_4N)_{19}[(MnMo_6O_{24})_4(C_{11}H_{11}N_4O)_3(C_{10}H_{14}NO)_3(C_4H_8N)_2]_2]^{5-}$ (predicted: 2506.44), and $[((C_4H_9)_4N)_{10}[(MnMo_6O_{24})_4(C_{11}H_{11}N_4O)_3(C_{10}H_{14}NO)_3(C_4H_8N)_2]]^{1-}$ (predicted: 3880.80), respectively.

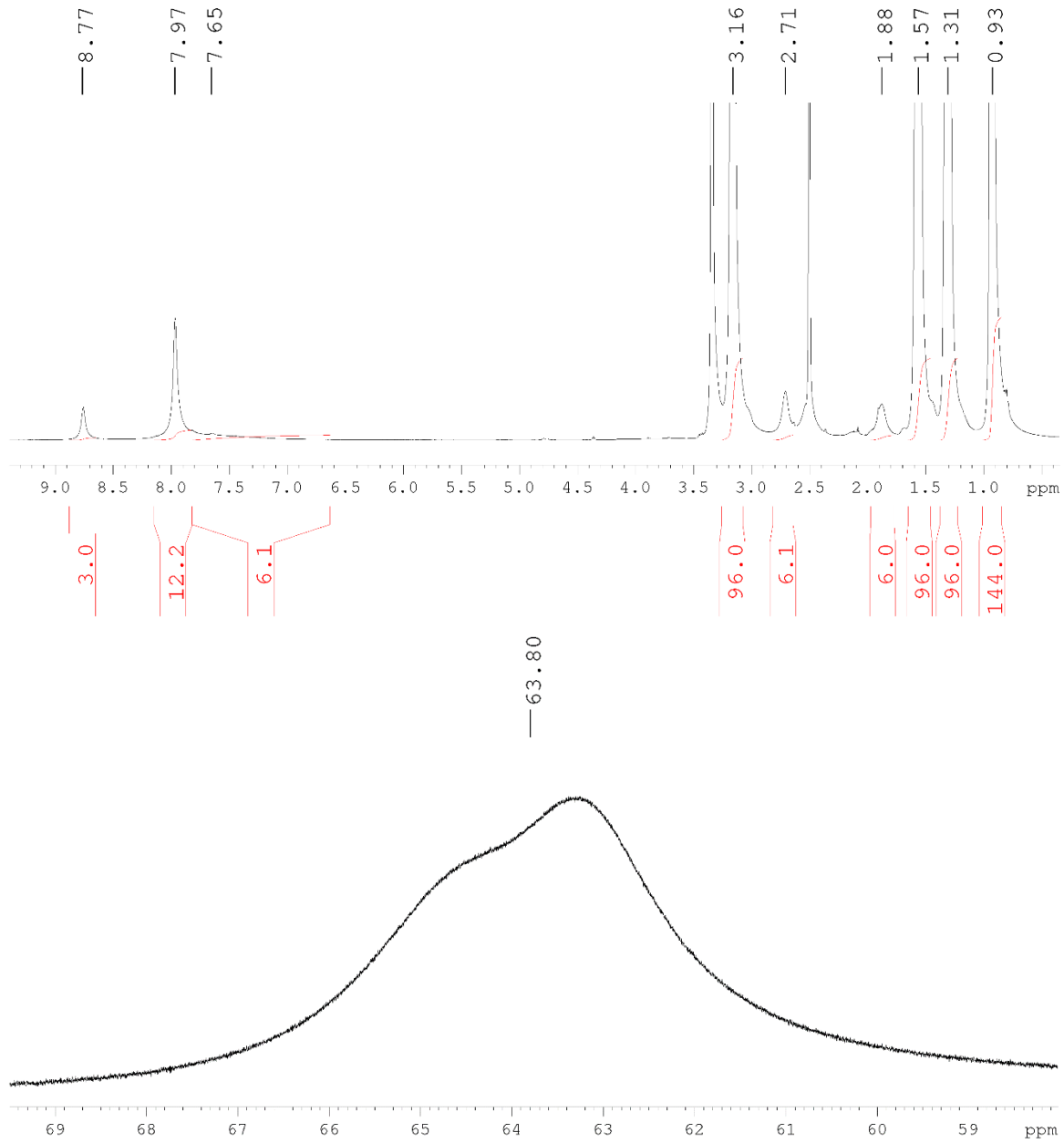

^{1}H NMR of the Mn-Anderson tetramer (**12**) in DMSO-d_6 at 500 MHz.

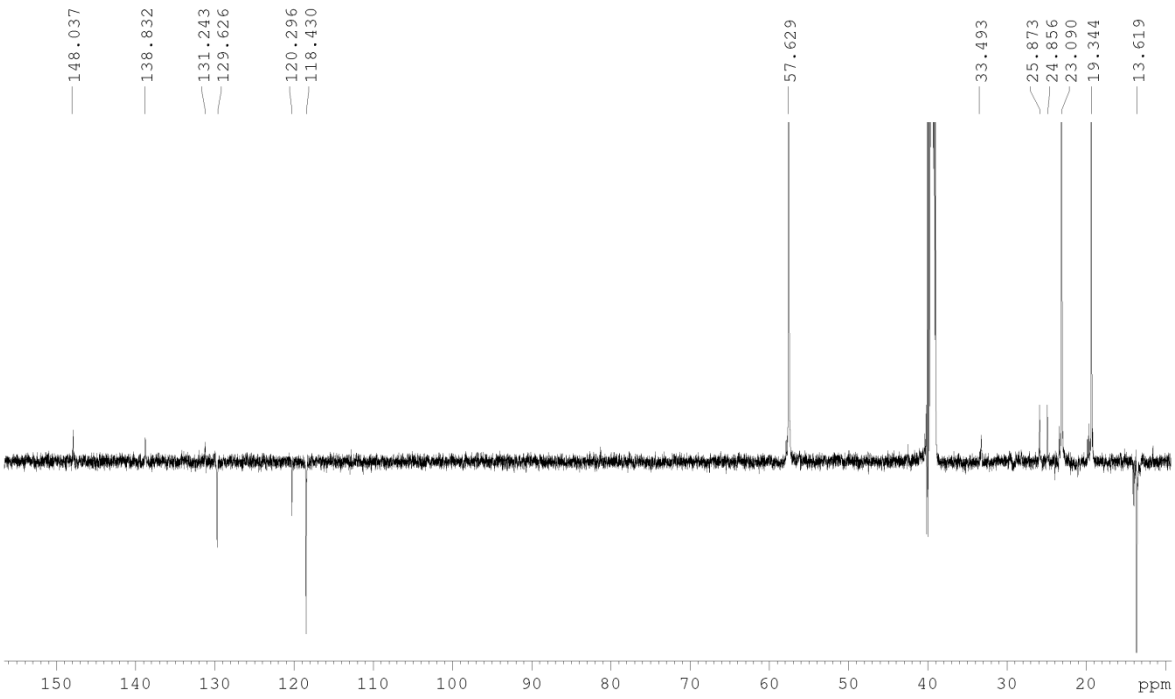

^{13}C DEPTQ NMR of the Mn-Anderson tetramer (**12**) in DMSO-d_6 at 125 MHz.

Compound 13 Mn-Anderson Pentamer

$((C_4H_9)_4N)_{15}[MnMo_6O_{24}(C_{11}H_{11}N_4O)_2]$-
$[MnMo_6O_{24}(C_{10}H_{14}NO)_2]_2[MnMo_6O_{24}(C_{11}H_{11}N_4O)(C_4H_8N)]_2$

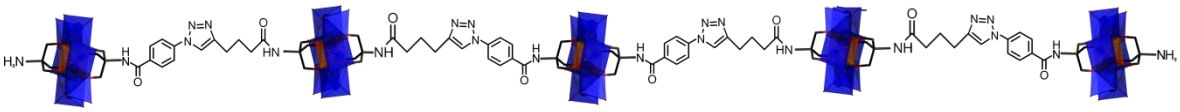

A mixture of asymmetric 4-azidobenzoic/TRIS Mn-Anderson (**6**) (379 mg, 0.06 mmol) and Mn-Anderson trimer (5-hexynoic) (**11**) (302 mg, 0.05 mmol) was dissolved in a Schlenk tube in 6 mL of DMF, to which DIEA was added (20 µL, 0.12 mmol). The solution was then degassed by bubbling nitrogen through it for 5 minutes, then CuI (11 mg, 0.06 mmol) was added and the tube was sealed under nitrogen. The mixture was then stirred at 40°C for 16h. The product was then precipitated from the DMF with diethyl ether, redissolved in MeCN and loaded onto silica. The product was then separated from the remaining starting material using a Reveleris flash chromatography system with a C-18 column with MeCN and a 10 mM aqueous solution of TBABr as eluents. Fractions were combined, MeCN was removed and the precipitate was collected by centrifugation. The residue was then recrystallised from MeCN with diethyl ether diffusion.

Yield: 195 mg, 0.02 mmol, 39.3%; **^{1}H NMR** (DMSO-d_6, 500 MHz): δ = 0.93 (m, 180H, CH_3 from TBA^+), 1.31 (m, 120H, CH_2 from TBA^+), 1.57 (m, 120H, CH_2 from TBA^+), 1.88 (bs, 8H, CH_2), 2.71 (bs, 8H, CH_2), 3.16 (m, 120H, CH_2 from TBA^+), 6.7 – 7.7 (m, 8H, NH), 7.97 (m, 16H, CH), 8.76 (s, 4H, Triazole-H), 63.73 ppm (m, 60H, CH_2) **^{13}C DEPTQ NMR** (DMSO-d_6, 125 MHz): δ = 13.6 (CH_3), 19.3 (CH_2), 23.1 (CH_2), 24.9 (CH_2), 25.9 (CH_2), 33.2 (CH_2), 57.5 (CH_2), 60.2 (CH_2), 60.8 (C), 63.9 (C), 118.5 (CH), 120.2 (CH), 129.8 (CH), 138.9 (C), 144.0 (C), 148.0 (C), 173.5 and 174.5 ppm (CO); **Elemental analysis:** Calc. for $C_{332}H_{656}Mn_5Mo_{30}N_{37}O_{128}$ (10367.12 g.mol^{-1}): C 38.46, H 6.38, N 5.00 Found: C 38.58, H 6.43, N 4.78. **ESI-MS:** Peak envelopes were observed with central peaks at *m/z* 2349.69 (z = -4), 3213.94 (z = -3) and 3904.93 (z = -5) were assigned as $[((C_4H_9)_4N)_{11}[(MnMo_6O_{24})_5(C_{11}H_{11}N_4O)_4$-$(C_{10}H_{14}NO)_4(C_4H_8N)_2]]^{4-}$ (predicted: 2349.58), $[((C_4H_9)_4N)_{12}[(MnMo_6O_{24})_5(C_{11}H_{11}N_4O)_4$-$(C_{10}H_{14}NO)_4(C_4H_8N)_2]]^{3-}$ (predicted: 3213.54) and $[((C_4H_9)_4N)_{25}[(MnMo_6O_{24})_5$-$(C_{11}H_{11}N_4O)_4(C_{10}H_{14}NO)_4(C_4H_8N)_2]_2]^{5-}$ (predicted: 3904.70), respectively.

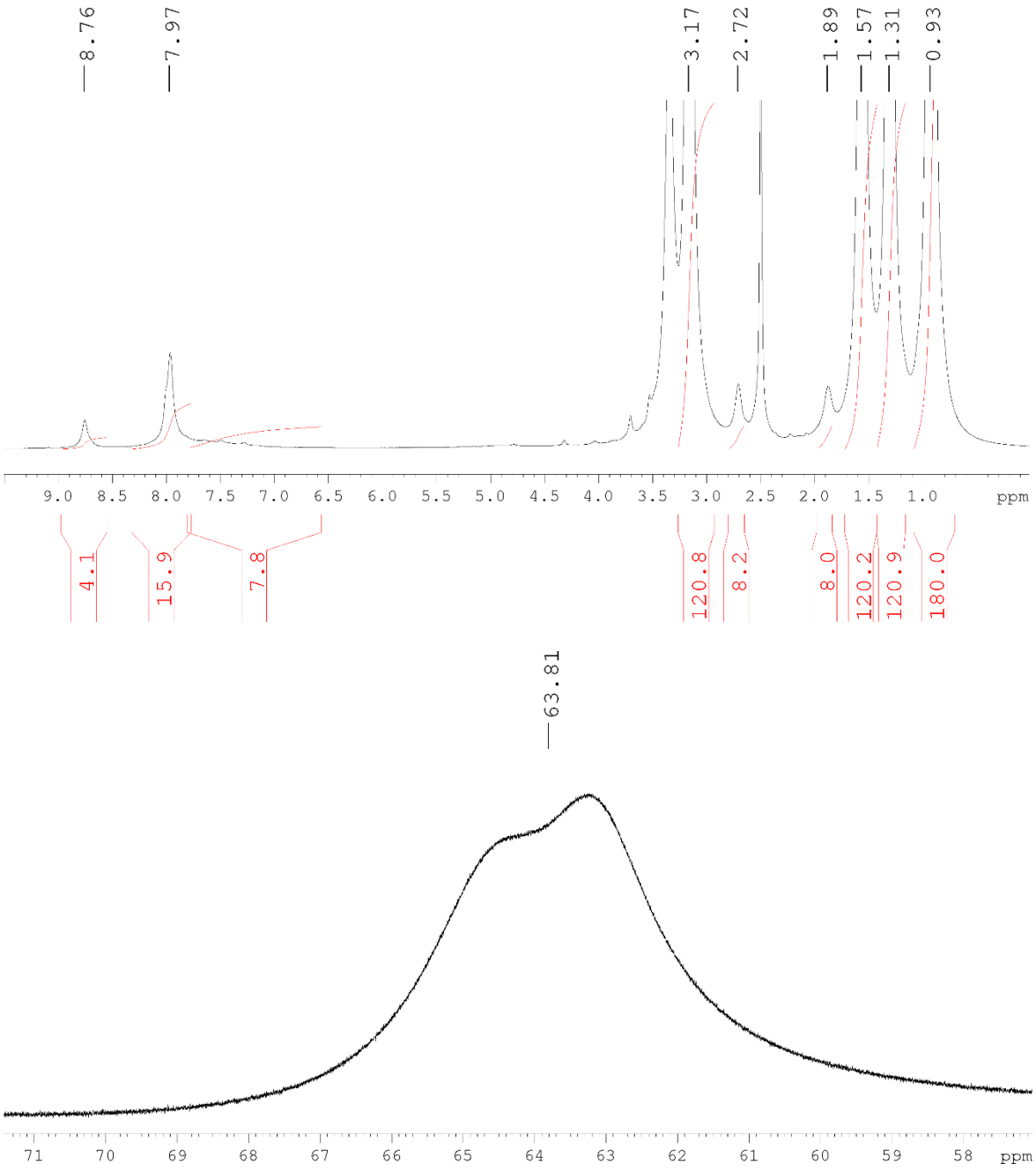

^{1}H NMR of the Mn-Anderson pentamer (**13**) in DMSO-d_6 at 500 MHz.

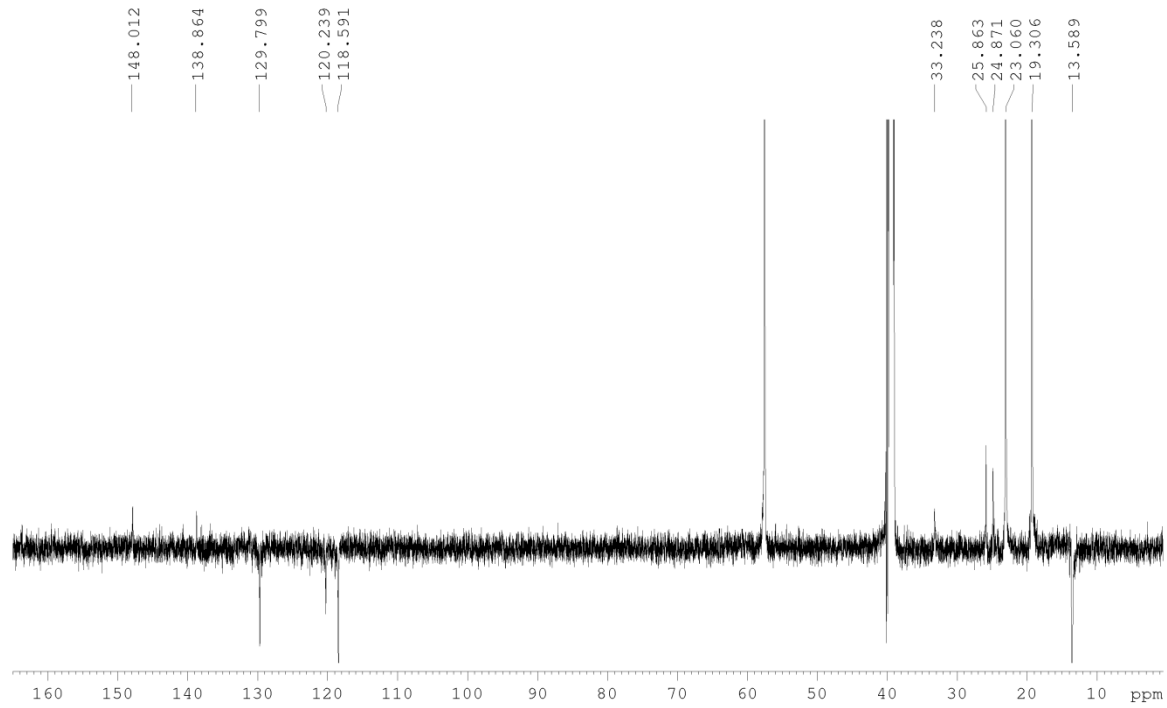

^{13}C DEPTQ NMR of the Mn-Anderson pentamer (**13**) in DMSO-d_6 at 125 MHz.

Compound 14 Decavanadate

$H_3V_{10}O_{28}(N(C_4H_9)_4)_3$

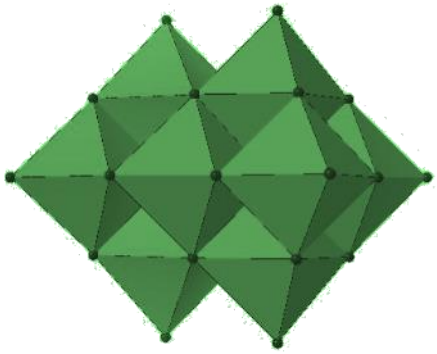

Adapted from a published procedure.[377]

3M HCl (50 mL) was added at a rate of 2 drops sec $^{-1}$ to a solution of sodium vanadate, Na_3VO_4 (10 g, 183.91 gmol^{-1}, 0.054 mol) in H_2O (70 mL). This orange solution was then added, at the same rate, to TBABr (40 g, 322.37 gmol^{-1}, 0.124 mol) dissolved in H_2O (60 mL) forming a cloudy yellow mixture that was left to stir for 20 minutes. The solid was collected and washed with H_2O, EtOH and Et_2O via centrifugation and then left to dry overnight under vacuum.

This solid was combined with a second identical batch of crude material and stirred at 26°C in MeCN (300 mL) for 30 minutes and undissolved material removed leaving a red/orange solution that was heated for a further hour to 30°C before addition of Et_2O (800 mL) to precipitate and collect yellow solid. This solid was redissolved once more in MeCN and set up for slow Et_2O diffusion, forming orange crystals after 20 days.

Yield: 2321 g, 1.576 mmol, 14.5 %; **Characteristic FT-IR** (solution) bands (cm^{-1}): 3290 (b, H_2O), 2959 (sh, -CH_2/-CH_3), 1481 (sh, TBA^+), 968 (s, =O), 847 (sh), 609 (sh, -O-); **Elemental analysis**: Calc. for $C_{48}H_{111}N_3O_{28}V_{10}$ (1687.82 g.mol^{-1}): C 34.16, H 6.63, N 2.49; Found: C 34.48, H 6.28, N 2.41; **ESI-MS**: Peak envelope was observed with central peaks at *m/z* 1445 (z = -1) and 1929.46 (z = +1) assigned as $[H_3V_{10}O_{28}(N(C_4H_9)_4)_2]^{1-}$ (predicted: 1444.89) and $[H_3V_{10}O_{28}(N(C_4H_9)_4)_4]^{1+}$ (predicted: 1929.46), respectively.

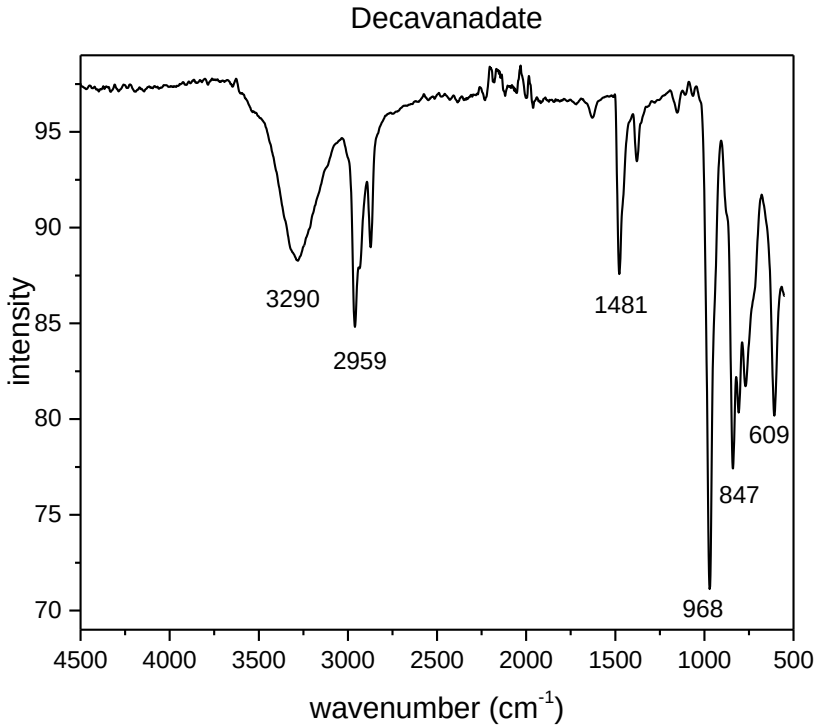

FT-IR measurement for decavanadate (**14**).

Compound 15 FMOC Lindqvist Hybrid

$V_6O_{13}(C_4H_6NHC_{15}H_{11}O_2)(N(C_4H_9)_4)_2$

TRIS ligand (10 mg, 0.083 mmol), FMOC-TRIS ligand (30 mg, 0.087 mmol) and decavanadate (**14**) (100 mg, 0.059 mmol) were dissolved in DMA (15 mL) and refluxed at 90C for 42 hours. Diethyl ether was added to the solution and the solid left to fully precipitate and isolated through centrifugation. The solid was then collected, dried and redissolved in MeCN and left to crystallise by Et_2O diffusion and a small amount of red solid formed after a week

Yield: trace. **ESI-MS**: Peak envelope was observed with central peaks at m/z 1680 (z = +1) assigned as $[V_6O_{13}((OCH_2)_3CNHC_{15}H_{11}O_2)_2(N(C_4H_9)_4)_2H_2]^{1+}$ (predicted: 1680.42).

Compound 16 FMOC/TRIS Lindqvist Hybrid

$V_6O_{13}((OCH_2)_3CNH_2)(C_4H_6NHC_{15}H_{11}O_2)(N(C_4H_9)_4)_2$

Same procedure as FMOC Lindqvist hybrid (**15**).

Yield: trace. **ESI-MS**: Peak envelope was observed with central peaks at m/z 1458 (z = +1) assigned as $[V_6O_{13}((OCH_2)_3CNHC_{15}H_{11}O_2)((OCH_2)_3CNH_2)(N(C_4H_9)_4)_2H_2]^{1+}$ (predicted: 1458.35).

Compound 17 TRIS Lindqvist Hybrid

$V_6O_{13}((OCH_2)_3CNH_2)_2(N(C_4H_9)_4)_2$

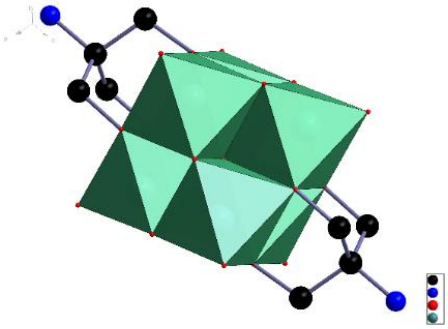

Adapted from a published procedure.[373,376,378,379]

FMOC-TRIS Ligand (130 mg, 343.14 $gmol^{-1}$, 0.379 mmol) and decavanadate (**14**) (198 mg, 1687.175 $gmol^{-1}$, 0.117 mmol) was stirred under nitrogen in anhydrous DMA (10 mL) for 20 hours. Diethyl ether (40 mL) was added to the solution and the solid left to fully precipitate out overnight at -4°C. The solid was then collected, dried and redissolved in MeCN (60 mL). The solution was split into to two equal parts, one part of which was stirred for 2 hours with TBAOH 10% in methanol (5 mL). After filtering, the flask was left to crystallise by Et_2O diffusion and small red needles were collected some days later.

Yield: 12 mg, 0.008 mmol, 4.1 % based on Mo; **^{1}H NMR** (DMSO-d_6, 600 MHz): δ = 0.94 (CH_3 from TBA^+), 1.32 (dd, CH_2 from TBA^+), 1.57 (q, CH_2 from TRIS), 3.17 (t, CH_2 from TBA^+), 4.78 (s, NH) ppm (s); **^{13}C DEPTQ NMR** (DMSO-d_6, 150.9 MHz): δ = 13.5 (CH_3 from TBA^+), 19.2 (CH_2 from TBA^+), 23.1 (CH_2 from TBA^+), 49.0 (CH_2 from TRIS), 57.5 (CH_2 from TBA^+), 84.5 ppm (C from TRIS); **Characteristic FT-IR** (solution) bands (cm^{-1}): 2953 (m, H_2O/-NH_2), 1983 (w), 1481 (sh, TBA^+), 1059 (s, TRIS), 951 (s, =O), 723 (s, -O-); **Elemental analysis**: Calc. for $C_8H_{16}N_2O_{19}V_6(C_{16}H_{36}N)_2$ (1234.79 $g.mol^{-1}$): C 38.91, H 8.46, N 7.18; Found: C 39.57, H 7.25, N 4.67.

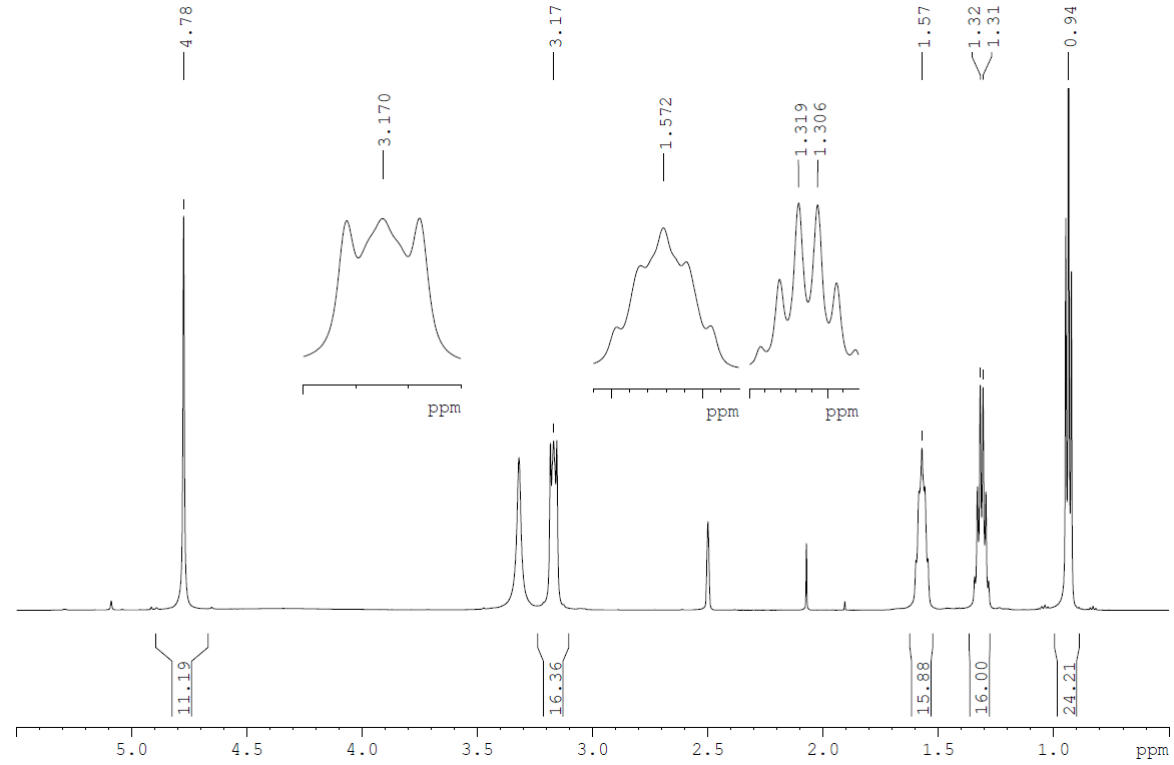

^{1}H NMR of the TRIS Lindqvist hybrid (**17**) in DMSO-d_6 at 600 MHz.

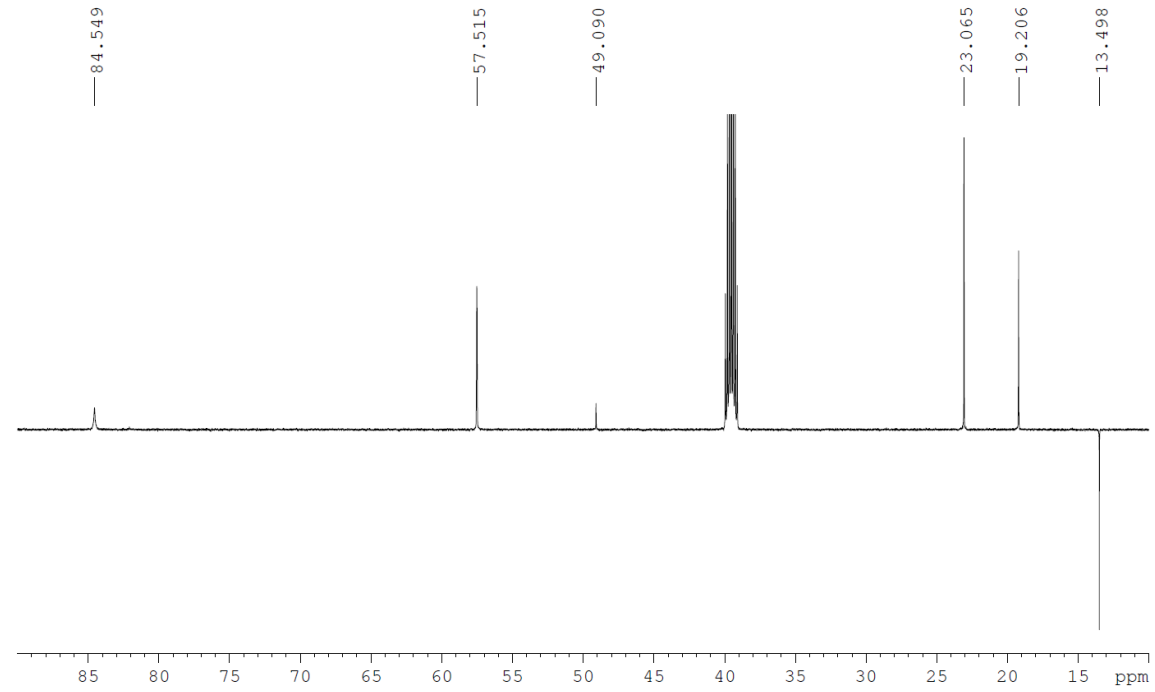

^{13}C DEPTQ NMR of the TRIS Lindqvist hybrid (**17**) in DMSO-d_6 at 150.9 MHz

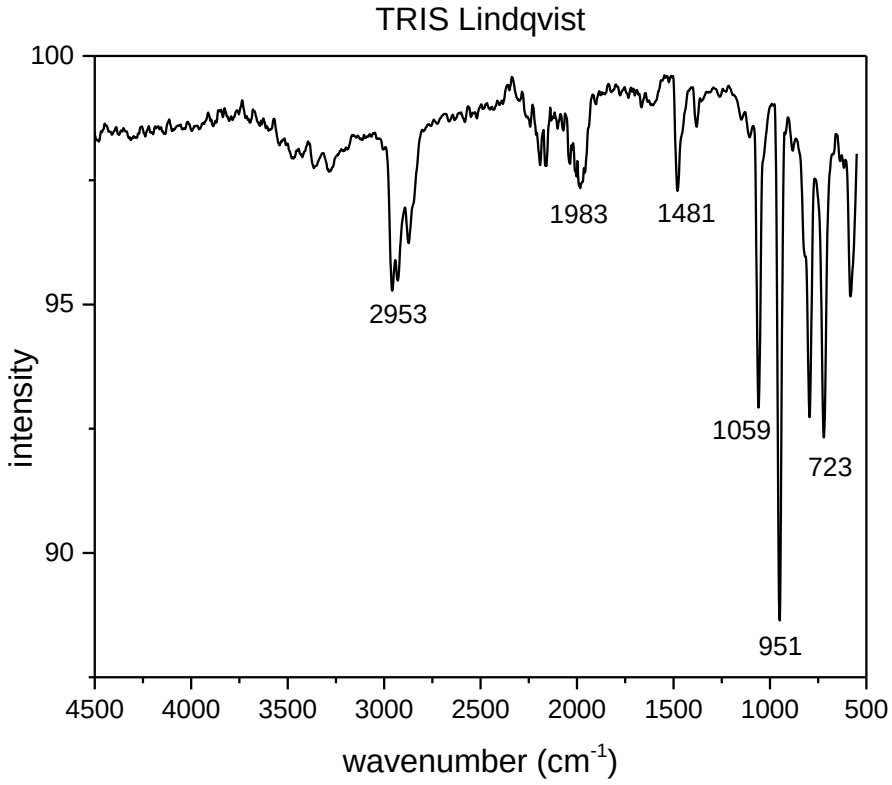

FT-IR measurement for TRIS Lindqvist (**17**).

Compound 18 TRIS Fe-Anderson Hybrid

$(FeMo_6O_{24})(C_4H_6NH_2)_2(N(C_4H_9)_4)_3$

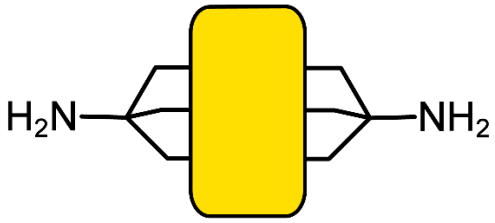

Method A

A mixture of $(TBA)_4[\alpha\text{-}Mo_8O_{26}]$ (3.78 g, 1.76 mmol), $Fe_3O(CH_3CO_2)_7(H_2O)_3$ (696 mg, 1.07 mmol) and TRIS ligand (756 mg; 6.24 mmol) was refluxed in MeCN (50 mL) for 16 h. After removal of any precipitate, the resulting bright yellow solution was allowed to cool to room temperature. This crude mixture was purified via crystallisation by Et_2O diffusion. After 5 days, yellow crystals/solid formed, isolated and analysed.

Method B

Symmetric FMOC Fe-Anderson was dissolved in MeCN (20% piperidine) and left to stir at room temperature for an hour. The solid was then precipitated out with Et_2O, collected and combined with celite in MeCN then evaporated under vacuum to obtain a powder. The crude material adsorbed on celite was purified by flash chromatography and the MeCN removed causing a white/yellow powder to precipitate from the remaining water. This precipitate was isolated by centrifugation then dissolved in MeCN then set up for crystallisation with Et_2O diffusion. Within a week, crystals were formed, dried and analysed.

Yield: 1.886 g, 1.002 mmol, 42.7 %; **^{13}C DEPTQ NMR** (DMSO-d_6, 150.9 MHz) δ = 13.5 (CH_3 from TBA^+), 19.2 (CH_2 from TBA^+), 23.0 (CH_2 from TRIS), 57.5 ppm (CH_2 from TBA^+); **Characteristic FT-IR** (solution) bands (cm^{-1}): 2963 (sh, -CH_2/-CH_3), 1480 (sh, TBA^+), 924 (s, =O) 661(s, -O-); **Elemental analysis:** Calc. for $C_8H_{16}FeMo_6N_2O_{24}(C_{16}H_{36}N)_3H_3$ (1886.06 $g.mol^{-1}$): C 35.66, H 6.79, N 3.71; Found: C 35.15, H 6.79, N 3.7; **ESI-MS:** Peak envelope was observed with central peaks at *m/z* 1640.96 (z = -1) and 1398.66 (z = -1) assigned as

$[((C_4H_9)_4N)_2FeMo_6O_{24}(C_4H_6NH_2)_2]^-$ (predicted: 1640.95) and $[((C_4H_9)_4N)_2FeMo_6O_{24}(C_4H_6NH_2)H]^-$ (predicted: 1398.67), respectively.

Yield: 438 g, 0.46 mmol, 39.47 % for sym FMOC Fe-Anderson

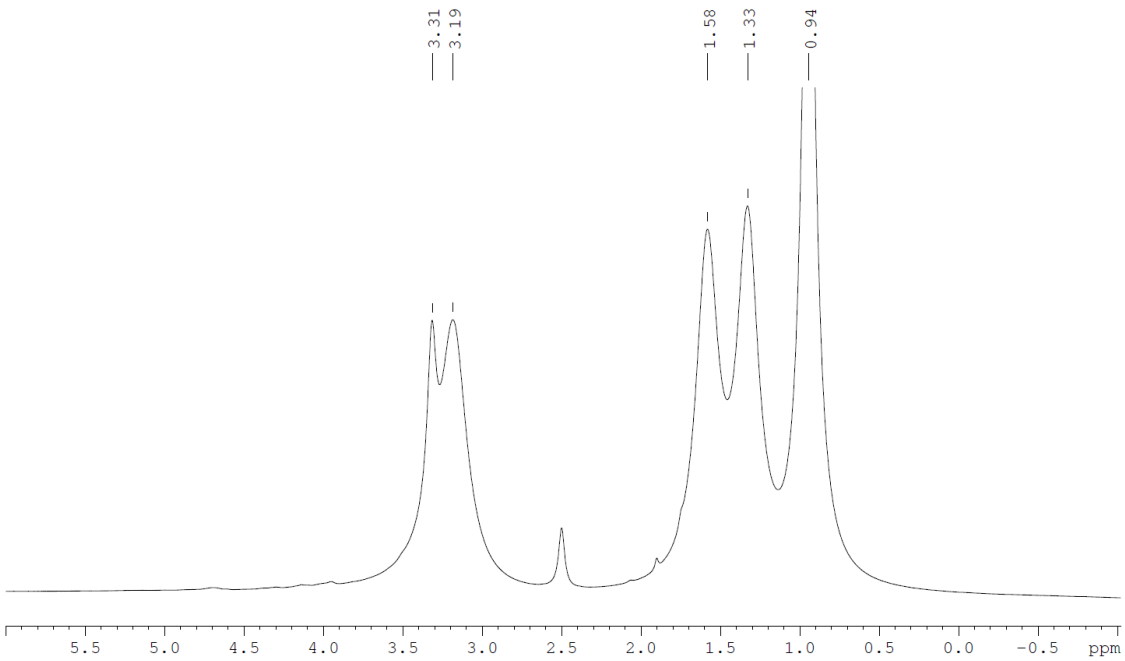

^{1}H NMR of the TRIS Fe-Anderson (**18**) in DMSO-d_6 at 600 MHz.

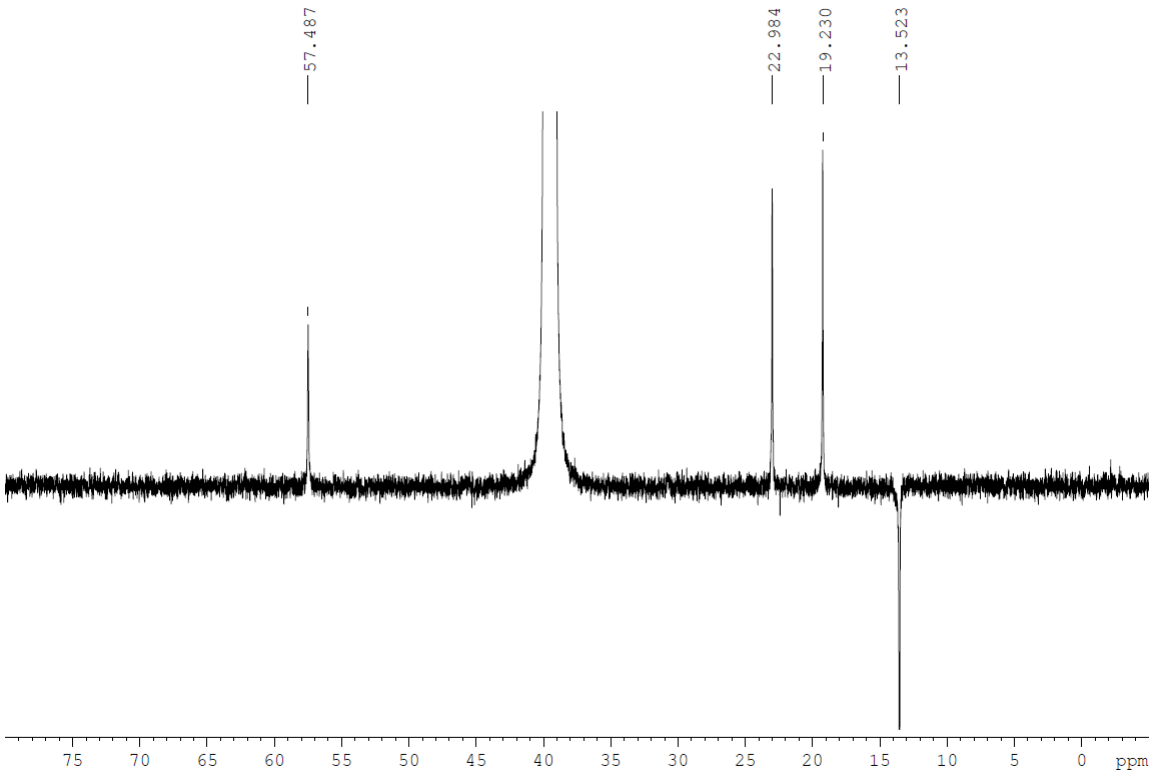

^{13}C DEPTQ NMR of the TRIS Fe-Anderson (**18**) in DMSO-d_6 at 150.9 MHz

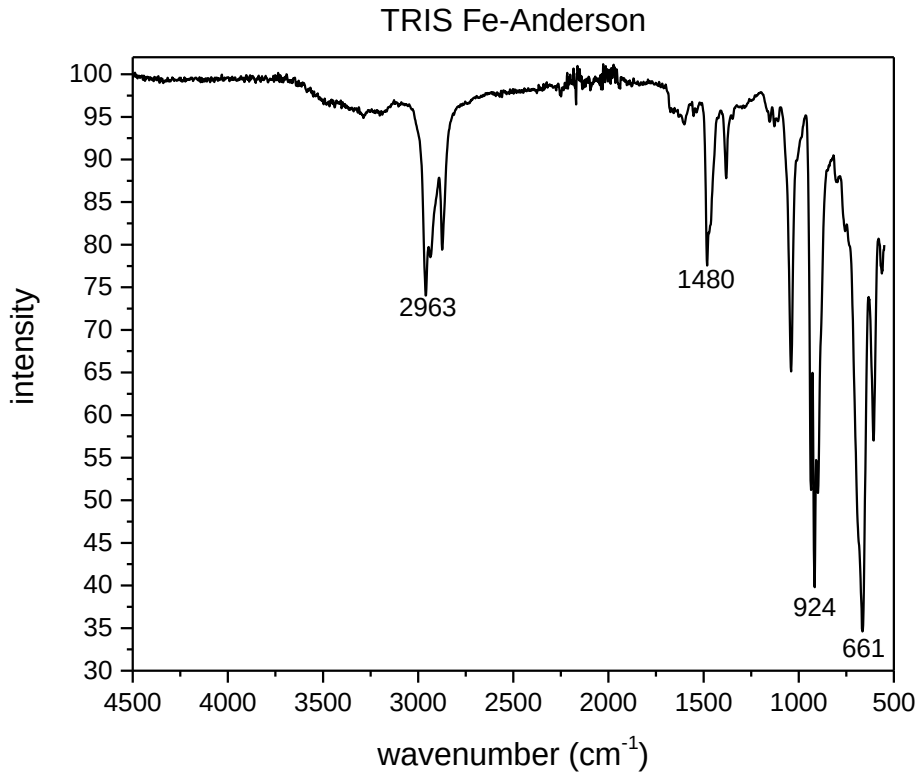

FT-IR measurement for TRIS Fe-Anderson (**18**).

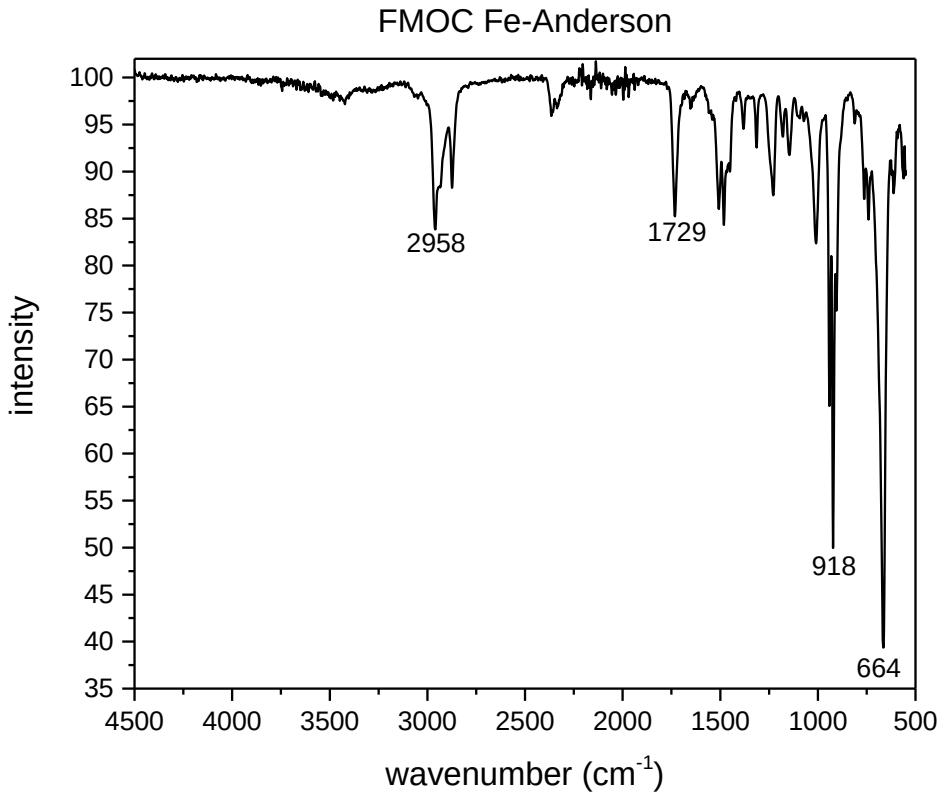

FT-IR measurement for FMOC Fe-Anderson.

Compound 19 FMOC/TRIS Fe-Anderson Hybrid

$FeMo_6O_{24}(C_4H_6NH_2)(C_4H_6NHC_{15}H_{11}O_2)(N(C_4H_9)_4)_3$

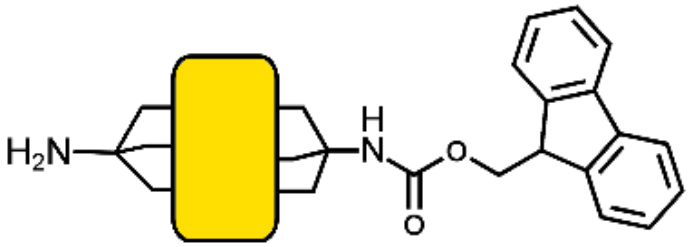

A mixture of $((C_4H_9)_4N)_4[\alpha\text{-}Mo_8O_{26}]$ (7.127 g, 3.31 mmol, 2153.8 $gmol^{-1}$), $Fe(C_5H_7O_2)_3$ (2.338 g, 6.62 mmol, 353.17 $gmol^{-1}$), TRIS ligand (0.808 g, 6.67 mmol, 121.14 $gmol^{-1}$) and FMOC-TRIS ligand, (2.277 g, 6.64 mmol, 343.142 $gmol^{-1}$) was refluxed in MeCN (150 mL) for 18 h. The resulting brown mixture was cooled down to room temperature and the precipitate removed by centrifugation to lead to a bright yellow solution. The crude mixture was isolated by crystallisation by Et_2O diffusion, giving yellow crystals after 5 days, which were isolated. These were adsorbed on celite and purified by flash chromatography and the pure fractions were combined. The MeCN was evaporated under vacuum causing a white/yellow powder to precipitate from the remaining water. This precipitate was isolated by centrifugation then dissolved in MeCN then set up for crystallisation with Et_2O diffusion. Within a week, crystals were formed, dried and analysed.

Yield: 791 mg, 0.376 mmol, 40.4 %, **ESI-MS**: Peak envelope was observed with central peaks at *m/z* 1621.95 (z = -1) and 1863.26 (z = -1) assigned as $[FeMo_6O_{24}(C_4H_6NH_2)(C_4H_6NHC_{15}H_{11}O_2)(N(C_4H_9)_4)H]^{1-}$ (predicted: 1621.74) and $[FeMo_6O_{24}(C_4H_6NH_2)(C_4H_6NHC_{15}H_{11}O_2)(N(C_4H_9)_4)_2]^{1-}$ (predicted: 1863.02), respectively. Characterisation limited as all material used imediately for 5-hexynoic/TRIS Fe-Anderson synthesis.

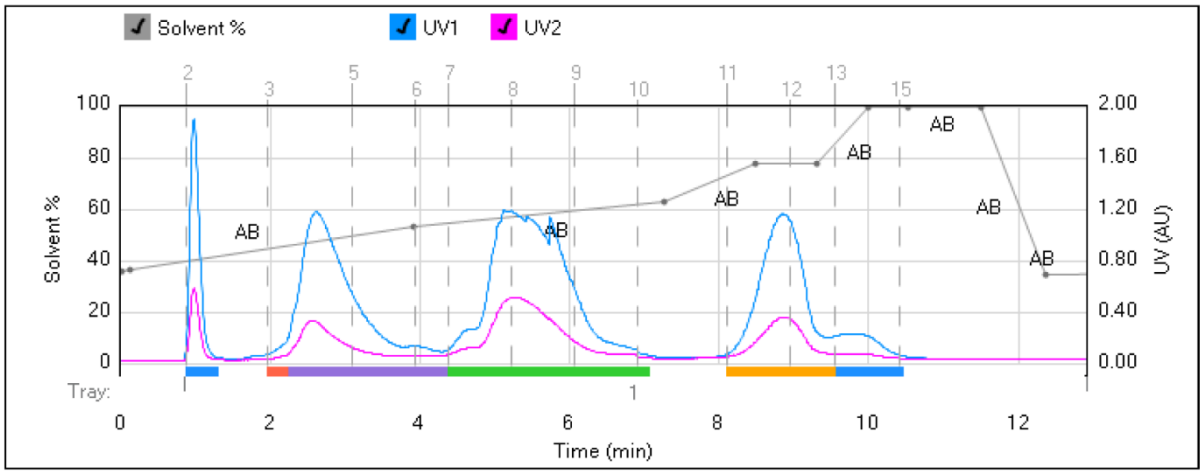

UV trace for the RP-LC separation of FMOC/TRIS Fe-Anderson (**19**).

Compound 20 4-azidobenzoic/TRIS Fe-Anderson

$(N(C_4H_9)_4)_3\ FeMo_6O_{24}(C_4H_6NH_2)(C_4H_6NHC_{15}H_{11}O_2)$

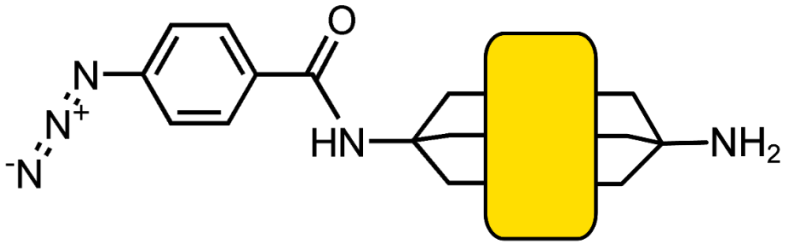

Method A

A mixture of $((C_4H_9)_4N)_4[\alpha\text{-}Mo_8O_{26}]$ (1092 mg, 0.51 mmol), $Fe(acac)_3$ (358 mg, 1.01 mmol), TRIS (123 mg, 1.01 mmol) and 4-azidobenzoic-TRIS (270 mg, 1.01 mmol) was refluxed in MeCN (50 mL) for 18 h. The mixture was left to cool, then the precipitate was removed by centrifugation, resulting in a bright red solution. The crude mixture was isolated by crystallisation by Et_2O diffusion, giving yellow crystals after 5 days, which were isolated. The crude mixture was combined with celite (10 g) in 40 mL of MeCN then evaporated under vacuum to obtain a powder. The crude material adsorbed on celite was purified by flash chromatography and the pure fractions were combined and a large excess of TBABr (0.5 g, 1.55 mmol) was added to the resulting light yellow solution. The MeCN was evaporated under vacuum causing a white/yellow powder to precipitate from the remaining water. This precipitate was isolated by centrifugation then dissolved in MeCN then set up for crystallisation with Et_2O diffusion. Within a week, crystals were formed, dried and analysed.

Yield: 45 mg, 0.22 mmol, 3 % based on Mo; **^{1}H NMR** (DMSO-d_6, 600 MHz): δ = 0.94 (CH_3 from TBA^+), 1.32 (CH_2 from TBA^+), 1.57 (CH_2 from TBA^+), 3.16 ppm (CH_2 from TBA^+); **^{13}C DEPTQ NMR** (DMSO-d_6, 150.9 MHz): δ = 13.6 (CH_3 from TBA^+), 19.2 (CH_2 from TBA^+), 23.0 (CH_2 from TRIS), 57.5 (CH_2 from TBA^+); **Elemental analysis**: Calc. for $(FeMo_6O_{24})(C_4H_6NHCOC_6H_4N_3)(C_4H_6NH_2)(N(C_4H_9)_4)_2(H_2O)_7$ (1911.80 $g.mol^{-1}$): C 29.53, H 5.54, N 5.13; Found: C 30.38, H 4.78, N 4.27; **ESI-MS:** Peak envelopes were observed with central peaks at *m/z* 1785.83 (z = -1/-2) was assigned to $[((C_4H_9)_4N)_2\ FeMo_6O_{24}(C_4H_6NH_2)(C_4H_6NHCOC_6H_4N_3)_2]^-$ (predicted: 1785.98). Many other unassigned peaks left.

Method B

A mixture of $((C_4H_9)_4N)_4[\alpha\text{-}Mo_8O_{26}]$ (400 mg, 1.80 mmol), $Fe_3O(CH_3CO_2)_7(H_2O)_3$ (300 mg, 0.461 mmol), TRIS (112 mg, 0.922 mmol) and 4-azidobenzoic-TRIS, 245 mg, 0.922 mmol) was refluxed in MeCN (20 mL) for 18 h. The resulting brown mixture was cooled down to room temperature and the precipitate removed by centrifugation to lead to a bright yellow solution. The crude mixture was isolated by crystallisation by Et_2O diffusion, giving yellow crystals after 5 days, which were isolated. The crude mixture was combined with celite in MeCN then evaporated under vacuum to obtain a powder. The crude material adsorbed on celite was purified by flash chromatography and the pure fractions were combined and a large excess of TBABr (0.5 g, 1.55 mmol) was added to the resulting light yellow solution. The MeCN was evaporated under vacuum causing a white/yellow powder to precipitate from the remain-ing water. This precipitate was isolated by centrifugation then dissolved in MeCN then set up for crystallisation with Et_2O diffusion. Within a week, crystals were formed, dried and analysed.

Yield: not recorded; **ESI-MS:** Peak envelopes were observed with central peaks at *m/z* 1785.98 (z = -1/-2) was assigned to $[((C_4H_9)_4N)_2\ FeMo_6O_{24}(C_4H_6NH_2)(C_4H_6NHCOC_6H_4N_3)_2]^-$ (predicted: 1785.98).

Method C

A mixture of $((C_4H_9)_4N)_4[\alpha\text{-}Mo_8O_{26}]$ (334 mg, 1.315 mmol), $Fe_3O(CH_3CO_2)_7(H_2O)_3$ (122 mg, 0.188 mmol), 4-azidobenzoic-TRIS (100 mg, 0.376 mmol) and FMOC-TRIS, 129 mg, 0.376 mmol) was re-fluxed in MeCN (50 mL) for 18 h. The resulting brown mixture was cooled down to room temperature and the precipitate removed by centrifugation to lead to a bright yellow solution. The crude mixture was isolated by crystallisation by Et_2O diffusion, giving yellow crystals after 5 days, which were isolated. The crude mixture was redissolved in 50mL MeCN (20% piperidine) and left to stir at room temperature for an hour. The solid was then precipitated out with Et_2O, collected and combined with celite (10 g) in 40 mL of MeCN then evaporated under vacuum to obtain a powder. The crude material adsorbed on celite was purified by flash chromatography and the pure fractions were combined and a large excess of TBA bromide (0.5 g, 1.55 mmol) was added to the resulting light yellow solution. The MeCN was evaporated under vacuum causing a white/yellow powder to precipitate from the remaining water. This precipitate was

isolated by centrifugation then dissolved in MeCN then set up for crystallisation with Et_2O diffusion. Within a week, crystals were formed, dried and analysed.

Yield: 25 mg, 0.0123 mmol, 4 % based on Fe; **Elemental analysis:** Calc. for $C_{15}H_{19}FeMo_6N_5O_{25}·2C_{16}H_{36}N·H·0.5C_{15}H_{11}O_2$ (1898.37 g.mol-1): C 34.48, H 5.18, N 5.52; Found: C 34.49, H 5.74, N 5.16; **ESI-MS:** Peak envelopes were observed with central peaks at *m/z* 1785.93 (z = -1/-2) and 1544.67 (z = -1), assigned as $[((C_4H_9)_4N)_2\ FeMo_6O_{24}(C_4H_6NH_2)(C_4H_6NHCOC_6H_4N_3)]^-$ (predicted: 1785.98) and $[((C_4H_9)_4N)H\ FeMo_6O_{24}(C_4H_6NH_2)(C_4H_6NHCOC_6H_4N_3)]^-$ (predicted: 1544.72), respectively.

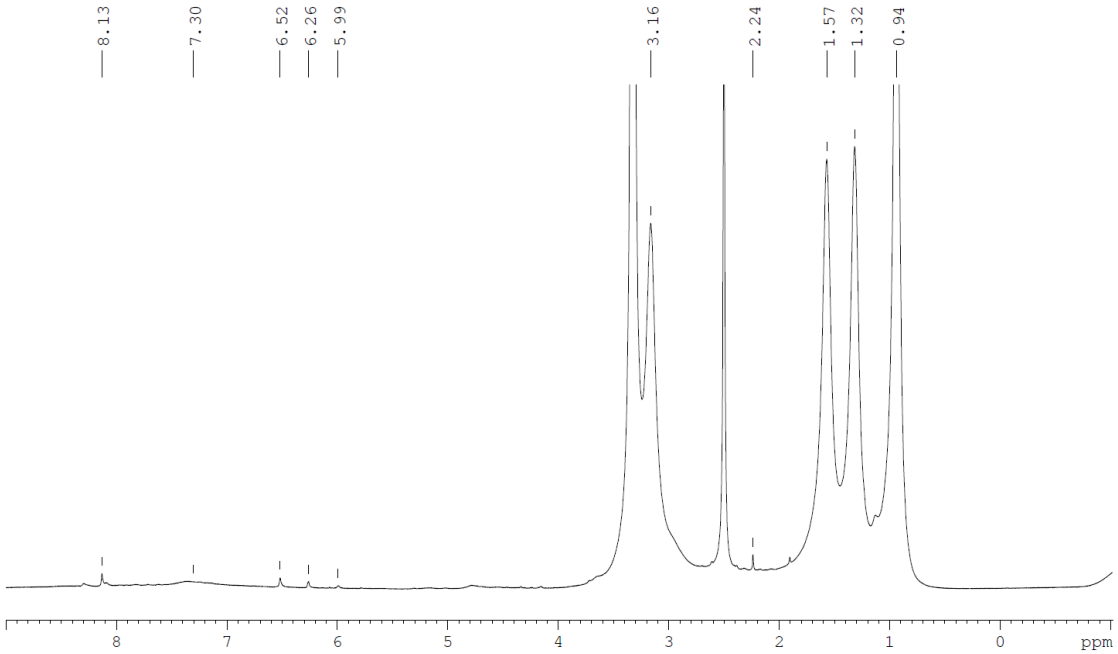

^{1}H NMR of the 4-azidobenzoic/TRIS Fe-Anderson (**20**) in DMSO-d_6 at 600 MHz.

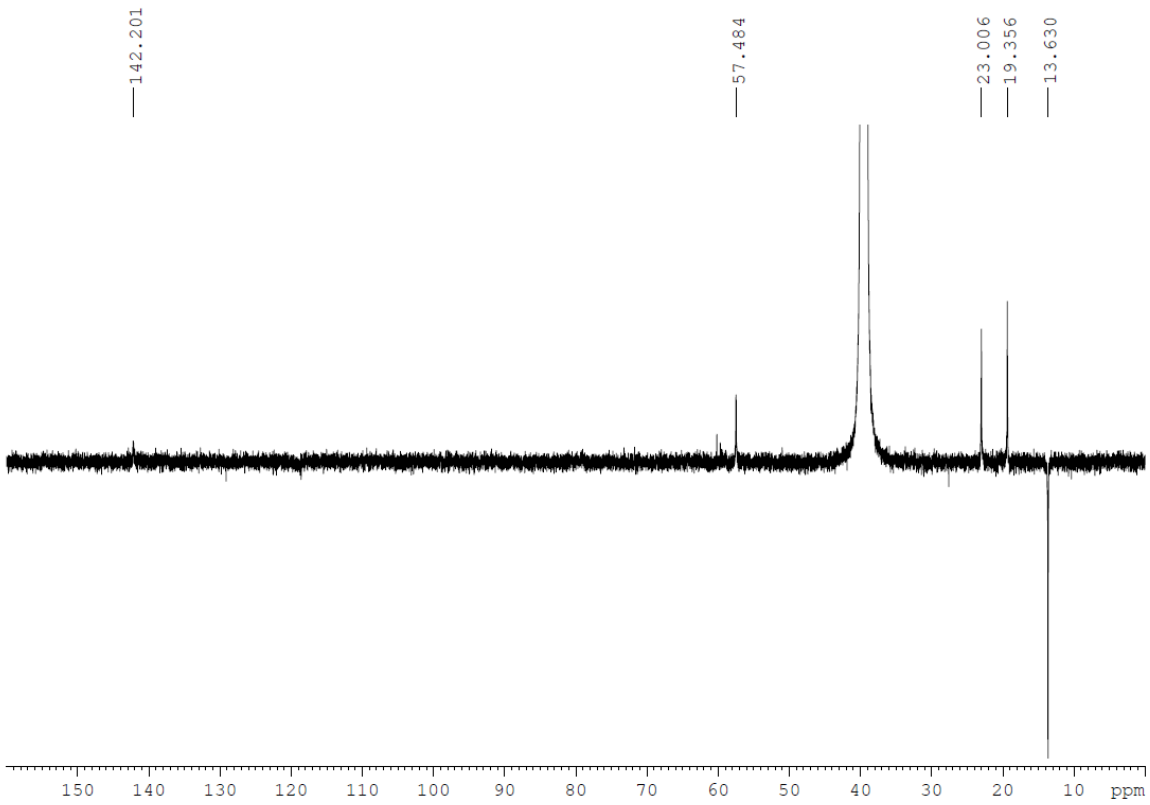

^{13}C DEPTQ NMR of the 4-azidobenzoic/TRIS Fe-Anderson (**20**) in DMSO-d_6 at 150.9 MHz

Compound 21 5-hexynoic Fe-Anderson Hybrid

$(FeMo_6O_{24})(C_4H_6NHCOC_5H_7)_2(N(C_4H_9)_4)_3$

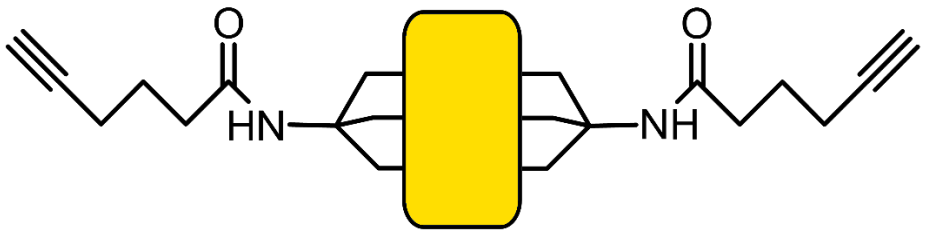

5-hexynoic acid (1.00 mL, 1.016 g, 9.061 mmol, 112.13 $gmol^{-1}$), EEDQ (2.00 g, 8.088 mmol, 247.29 $gmol^{-1}$) and symmetric TRIS Fe-Anderson (**18**) (3.00 g, 1.595 mmol, 1881.24 $gmol^{-1}$) were combined in MeCN (50 mL) and refluxed for 18 h. The deep brown solution was then allowed to cool to room temperature, filtered and the resulting solution was poured into Et_2O (100 mL). Solid collected through centrifugation and washed by redissolving in MeCN and crashing in Et_2O. Solid dried under vacuum before analysis.

Yield: 547 mg, 0.264 mmol, 16.6 %, **^{1}H NMR** (DMSO-d_6, 600 MHz): δ = 0.94 (CH_3 from TBA^+), 1.32 (CH_2 from TBA^+), 1.57 (CH_2 from TBA^+), 3.19 ppm (CH_2 from TBA^+); **^{13}C DEPTQ NMR** (DMSO-d_6, 150.9 MHz): δ = 13.6 (CH_3 from TBA^+), 17.2 (CH_2), 19.3 (CH_2 from TBA^+), 23.4 (CH_2 from TRIS), 32.3 (CH_2), 57.5 (CH_2 from TBA^+), 60.5 ppm (CH_2); **Characteristic FT-IR** (solution) bands (cm^{-1}): 3284 (w, H_2O/-NH_2), 2959 (w, -CH_2/-CH_3), 1481 (w, TBA^+), 916 (sh, =O), 660 (s, -O-); **Elemental analysis**: Calc. for $C_{20}H_{28}FeMo_6N_2O_{26}(C_{16}H_{36}N)_3$ (2071.26 $g.mol^{-1}$): C 39.43, H 6.62, N 3.38; Found: C 39.43, H 6.62, N 3.38; **ESI-MS**: Peak envelope was observed with central peaks at *m/z* 1640.96 (z = -1) and 1398.66 (z = -1) assigned as $[((C_4H_9)_4N)_2FeMo_6O_{24}(C_4H_6NH_2)_2]^-$ (predicted: 1640.95) and $[((C_4H_9)_4N)_2FeMo_6O_{24}(C_4H_6NH_2)H]^-$ (predicted: 1398.67), respectively.

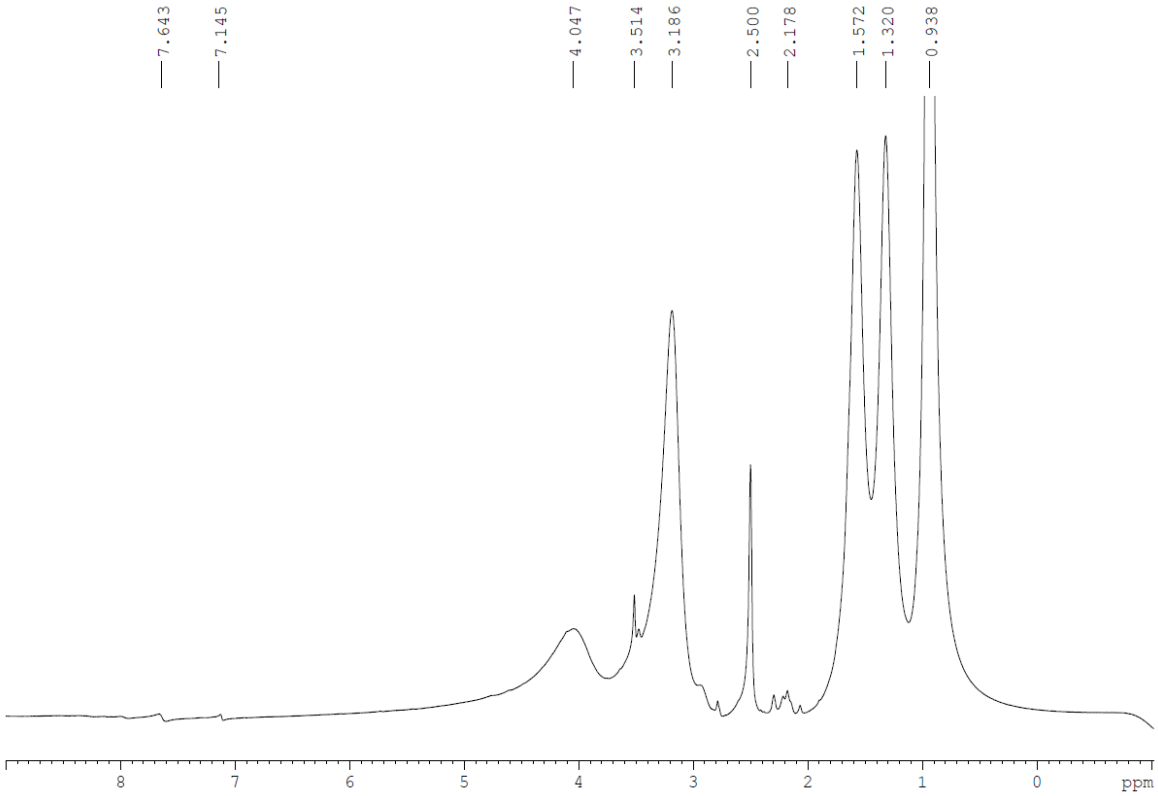

^{1}H NMR of the 5-hexynoic Fe-Anderson (**21**) in DMSO-d_6 at 600 MHz.

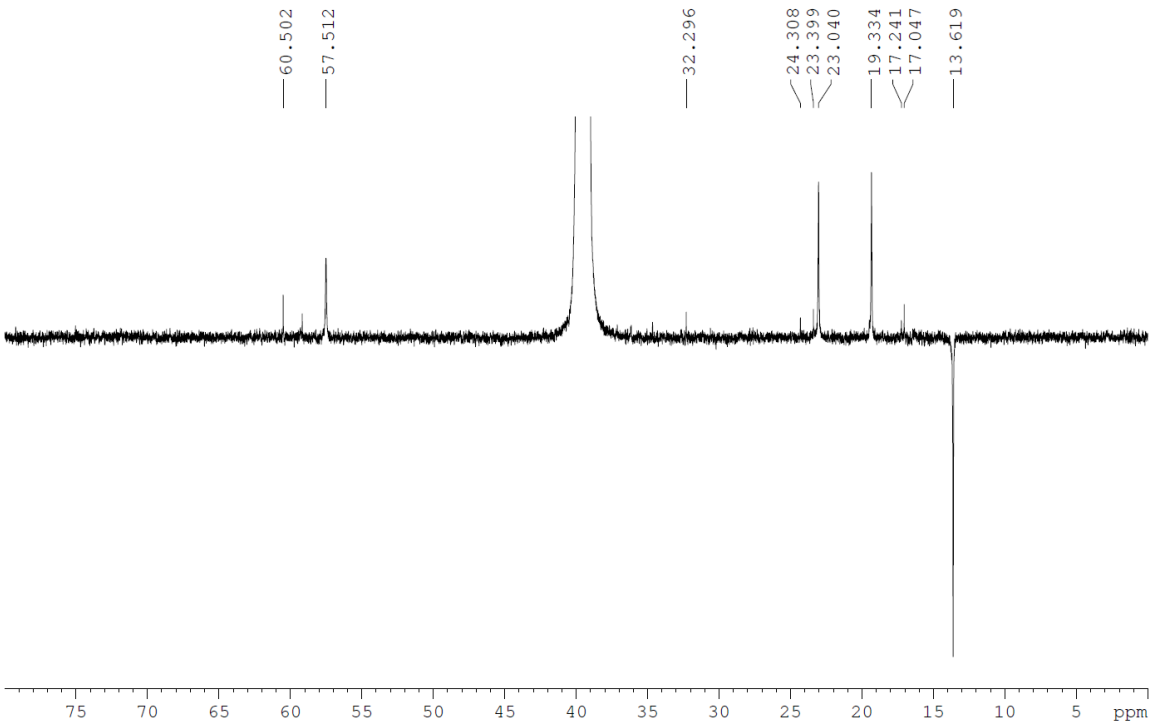

^{13}C DEPTQ NMR of the 5-hexynoic Fe-Anderson (**21**) in DMSO-d_6 at 150.9 MHz

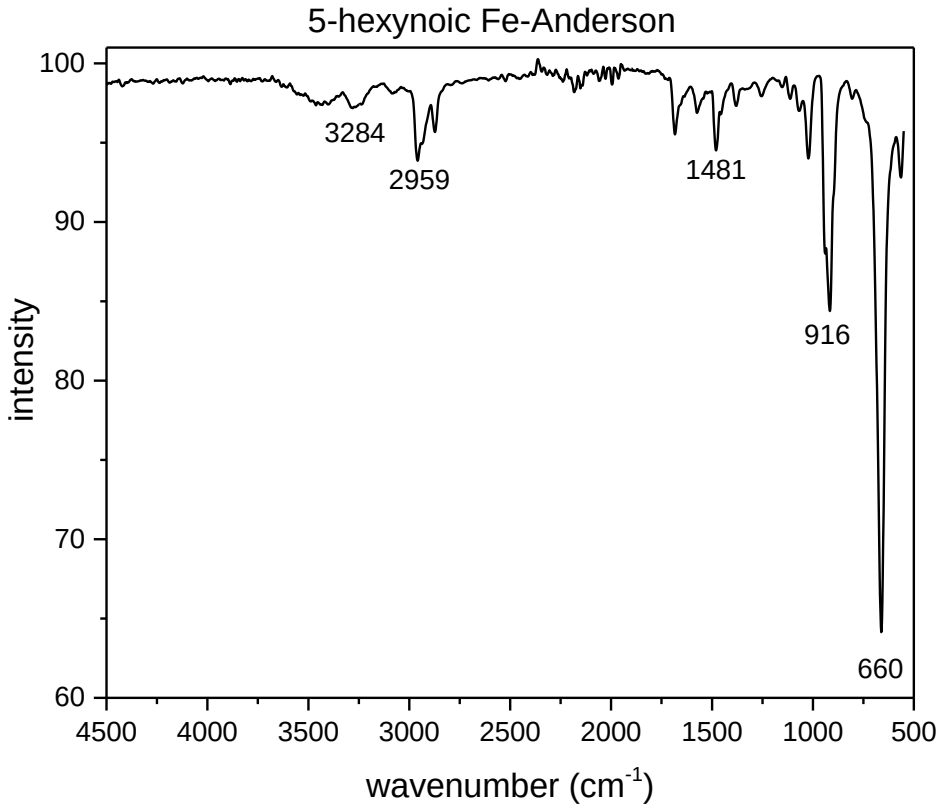

FT-IR measurement for 5-hexynoic Fe-Anderson (**21**).

Compound 22 5-hexynoic/TRIS Fe-Anderson Hybrid

$(FeMo_6O_{24})(C_4H_6NHCOC_5H_7)(C_4H_6NH_2)(N(C_4H_9)_4)_3$

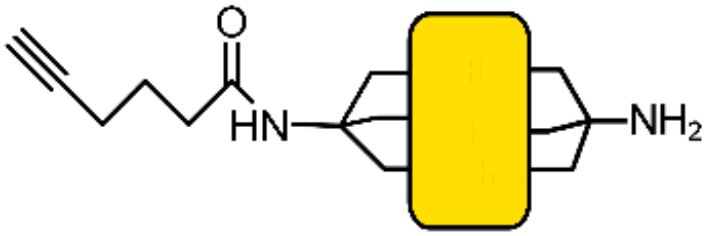

FMOC/TRIS Fe-Anderson (**19**) (1.258 g, 2106 $gmol^{-1}$, 0.597 mmol), EEDQ (739 mg, 247.29 $gmol^{-1}$, 2.987 mmol) and 5-hexynoic acid (0.82 mL, 112.13 $gmol^{-1}$, 29.87 mmol) refluxed in MeCN (15 mL) for 18 h, after which starting material could still be observed via ESI-MS and so another 780 mg of EEDQ was added and left for another night. The reaction mixture was then precipitated out with Et_2O and redissolved in 20 mL of MeCN (20% piperidine) and stirred for half an hour. ESI-MS demonstrated successful deprotection from the FMOC group and so the mixture was precipitated out in Et_2O and dried under vacuum.

Yield: 593 mg, 0.300 mmol, 50.2 %, **^{1}H NMR** (DMSO-d_6, 600 MHz): δ = 0.94 (CH_3 from TBA^+), 1.31 (CH_2 from TBA^+), 1.60 (CH_2 from TBA^+), 3.20 ppm (CH_2 from TBA^+); **^{13}C DEPTQ NMR** (DMSO-d_6, 150.9 MHz): δ = 13.5 (CH_3 from TBA^+), 19.2 (CH_2 from TBA^+), 21.6 (CH_2), 22.2 (CH_2), 23.0 (CH_2 from TRIS), 43.7 (CH_2), 57.5 (CH_2 from TBA^+); **Characteristic FT-IR** (solution) bands (cm^{-1}): 2959 (sh, -CH_2/-CH_3), 1476 (sh, TRIS), 916 (s, =O), 665 (s, -O-); **Elemental analysis**: Calc. for $C_{14}H_{22}FeMo_6N_2O_{25}(C_{16}H_{36}N)_2H_3$ (1737.70 $g.mol^{-1}$): C 31.79, H 5.63, N 3.22; Found: C 32.29, H 5.89, N 3.22; **ESI-MS**: Peak envelope was observed with central peaks at *m/z* 1492.89 (z = -1) and 1734.18 (z = -1) assigned as $[(FeMo_6O_{24})(C_4H_6NHCOC_5H_7)(C_4H_6NH_2)(N(C_4H_9)_4)H]^{1-}$ (predicted: 1492.7) and $[(FeMo_6O_{24})(C_4H_6NHCOC_5H_7)(C_4H_6NH_2)(N(C_4H_9)_4)_2]^{1-}$ (predicted: 1733.99), respectively.

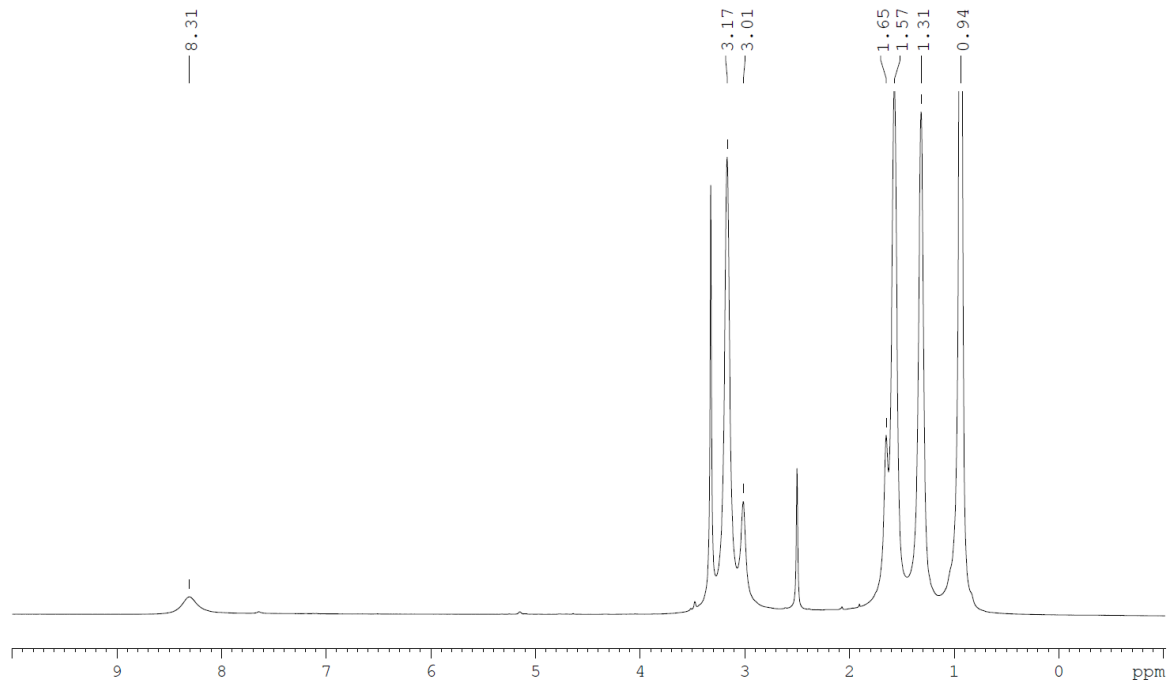

^{1}H NMR of the 5-hexynoic/TRIS Fe-Anderson (**22**) in DMSO-d_6 at 600 MHz.

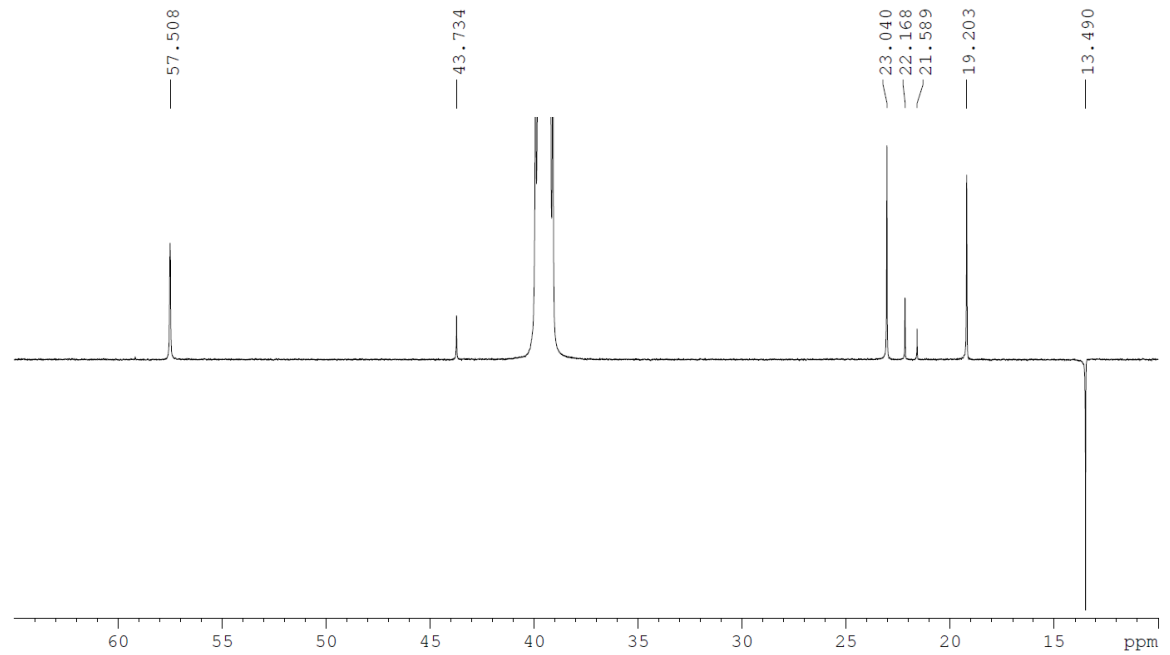

^{13}C DEPTQ NMR of the 5-hexynoic/TRIS Fe-Anderson (**22**) in DMSO-d_6 at 150.9 MHz

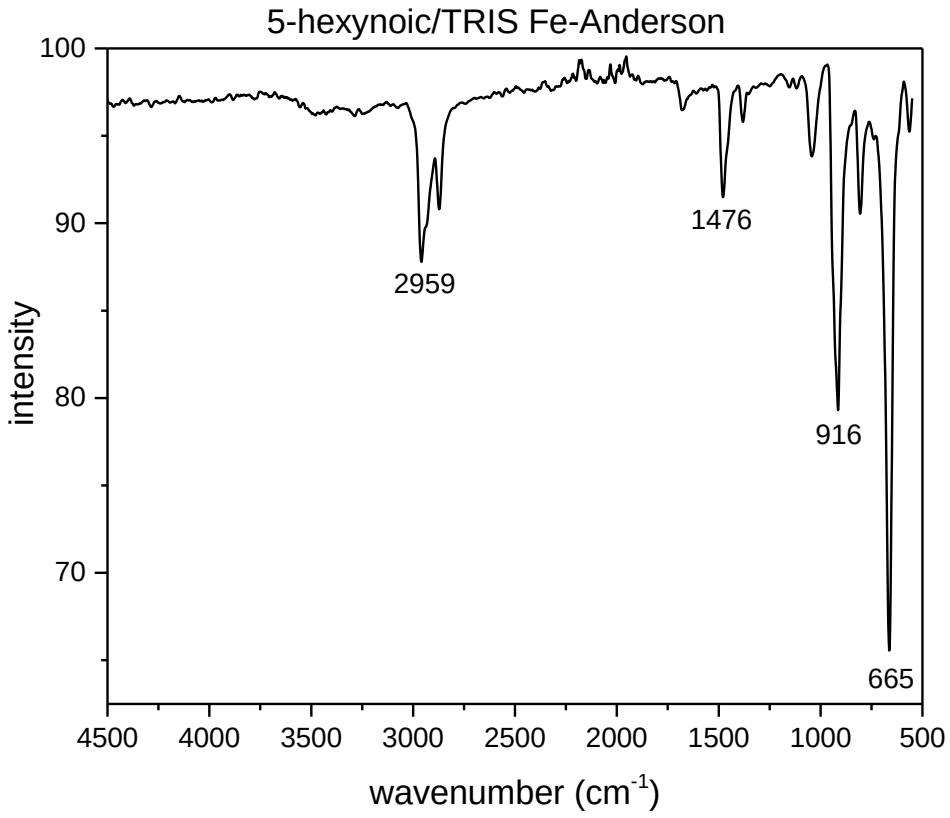

FT-IR measurement for 5-hexynoic/TRIS Fe-Anderson (**22**).

Compound 23 4-azidobenzoic Fe-Anderson Hybrid

$(FeMo_6O_{24})(C_4H_6NHCOC_6H_4N_3)_2(N(C_4H_9)_4)_3$

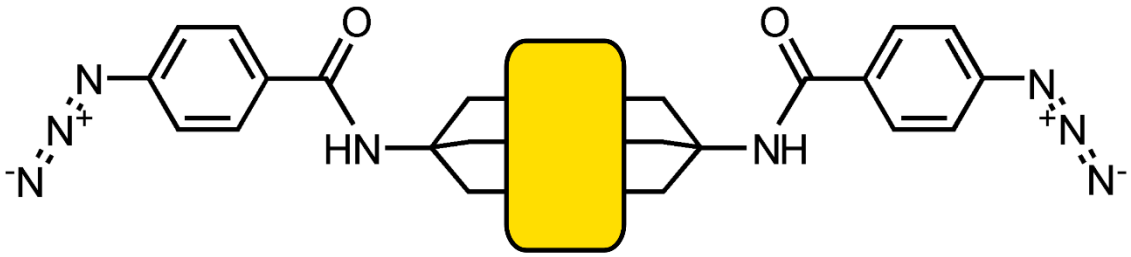

Method A

Isolated during automatic RP-LC separation in Synthesis Method 3A of Compound 3.

Yield: 117 mg, 0.054 mmol, 16 % based on Mo; **ESI-MS:** Peak envelope was observed with central peaks at *m/z* 1930.84 (z = -1/-2), assigned as $[((C_4H_9)_4N)_2FeMo_6O_{24}(C_4H_6NHCOC_6H_4N_3)_2]^-$ (predicted: 1931.01).

Method B

Isolated during automatic RP-LC separation in Synthesis Method 3B of Compound 3.

Yield: not recorded; **ESI-MS:** Peak envelope was observed with central peaks at *m/z* 1931.01 (z = -1/-2), assigned as $[((C_4H_9)_4N)_2\ FeMo_6O_{24}(C_4H_6NHCOC_6H_4N_3)_2]^-$ (predicted: 1931.01).

Method C

Isolated during automatic RP-LC separation in Synthesis Method 3C of Compound 3.

Yield: 12 mg, 0.006 mmol, 4 % based on Fe; **Elemental analysis:** Calc. for $C_{70}H_{130}FeMo_6N_{11}O_{26}$ (2173.28 g.mol-1): C 38.69, H 6.03, N 7.09 Found: C 37.89, H 6.02, N 7.09. **ESI-MS:** Peak envelope was observed with central peaks at *m/z* 1930.96 (z = -1/-2), assigned as $[((C_4H_9)_4N)_2\ FeMo_6O_{24}(C_4H_6NsHCOC_6H_4N_3)_2]^-$ (predicted: 1931.01).

Method D

A mixture of $((C_4H_9)_4N)4[\alpha\text{-}Mo_8O_{26}]$ (2.000 g, 0.929 mmol, 2153.8 $gmol^{-1}$), Fe(III) acetate (0.815 g, 1.252 mmol, 650.89 $gmol^{-1}$) and 4-azidobenzoic-TRIS (2.025 g, 7.606 mmol, 266.25 $gmol^{-1}$) was refluxed in MeCN (75 mL) for 18 h. The mixture was left to cool, then the precipitate was removed by centrifugation, resulting in a bright red solution. This solution was poured into 150 mL Et_2O and the solid collected and washed by centrifugation.

Yield: 332 mg, 0.153 mmol, 14.1 %, **^{1}H NMR** (DMSO-d_6, 600 MHz): δ = 0.94 (CH_3 from TBA^+), 1.33 (CH_2 from TBA^+), 1.57 (CH_2 from TBA^+), 3.17 ppm (CH_2 from TBA^+); **^{13}C DEPTQ NMR** (DMSO-d_6, 150.9 MHz): δ = 13.6 (CH_3 from TBA^+), 19.4 (CH_2 from TBA^+), 23.0 (CH_2 from TRIS), 57.5 (CH_2 from TBA^+); **Characteristic FT-IR** (solution) bands (cm^{-1}): 2953 (sh, -CH_2/-CH_3), 2121 (sh, -N_3), 923 (sh, =O), 665 (s, -O-); **Elemental analysis**: Calc. for $C_{22}H_{22}FeMo_6N_8O_{26}(C_{16}H_{36}N)_3H_3$ (2176.30 $g.mol^{-1}$): C 38.63, H 6.16, N 7.08; Found: C 38.01, H 6.29, N 6.22.

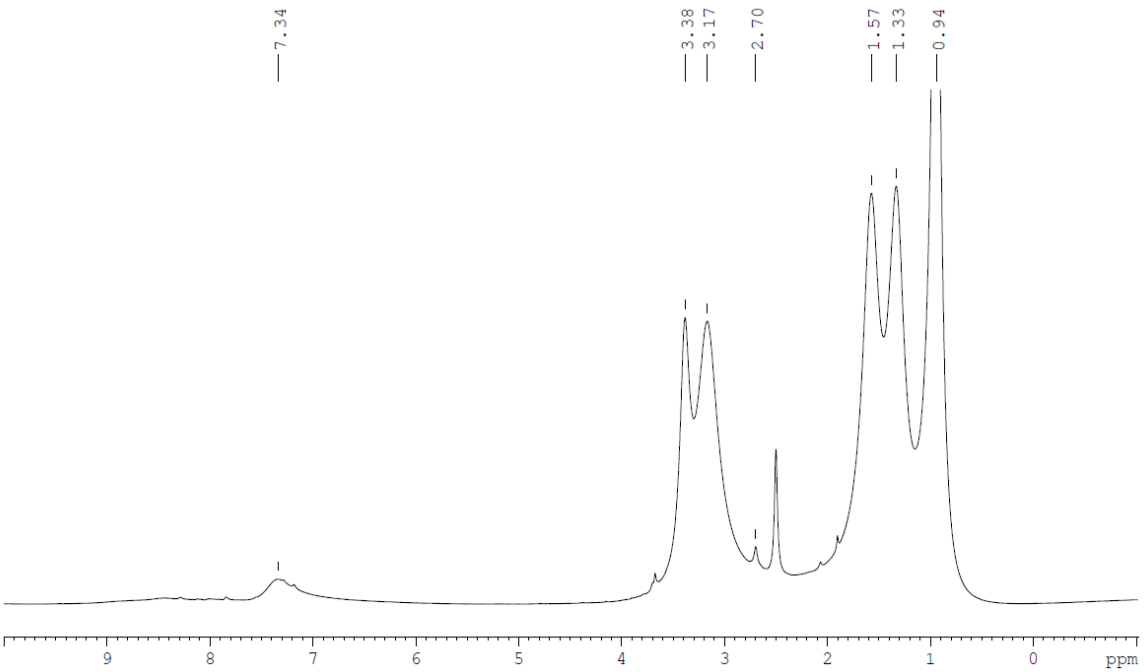

^{1}H NMR of the 4-azidobenzoic Fe-Anderson (**23**) in DMSO-d_6 at 600 MHz.

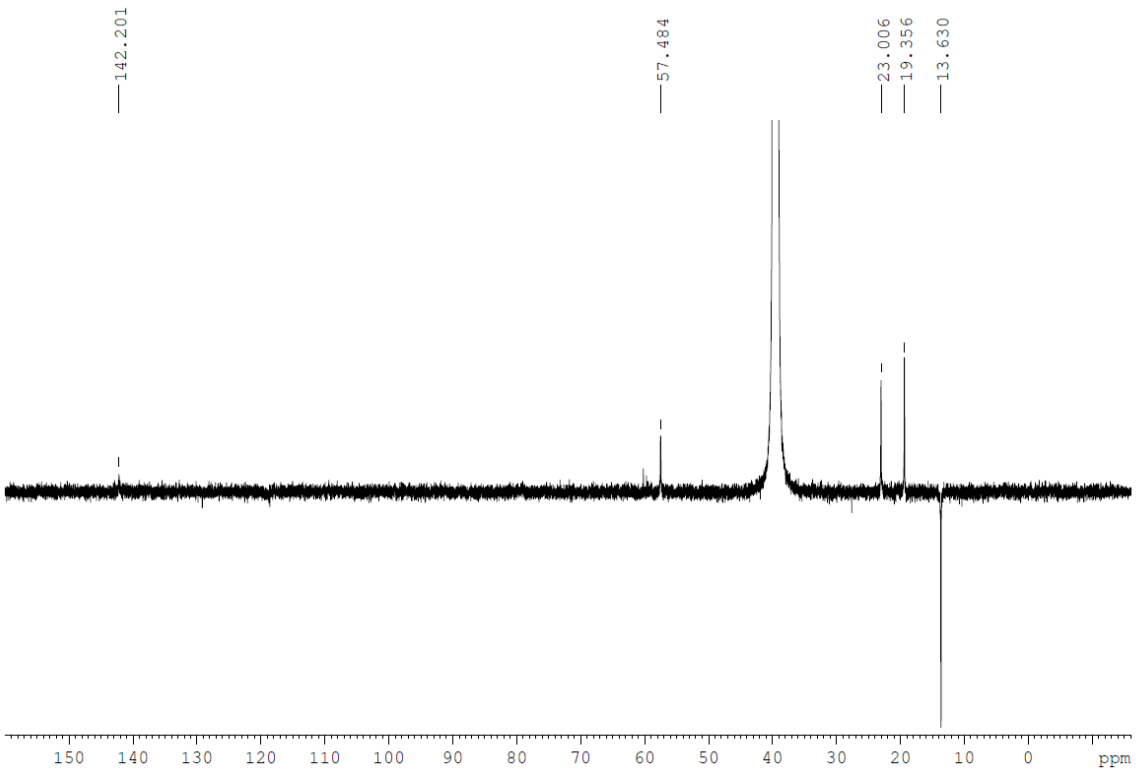

^{13}C DEPTQ NMR of the 4-azidobenzoic Fe-Anderson (**23**) in DMSO-d_6 at 150.9 MHz

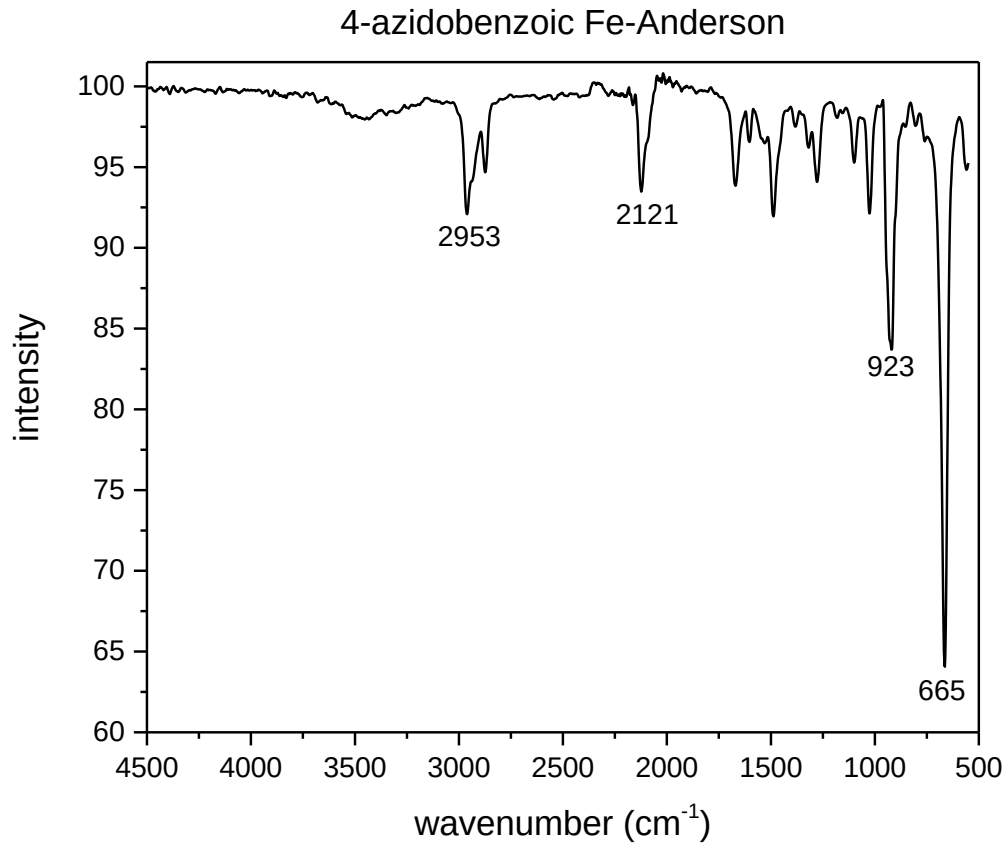

FT-IR measurement for 4-azidobenzoic acid Fe-Anderson (**23**).

Compound 24 {$CoMo_3$} Hybrid

$(CoMo_3O_{13})(C_4H_6OHNH)_3H_3$

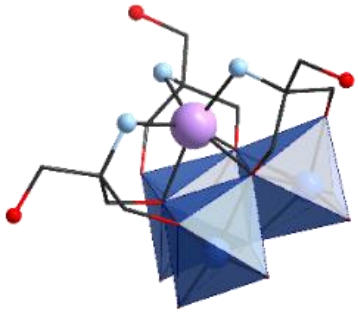

Cobalt acetate tetrahydrate (105 mg, 177.02 $gmol^{-1}$, 0.593 mmol), {Mo-8} (298 mg, 2153.8 $gmol^{-1}$, 0.138 mmol) and TRIS ligand hydrochloride (226 mg, 157.6 $gmol^{-1}$, 1.434 mmol) was dissolved in DMF (8 mL) forming a blue solution immediately and stirred at 85°C overnight. After cooling to room temperature, the solution was left to crystallise under slow Et_2O forming diffraction-quality violet block crystals after 3 days.

Yield: 451 mg, 0.153 mmol, 32%; **^{1}H NMR** (DMSO-d_6, 600 MHz): δ = 1.00, 1.16, 1.44, 1.78, 2.50, 2.69, 2.86, 4.01, 4.81, 5.07, 7.92 ppm; **^{13}C DEPTQ NMR** (DMSO-d_6, 150.9 MHz): δ = 30.7 (C), 35.7 (CH_2), 162.3 (CH_2) ppm; **Characteristic FT-IR** (solution) bands (cm^{-1}): 3347 (b, H_2O/-NH_2), 2976 (sh, -CH_2/-CH_3), 1378 (w, TBA^+), 1042 (s, TRIS), 882 (s, =O/ -O-); **Elemental analysis**: Calc. for $(CoMo_3O_{13})(C_4H_6NHOH)_3H_6(C_3H_7NO)_2$ (965.29 $g.mol^{-1}$): C 22.40, H 4.59, N 7.26; Found: C 22.15, H 4.08, N 7.10.

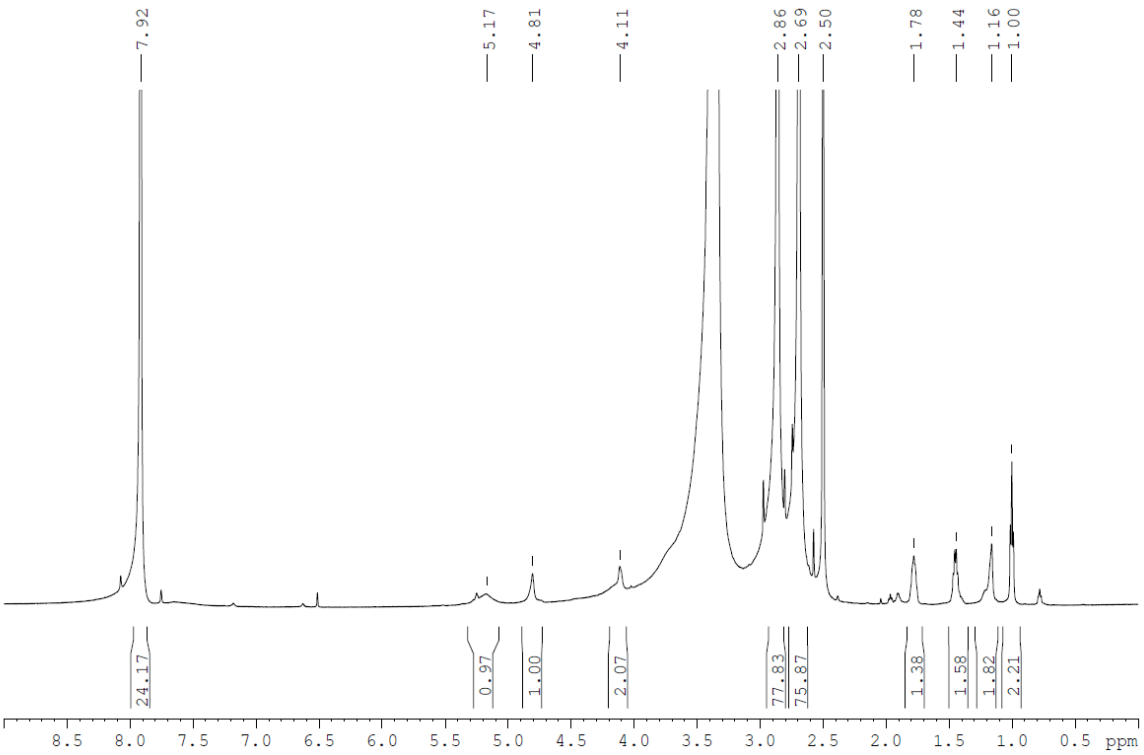

^{1}H NMR of the {$CoMo_3$} hybrid (**24**) in DMSO-d_6 at 600 MHz.

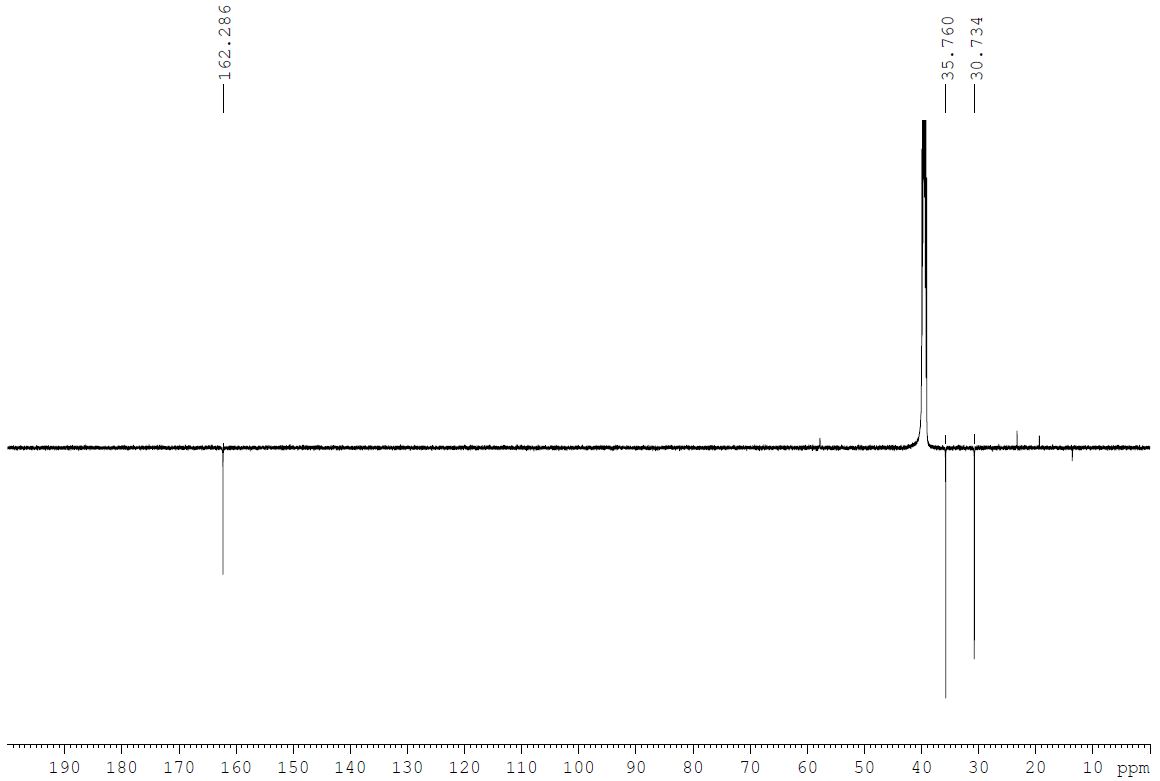

^{13}C DEPTQ NMR of the {$CoMo_3$} hybrid (**24**) in DMSO-d_6 at 150.9 MHz

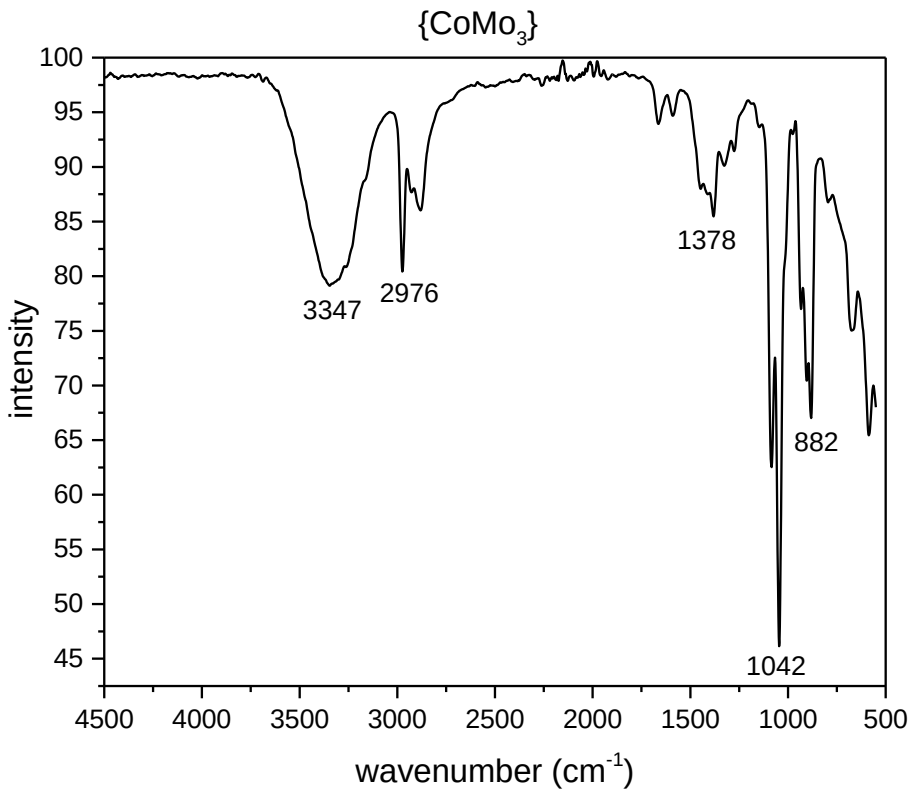

FT-IR measurement for {$CoMo_3$} hybrid (**24**).

Compound 25 Cr-Anderson POM

$CrMo_6O_{24}H_6(Na)_3$

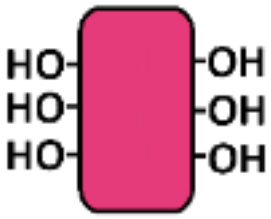

Adapted from a published procedure.[224]

$Na_2MoO_4.2H_2O$ (145 g) was dissolved in H_2O (300 mL) and pH adjusted from 9.50 to 4.50 with conc. HNO3. This was combined with a dark blue aqueous solution (40 mL) of $Cr(NO_3)_3.9H_2O$ forming a dark green solution that was left in a beaker to evaporate at room temperature, forming pink crystals after 3 days.

Yield: not recorded; **Characteristic FT-IR** (solution) bands (cm^{-1}): 3575 (w, H_2O), 3153 (b, H_2O), 1618 (w), 916 (s, =O), 665 (s, -O-).

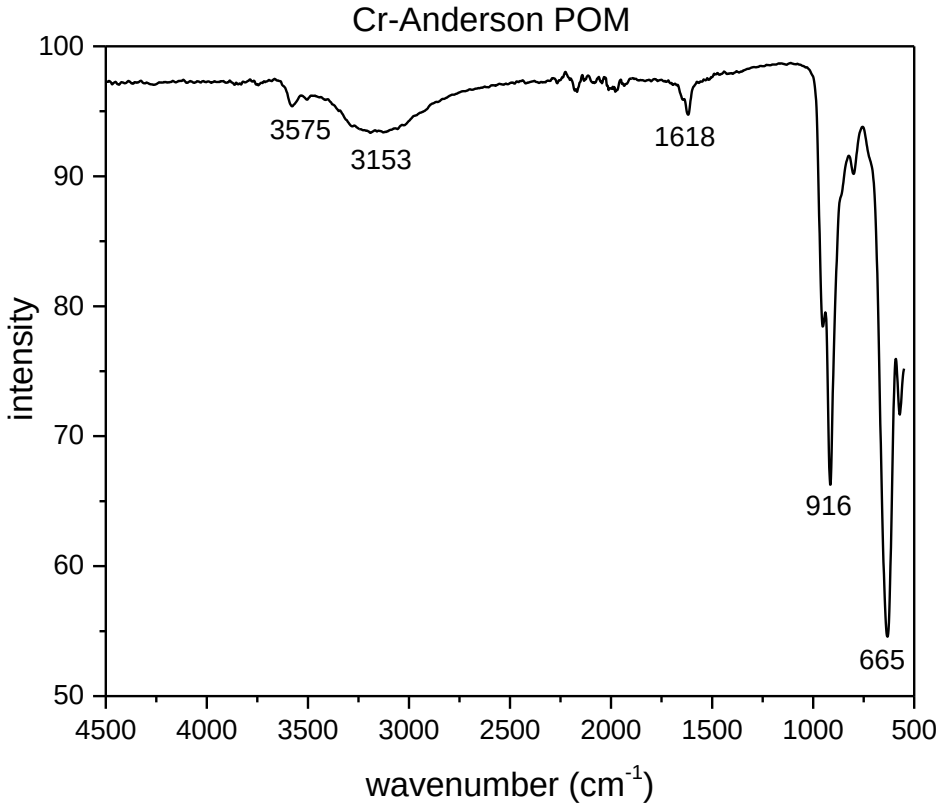

FT-IR measurement for Cr-Anderson (**25**).

Compound 26 Single-sided TRIS Cr-Anderson Hybrid

$CrMo_6O_{24}(OH)_3(C_4H_6NH_2)(N(C_4H_9)_4)_3$

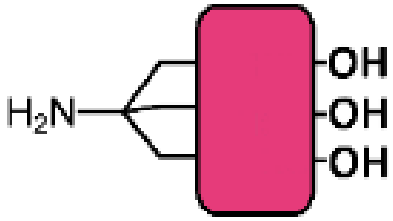

Cr-Anderson POM (**25**) (22 g, 1086.64 $gmol^{-1}$, 20.2 mmol) and TRIS ligand hydrochloride (11 g, 157.60 $gmol^{-1}$, 70.0 mmol) was dissolved in H_2O (220 mL) and separated evenly between 11 large hydrothermal bombs. Once sealed, they were heated to 140°C for 24 hours and allowed to cool slowly. The pink solutions were then recombined and stirred with TBABr (39 g, 322.37 $gmol^{-1}$, 121.2 mmol) for half an hour forming a pink precipitate which was filtered off leaving the solution to crystallise through slow evaporation at room temperature. After several days, large pale pink crystals formed which were collected and dried under vacuum.

Yield: 4.389 g, 4.039 mmol, 72.1 %, **^{1}H NMR** (DMSO-d_6, 600 MHz): δ = 0.94 (CH_3 from TBA^+), 1.31 (CH_2 from TBA^+), 1.57 (CH_2 from TBA^+), 3.17 ppm (CH_2 from TBA^+); **^{13}C DEPTQ NMR** (DMSO-d_6, 150.9 MHz): δ = 13.5 (CH_3 from TBA^+), 19.2 (CH_2 from TBA^+), 23.1 (CH_2 from TRIS), 57.5 (CH_2 from TBA^+); **Characteristic FT-IR** (solution) bands (cm^{-1}): 3216 (b, H_2O/-NH_2), 2965 (sh, -CH_2/-CH_3), 1469 (sh, TBA^+), 899 (s, =O), 665 (s, -O-); **Elemental analysis**: Calc. for $C_4H_{11}CrMo_6NO_{27}(C_{16}H_{36}N)_2H_3$ (1620.66 $g.mol^{-1}$): C 26.68, H 5.35, N 2.59; Found: C 27.82, H 5.80, N 2.67; **ESI-MS**: Peak envelope was observed with central peaks at *m/z* 2899.56 (z = -1) and 3140.86 (z = -1) assigned as $[((Cr(OH)_3Mo_6O_{18})(O_3C_4H_6NH_2))_2(N(C_4H_9)_4)_3H_2]^{1-}$ (predicted: 2899.56) and $[((Cr(OH)_3Mo_6O_{18})(O_3C_4H_6NH_2))_2(N(C_4H_9)_4)_4H]^{1-}$ (predicted: 3140.84), respectively.

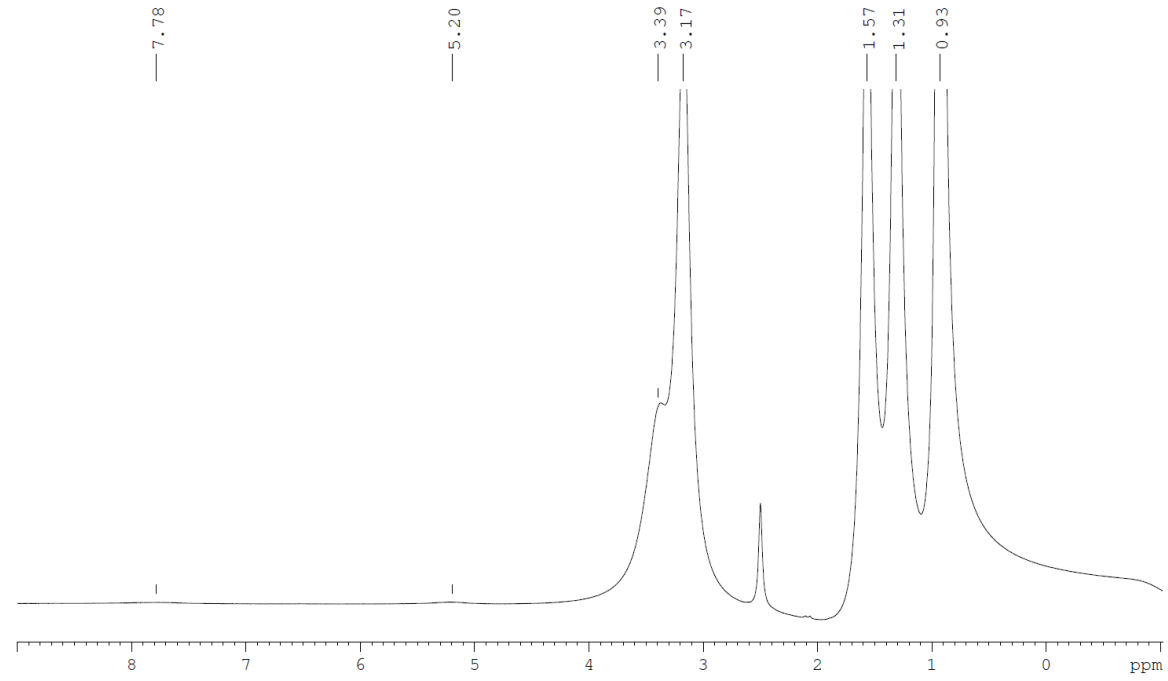

^{1}H NMR of the single-sided TRIS Cr-Anderson (**26**) in DMSO-d_6 at 600 MHz.

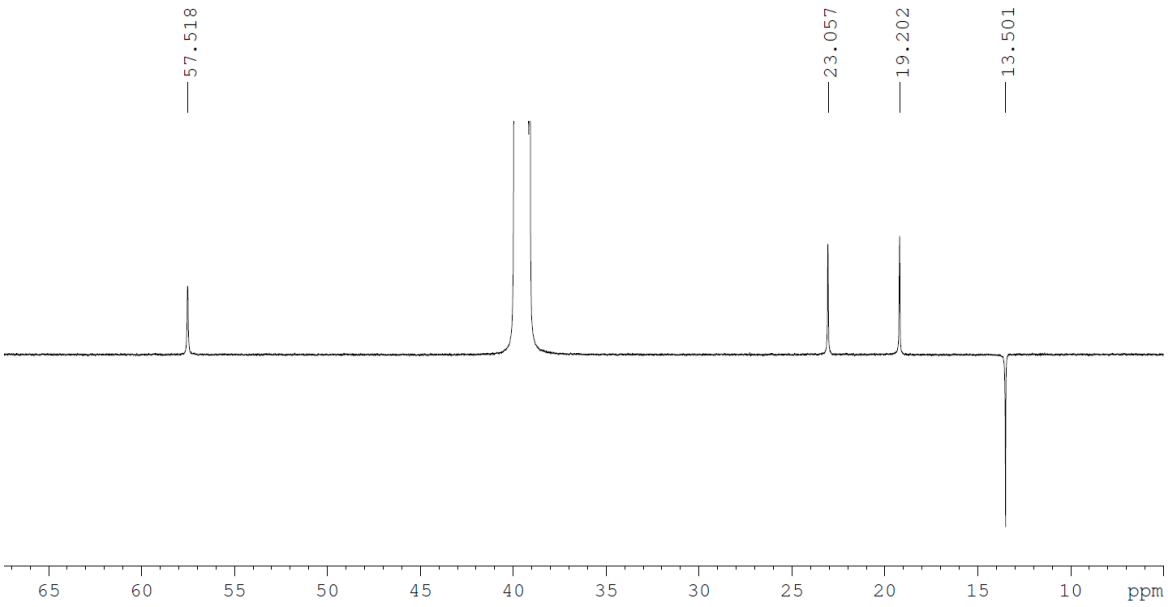

^{13}C DEPTQ NMR of the single-sided TRIS Cr-Anderson (**26**) in DMSO-d_6 at 150.9 MHz

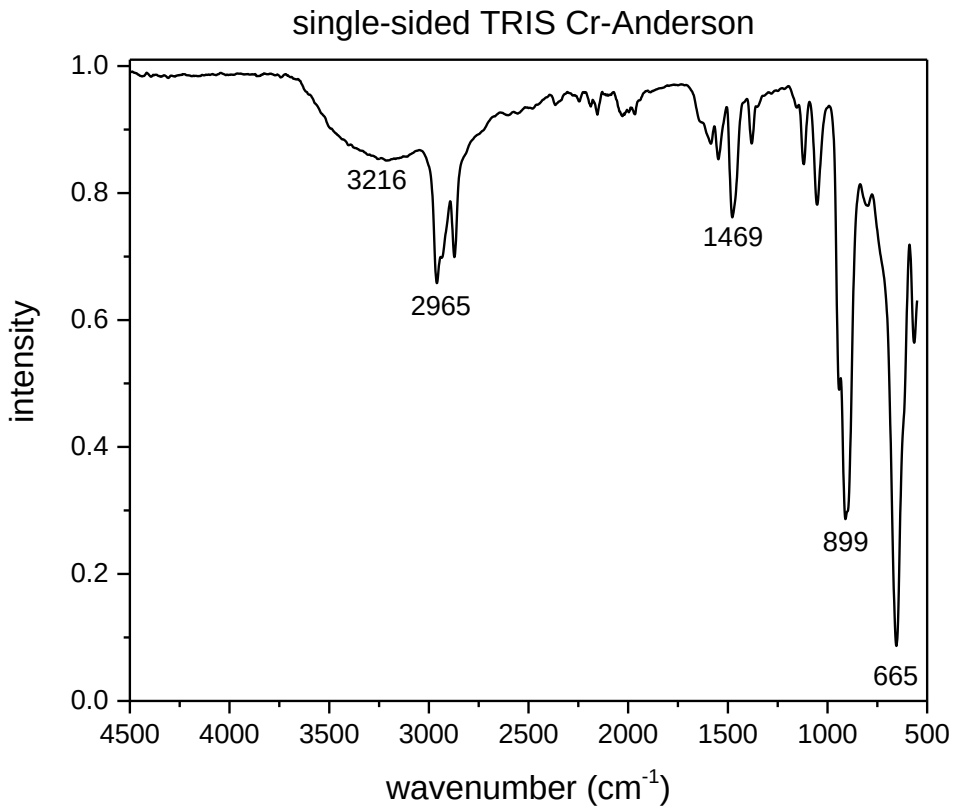

FT-IR measurement for single-sided TRIS Cr-Anderson (**26**).

Compound 27 4-azidobenzoic/tris Cr-Anderson Hybrid

$(CrMo_6O_{24})(C_4H_6NHCOC_6H_4N_3)(C_4H_6NH_2)(N(C_4H_9)_4)_3$

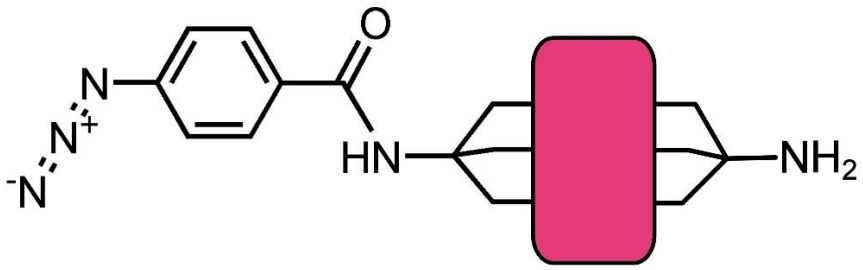

Single-sided TRIS Cr-Anderson (**26**) (2.00 g, 1.104 mmol, 1812 $gmol^{-1}$) and 4-azidobenzoic-TRIS ligand (0.441 g, 1.656 mmol, 266.25 $gmol^{-1}$) was refluxed in EtOH (30 mL) for 3 h. Et_2O (100mL) was added to the resulting dark purple solution and the precipitated solid collected via centrifugation. This solid was washed twice by redissolving in EtOH followed by Et_2O addition and the resulting solid dried under vacuum for analysis.

Yield: 2.009 g**,** 0.992 mmol, 89.9 %, **^{1}H NMR** (DMSO-d_6, 600 MHz): δ = 0.93 (CH_3 from TBA^+), 1.31 (CH_2 from TBA^+), 1.56 (CH_2 from TBA^+), 3.17 ppm (CH_2 from TBA^+), 7.19 (CH), 7.85 (CH); **^{13}C DEPTQ NMR** (DMSO-d_6, 150.9 MHz): δ = 13.5 (CH_3 from TBA^+), 19.2 (CH_2 from TBA^+), 23.1 (CH_2 from TRIS), 57.5 (CH_2 from TBA^+) 118.7 (CH), 129.3 (C), 132 (CH), 142 (C), 166.3 ppm (CO); **Characteristic FT-IR** (solution) bands (cm^{-1}): 3193 (b, H_2O/-NH_2), 2959 (sh, -CH_2/-CH_3), 2120 (w, -N_3) 1459 (sh, TBA^+), 893 (s, =O), 654 (s, -O-); **Elemental analysis**: Calc. for $C_{15}H_{19}CrMo_6N_5O_{25}(C_{16}H_{36}N)_2H_3$ (1784.87 $g.mol^{-1}$): C 31.63, H 5.31, N 5.49; Found: C 28.41, H 5.57, N 3.27.

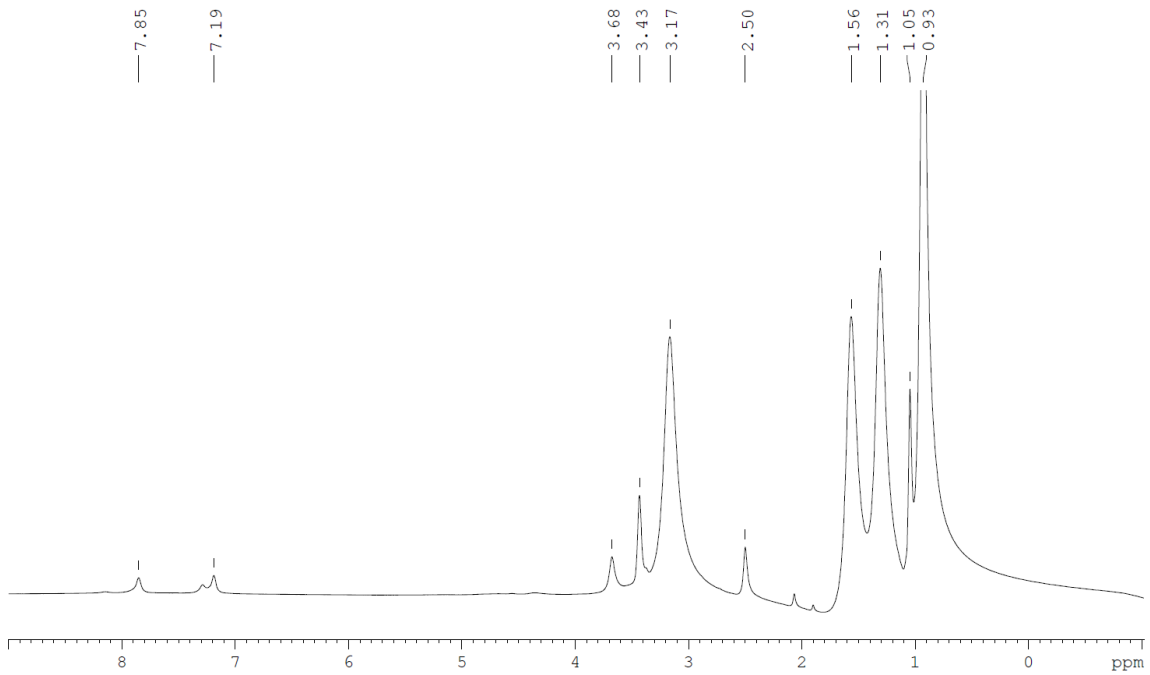

^{1}H NMR of the 4-azidobenzoic/TRIS Cr-Anderson (**27**) in DMSO-d_6 at 600 MHz.

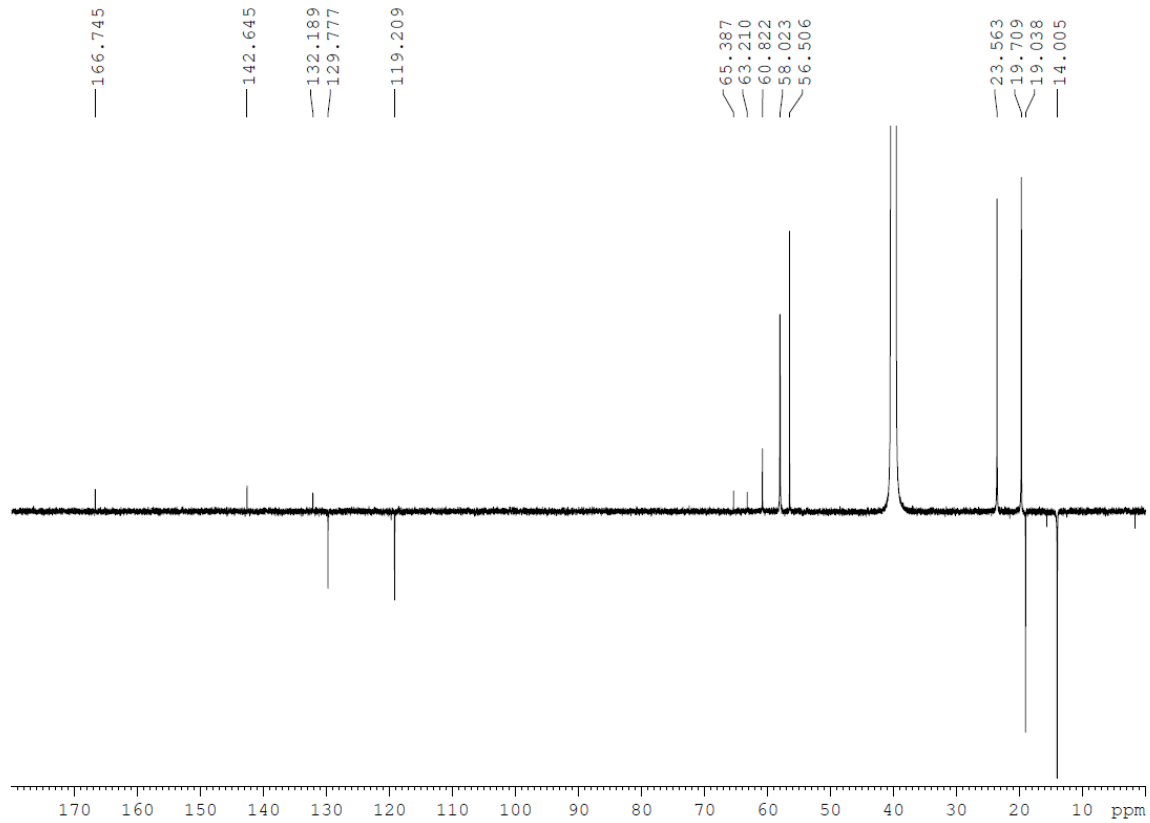

^{13}C DEPTQ NMR of the 4-azidobenzoic/TRIS Cr-Anderson (**27**) in DMSO-d_6 at 150.9 MHz

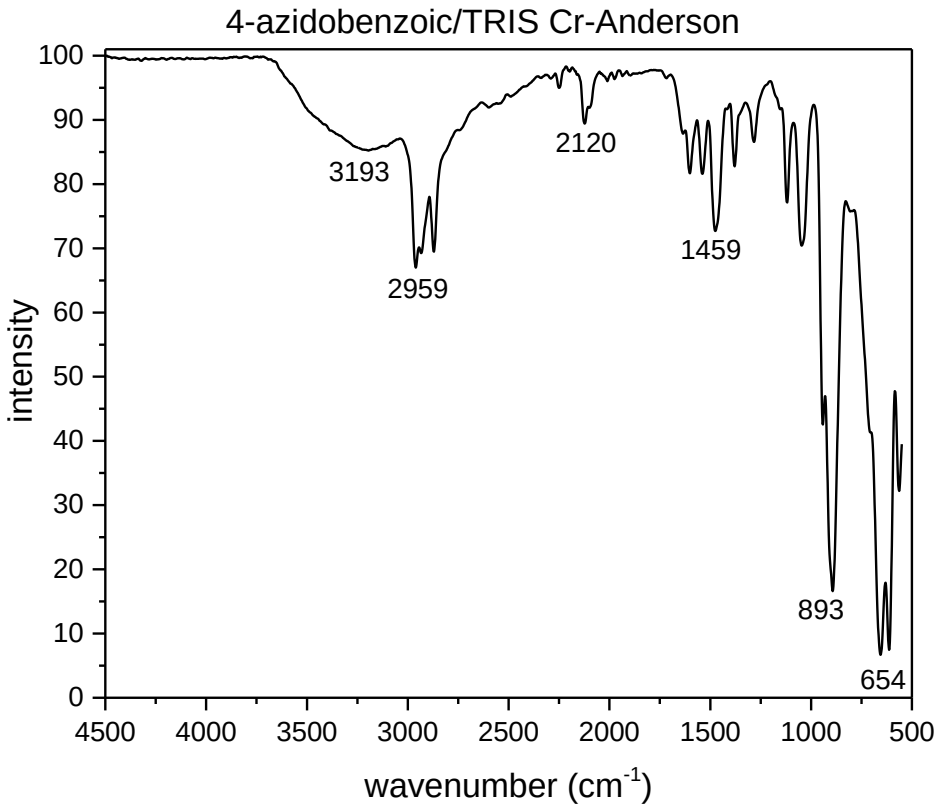

FT-IR measurement for 4-azidobenzoic/TRIS Cr-Anderson (**27**).

Compound 28 Mn/Fe/Mn-Anderson Trimer (TRIS)

$(MnMo_6O_{24})_2(C_4H_6NHCOC_6H_4N_3)_2(C_4H_6NHCOC_5H_7)_2(FeMo_6O_{24})(C_4H_6NH_2)_2(N(C_4H_9)_4)_9$

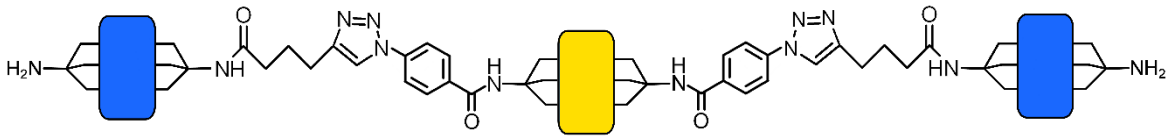

Symmetric 4-azidobenzoic Fe-Anderson (**23**) (1.5 g, 0.690 mmol, 2173.28 $gmol^{-1}$), 5-hexynoic/TRIS Mn-Anderson (**22**) (3.00 g, 0.278 mmol, 1946.41 $gmol^{-1}$) and CuI (53 mg, 0.278 mmol, 190.45 $gmol^{-1}$) were dissolved in DMF (10 mL) in an oven-dried two-necked 100mL round-bottomed flask and left under a nitrogen atmosphere. Dry DIEA (1.5 mL, 8.611 mmol) was then added and the mixture stirred at 40°C for 16 h. The product was then precipitated from the DMF with diethyl ether, redissolved in MeCN and loaded onto silica. The product was then separated from the remaining starting material using a Reveleris flash chromatography system with a C-18 column with MeCN and a 10 mM aqueous solution of TBABr as eluents. Fractions were combined, MeCN was removed and the precipitate was collected by centrifugation. The residue was then recrystallised from MeCN with diethyl ether diffusion.

Yield: 700 mg**,** 0.114 mmol, 16.5 %, **^{13}C DEPTQ NMR** (DMSO-d_6, 150.9 MHz): δ = 13.5 (CH_3), 19.2 (CH_2), 23.0 (CH_2), 57.4 (CH_2), 119.0 (CH), 120.4 (CH), 129.0 (CH); **Characteristic FT-IR** (solution) bands (cm^{-1}): 3473 (b, H_2O/-NH_2), 2959 (sh, -CH_2/-CH_3), 1476 (m, TBA^+), 916 (s, =O), 665 (s, -O-); **Elemental analysis**: Calc. for $C_{50}H_{66}FeMn_2Mo_{18}N_{12}O_{76}(C_{16}H_{36}N)_8H_2$ (5885.31 $g.mol^{-1}$): C 36.33, H 6.10, N 4.76; Found: C 35.86, H 6.13, N 4.75; **ESI-MS**: Peak envelope was observed with central peaks at *m/z* 2820.60 (z = -2) assigned as $[(MnMo_6O_{24})_2(C_4H_6NHCOC_6H_4N_3)_2(C_4H_6NHCOC_5H_7)_2(FeMo_6O_{24})(C_4H_6NH_2)_2(N(C_4H_9)_4)_7]^{2-}$ (predicted: 2820.64).

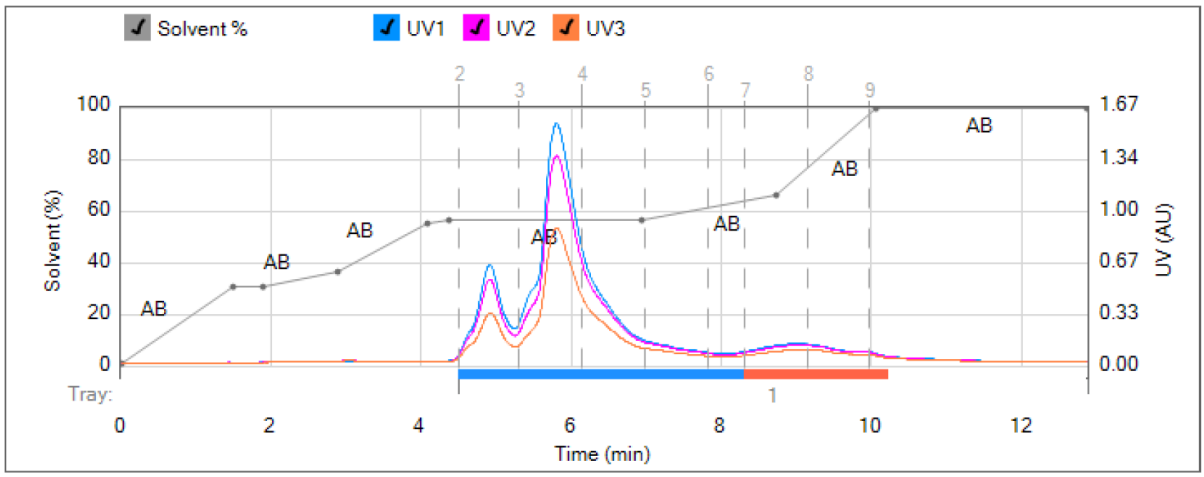

UV trace for the RP-LC separation of the Mn/Fe/Mn-Anderson trimer (TRIS) (**28**).

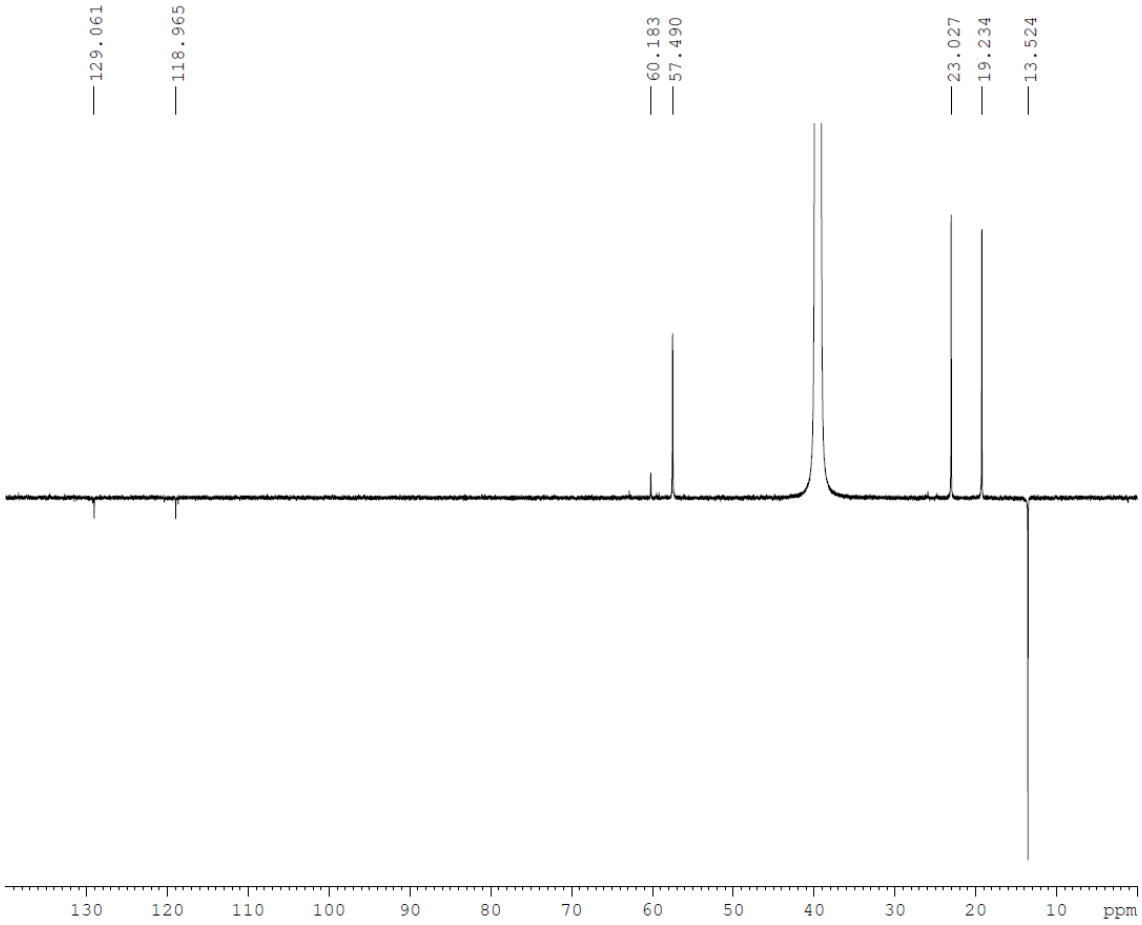

^{13}C DEPTQ NMR of the Mn/Fe/Mn-Anderson trimer (TRIS) (**28**) in DMSO-d_6 at 150.9 MHz

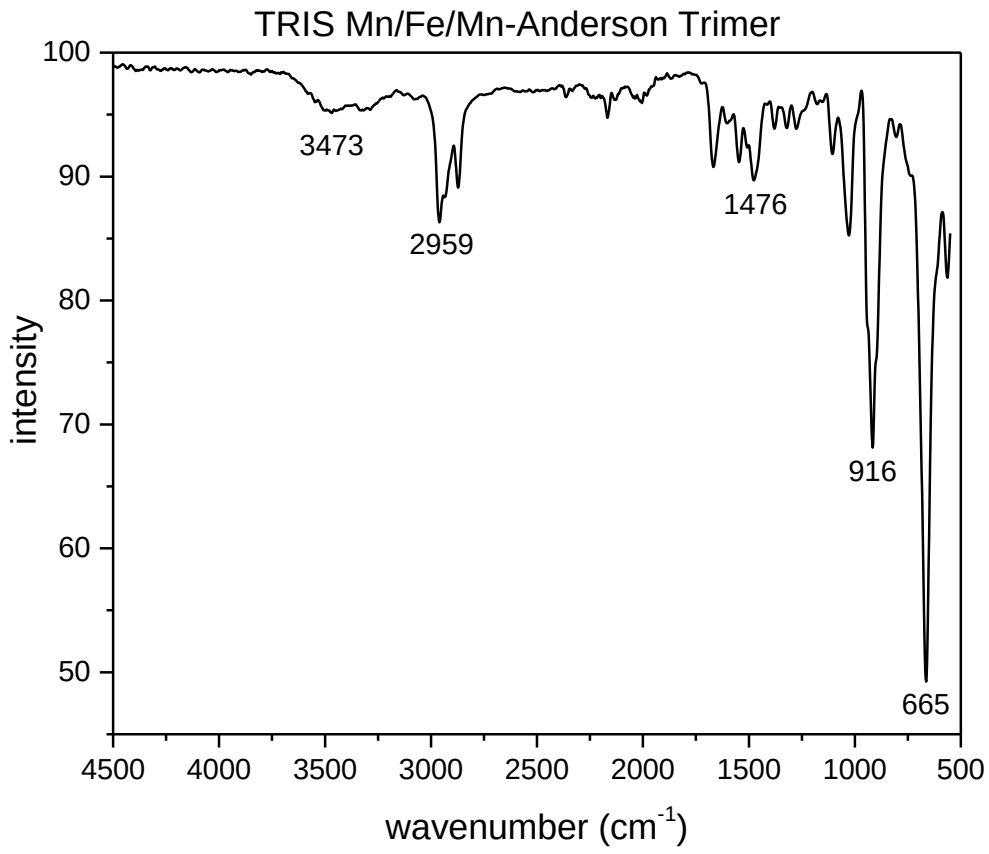

FT-IR measurement for TRIS Mn/Fe/Mn-Anderson Trimer (**28**).

Compound 29 Cr/Fe/Cr-Anderson Trimer (TRIS)

$(CrMo_6O_{24})_2(C_4H_6NHCOC_6H_4N_3)_2(C_4H_6NHCOC_5H_7)_2(FeMo_6O_{24})(C_4H_6NH_2)_2(N(C_4H_9)_4)_9$

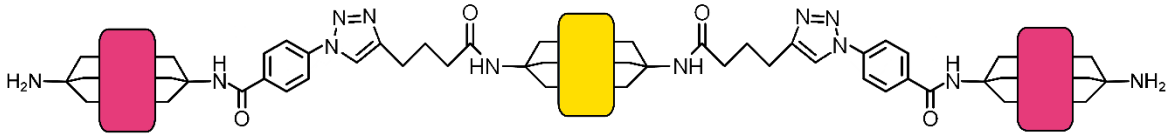

Symmetric 5-hexynoic Fe-Anderson (**21**) (800 mg, 2071.26 $gmol^{-1}$, 0.386 mmol), 4-azidobenzoic/TRIS Cr-Anderson (**27**) (1.866 g, 2024.31 $gmol^{-1}$, 0.922 mmol) and CuI (47 mg, 190.45 $gmol^{-1}$, 0.246 mmol) were dissolved in dry DMF (10 mL) in an oven-dried two-necked 100mL round-bottomed flask and left under a nitrogen atmosphere. Dry DIEA (1 mL) was then added and the mixture stirred at 40°C for 16 h. Solid (2.445 g) precipitated from the DMF with diethyl ether, redissolved in MeCN and loaded onto silica. The product was then separated from the remaining starting material using a Reveleris flash chromatography system with a C-18 column with MeCN and a 10 mM aqueous solution of TBABr as eluents. Fractions were collected: 1, 2.1, 2.2, 3.1, 3.2, 3.3, 4. IMS-MS run immediately. After 2-week Et_2O diffusion crystallization attempt, dried and ^1H NMR run.

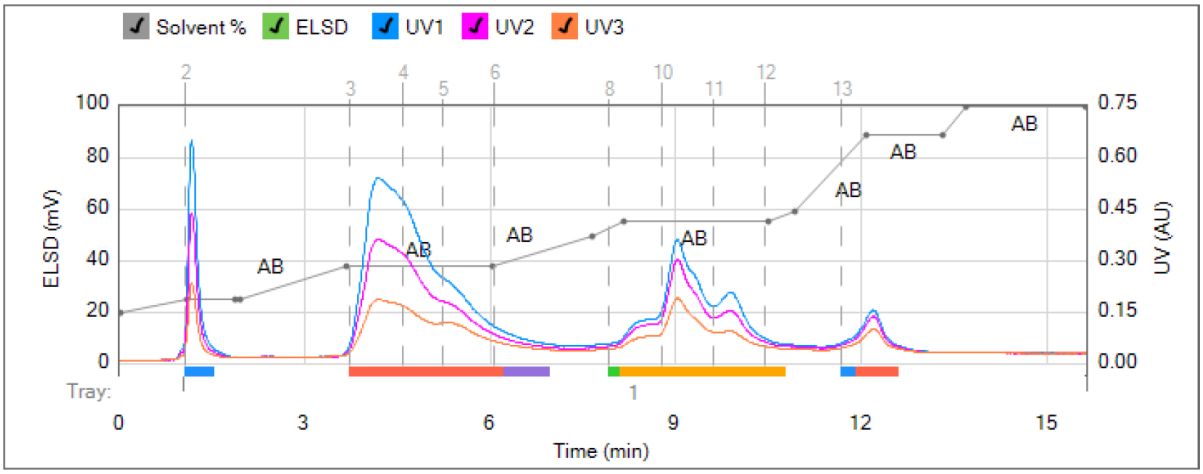

UV trace for the RP-LC separation of the Cr/Fe/Cr-Anderson trimer (TRIS) (**29**).

Compound 30 Cr/Mn/Cr-Anderson Trimer (TRIS)

$(CrMo_6O_{24})_2(C_4H_6NHCOC_6H_4N_3)_2(C_4H_6NHCOC_5H_7)_2(MnMo_6O_{24})(C_4H_6NH_2)_2(N(C_4H_9)_4)_9$

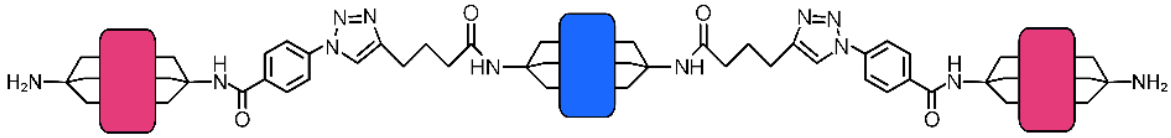

Symmetric 5-hexynoic Mn-Anderson (453 mg, 2070.354 $gmol^{-1}$, 0.219 mmol), 4-azidobenzoic/TRIS Cr-Anderson (**27**) (933 mg, 2024.31 $gmol^{-1}$, 0.461 mmol) and CuI (24 mg, 190.45 $gmol^{-1}$, 0.126 mmol) were dissolved in dry DMF (3 mL) in an oven-dried two-necked 50mL round-bottomed flask and left under a nitrogen atmosphere. Dry DIEA (0.50 mL) was then added and the mixture stirred at 40°C for 16 h. Solid precipitated from the DMF with diethyl ether, washed several times and left to dry.

Compound 31 Fe/Mn/Fe-Anderson Trimer (TRIS)

$(FeMo_6O_{24})_2(C_4H_6NHCOC_6H_4N_3)_2(C_4H_6NHCOC_5H_7)_2(MnMo_6O_{24})(C_4H_6NH_2)_2(N(C_4H_9)_4)_9$

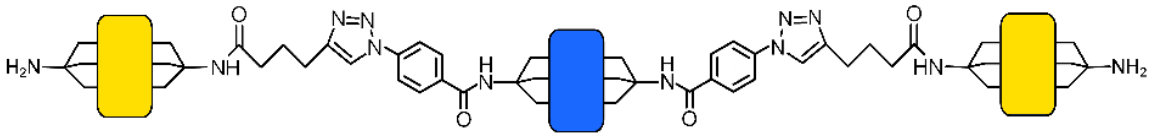

Symmetric 4-azidobenzoic Mn-Anderson (**5**) (220 mg, 2172.368 $gmol^{-1}$, 0.1012 mmol), 5-hexynoic/TRIS Fe-Anderson (**22**) (400 mg, 1977.15 $gmol^{-1}$, 0.2023 mmol) and CuI (10 mg, 190.45 $gmol^{-1}$, 0.506 mmol) were dissolved in dry DMF (6 mL) in an oven-dried two-necked 50mL round-bottomed flask and left under a nitrogen atmosphere. Dry DIEA (0.30 mL) was then added and the mixture stirred at 40°C for 16 h. Et_2O was added to the reaction mixture to precipitate out the solid which was washed several times before drying under vacuum.

Compound 32 Mn/Fe/Mn-Anderson Trimer (5-hexynoic)

$(MnMo_6O_{24})_2(C_4H_6NHCOC_6H_4N_3)_2(C_4H_6NHCOC_5H_7)_4(FeMo_6O_{24})(N(C_4H_9)_4)_9$

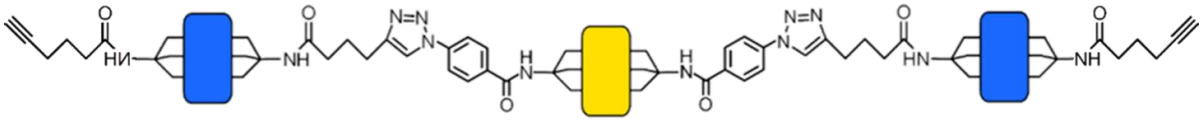

5-hexynoic acid (45 µL, 112.13 $gmol^{-1}$, 0.408 mmol), EEDQ (101 mg, 247.29 $gmol^{-1}$, 0.408 mmol) and Mn/Fe/Mn-Anderson trimer (TRIS) (**28**) (500 g, 6125.761 $gmol^{-1}$, 0.0816 mmol) were combined in MeCN and this was stirred under reflux overnight. Additional 5-hexynoic acid (50 µL) and EEDQ (202 mg) was added and left for another 18 hours. The solution was then allowed to cool to room temperature and precipitated from the MeCN with diethyl ether. The solid was collected, washed and dried under vacuum.

Yield: 462 mg, 0.0732 mmol, 89.7 %, **^{1}H NMR** (DMSO-d_6, 600 MHz): δ = 0.93 (t, 108H, CH_3 from TBA^+, J = 6.95 Hz), 1.31 (CH_2 from TBA^+), 1.56 (CH_2 from TBA^+), 1.90 (CH_2), 2.75 (CH_2), 3.16 (CH_2 from TBA^+), 7.42 (NH), 7.99 (s, CH), 8.74 (Triazole-H); **^{13}C DEPTQ NMR** (DMSO-d_6, 150.9 MHz): δ = 13.5 (CH_3), 19.3 (CH_2), 23.0 (CH_2), 57.5 (CH_2), 118.9 (CH), 129.0 (CH); **Characteristic FT-IR** (solution) bands (cm^{-1}): 3296 (b, H_2O/-NH_2), 2959 (m, -CH_2/-CH_3), 1669 (m), 916 (sh, =O), 665 (s, -O-); **Elemental analysis**: Calc. for $C_{62}H_{78}FeMn_2Mo_{18}N_{12}O_{78}(C_{16}H_{36}N)_8H_2$ (6073.53 $g.mol^{-1}$): C 37.57, H 6.11, N 4.61; Found: C 37.54, H 6.20, N 4.70; **ESI-MS**: Peak envelope was observed with central peaks at *m/z* 2914.49 (z = -2) assigned as $[(MnMo_6O_{24})_2(C_4H_6NHCOC_6H_4N_3)_2(C_4H_6NHCOC_5H_7)_4(FeMo_6O_{24})(N(C_4H_9)_4)_7]^{2-}$ (predicted: 2914.68).

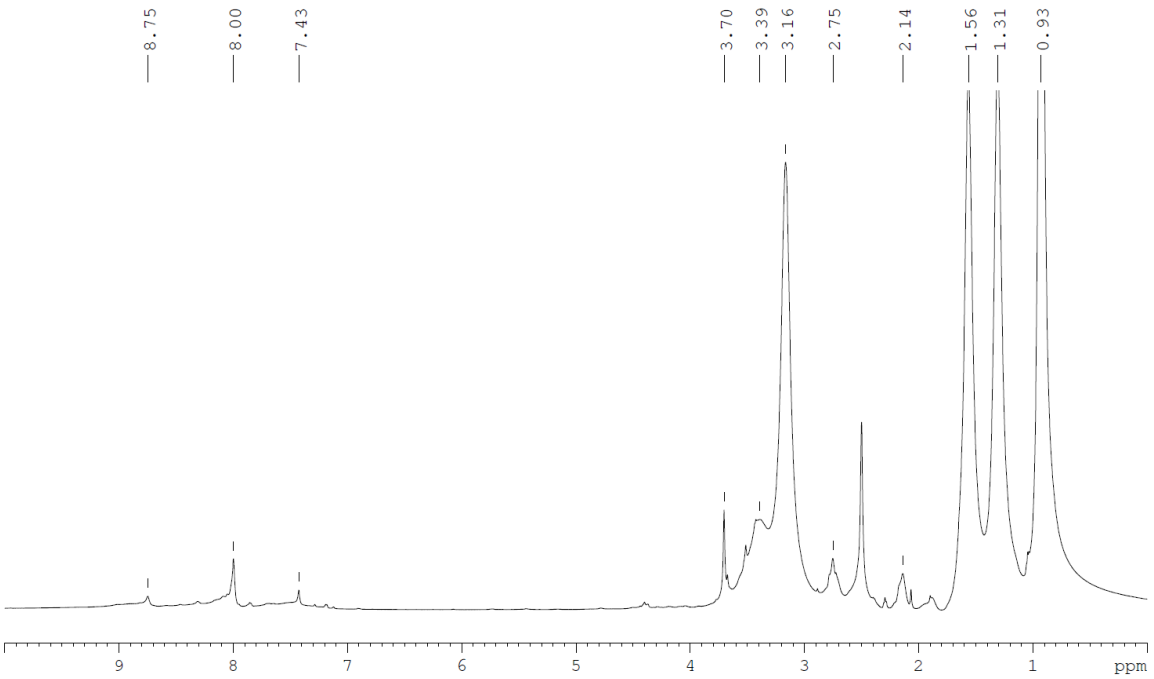

^{1}H NMR of the 5-hexynoic Mn/Fe/Mn-Anderson (**32**) in DMSO-d_6 at 600 MHz.

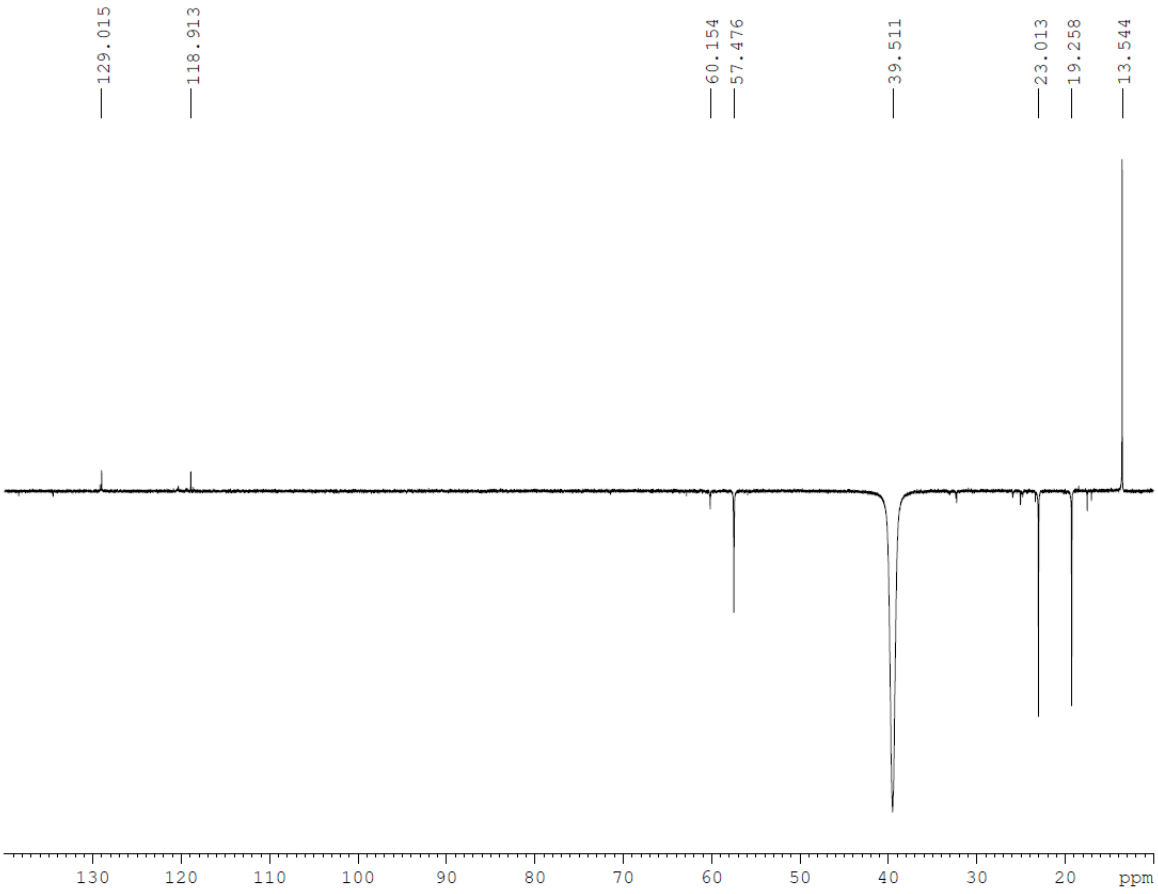

^{13}C DEPTQ NMR of the 5-hexynoic Mn/Fe/Mn-Anderson (**32**) in DMSO-d_6 at 150.9 MHz

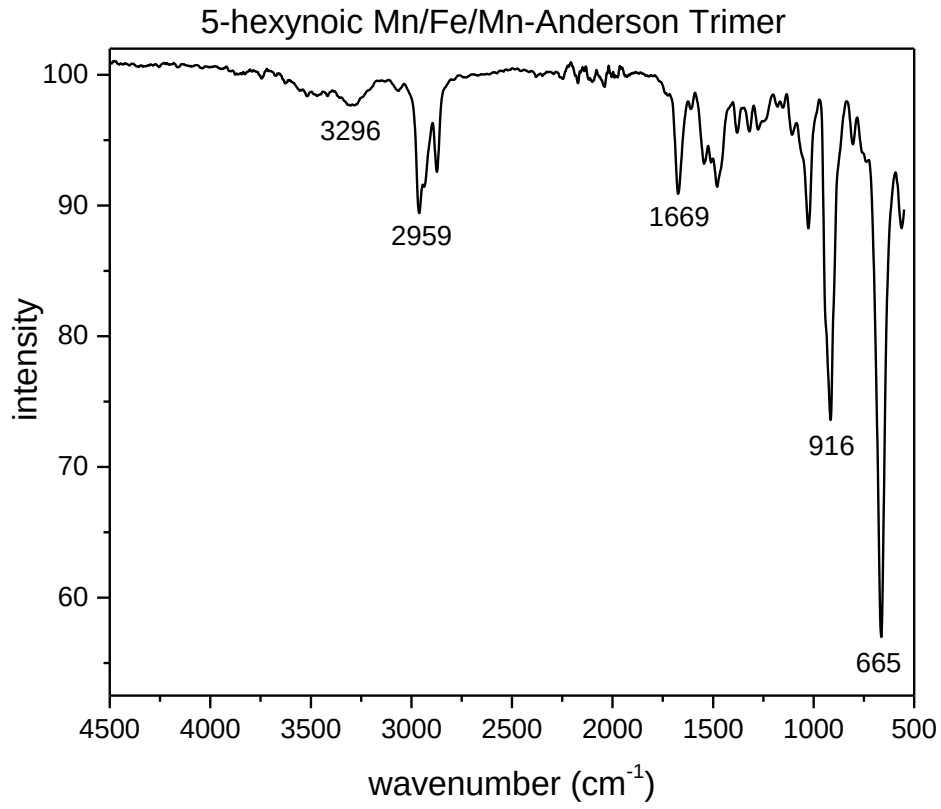

FT-IR measurement for 5-hexynoic Mn/Fe/Mn-Anderson Trimer (**32**).

Compound 33 Cr/Mn/Fe/Mn/Cr-Anderson Pentamer

$(MnMo_6O_{24})_2(C_4H_6NHCOC_6H_4N_3)_4(C_4H_6NHCOC_5H_7)_4(FeMo_6O_{24})(CrMo_6O_{24})_2(C_4H_6NH_2)_2(N(C_4H_9)_4)_{15}$

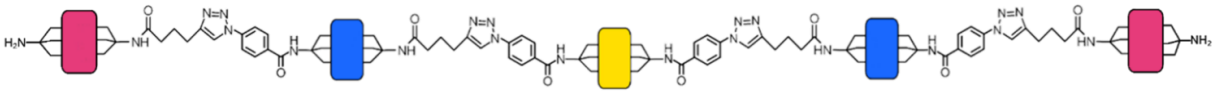

A mixture of asymmetric 4-azidobenzoic/TRIS Cr-Anderson (**26**) (273 mg, 2024.31 $gmol^{-1}$, 0.134 mmol) and Mn/Fe/Mn-Anderson trimer (5-hexynoic) (**32**) (340 g, 6313.98 $gmol^{-1}$, 0.054 mmol) and CuI (12 mg, 190.45 $gmol^{-1}$, 0.063 mmol) were dissolved in dry DMF (3 mL) in an oven-dried two-necked 50mL round-bottomed flask and left under a nitrogen atmosphere. Dry DIEA (150 µL, 129.25 $gmol^{-1}$, 0.879 mmol) was then added and the mixture stirred at 40°C for 16 h. The product was then precipitated from the DMF with diethyl ether, redissolved in MeCN and loaded onto silica. The product was then separated from the remaining starting material using a Reveleris flash chromatography system with a C-18 column with MeCN and a 10 mM aqueous solution of TBABr as eluents. The fractions were collected (1, 2.1, 2.2, 2.3, 3, 4.1, 4.2, 5), the MeCN removed under rotavap and the solid filtered off. IMS-MS run. These were redissolved in MeCN and left for two weeks in an attempt to crystallise under Et_2O diffusion. The solids formed from the fractions collected and dried under vacuum and then samples used for ^1H NMR.

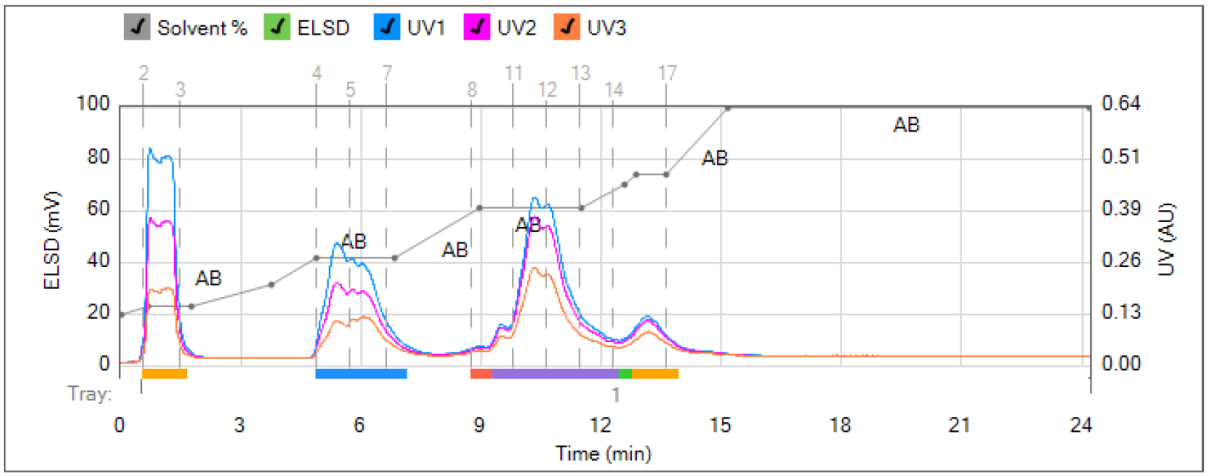

UV trace for the RP-LC separation of the Cr/Mn/Fe/Mn/Cr-Anderson pentamer (TRIS) (**33**).

6 Crystallographic Section

6.1 Guanosine Strandberg (Compound 1)

$Na_2[C_{20}H_{26}Mo_5N_{10}P_2O_{31}](H_2O)_7$

Identification code	naj256	
Empirical formula	$C_{20}\ H_{40}\ Mo_5\ N_{10}\ Na_2\ O_{38}\ P_2$	
Formula weight	1616.24	
Temperature	150(2) K	
Wavelength	1.54178 Å	
Crystal system	Hexagonal	
Space group	P 65 2 2	
Unit cell dimensions	a = 16.0517(3) Å	α= 90°.
	b = 16.0517(3) Å	β= 90°.
	c = 42.8082(7) Å	γ = 120°.
Volume	9552.1(4) $Å^3$	
Z	6	
Density (calculated)	1.686 Mg/m^3	
Absorption coefficient	9.306 mm^{-1}	
F(000)	4776	
Crystal size	0.352 x 0.182 x 0.156 mm^3	
Theta range for data collection	3.343 to 61.499°.	
Index ranges	-18<=h<=17, -18<=k<=18, -48<=l<=48	
Reflections collected	75586	
Independent reflections	4943 [R(int) = 0.0394]	
Completeness to theta = 61.499°	99.9 %	
Absorption correction	Analytical	
Max. and min. transmission	0.361 and 0.114	
Refinement method	Full-matrix least-squares on F^2	
Data / restraints / parameters	4943 / 1 / 357	
Goodness-of-fit on F^2	1.045	
Final R indices [I>2sigma(I)]	R1 = 0.0887, wR2 = 0.2512	
R indices (all data)	R1 = 0.0946, wR2 = 0.2603	
Absolute structure parameter	-0.004(8)	
Extinction coefficient	n/a	
Largest diff. peak and hole	0.69 and -0.93 $e.Å^{-3}$	

6.2 FMOC/TRIS Mn-Anderson (Compound 3)

Empirical formula	$C_{80}H_{155}MnMo_6N_8O_{29}$	
Formula weight	2323.70	
Temperature	150(2) K	
Wavelength	0.71073 Å	
Crystal system, space group	Orthorhombic, *Pnma*	
Unit cell dimensions	*a* = 28.257(2) Å	*α* = 90 º
	b = 21.8128(16) Å	*β* = 90 º
	c = 16.5796(14) Å	*γ* = 90 º
Volume	10219.1(14) $Å^3$	
Z, Calculated density	4, 1.510 Mg/m^3	
Absorption coefficient	0.906 mm^{-1}	
F(000)	4800	
Crystal size	0.12 x 0.06 x 0.03 mm	
Theta range for data collection	1.89 to 26.00 º	
Limiting indices	-34<=h<=30, -26<=k<=23, -20<=l<=19	
Reflections collected / unique	77882 / 10308 [R(int) = 0.0862]	
Completeness to theta = 26.00	99.9 %	
Absorption correction	Empirical	
Max. and min. transmission	0.9733 and 0.8991	
Refinement method	Full-matrix least-squares on F2	
Data / restraints / parameters	10308 / 39 / 440	
Goodness-of-fit on F2	1.068	
Final R indices [I>2sigma(I)]	R1 = 0.0823, wR2 = 0.2554	
R indices (all data)	R1 = 0.1193, wR2 = 0.2777	
Largest diff. peak and hole	1.18 and -0.97 $e.Å^{-3}$	

6.3 TRIS Lindqvist (Compound 17)

$(C_{16}H_{36}N)_2[C_8H_{16}N_2O_{19}V_6]$

Published Structure.[392]

Identification code	platon_sq	
Empirical formula	C_{40} H_{88} N_4 O_{19} V_6	
Formula weight	1234.78	
Temperature	150(2) K	
Wavelength	0.71073 Å	
Crystal system	Orthorhombic	
Space group	I b c a	
Unit cell dimensions	a = 23.073(5) Å	α = 90°.
	b = 20.360(3) Å	β = 90°.
	c = 24.666(4) Å	γ = 90°.
Volume	11587(3) $Å^3$	
Z	8	
Density (calculated)	1.416 Mg/m^3	
Absorption coefficient	0.995 mm^{-1}	
F(000)	5168	
Crystal size	0.100 x 0.100 x 0.100 mm^3	
Theta range for data collection	1.765 to 27.215°.	
Index ranges	-29<=h<=29, -26<=k<=26, -31<=l<=31	
Reflections collected	91279	
Independent reflections	6467 [R(int) = 0.0452]	
Completeness to theta = 25.242°	99.9 %	
Refinement method	Full-matrix least-squares on F^2	
Data / restraints / parameters	6467 / 0 / 318	
Goodness-of-fit on F^2	1.069	
Final R indices [I>2sigma(I)]	R1 = 0.0341, wR2 = 0.0901	
R indices (all data)	R1 = 0.0455, wR2 = 0.0986	
Extinction coefficient	n/a	
Largest diff. peak and hole	0.612 and -0.510 $e.Å^{-3}$	

6.4 {$CoMo_3$} Hybrid (Compound 17)

$[Mo_3CoO_7(C_4H_9NO_3)_3](C_3H_7NO)_{5.5}$

Identification code	naj425-3	
Empirical formula	$C_{28.50}\ H_{65.50}\ Co\ Mo_3\ N_{8.50}\ O_{21.50}$	
Formula weight	1218.14	
Temperature	150(2) K	
Wavelength	0.71073 Å	
Crystal system	Monoclinic	
Space group	P 21/c	
Unit cell dimensions	a = 13.9098(19) Å	α = 90°.
	b = 14.951(2) Å	β = 94.717(5)°.
	c = 21.871(3) Å	γ = 90°.
Volume	4533.1(11) $Å^3$	
Z	4	
Density (calculated)	1.785 Mg/m^3	
Absorption coefficient	1.257 mm^{-1}	
F(000)	2484	
Crystal size	0.100 x 0.100 x 0.100 mm^3	
Theta range for data collection	2.003 to 25.999°.	
Index ranges	-15<=h<=17, -18<=k<=9, -26<=l<=26	
Reflections collected	23185	
Independent reflections	8729 [R(int) = 0.0270]	
Completeness to theta = 25.242°	98.1 %	
Refinement method	Full-matrix least-squares on F^2	
Data / restraints / parameters	8729 / 0 / 596	
Goodness-of-fit on F^2	1.043	
Final R indices [I>2sigma(I)]	R1 = 0.0238, wR2 = 0.0608	
R indices (all data)	R1 = 0.0291, wR2 = 0.0636	
Extinction coefficient	n/a	
Largest diff. peak and hole	0.985 and -0.478 $e.Å^{-3}$	

6.5 Single-sided Cr-Anderson (Compound 26)

$(C_{16}H_{36}N)_4Br[C_4H_{11}NCrMo_6O_{24}]$

Published Structure.[281]

Identification code	naj401	
Empirical formula	C_{68} H_{155} Br Cr Mo_6 N_5 O_{24}	
Formula weight	2134.51	
Temperature	150(2) K	
Wavelength	0.71073 Å	
Crystal system	Monoclinic	
Space group	P 21	
Unit cell dimensions	a = 16.2964(11) Å	α = 90°.
	b = 15.4110(11) Å	β = 92.660(3)°.
	c = 18.1624(11) Å	γ = 90°.
Volume	4556.5(5) $Å^3$	
Z	2	
Density (calculated)	1.556 Mg/m^3	
Absorption coefficient	1.419 mm^{-1}	
F(000)	2202	
Crystal size	0.100 x 0.100 x 0.100 mm^3	
Theta range for data collection	2.107 to 25.999°.	
Index ranges	-20<=h<=20, -19<=k<=18, -21<=l<=22	
Reflections collected	67688	
Independent reflections	17654 [R(int) = 0.0492]	
Completeness to theta = 25.242°	99.9 %	
Refinement method	Full-matrix least-squares on F^2	
Data / restraints / parameters	17654 / 13 / 907	
Goodness-of-fit on F^2	1.056	
Final R indices [I>2sigma(I)]	R1 = 0.0380, wR2 = 0.0954	
R indices (all data)	R1 = 0.0518, wR2 = 0.1013	
Absolute structure parameter	0.063(5)	
Extinction coefficient	n/a	
Largest diff. peak and hole	1.521 and -0.497 e.$Å^{-3}$	

$(C_{16}H_{36}N)_3Br[C_4H_{12}NCrMoO_{24}](H_2O)_8$

Identification code	naj472a2	
Empirical formula	C_{52} H_{136} Br Cr Mo_6 N_4 O_{32}	
Formula weight	2037.19	
Temperature	150(2) K	
Wavelength	0.71073 Å	
Crystal system	Monoclinic	
Space group	C 2/c	
Unit cell dimensions	a = 27.002(3) Å	α = 90°.
	b = 15.4434(18) Å	β = 90.477(3)°.
	c = 39.641(5) Å	γ = 90°.
Volume	16530(3) $Å^3$	
Z	8	
Density (calculated)	1.637 Mg/m^3	
Absorption coefficient	1.567 mm^{-1}	
F(000)	8344	
Crystal size	0.115 x 0.079 x 0.022 mm^3	
Theta range for data collection	1.508 to 26.000°.	
Index ranges	-33<=h<=33, -19<=k<=19, -48<=l<=48	
Reflections collected	125417	
Independent reflections	16237 [R(int) = 0.0763]	
Completeness to theta = 25.242°	100.0 %	
Refinement method	Full-matrix least-squares on F^2	
Data / restraints / parameters	16237 / 0 / 865	
Goodness-of-fit on F^2	1.057	
Final R indices [I>2sigma(I)]	R1 = 0.0615, wR2 = 0.1317	
R indices (all data)	R1 = 0.0931, wR2 = 0.1516	
Extinction coefficient	n/a	
Largest diff. peak and hole	2.198 and -1.507 $e.Å^{-3}$	

$C_{16}H_{36}N)_2[C_4H_{12}NCrMo_6O_{24}](H_2O)_6$

Identification code	naj511-2	
Empirical formula	C_{36} H_{96} Cr Mo_6 N_3 O_{30}	
Formula weight	1678.79	
Temperature	150(2) K	
Wavelength	0.71073 Å	
Crystal system	Monoclinic	
Space group	P 21/c	
Unit cell dimensions	a = 9.1942(18) Å	α = 90°.
	b = 15.189(3) Å	β = 93.097(11)°.
	c = 43.368(9) Å	γ = 90°.
Volume	6047(2) $Å^3$	
Z	4	
Density (calculated)	1.844 Mg/m^3	
Absorption coefficient	1.461 mm^{-1}	
F(000)	3396	
Crystal size	0.100 x 0.100 x 0.100 mm^3	
Theta range for data collection	1.421 to 25.999°.	
Index ranges	-11<=h<=11, -18<=k<=17, -53<=l<=53	
Reflections collected	67924	
Independent reflections	11558 [R(int) = 0.0937]	
Completeness to theta = 25.242°	97.0 %	
Refinement method	Full-matrix least-squares on F^2	
Data / restraints / parameters	11558 / 12 / 689	
Goodness-of-fit on F^2	1.098	
Final R indices [I>2sigma(I)]	R1 = 0.1103, wR2 = 0.2572	
R indices (all data)	R1 = 0.1530, wR2 = 0.2807	
Extinction coefficient	n/a	
Largest diff. peak and hole	1.527 and -1.882 e.$Å^{-3}$	

$(C_{16}H_{36}N)_6Br_4[C_4H_{12}NCrMo_6O_{24}](H_2O)_3$

Identification code	naj4053-3	
Empirical formula	C_{100} H_{234} Br_4 Cr Mo_6 N_7 O_{27}	
Formula weight	2914.21	
Temperature	150(2) K	
Wavelength	0.71073 Å	
Crystal system	Orthorhombic	
Space group	P n m a	
Unit cell dimensions	a = 31.391(3) Å	α = 90°.
	b = 21.609(2) Å	β = 90°.
	c = 17.7457(19) Å	γ = 90°.
Volume	12038(2) $Å^3$	
Z	4	
Density (calculated)	1.608 Mg/m^3	
Absorption coefficient	2.090 mm^{-1}	
F(000)	6060	
Crystal size	0.100 x 0.100 x 0.100 mm^3	
Theta range for data collection	1.732 to 25.999°.	
Index ranges	-38<=h<=38, -25<=k<=26, -21<=l<=21	
Reflections collected	174828	
Independent reflections	12161 [R(int) = 0.0600]	
Completeness to theta = 25.242°	100.0 %	
Refinement method	Full-matrix least-squares on F^2	
Data / restraints / parameters	12161 / 56 / 576	
Goodness-of-fit on F^2	1.095	
Final R indices [I>2sigma(I)]	R1 = 0.0666, wR2 = 0.1808	
R indices (all data)	R1 = 0.0915, wR2 = 0.2056	
Extinction coefficient	n/a	
Largest diff. peak and hole	1.756 and -1.131 $e.Å^{-3}$	

References

1 M. T. Pope and A. Müller, in *Polyoxometalate Chemistry From Topology via Self-Assembly to Applications*, Kluwer Academic Publishers, Dordrecht, 2006, pp. 1–6.
2 M. Achim, E. Beckmann, H. Bögge, M. Schmidtmann and A. Dress, *Angew. Chem., Int. Ed.*, 2002, **41**, 1162–1167.
3 H. Wang, S. Hamanaka, Y. Nishimoto, S. Irle, T. Yokoyama, H. Yoshikawa and K. Awaga, *J. Am. Chem. Soc.*, 2012, **134**, 4918–4924.
4 M. Sadakane and E. Steckhan, *Chem. Rev.*, 1998, **2665**, 219–237.
5 I. V. Kozhevnikov, *Chem. Rev.*, 1998, **98**, 171–198.
6 C. L. Hill, *J. Mol. Catal. A Chem.*, 2007, **262**, 2–6.
7 E. Coronado and C. J. Go, *Chem. Rev.*, 1998, **98**, 273–296.
8 M. Hutin, D. L. Long and L. Cronin, *Isr. J. Chem.*, 2011, **51**, 205–214.
9 D. Fan, J. Hao and Q. Wei, *J. Inorg. Organomet. Polym. Mater.*, 2012, **22**, 301–306.
10 D.-Y. Du, J.-S. Qin, S.-L. Li, Z.-M. Su and Y.-Q. Lan, *Chem. Soc. Rev.*, 2014, **43**, 4615–32.
11 C. Busche, L. Vilà-Nadal, J. Yan, H. N. Miras, D.-L. Long, V. P. Georgiev, A. Asenov, R. H. Pedersen, N. Gadegaard, M. M. Mirza, D. J. Paul, J. M. Poblet and L. Cronin, *Nature*, 2014, **515**, 545–549.
12 A. Müller, P. Kögerler and A. W. M. Dress, *Coord. Chem. Rev.*, 2001, **222**, 193–218.
13 J. M. Clemente-Juan, E. Coronado and A. Gaita-Ariño, *Chem. Soc. Rev.*, 2012, **41**, 7464.
14 B. Hasenknopf, *Front. Biosci.*, 2005, **10**, 275.
15 C. E. Müller, J. Iqbal, Y. Baqi, H. Zimmermann, A. Röllich and H. Stephan, *Bioorganic Med. Chem. Lett.*, 2006, **16**, 5943–5947.
16 C. W. Scheele, *Sämmtliche physische und chemische Werke*, 1793, vol. 4.
17 J. J. Berzelius, *Ann. Phys.*, 1826, **82**, 369–392.
18 J.-C. Galissard de Marignac, *Ann. Chim. Phys.*, 1862, **25**, 362.
19 J.-C. Galissard de Marignac, *Recherches sur les acides silicotungstiques et note sur la constitution de l'acide tungstique*, 1864.
20 A. Werner, *Zeitschrift für Anorg. Chemie*, 1893, **3**, 267–330.
21 A. Miolati and R. Pizzighelli, *J. für Prakt. Chemie*, 1908, **77**, 417–456.
22 A. Rosenheim and J. Jaenicke, *Zeitschrift für Anorg. und Allg. Chemie*, 1917, **101**, 235–275.
23 L. Pauling, *J. Am. Chem. Soc.*, 1929, **51**, 2868–2880.
24 P. W. H. Bragg and W. L. Bragg, 1913, **17**, 428–438.
25 W. L. Bragg, *Proc. R. Soc. A Math. Phys. Eng. Sci.*, 1913, **89**, 248–277.
26 J. F. Keggin, *Nature*, 1933, **132**, 351–351.
27 J. F. Keggin, *Proc. R. Soc. A Math. Phys. Eng. Sci.*, 2006, **144**, 75–100.
28 B. Dawson, *Acta Crystallogr.*, 1953, **6**, 113–126.
29 J. S. Anderson, *Nature*, 1937, **140**, 850–850.
30 H. T. Evans, *J. Am. Chem. Soc.*, 1948, **70**, 1291–1292.
31 M. T. Pope and A. Müller, *Angew. Chemie Int. Ed. English*, 1991, **30**, 34–48.
32 L. C. W. Baker and D. C. Glick, *Chem. Rev.*, 1998, **98**, 3–50.
33 A. Müller, J. Meyer, E. Krickemeyer and E. Diemann, *Angew. Chemie Int. Ed. English*, 1996, **35**, 1206–1208.
34 S. R. Hall, H. Bolger and S. Mann, *Chem. Commun.*, 2003, **3**, 2784–2785.
35 G. M. Sheldrick, *Acta Crystallogr. Sect. A Found. Crystallogr.*, 2008, **64**, 112–122.
36 P. Mialane, A. Dolbecq, L. Lisnard, A. Mallard, J. Marrot and F. Sécheresse, *Angew.*

Chemie Int. Ed., 2002, **41**, 2398.
37 M. Šimuneková, D. Prodius, V. Mereacre, P. Schwendt, C. Turta, M. Bettinelli, A. Speghini, Y. Lan, C. E. Anson and A. K. Powell, *RSC Adv.*, 2013, **3**, 6299.
38 J. R. Winkler and H. B. Gray, in *Structure and Bonding*, 2011, vol. 142, pp. 17–28.
39 N. V. Izarova, M. T. Pope and U. Kortz, *Angew. Chemie Int. Ed.*, 2012, **51**, 9492–9510.
40 J. Zhang, Q. Li, M. Zeng, Y. Huang, J. Zhang, J. Hao and Y. Wei, *Chem. Commun. (Camb).*, 2016, **52**, 2378–81.
41 M. Filowitz, R. K. C. Ho, W. G. Klemperer and W. Shum, *Inorg. Chem.*, 1979, **18**, 93–103.
42 M. Kunz and I. D. Brown, *J. Solid State Chem.*, 1995, **115**, 395–406.
43 B. J. Coe and S. J. Glenwright, *Coord. Chem. Rev.*, 2000, **203**, 5–80.
44 W. X. Lipscomb, *Inorg. Chem.*, 1965, **4**, 132–134.
45 L. Ma, S. Liu and J. Zubieta, *Inorg. Chem.*, 1989, 28, 175–177.
46 A. Müller, E. Krickemeyer, M. Penk, V. Wittneben and J. Döring, *Angew. Chemie Int. Ed. English*, 1990, **29**, 88–90.
47 M. I. Khan, A. Müller, S. Dillinger, H. Bögge, Q. Chen and J. Zubieta, *Angew. Chemie Int. Ed. English*, 1993, **32**, 1780–1782.
48 M. T. Pope, *Inorg. Chem.*, 1972, **11**, 1973–1974.
49 K. Eguchi, T. Seiyama, N. Yamazoe, S. Katsuki and H. Taketa, *J. Catal.*, 1988, **111**, 336–344.
50 J. M. Poblet, X. López and C. Bo, *Chem. Soc. Rev.*, 2003, **32**, 297–308.
51 S. Gambarelli, B. Tsukerblat, S. Bertaina, A. Müller, B. Barbara and T. Mitra, *Nature*, 2008, **453**, 203–206.
52 M. T. Pope, *Heteropoly and Isopoly Oxometalates (Inorganic Chemistry Concepts 8)*, 1983.
53 T. Kurata, A. Uehara, Y. Hayashi and K. Isobe, *Inorg. Chem.*, 2005, **44**, 2524–2530.
54 R. J. Errington, M. D. Kerlogue and D. G. Richards, *J. Chem. Soc. Chem. Commun.*, 1993, 649.
55 T. R. Mohs, G. P. a Yap, A. L. Rheingold and E. a. Maatta, *Inorg. Chem.*, 1995, **34**, 9–10.
56 M. H. Rosnes, C. Yvon, D. L. Long and L. Cronin, *Dalt. Trans.*, 2012, **41**, 10071–10079.
57 H. Abbas, A. L. Pickering, D. L. Long, P. Kögerler and L. Cronin, *Chem. - A Eur. J.*, 2005, **11**, 1071–1078.
58 A. Michailovski and G. R. Patzke, *Chem. - A Eur. J.*, 2006, **12**, 9122–9134.
59 G. Fraqueza, L. A. E. Batista De Carvalho, M. P. M. Marques, L. Maia, C. A. Ohlin, W. H. Casey and M. Aureliano, *Dalt. Trans.*, 2012, **41**, 12749–12758.
60 L. Lisnard, A. Dolbecq, P. Mialane, J. Marrot and F. Sécheresse, *Inorganica Chim. Acta*, 2004, **357**, 845–852.
61 J. Zhao, J. Li, P. Ma, J. Wang and J. Niu, *Inorg. Chem. Commun.*, 2009, **12**, 450–453.
62 E. Antonova, C. Näther and W. Bensch, *Dalt. Trans.*, 2011, **41**, 1338–1344.
63 A. Wutkowski, F. Niefind, C. Näther and W. Bensch, *Zeitschrift fur Anorg. und Allg. Chemie*, 2011, **637**, 2198–2204.
64 E. Ahmed and M. Ruck, *Angew. Chemie - Int. Ed.*, 2012, **51**, 308–309.
65 H. Fu, C. Qin, Y. Lu, Z.-M. Zhang, Y.-G. Li, Z.-M. Su, W.-L. Li and E.-B. Wang, *Angew. Chemie*, 2012, **124**, 8109–8113.
66 S. Lin, W. Liu, Y. Li, Q. Wu, E. Wang and Z. Zhang, *Dalt. Trans.*, 2010, **39**, 1740–1744.
67 C. J. Richmond, H. N. Miras, A. R. De La Oliva, H. Zang, V. Sans, L. Paramonov, C. Makatsoris, R. Inglis, E. K. Brechin, D. L. Long and L. Cronin, *Nat. Chem.*, 2012, **4**,

1037–1043.
68 A. R. De La Oliva, V. Sans, H. N. Miras, J. Yan, H. Zang, C. J. Richmond, D. L. Long and L. Cronin, *Angew. Chemie - Int. Ed.*, 2012, **51**, 12759–12762.
69 P. J. Kitson, M. D. Symes, V. Dragone and L. Cronin, *Chem. Sci.*, 2013, **4**, 3099–3103.
70 M. D. Symes, P. J. Kitson, J. Yan, C. J. Richmond, G. J. T. Cooper, R. W. Bowman, T. Vilbrandt and L. Cronin, *Nat. Chem.*, 2012, **4**, 349–354.
71 M. J. Deery, O. W. Howarth and K. R. Jennings, *J. Chem. Soc. Dalt. Trans.*, 1997, 4783–4788.
72 T. Waters, R. A. J. O'Hair and A. G. Wedd, *J. Am. Chem. Soc.*, 2003, **125**, 3384–3396.
73 C. A. Ohlin, E. M. Villa, J. C. Fettinger and W. H. Casey, *Angew. Chemie*, 2008, **120**, 8375–8378.
74 L. Vilà-Nadal, A. Rodríguez-Fortea, L.-K. Yan, E. F. Wilson, L. Cronin and J. M. Poblet, *Angew. Chemie Int. Ed.*, 2009, **48**, 5452–5456.
75 R. A. Scullion, A. J. Surman, F. Xu, J. S. Mathieson, D. L. Long, F. Haso, T. Liu and L. Cronin, *Angew. Chemie - Int. Ed.*, 2014, **53**, 10032–10037.
76 L. G. Christie, S. Asche, J. S. Mathieson, L. Vilà-Nadal and L. Cronin, *J. Am. Chem. Soc.*, 2018, **140**, 9379–9382.
77 P. S. Gromski, A. B. Henson, J. M. Granda and L. Cronin, *Nat. Rev. Chem.*, 2019, **3**, 119–128.
78 A. B. Henson, P. S. Gromski and L. Cronin, *ACS Cent. Sci.*, 2018, **4**, 793–804.
79 W. H. KNOTH and R. L. HARLOW, *Chem. Informationsd.*, 1981, **12**, 1865–1867.
80 J. F. Kirby and L. C. W. Baker, *Inorg. Chem.*, 1998, **37**, 5537–5543.
81 C. P. Pradeep, D.-L. Long and L. Cronin, *Dalt. Trans.*, 2010, **39**, 9443–9457.
82 F. Li, D. L. Long, J. M. Cameron, H. N. Miras, C. P. Pradeep, L. Xu and L. Cronin, *Dalt. Trans.*, 2012, **41**, 9859–9862.
83 D.-L. Long, D. Gabb, H. N. Miras, C. P. Pradeep, L. Cronin and S. G. Mitchell, *Dalt. Trans.*, 2012, **41**, 10000.
84 Jun Yan, De-Liang Long, N. M. Haralampos and L. Cronin, *Inorg. Chem.*, 2010, **49**, 1819–1825.
85 D. L. Long, H. Abbas, P. Kögerler and L. Cronin, *J. Am. Chem. Soc.*, 2004, **126**, 13880–13881.
86 D.-L. Long, P. Kögerler, A. D. C. C. Parenty, J. Fielden and L. Cronin, *Angew. Chemie - Int. Ed.*, 2006, **45**, 4798–4803.
87 J. Peng, T. Wang, E. Wang, Y. Kong, L. Li, B. Xue and Z. Xin, *Inorg. Chem.*, 2006, **45**, 8856–8858.
88 D. A. MacLaren, C. Streb, H. Yin, C. Ritchie, G. J. T. Cooper, L. Cronin, A. D. C. Parenty and Y.-F. Song, *Nat. Chem.*, 2009, **1**, 47–52.
89 Y. Shen, J. Peng, H. Pang, P. Zhang, D. Chen, C. Chen, H. Zhang, C. Meng and Z. Su, *Chem. - A Eur. J.*, 2011, **17**, 3657–3662.
90 A. G. Boulay, G. J. T. Cooper and L. Cronin, *Chem. Commun.*, 2012, **48**, 5088–5090.
91 T. Liu, E. Diemann, H. Li, A. W. M. Dress and A. Müller, *Nature*, 2003, **426**, 59–62.
92 G. Liu, T. Liu, S. S. Mal and U. Kortz, *J. Am. Chem. Soc.*, 2006, **128**, 10103–10110.
93 A. A. Verhoeff, M. L. Kistler, A. Bhatt, J. Pigga, J. Groenewold, M. Klokkenburg, S. Veen, S. Roy, T. Liu and W. K. Kegel, *Phys. Rev. Lett.*, 2007, **99**, 066104.
94 P. P. Mishra, J. Jing, L. C. Francesconi and T. Liu, *Langmuir*, 2008, **24**, 9308–9313.
95 T. Liu, *J. Am. Chem. Soc.*, 2003, **125**, 312–313.
96 G. J. T. Cooper, P. J. Kitson, R. Winter, M. Zagnoni, D. L. Long and L. Cronin, *Angew. Chemie - Int. Ed.*, 2011, **50**, 10373–10376.
97 A. Dolbecq, E. Dumas, R. Mayer, P. Mialane, C. R. Mayer and P. Mialane, *Chem. Rev.*, 2010, **110**, 6009–6048.

98 A. Proust, R. Thouvenot and P. Gouzerh, *Chem. Commun. (Camb).*, 2008, 1837–52.
99 V. Shivaiah, M. Nagaraju and S. K. Das, *Inorg. Chem.*, 2003, **42**, 6604–6606.
100 X. Feng, W. Zhou, Y. Li, H. Ke, J. Tang, R. Clérac, Y. Wang, Z. Su and E. Wang, *Inorg. Chem.*, 2012, **51**, 2722–2724.
101 Z. Shi, F. Li, J. Zhao, X.-Y. Yu, Y. Zheng, Z. Chen, Q. Guo, G. Zhang and Y. Luo, *Inorg. Chem. Commun.*, 2019, **102**, 104–107.
102 H. K. Chae, W. G. Klemperer and V. W. Day, *Inorg. Chem.*, 1989, **28**, 1423–1424.
103 B. Hasenknopf, R. Delmont, P. Herson and P. Gouzerh, *Eur. J. Inorg. Chem.*, 2002, **2002**, 1081–1087.
104 B. Matt, S. Renaudineau, L.-M. Chamoreau, C. Afonso, G. Izzet and A. Proust, *J. Org. Chem.*, 2011, **76**, 3107–3112.
105 A. Proust, B. Matt, R. Villanneau, G. Guillemot, P. Gouzerh and G. Izzet, *Chem. Soc. Rev.*, 2012, **41**, 7605.
106 A. J. Wilson, W. T. Robinson and C. J. Wilkins, *Acta Crystallogr. Sect. C Cryst. Struct. Commun.*, 1983, **39**, 54–56.
107 A. No, J. Oble, M. Malacria, S. Thorimbert, N. Cnrs, A. De Terrasse and G. Cedex, 2011, 4388–4391.
108 J. Li, I. Huth, L. M. Chamoreau, B. Hasenknopf, E. Lacôte, S. Thorimbert and M. Malacria, *Angew. Chemie - Int. Ed.*, 2009, **48**, 2035–2038.
109 J. J. Zhang, Y. Huang, J. J. Zhang, S. She, J. Hao, Y. G. Wei, Y. G. Wei, D. V. Vezenov, T. B. Liu and Y. G. Wei, *Dalt. Trans.*, 2014, **43**, 2722–2725.
110 K. Nwe and M. W. Brechbiel, *Cancer Biother. Radiopharm.*, 2009, **24**, 289–302.
111 H. C. Kolb, M. G. Finn and K. B. Sharpless, *Angew. Chemie Int. Ed.*, 2001, **40**, 2004–2021.
112 V. D. Bock, H. Hiemstra and J. H. Van Maarseveen, *European J. Org. Chem.*, 2006, **2006**, 51–68.
113 H.-K. Yang, M.-M. Su, L.-J. Ren, J. Tang, Y.-K. Yan, W.-K. Miao, P. Zheng and W. Wang, *Eur. J. Inorg. Chem.*, 2013, **2013**, 1381–1389.
114 R. C. Boutelle and B. H. Northrop, *J. Org. Chem.*, 2011, **76**, 7994–8002.
115 K. Micoine, B. Hasenknopf, S. Thorimbert, E. Lacôte and M. Malacria, *Org. Lett.*, 2007, **9**, 3981–3984.
116 I. Lindqvist, *Ark. Kemi*, 1950, **2**, 349–355.
117 Lindqvist, *ark.kemi*, 1952, **5**, 247–250.
118 M. Nyman, T. M. Alam, F. Bonhomme, M. A. Rodriguez, C. S. Frazer and M. E. Welk, *J. Clust. Sci.*, 2006, **17**, 197–219.
119 I. Lindqvist and B. Aronsson, *Ark. Kemi*, 1954, **7**, 49–52.
120 W. Clegg, G. M. Sheldrick, C. D. Garner and I. B. Walton, *Acta Crystallogr. Sect. B Struct. Crystallogr. Cryst. Chem.*, 1982, **38**, 2906–2909.
121 C. D. Garner, N. C. Howlader, F. E. Mabbs, A. T. McPhail, R. W. Miller and K. D. Onan, *J. Chem. Soc. Dalt. Trans.*, 1978, 1582–1589.
122 J. Fuchs, W. Freiwald and H. Hartl, *Acta Crystallogr., Sect. B Struct. Sci.*, 1978, **9**, 1764–1770.
123 A. Müller, J. Meyer, H. Bögge, A. Stammler and A. Botar, *Zeitschrift für Anorg. und Allg. Chemie*, 1995, **621**, 1818–1831.
124 C. Daniel and H. Hartl, *J. Am. Chem. Soc.*, 2005, **127**, 13978–13987.
125 K. Hegetschweiler, H. Schmalle, H. M. Streit and W. Schneider, *Inorg. Chem.*, 1990, **29**, 3625–3627.
126 C. M. Flynn and M. T. Pope, *Inorg. Chem.*, 1971, **10**, 2524–2529.
127 C. M. Flynn and M. T. Pope, *Inorg. Chem.*, 1973, **12**, 1626–1634.
128 T. M. Anderson, J. B. Parise, J. N. Bixler, T. A. Stewart, M. A. Rodriguez, M. Nyman

and W. Xu, *Eur. J. Inorg. Chem.*, 2008, **2008**, 3286–3294.
129 J. Tucher, Y. Wu, L. C. Nye, I. Ivanovic-Burmazovic, M. M. Khusniyarov and C. Streb, *Dalt. Trans.*, 2012, **41**, 9938.
130 M. A. AlDamen, J. M. Clemente-Juan, E. Coronado, C. Martí-Gastaldo and A. Gaita-Ariño, *J. Am. Chem. Soc.*, 2008, **130**, 8874–8875.
131 S. Yerra, S. R. Amanchi and S. K. Das, *J. Mol. Struct.*, 2014, **1062**, 53–60.
132 Y. Liang, Z. M. Zhang, Z. J. Liu, Y. Zhang, J. Zhang and E. B. Wang, *CrystEngComm*, 2014, **16**, 1187–1191.
133 J. Zhang, F. Xiao, J. Hao and Y. Wei, *Dalt. Trans.*, 2012, **41**, 3599.
134 Y. Du, A. L. Rheingold and E. A. Maatta, *J. Am. Chem. Soc.*, 1992, **114**, 345–346.
135 A. Proust, R. Thouvenot, M. Chaussade, F. Robert and P. Gouzerh, *Inorganica Chim. Acta*, 1994, **224**, 81–95.
136 J. B. Strong, R. Ostrander, A. L. Rheingold and E. A. Maatta, *J. Am. Chem. Soc.*, 1994, **116**, 3601–3602.
137 J. B. Strong, G. P. A. Yap, R. Ostrander, L. M. Liable-Sands, A. L. Rheingold, R. Thouvenot, P. Gouzerh and E. A. Maatta, *J. Am. Chem. Soc.*, 2000, **122**, 639–649.
138 J. B. Strong, B. S. Haggerty, A. L. Rheingold and E. A. Maatta, *Chem. Commun.*, 1997, **0**, 1137–1138.
139 W. Clegg, R. J. Errington, K. a. Fraser, S. a. Holmes and A. Schäfer, *J. Chem. Soc. Chem. Commun.*, 1995, 455.
140 D. X. West, A. Castineiras, R. A. Roesner, J. T. Brockman, J. D. Moll, J. K. Swearingen and S. C. McGrath, *Inorganica Chim. Acta*, 2003, **342**, 37–47.
141 Y. Wei, B. Xu, C. L. Barnes and Z. Peng, *J. Am. Chem. Soc.*, 2001, **123**, 4083–4084.
142 Y. Zhu, L. Wang, J. Hao, Z. Xiao, Y. Wei and Y. Wang, *Cryst. Growth Des.*, 2009, **9**, 3509–3518.
143 Q. Li, P. Wu, Y. Xia, Y. Wei and H. Guo, *J. Organomet. Chem.*, 2006, **691**, 1223–1228.
144 J. L. Stark, V. G. Young and E. a Maatta, *Angew. Chemie Int. Ed. English*, 1995, **34**, 2547–2548.
145 M. Araghi, V. Mirkhani, M. Moghadam, S. Tangestaninejad and I. Mohammdpoor-Baltork, *Dalt. Trans.*, 2012, **41**, 3087–3094.
146 B. Xu, Y. Wei, C. L. Barnes and Z. Peng, *Angew. Chemie Int. Ed.*, 2001, **40**, 2290–2292.
147 C. Streb, *Dalt. Trans.*, 2012, 41, 1651–1659.
148 Q. Chen, D. P. Goshorn, C. P. Scholes, X. Tan and J. Zubieta, *J. Am. Chem. Soc.*, 1992, **114**, 4667–4681.
149 M. I. Khan, M. I. Khan, Q. Chen, Q. Chen, H. Hope, H. Hope, S. Parkin, S. Parkin, C. J. Oconnor, C. J. Oconnor, J. Zubieta and J. Zubieta, *Inorg. Chem.*, 1993, **32**, 2929–2937.
150 L. J. Batchelor, R. Shaw, S. J. Markey, M. Helliwell and E. J. L. McInnes, *Chem. - A Eur. J.*, 2010, **16**, 5554–5557.
151 C. Allain, S. Favette, L. Chamoreau, J. Vaissermann, L. Ruhlmann and B. Hasenknopf, *Eur. J. Inorg. Chem.*, 2008, **2008**, 3433–3441.
152 J. Schulz, R. Gyepes, I. Císařová and P. Štpnička, *New J. Chem.*, 2010, **34**, 2749–2756.
153 P. Yin, J. Wang, Z. Xiao, P. Wu, Y. Wei and T. Liu, *Chem. - A Eur. J.*, 2012, **18**, 9174–9178.
154 A. J. Bridgeman, *J. Phys. Chem. A*, 2002, **106**, 12151–12160.
155 M. L. Niven, J. J. Cruywagen and J. B. B. Heyns, *J. Chem. Soc., Dalt. Trans.*, 1991, **0**, 2007–2011.
156 D. Xiao, Y. Hou, E. Wang, S. Wang, Y. Li, L. Xu and C. Hu, *Inorganica Chim. Acta*,

2004, **357**, 2525–2531.
157 D. G. Allis, E. Burkholder and J. Zubieta, *Polyhedron*, 2004, **23**, 1145–1152.
158 R. Strandberg, L. Niinistö, J. Møller, G. Schroll, K. Leander and C.-G. Swahn, *Acta Chem. Scand.*, 1973, **27**, 1004–1018.
159 V. Shivaiah, T. Arumuganathan and S. K. Das, *Inorg. Chem. Commun.*, 2004, **7**, 367–369.
160 I. Nagazi and A. Haddad, *J. Clust. Sci.*, 2014, **25**, 627–638.
161 W. Kwak, M. T. Pope and T. F. Scully, *J. Am. Chem. Soc.*, 1975, **97**, 5735–5738.
162 J. K. Stalick and C. O. Quicksall, *Inorg. Chem.*, 1976, **15**, 1577–1584.
163 G. Johansson, L. Pettersson and N. Ingri, *Acta Chem. Scand. A*, 1974, **28**, 1119–1128.
164 L. Pettersson, I. Andersson and L.-O. Ohman, *Acta Chem. Scand. A*, 1985, **39**, 53–58.
165 S. Sun, X. Liu, L. Yang, H. Tan and E. B. Wang, *Eur. J. Inorg. Chem.*, 2016, **2016**, 4179–4184.
166 T. Zhang, W. Guan, S. Wen, T. Ma, L. Yan and Z. Su, *J. Theor. Comput. Chem.*, 2015, **14**, 1550007.
167 S. Shi, L. Chen, X. Zhao, B. Ren, X. Cui and J. Zhang, *Inorganica Chim. Acta*, 2018, **482**, 870–877.
168 J. Niu, J. Ma, J. Zhao, P. Ma and J. Wang, *Inorg. Chem. Commun.*, 2011, **14**, 474–477.
169 T. Lu, S. L. Feng, Z. M. Zhu, X. J. Sang, F. Su and L. C. Zhang, *J. Solid State Chem.*, 2017, **253**, 52–57.
170 G. Hu, Y. Dong, X. He, H. Miao, S. Zhou and Y. Xu, *Inorg. Chem. Commun.*, 2015, **60**, 33–36.
171 Z. L. Li, Y. Wang, L. C. Zhang, J. P. Wang, W. S. You and Z. M. Zhu, *Dalt. Trans.*, 2014, **43**, 5840–5846.
172 Y. M. Ji, Y. Fang, P. P. Han, M. X. Li, Q. Q. Chen and Q. X. Han, *Inorg. Chem. Commun.*, 2017, **86**, 22–25.
173 M. Carraro, A. Sartorel, G. Scorrano, C. Maccato, M. H. Dickman, U. Kortz and M. Bonchio, *Angew. Chemie - Int. Ed.*, 2008, **47**, 7275–7279.
174 A. Tézé and G. Hervé, *J. Inorg. Nucl. Chem.*, 1977, **39**, 2151–2154.
175 S. Himeno, M. Takamoto, M. Hoshiba, A. Higuchi and M. Hashimoto, *Bull. Chem. Soc. Jpn.*, 2004, **77**, 519–524.
176 C. Rocchiccioli-Deltcheff, M. Fournier, R. Franck and R. Thouvenot, *Inorg. Chem.*, 1983, **22**, 207–216.
177 G. Johansson, *Acta Chem. Scand.*, 1960, **14**, 771–773.
178 E. Rather, J. T. Gatlin, P. G. Nixon, T. Tsukamoto, V. Kravtsov and D. W. Johnson, *J. Am. Chem. Soc.*, 2005, **127**, 3242–3243.
179 O. Sadeghi, L. N. Zakharov and M. Nyman, *Science*, 2015, **347**, 1359–1362.
180 W. Wernsdorfer, M. Nihei, S. Yamashita, J. Matsuno, H. Nojiri, G. N. Newton, T. Shiga, H. Oshio, K. Hasumi, M. Nakano and N. Yoshida, *Angew. Chemie Int. Ed.*, 2011, **50**, 5716–5720.
181 K. Y. Matsumoto, A. Kobayashi and Y. Sasaki, *Bull. Chem. Soc. Jpn.*, 1975, **48**, 3146–3151.
182 A. Tézé, E. Cadot, V. Béreau and G. Hervé, *Inorg. Chem.*, 2001, **40**, 2000–2004.
183 J. Rowsell and L. F. Nazar, *J. Am. Chem. Soc.*, 2000, **122**, 3777–3778.
184 P. Mialane, A. Dolbecq, L. Lisnard, A. Mallard, J. Marrot and F. Sécheresse, *Angew. Chemie Int. Ed.*, 2002, **41**, 2398.
185 T. Minato, K. Suzuki, K. Kamata and N. Mizuno, *Chem. - A Eur. J.*, 2014, **20**, 5946–5952.

186 Y. Ding, H. Chen, W. Chen, E. Wang and J. Meng, *Transit. Met. Chem.*, 2009, **34**, 281–288.
187 R. Contant and R. Thouvenot, *Inorganica Chim. Acta*, 1993, **212**, 41–50.
188 A. W. A. Mariotti, J. Xie, B. F. Abrahams, A. M. Bond and A. G. Wedd, *Inorg. Chem.*, 2007, **46**, 2530–2540.
189 A. F. Wells, *J. Mol. Struct.*, 1976, **32**, 408.
190 X. López, C. Bo, J.-M. Poblet and J. P. Sarasa, *Inorg. Chem.*, 2003, **42**, 2634–2638.
191 L. C. W. Baker and J. S. Figgis, *J. Am. Chem. Soc.*, 1970, **92**, 3794–3797.
192 H. Wu, *J. Biol. Chem.*, 1920, 189–221.
193 P. J. S. Richardt, R. W. Gable, A. M. Bond and A. G. Wedd, *Inorg. Chem.*, 2001, **40**, 703–709.
194 F. Q. Zhang, W. Guan, L. K. Yan, Y. T. Zhang, M. T. Xu, E. Hayfron-Benjamin and Z. M. Su, *Inorg. Chem.*, 2011, **50**, 4967–4977.
195 Q. Han, X. Sun, J. Li, P. Ma and J. Niu, *Inorg. Chem.*, 2014, **53**, 2006–2011.
196 Y. Jeannin and J. Martin-Frere, *Inorg. Chem.*, 1979, **18**, 3010–3014.
197 Y. Ozawa and Y. Sasaki, *Chem. Lett.*, 1987, **16**, 923–926.
198 D. L. Long, P. Kögerler and L. Cronin, *Angew. Chemie - Int. Ed.*, 2004, **43**, 1817–1820.
199 D.-L. Long, Y.-F. Song, E. F. Wilson, P. Kögerler, S.-X. Guo, A. M. Bond, J. S. J. Hargreaves and L. Cronin, *Angew. Chemie Int. Ed.*, 2008, **120**, 4456–4459.
200 C.-J. Yu, C.-D. Zhang, W. Zhang, D.-D. Liang, Y.-Y. Zhang, Q. Tang, S.-J. Li, R.-K. Tan, S.-X. Liu and F.-J. Ma, *Inorg. Chem. Commun.*, 2010, **13**, 1418–1420.
201 J. Yan, D.-L. Long, E. F. Wilson and L. Cronin, *Angew. Chemie*, 2009, **121**, 4440–4444.
202 L. Vilà-Nadal, K. Peuntinger, C. Busche, J. Yan, D. Lüders, D. L. Long, J. M. Poblet, D. M. Guldi and L. Cronin, *Angew. Chemie - Int. Ed.*, 2013, **52**, 9695–9699.
203 C. Marchal-Roch, E. Ayrault, L. Lisnard, J. Marrot, F. X. Liu and F. Sécheresse, *J. Clust. Sci.*, 2006, **17**, 283–290.
204 W. H. Knoth, *J. Am. Chem. Soc.*, 1979, **101**, 759–760.
205 F. Xin and M. T. Pope, *Organometallics*, 1994, **13**, 4881–4886.
206 C. R. Mayer, C. Roch-Marchal, H. Lavanant, R. Thouvenot, N. Sellier, J. C. Blais and F. Sécheresse, *Chem. - A Eur. J.*, 2004, **10**, 5517–5523.
207 N. Joo, S. Renaudineau, G. Delapierre, G. Bidan, L. M. Chamoreau, R. Thouvenot, P. Gouzerh and A. Proust, *Chem. - A Eur. J.*, 2010, **16**, 5043–5051.
208 V. Duffort, R. Thouvenot, C. Afonso, G. Izzet and A. Proust, *Chem. Commun.*, 2009, 6062–6064.
209 B. Matt, J. Moussa, L.-M. Chamoreau, C. Afonso, A. Proust, H. Amouri and G. Izzet, *Organometallics*, 2012, **31**, 35–38.
210 S. Gam Derouich, C. Rinfray, G. Izzet, J. Pinson, J. J. Gallet, F. Kanoufi, A. Proust and C. Combellas, *Langmuir*, 2014, **30**, 2287–2296.
211 V. Kogan, Z. Aizenshtat, R. Popovitz-Biro and R. Neumann, *Org. Lett.*, 2002, **4**, 3529–3532.
212 S. Bareyt, S. Piligkos, B. Hasenknopf, P. Gouzerh, E. Lacôte, S. Thorimbert and M. Malacria, *Angew. Chemie - Int. Ed.*, 2003, **42**, 3404–3406.
213 S. Bareyt, S. Piligkos, B. Hasenknopf, P. Gouzerh, E. Lacôte, S. Thorimbert and M. Malacria, *J. Am. Chem. Soc.*, 2005, **127**, 6788–6794.
214 K. Micoine, B. Hasenknopf, S. Thorimbert, E. Lacôte and M. Malacria, *Angew. Chemie - Int. Ed.*, 2009, **48**, 3466–3468.
215 Y. Q. Hou and C. L. Hill, *J. Am. Chem. Soc.*, 1993, **115**, 11823–11830.
216 B. Keita, I. M. Mbomekalle, L. Nadjo, P. de Oliveira, A. Ranjbari and R. Contant,

Comptes Rendus Chim., 2005, **8**, 1057–1066.
217 C. P. Pradeep, D. L. Long, G. N. Newton, Y. F. Song and L. Cronin, *Angew. Chemie - Int. Ed.*, 2008, **47**, 4388–4391.
218 H. Zeng, G. R. Newkome and C. L. Hill, *Angew. Chemie Int. Ed.*, 2000, **39**, 1841–1844.
219 C. P. Pradeep, F.-Y. Li, C. Lydon, H. N. Miras, D.-L. Long, L. Xu and L. Cronin, *Chem. - A Eur. J.*, 2011, **17**, 7472–7479.
220 M. F. Misdrahi, M. Wang, C. P. Pradeep, F.-Y. Y. Li, C. Lydon, L. Xu, L. Cronin and T. Liu, *Langmuir*, 2011, **27**, 9193–9202.
221 C. P. Pradeep, M. F. Misdrahi, F. Y. Li, J. Zhang, L. Xu, D. L. Long, T. Liu and L. Cronin, *Angew. Chemie - Int. Ed.*, 2009, **48**, 8309–8313.
222 H. T. Evans Jr, *Acta Crystallogr. Sect. B.,* 1974, **30**, 2095-2100.
223 H. T. Evans, *J. Am. Chem. Soc.*, 1968, **90**, 3275–3276.
224 A. Perloff, *Inorg. Chem.,* 1970, **9**, 2228-2239.
225 V. S. Sergienko, V. N. Molchanov and M. A. Porai-Koshits, *Sov. J. Coord. Chem.*, 1979, **5**, 740.
226 R. Dessapt, M. Gabard, M. Bujoli-Doeuff, P. Deniard and S. Jobic, *Inorg. Chem.*, 2011, **50**, 8790–8796.
227 A. L. Nolan, C. C. Allen, R. C. Burns, D. C. Craig and G. A. Lawrance, *Aust. J. Chem.*, 1998, **51**, 825–834.
228 U. Lee, H.-C. Joo and J.-S. Kwon, *Acta Crystallogr. Sect. E Struct. Reports Online*, 2002, **58**, i6–i8.
229 F. Ito, T. Ozeki, H. Ichida, H. Miyamae and Y. Sasaki, *Acta Crystallogr. Sect. C*, 1989, **45**, 946–947.
230 C. C. Allen, R. C. Burns, G. A. Lawrance, P. Turner and T. W. Hambley, *Acta Crystallogr. Sect. C Cryst. Struct. Commun.*, 1997, **53**, 7–9.
231 S. Himeno, S. Murata and K. Eda, *Dalton Trans.*, 2009, **35**, 6114–6119.
232 H. Y. Lee, K. M. Park, U. Lee and H. Ichida, *Acta Crystallogr. Sect. C Cryst. Struct. Commun.*, 1991, **47**, 1959–1961.
233 Y. Ozawa, Y. Hayashi and K. Isobe, *Acta Crystallogr. Sect. C*, 1991, **47**, 637–638.
234 L. A. Kushch, V. A. Emel'yanov, S. Golhen, O. Cador, D. Schaniel, T. Woike, L. Ouahab and E. B. Yagubskii, *Inorganica Chim. Acta*, 2009, **362**, 2279–2282.
235 U. Lee, *Acta Crystallogr. Sect. C Cryst. Struct. Commun.*, 1994, **50**, 1657–1659.
236 H. Kondo, a. Kobayashi and Y. Sasaki, *Acta Crystallogr. Sect. B Struct. Crystallogr. Cryst. Chem.*, 1980, **36**, 661–664.
237 K. J. Schmidt, G. J. Schrobilgen and J. F. Sawyer, *Acta Crystallogr. Sect. C Cryst. Struct. Commun.*, 1986, **42**, 1115–1118.
238 C. Wu, X. Lin, R. Yu, W. Yang, C. Lu and H. Zhuang, *Sci. China, Ser. B Chem.*, 2001, **44**, 49–54.
239 A. Ogawa, H. Yamato, U. Lee, H. Ichida, A. Kobayashi and Y. Sasaki, *Acta Crystallogr. Sect. C Cryst. Struct. Commun.*, 1988, **44**, 1879–1881.
240 U. Lee and Y. Sasaki, *Bull. Korean Chem. Soc.*, 1994, **15**, 37–45.
241 H. An, X. Liu, H. Chen, Z. Han, H. Zhang and Z. Chen, *CrystEngComm*, 2011, **13**, 5384–5393.
242 D. M. Shi, F. X. Ma, C. J. Zhang, S. Lu and Y. G. Chen, *Zeitschrift fur Anorg. und Allg. Chemie*, 2008, **634**, 758–763.
243 L. Zhao, S. Shen and H. Yu, *Zeitschrift fur Naturforsch. - Sect. B J. Chem. Sci.*, 2008, **63**, 799–803.
244 S. M. Wang, Y. W. Li, X. J. Feng, Y. G. Li and E. B. Wang, *Inorganica Chim. Acta*, 2010, **363**, 1556–1560.

245 S. Thabet, B. Ayed and A. Haddad, *Mater. Res. Bull.*, 2012, **47**, 3791–3796.
246 C. H. Zhang, C. J. Zhang and Y. G. Chen, *Solid State Sci.*, 2011, **13**, 1122–1126.
247 P. P. Zhang, J. Peng, A. X. Tian, J. Q. Sha, H. J. Pang, Y. Chen, M. Zhu and Y. H. Wang, *J. Mol. Struct.*, 2009, **931**, 50–54.
248 D. Dutta, A. D. Jana, M. Debnath, A. Bhaumik, J. Marek and M. Ali, *Dalt. Trans.*, 2010, **39**, 11551–11559.
249 L. Yang, Z. Zhou, P.-T. Ma, X.-F. Zhang, J.-P. Wang and J.-Y. Niu, *J. Coord. Chem.*, 2013, **66**, 1058–1067.
250 Q. Gao, F. Li, Y. Wang, L. Xu, J. Bai and Y. Wang, *Dalt. Trans.*, 2014, **43**, 941–944.
251 S. A. Adonin, N. V. Izarova, C. Besson, P. A. Abramov, B. Santiago-Schübel, P. Kögerler, V. P. Fedin and M. N. Sokolov, *Chem. Commun.*, 2015, **51**, 1222–1225.
252 R. Ran, H. Pang, Z. Yu, H. Ma and Y. Xun, *J. Coord. Chem.*, 2011, **64**, 2388–2398.
253 J. Yan, K. Gong, X. Xue, X. He, C. Zhao, Z. Han and H. Yu, *Eur. J. Inorg. Chem.*, 2014, **2014**, 5969–5976.
254 P. A. Lorenzo-Luis, P. Gili, A. Sánchez, E. Rodriguez-Castellón, J. Jiménez-Jiménez, C. Ruiz-Pérez and X. Solans, *Transit. Met. Chem.*, 1999, **24**, 686–692.
255 S. Zhang, Y. Li, Y. Liu, R. Cao, C. Sun, H. Ji and S. Liu, *J. Mol. Struct.*, 2009, **920**, 284–288.
256 S. Li, P. Ma, J. Wang, Y. Guo, H. Niu, J. Zhao and J. Niu, *CrystEngComm*, 2010, **12**, 1718–1721.
257 R. Cao, S. Liu, L. Xie, Y. Pan, J. Cao and Y. Liu, *Inorganica Chim. Acta*, 2008, **361**, 2013–2018.
258 D. Kumar, S. Ahmad, G. V. Prakash, K. V. Ramanujachary and A. Ramanan, *CrystEngComm*, 2014, **16**, 7097–7105.
259 H. Naruke and T. Yamase, *Acta Crystallogr. Sect. C Cryst. Struct. Commun.*, 1992, **48**, 597–599.
260 Q. Wu, W.-L. Chen, D. Liu, C. Liang, Y.-G. Li, S.-W. Lin and E. Wang, *Dalt. Trans.*, 2011, **40**, 56–61.
261 A. Blazevic and A. Rompel, *Coord. Chem. Rev.*, 2016, **307**, 42–64.
262 N. I. Gumerova, A. Roller and A. Rompel, *Chem. Commun.*, 2016, **52**, 9263–9266.
263 J. Zhang, Y. Huang, J. Hao and Y. Wei, *Inorg. Chem. Front.*, 2017, **4**, 1215–1218.
264 Z. Jin, H. Jian, W. Yongge, X. Fengping, Y. Panchao, W. Longsheng, J. Zhang, J. Hao, Y. Wei, F. Xiao, P. Yin and L. Wang, *J. Am. Chem. Soc.*, 2010, **132**, 14–15.
265 E. F. Wilson, H. N. Miras, M. H. Rosnes and L. Cronin, *Angew. Chemie Int. Ed.*, 2011, **50**, 3720–3724.
266 J. Thiel, D. Yang, M. H. Rosnes, X. Liu, C. Yvon, S. E. Kelly, Y. F. Song, D. L. Long and L. Cronin, *Angew. Chemie - Int. Ed.*, 2011, **50**, 8871–8875.
267 P. R. R. Marcoux, B. Hasenknopf, J. Vaissermann and P. Gouzerh, *Eur. J. Inorg. Chem.*, 2003, **2003**, 2406–2412.
268 S. Favette, B. Hasenknopf, J. Vaissermann, P. Gouzerh and C. Roux, *Chem. Commun.*, 2003, 2664.
269 D. Schaming, C. Allain, R. Farha, M. Goldmann, S. Lobstein, A. Giraudeau, B. Hasenknopf and L. Ruhlmann, *Langmuir*, 2010, **26**, 5101–5109.
270 Y. F. Song, N. McMillan, D. L. Long, J. Thiel, Y. Ding, H. Chen, N. Gadegaard and L. Cronin, *Chem. - A Eur. J.*, 2008, **14**, 2349–2354.
271 J. Zhang, Y. F. Song, L. Cronin and T. Liu, *J. Am. Chem. Soc.*, 2008, **130**, 14408–14409.
272 Y. F. Song, D. L. Long, S. E. Kelly and L. Cronin, *Inorg. Chem.*, 2008, **47**, 9137–9139.
273 Y. F. Song, N. McMillan, D. L. Long, S. Kane, J. Malm, M. O. Riehle, C. P. Pradeep, N. Gadegaard and L. Cronin, *J. Am. Chem. Soc.*, 2009, **131**, 1340–1341.

274 M. H. Rosnes, C. Musumeci, C. P. Pradeep, J. S. Mathieson, D.-L. Long, Y.-F. Song, B. Pignataro, R. Cogdell and L. Cronin, *J. Am. Chem. Soc.*, 2010, **132**, 15490–15492.

275 C. Musumeci, A. Luzio, C. P. Pradeep, H. N. Miras, M. H. Rosnes, Y. F. Song, D. L. Long, L. Cronin and B. Pignataro, *J. Phys. Chem. C*, 2011, **115**, 4446–4455.

276 C. Musumeci, M. H. Rosnes, F. Giannazzo, M. D. Symes, L. Cronin and B. Pignataro, *ACS Nano*, 2011, **5**, 9992–9999.

277 C. Yvon, A. Macdonell, S. Buchwald, A. J. Surman, N. Follet, J. Alex, D. L. Long and L. Cronin, *Chem. Sci.*, 2013, **4**, 3810–3817.

278 J. Zhang, J. Luo, P. Wang, B. Ding, Y. Huang, Z. Zhao, J. Zhang and Y. Wei, *Inorg. Chem.*, 2015, **54**, 2551–2559.

279 W. Zhang, J. Gong, L. Zhang, Y. Yang, Y. Liu, H. Zhang, G. Zhang, H. Dong, H. Hu, F. Zhao and Z. Kang, *Dalt. Trans.*, 2013, **42**, 1760–1769.

280 B. Zhang, L. Yue, Y. Wang, Y. Yang and L. Wu, *Chem. Commun.*, 2014, **50**, 10823–10826.

281 J. Zhang, Z. Zhao, J. Zhang, S. She, Y. Huang and Y. Wei, *Dalt. Trans.*, 2014, **43**, 17296–17302.

282 J. J. zhang, Z. Liu, Y. Huang, J. J. zhang, J. Hao and Y. Wei, *Chem. Commun.*, 2015, **51**, 9097–9100.

283 A. Blazevic and A. Rompel, *Coord. Chem. Rev.*, 2016, **307**, 42–64.

284 A. R. Moore, H. Kwen, A. M. Beatty and E. A. Maatta, *Chem. Commun.*, 2000, **996**, 1793–1794.

285 S. Chakraborty, A. Keightley, V. Dusevich, Y. Wang and Z. Peng, *Chem. Mater.*, 2010, **22**, 3995–4006.

286 W. K. Miao, Y. K. Yan, X. Le Wang, Y. Xiao, L. J. Ren, P. Zheng, C. H. Wang, L. X. Ren and W. Wang, *ACS Macro Lett.*, 2014, **3**, 211–215.

287 Y. Han, Y. Xiao, Z. Zhang, B. Liu, P. Zheng, S. He and W. Wang, *Macromolecules*, 2009, **42**, 6543–6548.

288 Y. Xiao, Y. K. Han, N. Xia, M. B. Hu, P. Zheng and W. Wang, *Chem. - A Eur. J.*, 2012, **18**, 11325–11333.

289 Y. K. Han, Z. J. Zhang, Y. L. Wang, N. Xia, B. Liu, Y. Xiao, L. X. Jin, P. Zheng and W. Wang, *Macromol. Chem. Phys.*, 2011, **212**, 81–87.

290 N. Xia, W. Yu, Y. Wang, Y. Han, P. Zheng, W. Wang, G. Sakaguchi, K. Matsuda, K. Saijo, M. Takenaka and H. Hasegawa, *Polymer*, 2011, **52**, 1772–1780.

291 U. Tong, W. Chen, C. Ritchie, X. Wang and Y. F. Song, *Chem. - A Eur. J.*, 2014, **20**, 1500–1504.

292 G. M. Peters and J. T. Davis, *Chem. Soc. Rev.*, 2016, **45**, 3188–3206.

293 P. Weiss, Richard G.; Terech, *Molecular Gels: Materials with Self-Assembled Fibrillar Networks*, 2006.

294 K. Nishinari, *Prog. Colloid Polym. Sci.*, 2009, **136**, 87–94.

295 T. F. A. De Greef, M. M. J. Smulders, M. Wolffs, A. P. H. J. Schenning, R. P. Sijbesma and E. W. Meijer, *Chem. Rev.*, 2009, **109**, 5687–5754.

296 A. R. Hirst, B. Escuder, J. F. Miravet and D. K. Smith, *Angew. Chemie Int. Ed.*, 2008, **47**, 8002–8018.

297 K. J. Skilling, F. Citossi, T. D. Bradshaw, M. Ashford, B. Kellam and M. Marlow, *Soft Matter*, 2014, **10**, 237–256.

298 X. Y. Liu and J. L. Li, *Soft Fibrillar Materials: Fabrication and Applications*, Wiley-VCH, 2013.

299 W. Saenger, *Principles of Nucleic Acid Structure*, Springer-Verlag, 1984.

300 E. Yu, D. Nakamura, K. DeBoyace, A. W. Neisius and L. B. McGown, *J. Phys. Chem. B*, 2008, **112**, 1130–1134.

301 V. N. Potaman and R. R. Sinden, *Biochemistry*, 1995, **34**, 14885–14892.
302 J. T. Davis, *Angew. Chemie - Int. Ed.*, 2004, **43**, 668–698.
303 W. Fritzsche and L. Spindler, *Guanine Quartets: Structure and Application*, Royal Society of Chemistry, 2012.
304 K. Araki and I. Yoshikawa, *Top. Curr. Chem.*, 2005, **256**, 133–165.
305 M. El Garah, R. C. Perone, A. S. Bonilla, S. Haar, M. Campitiello, R. Gutierrez, G. Cuniberti, S. Masiero, A. Ciesielski and P. Samorì, *Chem. Commun.*, 2015, **51**, 11677–11680.
306 T. C. Marsh, J. Vesenka and E. Henderson, *Nucleic Acids Res.*, 1995, **23**, 696–700.
307 I. Bang, *Biochem. Z.*, 1910, **26**, 293–311.
308 P. A. Levene and W. A. Jacobs, *J. Biol. Chem.*, 1913, **12**, 421–426.
309 I. Gellert, M. N. Lipsett, D. R. Davies, M. Gellert, M. N. Lipsett and D. R. Davies, *Proc. Natl. Acad. Sci. U. S. A.*, 1962, **48**, 2013–2018.
310 A. Calzolari, R. Di Felice, E. Molinari and A. Garbesi, *Appl. Phys. Lett.*, 2002, **80**, 3331–3333.
311 J. Dash and P. Saha, *Org. Biomol. Chem.*, 2016, **14**, 2157–2163.
312 E. Mezzina, P. Mariani, R. Itri, S. Masiero, S. Pieraccini, G. P. Spada, F. Spinozzi, J. T. Davis and G. Gottarelli, *Chem. - A Eur. J.*, 2001, **7**, 388–395.
313 V. Andrisano, G. Gottarelli, S. Masiero, E. H. Heijne, S. Pieraccini and G. P. Spada, *Angew. Chemie Int. Ed.*, 1999, **38**, 2386–2388.
314 V. A. Dowling, J. A. M. Charles, E. Nwakpuda and L. B. McGown, *Anal. Chem.*, 2004, **76**, 4558–4563.
315 W. S. Case, K. D. Glinert, S. LaBarge and L. B. McGown, *Electrophoresis*, 2007, **28**, 3008–3016.
316 J.-F. Chantot, T. Haertle and W. Guschlbauer, *Biochimie*, 1974, **56**, 501–507.
317 L. Spindler, I. Drevenšek Olenik, M. Čopič, R. Romih, J. Cerar, J. Škerjanc and P. Mariani, *Eur. Phys. J. E*, 2002, **7**, 95–102.
318 V. Sasisekharan, S. Zimmerman and D. R. Davies, *J. Mol. Biol.*, 1975, **92**, 171–179.
319 G. Proni, G. Gottarelli, P. Mariani and G. P. Spada, *Chem. - A Eur. J.*, 2000, **6**, 3249–3253.
320 P. Mariani, F. Ciuchi and L. Saturni, *Biophys. J.*, 1998, **74**, 430–435.
321 R. T. West, L. A. Garza, W. R. Winchester and J. A. Walmsely, *Nucleic Acids Res.*, 1994, **22**, 5128–5134.
322 J. A. Walmsley and J. F. Burnett, *Biochemistry*, 1999, **38**, 14063–14068.
323 S. Pieraccini, T. Giorgi, G. Gottarelli, S. Masiero and G. P. Spada, *Mol. Cryst. Liq. Cryst.*, 2003, **398**, 57–73.
324 F. H. C. Crick, *Nature*, 1953, **171**, 737–738.
325 A. H. Wang, G. J. Quigley, F. J. Kolpak, J. L. Crawford, J. H. van Boom, G. van der Marel and A. Rich, *Nature*, 1979, **282**, 680–686.
326 D. Voet and J. G. Voet, *Biochemistry*, John Wiley & Sons, 4th edn., 2011.
327 D. S. Su, *Angew. Chemie Int. Ed.*, 2011, **50**, 4747–4750.
328 P. E. Nielsen, *Curr. Opin. Biotechnol.*, 2001, **12**, 16–20.
329 D. Haldar and C. Schmuck, *Chem. Soc. Rev.*, 2009, **38**, 363–371.
330 M. Albrecht, *Chem. Rev.*, 2001, **101**, 3457–3498.
331 S. Hanessian, A. Gomtsyan, M. Simard and S. Roelens, *J. Am. Chem. Soc.*, 1994, **116**, 4495–4496.
332 S. Hanessian, M. Simard and S. Roelens, *J. Am. Chem. Soc.*, 1995, **117**, 7630–7645.
333 J. M. Lehn, *Chem. - A Eur. J.*, 2000, **6**, 2097–2102.
334 A. E. Rowan and R. J. M. Nolte, *Angew. Chemie - Int. Ed.*, 1998, **37**, 63–68.
335 V. Berl, I. Huc, R. G. Khoury, M. J. Krische and J. M. Lehn, *Nature*, 2000, **407**, 720–

723.
336 E. Yashima, K. Maeda and Y. Furusho, *Acc. Chem. Res.*, 2008, **41**, 1166–1180.
337 K. Akagi, *Chem. Rev.*, 2009, **109**, 5354–5401.
338 J. H. Jung, Y. Ono, K. Hanabusa and S. Shinkai, *J. Am. Chem. Soc.*, 2000, **122**, 5008–5009.
339 Y. Oaki and H. Imai, *Cryst. Growth Des.*, 2003, **3**, 711–716.
340 H. Imai and Y. Oaki, *CrystEngComm*, 2010, **12**, 1679–1687.
341 V. Soghomonian, Q. Chen, R. C. Haushalter, J. Zubieta and C. J. O'Connor, *Science.*, 1993, **259**, 1596–1599.
342 J. Heo, Y. M. Jeon and C. A. Mirkin, *J. Am. Chem. Soc.*, 2007, **129**, 7712–7713.
343 D. Pfister, K. Schäfer, C. Ott, B. Gerke, R. Pöttgen, O. Janka, M. Baumgartner, A. Efimova, A. Hohmann, P. Schmidt, S. Venkatachalam, L. van Wüllen, U. Schürmann, L. Kienle, V. Duppel, E. Parzinger, B. Miller, J. Becker, A. Holleitner, R. Weihrich and T. Nilges, *Adv. Mater.*, 2016, **28**, 9783–9791.
344 S. Doonan and E. J. Wood, *Biochem. Mol. Biol. Educ.*, 2003, **31**, 276–276.
345 A. Cornish-Bowden, *Eur. J. Biochem.*, 1984, **138**, 9–37.
346 R. B. Merrifield, *J. Am. Chem. Soc.*, 1963, **85**, 2149–2154.
347 J. a Moss, in *Current Protocols in Protein Science*, John Wiley & Sons, Inc., Hoboken, NJ, USA, 2005, vol. Chapter 18, pp. 18.7.1-18.7.19.
348 F. Guillier, D. Orain and M. Bradley, *Chem. Rev.*, 2000, **100**, 3859.
349 A. G. Kreutzer and P. J. Salveson, *Standard practices for Fmoc-based solid-phase peptide synthesis in the Nowick laboratory*, 2015.
350 C. Yvon, A. J. Surman, M. Hutin, J. Alex, B. O. Smith, D.-L. Long and L. Cronin, *Angew. Chem. Int. Ed. Engl.*, 2014, **53**, 3336–41.
351 F. Crick, *Nature*, 1970, **227**, 561–563.
352 A. G. Cairns-Smith, *Seven Clues to the Origin of Life: A Scientific Detective Story*, Cambridge, 2nd edn., 1987.
353 A. G. Cairns-Smith, *Chem. - A Eur. J.*, 2008, **14**, 3830–3839.
354 A. G. Cairns-Smith and G. L. Walker, *J. Theor. Biol.*, 1966, **10**, 53–88.
355 B. J. Cafferty and N. V. Hud, *Curr. Opin. Chem. Biol.*, 2014, **22**, 146–157.
356 T. M. Parker, E. G. Hohenstein, R. M. Parrish, N. V. Hud and C. D. Sherrill, *J. Am. Chem. Soc.*, 2013, **135**, 1306–1316.
357 D. J. Ritson and J. D. Sutherland, *J. Mol. Evol.*, 2014, **78**, 245–250.
358 W. Gilbert, *Nature*, 1986, **319**, 618–618.
359 V. Kulikov, N. A. B. Johnson, A. J. Surman, M. Hutin, S. M. Kelly, M. Hezwani, D. L. Long, G. Meyer and L. Cronin, *Angew. Chemie - Int. Ed.*, 2017, **56**, 1141–1145.
360 L. M. R. Hill, G. N. George, A. K. Duhme-Klair and C. G. Young, *J. Inorg. Biochem.*, 2002, **88**, 274–283.
361 M. Inoue and T. Yamase, *Bull. Chem. Soc. Jpn.*, 1996, **69**, 2863–2868.
362 W. Humphrey, A. Dalke and K. Schulten, *J. Mol. Graph.*, 1996, **14**, 33–38.
363 R. Strandberg, *Acta Chem Scand*, 1973, **3**, 1004–1018.
364 G. Wu and I. C. M. Kwan, *J. Am. Chem. Soc.*, 2009, **131**, 3180–3182.
365 J. E. Bell, *Spectroscopy in Biochemistry*, CRC Press, 2018, vol. 2.
366 J. Gawronski and P. Skowronek, in *Chiral Analysis*, Elsevier, 2006, pp. 397–459.
367 C. Parigger, *Handbook of Physics in Medicine and Biology*, CRC Press, 2010, vol. 56.
368 H. Vorbrüggen, I. M. Lagoja and P. Herdewijn, in *Current Protocols in Nucleic Acid Chemistry*, John Wiley & Sons, Inc., Hoboken, NJ, USA, 2006, vol. Chapter 1, pp. 1.13.1-1.13.16.
369 S. A. Thadke, B. Mishra and S. Hotha, *J. Org. Chem.*, 2014, **79**, 7358–7371.
370 C. P. Ashcroft, Y. Dessi, D. A. Entwistle, L. C. Hesmondhalgh, A. Longstaff and J. D.

Smith, *Org. Process Res. Dev.*, 2012, **16**, 470–483.
371 P. J. Robbins, A. J. Surman, J. Thiel, D.-L. Long and L. Cronin, *Chem. Commun.*, 2013, **49**, 1909.
372 S. Liu, Z. Li and P. S. Conti, *Molecules*, 2014, **19**, 4246–4255.
373 H. Jia, Q. Li, A. Bayaguud, S. She, Y. Huang, K. Chen and Y. Wei, *Sci. Rep.*, 2017, **7**, 12523.
374 T. J. Dunn, W. L. Neumann, M. M. Rogic and S. R. Woulfe, *J. Org. Chem.*, 1990, **55**, 6368–6373.
375 A. Zill, A. L. Rutz, R. E. Kohman, A. M. Alkilany, C. J. Murphy, H. Kong and S. C. Zimmerman, *Chem. Commun.*, 2011, **47**, 1279–1281.
376 O. Linnenberg, A. Kondinski, C. Stöcker and K. Y. Monakhov, *Dalt. Trans.*, 2017, **46**, 15636–15640.
377 V. W. Day, W. G. Klemperer, D. J. Maltbie, W. G. Klemparer and D. J. Maltbie, *J. Am. Chem. Soc.*, 1987, **109**, 2991–3002.
378 P. Wu, J. Chen, P. Yin, Z. Xiao, J. Zhang, A. Bayaguud and Y. Wei, *Polyhedron*, 2013, **52**, 1344–1348.
379 C. Allain, S. Favette, L. M. Chamoreau, J. Vaissermann, L. Ruhlmann and B. Hasenknopf, *Eur. J. Inorg. Chem.*, 2008, **2008**, 3433–3441.
380 A. Pénicaud, P. Poulin, A. Derré, E. Anglaret and P. Petit, *J. Am. Chem. Soc.*, 2005, **127**, 8–9.
381 W. Q. Tian and Y. A. Wang, *J. Org. Chem.*, 2004, **69**, 4299–4308.
382 C.-G. Lin, W. Chen, D.-L. Long, L. Cronin and Y.-F. Song, *Dalt. Trans.*, 2014, **43**, 8587.
383 P. Wu, P. Yin, J. Zhang, J. Hao, Z. Xiao and Y. Wei, *Chem. - A Eur. J.*, 2011, **17**, 12002–12005.
384 C. Yvon, University of Glasgow, 2014.
385 C. Dekker, *Nat. Nanotechnol.*, 2007, **2**, 209–215.
386 D. W. Deamer and M. Akeson, *Trends Biotechnol.*, 2000, **18**, 147–151.
387 V. Shivaiah and S. K. Das, *J. Chem. Sci*, 2005, **117**, 227–233.
388 R. C. Clark and J. S. Reid, *Acta Crystallogr. Sect. A Found. Crystallogr.*, 1995, **51**, 887–897.
389 R. H. Blessing, *Acta Crystallogr. Sect. A*, 1995, **51**, 33–38.
390 L. J. Farrugia, *J. Appl. Crystallogr.*, 1999, **32**, 837–838.
391 L. A. Carpino and G. Y. Han, *J. Org. Chem.*, 1972, **37**, 3404–3409.
392 D. Li, J. Song, P. Yin, S. Simotwo, A. J. Bassler, Y. Aung, J. E. Roberts, K. I. Hardcastle, C. L. Hill and T. Liu, *J. Am. Chem. Soc.*, 2011, **133**, 14010–14016.